SYNTHESIS AND CHARACTERIZATION OF ETHANOL ELECTRO-OXIDATION CATALYSTS

A THESIS SUBMITTED TO
THE GRADUATE SCHOOL OF NATURAL AND APPLIED SCIENCES
OF
MIDDLE EAST TECHNICAL UNIVERSITY

BY

HILAL DEMIR-KIVRAK

IN PARTIAL FULFILLMENT OF THE REQUIREMENTS
FOR
THE DEGREE OF DOCTOR OF PHILOSOPHY
IN
CHEMICAL ENGINEERING

OCTOBER 2010

Approval of the Thesis

"SYNTHESIS AND CHARACTERIZATION OF ETHANOL ELECTRO-OXIDATION CATALYSIS"

Submitted by **HILAL DEMIR-KIVRAK** in partial fulfillment of the requirements for the degree of **Doctor of Philosophy in Chemical Engineering Department, Middle East Technical University** by,

Prof. Dr. Canan Özgen
Dean, Graduate School of **Natural and Applied Sciences** _____

Prof. Dr. Gürkan Karakaş
Head of Department, **Chemical Engineering** _____

Prof. Dr. Deniz Üner
Supervisor, **Chemical Engineering Dept., METU** _____

Dr. Sadig Kuliyev
Co-supervisor, **Vestel Defence Industry** _____

Examining Committee Members:

Prof. Dr. Hayrettin Yücel
Chemical Engineering Dept., METU _____

Prof. Dr. Deniz Üner
Chemical Engineering Dept., METU _____

Prof. Dr. Gürkan Karakaş
Chemical Engineering Dept., METU _____

Assoc. Prof. Dr. Aysen Yılmaz
Chemistry Dept., METU _____

Assoc. Prof. Dr. N. Alper Tapan
Chemical Engineering Dept., Gazi University _____

Date: _____

I hereby declare that all information in this document has been obtained and presented in accordance with academic rules and ethical conduct. I also declare that, as required by these rules and conduct, I have fully cited and referenced all material and results that are not original to this work.

Name, Last name: Hilal DEMIR KIVRAK

Signature:

ABSTRACT

SYNTHESIS AND CHARACTERIZATION OF ETHANOL ELECTRO-OXIDATION CATALYSIS

Demir-Kivrak, Hilal

Ph.D., Department of Chemical Engineering

Supervisor : Prof. Dr. Deniz Üner

Co-supervisor : Dr. Sadig Kuliyev

October 2010, 196 pages

In this study, the role of defects, the role of Sn in relation to defects, and the role of oxide phase of tin in ethanol electro-oxidation reaction were investigated. Firstly, adsorption calorimetry measurements were conducted on monometallic (1%Pt, 2%Pt, and 5%Pt) and bi-metallic (5% Pt-Sn) γ-Al_2O_3 supported Pt catalysts. It was observed that while saturation coverage values decreased, intermediate heats remained same for Pt-Sn catalysts by the increasing amount of tin. The effect of particle size was investigated on Pt/C (pH=5), Pt/C (pH=11) catalysts at different scan rates. At high scan rates (quite above diffusion limitations), current per site activities were nearly the same for 20% Pt/C (E-Tek), Pt/C (pH=11), and Pt/C (pH=5) catalysts, which explained as electro-oxidation reaction takes place at the defects sites. Furthermore, the effect of support on ethanol electro-oxidation was investigated on CNT supported Pt catalyst. Results indicate that only the metal

dispersions improved ethanol electro-oxidation reaction and support did not have any effect on ethanol electro-oxidation reaction. Results on the 20% Pt-Sn/C (15:1 to 1:1 Pt: Sn atomic ratios) and 20% Pt-SnO_2/C (6:1 and 1:1) catalysts indicated that ethanol electro-oxidation activity increased by increasing tin amount. For 20% Pt-Sn/C catalysts, Pt-Sn (6:1)/C indicated best activity. On the other hand, 20% Pt-SnO_2 (6:1)/C catalyst was better than Pt-Sn (6:1)/C in terms of ethanol electro-oxidation activity due to the fact that there was low contact between Pt and tin oxide particles.

Keywords: Ethanol electro-oxidation, Pt, Pt-Sn, Pt-SnO_2, hydrogen adsorption, carbon monoxide adsorption, particle size, CNT support, tin addition, oxide phase.

ÖZ

ETANOL ELEKTRO-OKSİTLENME KATALİZÖRLERİNİN SENTEZLENMESİ VE KARAKTERİZASYONU

Demir-Kivrak, Hilal
Doktora, Kimya Mühendisliği Bölümü
Tez Yöneticisi : Prof. Dr. Deniz Üner
Ortak Tez Yöneticisi: Dr. Sadig Kuliyev

Ekim 2010, 196 Sayfa

Bu çalışmada, defekt sitelerin, kalayın defekt sitelerle olan ilişkisine bağlı olarak etanol elektro oksitlenmesine tepkimesine etkisi araştırılmıştır. İlk önce γ-Al_2O_3 destekli tek metalli Pt (1%Pt, 2%Pt, ve 5%Pt) ve iki metalli (5% Pt-Sn) katalizörler üzerinde adsorplanma kalorimetresi ölçümleri yapılmıştır. Artan kalay miktarı ile birlikte doygunluk konsantrasyonu (saturation coverage) düşmekte ve düşük enerjili sitelere ait olan herhangi bir değişiklik görülmemektedir. Pt/C (pH=5), Pt/C (pH=11) katalizörleri üzerinde farklı tarama hızlarında parçacık büyüklüğünün etanol elektro-oksitlenmesine etkisi araştırılmıştır. Yüksek tarama hızlarında bir siteye düşen akım değerleri 20% Pt/C (E-Tek), Pt/C (pH=11) ve Pt/C (pH=5) katalizörleri icin yakın bulunmuştur. Bu bulgu etanol elektro-oksitlenme reaksiyonunun bu katalizörler üzerinde defekt sitelerde gercekleştiği yönünde yorumlanmıştır. Diğer yandan katalizör desteğinin etanol elecktro-oksitlenme tepkimesine etkisi araştırılmıştır. Sonuçlar göstermiştir ki: sadece aktif metal yüzeylerinin dağılımı reaksiyonu etkilemekte ve katalizör desteğinin etanol

elektro-oksitlenme tepkimesi üzerinde herhangi bir etkisi görülmemektedir. Kalay miktarının ve kalay oksit fazının etanol eletro-oksitlenme tepkimesine etksi de bu araştırma kapsamında ele alınmıştır. Pt-Sn (6:1)/C katalizörü Pt:Sn/C katalizörleri içinde en iyi aktiviteyi gösterirken 20% Pt-SnO_2 (6:1)/C katalizörünün aktivitesinin Pt-Sn (6:1)/C katalizöründen daha iyi olduğu gözlenmiştir. Bunun sebebi Pt ve kalay oksit parçacıkları arasında ki temas noktasının az olmasından kaynaklandığı şeklinde yorumlanmıştır.

Anahtar Kelimeler: Etanol elektro-oksitlenmesi, Pt, Pt-Sn, Pt-SnO_2, hidrojen adsorpsiyonu, karbon monoksit adsorpsiyonu, parçacık boyutu, karbon nano tüp katalizör desteği, kalay miktarı, oksit faz.

To my dear husband and my family

ACKNOWLEDGMENTS

I would like to express my deepest sincere gratitude to my supervisor Prof. Dr. Deniz Üner for her scientific and academic guidance, suggestions, comments, encouragement, motivation and help during the course of this research. Also, I am thankful to her because of her kindly attitude not only related with the thesis but also in every occasion throughout this study.

I would like to express my deepest gratitude to my supervisor Prof. Dr. Deniz Üner and co-supervisor Dr. Sadig Kuliyev for giving me the opportunity to conduct Ph.D. studies under their supervision. Sincere appreciation is especially for their guidance, comments, constructive criticism, encouragement, patience.

The members of the PhD examining committee, Prof. Dr. Hayrettin Yücel and Assoc. Prof. Dr. Aysen Yılmaz are gratefully acknowledged for their positive attitude and constructive comments that help the progress of the thesis.

Selçuk University is gratefully acknowledged for providing opportunity to the author to conduct PhD in METU by OYP program.

I would like to thank to Vestel Defence Industry, İbrahim Pamuk and Beycan İbrahimoğlu for institutional support. Staff from Vestel; Yalçın Seven and Deniz Kozlu are deeply appreciated for the warm environment and the valuable technical help are kindly appreciated.

I also would like to thank Prof. Dr. Kurt Hebert for giving me opportunity to conduct my research in his laboratory in Iowa State University for a while and for his guidance, help, suggestions, comments and encouragement during my stay in U.S.A. The assistance of Jiahe Ai on electrochemical measurements and Newira Widharta on AFM measurements are acknowledged gratefully, as well as their friendship in Iowa State University.

I would like thank to Prof. Dr. Jorg J. Schneider for providing me research opportunities in his laboratory in Technical University of Darmstadt (Germany). I am also thankful to Herman Tempel, Mikail Paschanka, and Ravi Joshi for their guidance on the preparation of CNTs on PAOX membrane.

I am thankful to Prof. Dr. Hans J. Kleebe from Technical University of Darmstadt for providing the TEM images of the catalysts.

The technical assistance of Mr. Murat Üner for assistance in the microcalorimetry is appreciated.

I would like to thank to Assoc. Prof. Dr. Aysen Yılmaz from METU Chemistry Department for supplying the XRD measurements.

I would like to thank to METU Central Laboratory for XPS measurements.

I would like to thank to the technicians in the machine shop of METU Chemical Engineering Department.

Colleagues in the research group, “Cactus Group” are kindly appreciated namely; Mukaddes Can, Arzu Kanca, Bahar Ipek, Mert Mehmet Oymak, Saygın Aras,

Mustafa Yasin Aslan, Hale Ay, Osman Karslıoğlu, Başar Çağlar, Ebru Erünal, Berk Giray, Volkan Değirmenci, Hakan Önder Olcay, Özlem Özcan, Burcu Akça, Özge Güner. The authors kind regards are not enough to colleges Hermann Tempel, Emine Kayhan, Mikea Neumann, Ravi Joshi, Jorg Engstler, Eckhard Rikovsky, in Technical University of Darmstadt. My special thanks go to Tiffany Jo Myers, Barış Unal, Basak Çınlar for making life easier in Ames, Iowa. It is a great chance and a turning point to meet to these people for the rest of the life of the author. Colleges from the neighboring groups, Derya Düzenli, Ayse Bayrakçeken, Mehmet Ferdi Fellah are kindly appreciated.

The author is thankful for financial support by METU Research Fund Projects (BAP-08-11-DPT.2002K120510). The Scientific and Research Council of Turkey (TUBİTAK) is kindly acknowledged for the short term doctorate scholarship during seven months for research at Iowa State University and for financial support through Inten-C program during one month research study in Technical University of Darmstadt.

I am very grateful to my mother Nagihan Demir, my father Nejat Demir, and my brother N. Ceyhun Demir for their endless love and support and not leaving me alone although they were far away from me, without their endless support the realization of my goals would not be possible. Thanks a lot!

My last acknowledgement goes to my dear husband Arif Kıvrak for being there for me to share the life. Words are not enough to express my gratitude towards to him. He has been exceptionally supportive and loving throughout my career. His presence is great and it was impossible without him!

TABLE OF CONTENTS

ABSTRACT ..... **iv**

ÖZ ..... **vi**

ACKNOWLEDGMENTS ..... **ix**

TABLE OF CONTENTS ..... **xii**

LIST OF TABLES ..... **xvi**

LIST OF FIGURES ..... **xviii**

LIST OF SYMBOLS ..... **xxiv**

CHAPTERS

1. INTRODUCTION AND SCOPE **1**
1. 1 ENERGY MARKET 1
1. 2 FUEL CELLS 3
1. 3 ETHANOL MARKET 6
1. 4 SCOPE OF THESIS 7

2. LITERATURE REVIEW ON DEFC CATALYSIS **9**
2. 1 INTRODUCTION 9
2. 2 ETHANOL ELECTRO-OXIDATION CATALYSTS 10
2.2. 1 Pt-Ru Bi-metallic Anode Catalyst 11
2.2. 2 Pt-Sn Bi-metallic Anode Catalyst 14
2.2. 3 Other Pt-based Bi-metallic Anode Catalysts 19
2.2. 4 Trimetallic Anode Catalysts 22
2.2. 5 Pt-free Anode Catalysts 26
2.2. 6 Nanowires Anode Catalysts 27
2.2. 7 Ethanol Electro-oxidation Structure Sensitivity 30
2. 3 OXYGEN REDUCTION REACTION (ORR) CATALYSTS 32
2. 4 CATALYST SUPPORTS 34

3. BACKGROUND ON THE EXPERIMENTAL METHODS 36
3. 1 ADSORPTION CALORIMETRY STUDIES 36
3.1 1 Theoretical Background 36
3.1 2 Tian-Calvet Calorimetry 39
3.1 3 Adsorption Structure Sensitivity 41
3.1.3 1 *The Role of Particle Size* 43
3.1.3 2 *The Role of Second Metal Addition* 44
3.1.3 3 *The Detection of Active Sites Involving In Liquid Phase Reaction* 46
3. 2 ELECTRO-CHEMICAL CHARACTERIZATION STUDIES 46

4. EXPERIMENTAL 53
4. 1 INTRODUCTION 53
4. 2 PREPARATION METHODS 55
4.2. 1 Incipient Wetness Impregnation Method 55
4.2. 2 Polyol Method 56
4.2. 3 Preparation of CNTs 57
4. 3 CATALYST CHARACTERIZATION TECHNIQUES 57
4.3 1 X-Ray Diffraction Measurements 57
4.3 2 X-ray Photoelectron Spectroscopy Measurements 58
4.3 3 Transmission Electron Microscopy Measurements 58
4.3 4 Volumetric Chemisorption Measurements 58
4.3 5 Gas Phase Microcalorimetric Measurements 59
4.3 6 Voltammetric Measurements 60

5. RESULTS AND DISCUSSION 53
5. 1 THE CHARACTERIZATION OF γ-Al_2O_3 SUPPORTED Pt CATALYSTS 61
5.1. 1 Hydrogen Chemisorption Measurements 62
5.1. 2 Carbon Monoxide Chemisorption Measurement Results 66
5.1. 3 Oxygen Chemisorption Results 69
5.1. 4 Discussion 70
5. 2 DETERMINATION OF OPERATING PARAMETERS ON 20% Pt/C (E-TEK) CATALYST FOR ETHANOL ELECTRO-OXIDATION REACTION . 71
5.2. 1 The Effect of Scan Rate 72
5.2. 2 The Effect of Potential Change 77
5.2. 3 Discussion 79
5. 3 THE EFFECT OF PLATINUM PARTICLE SIZE FOR ETHANOL ELECTRO-OXIDATION 80
5.3. 1 XRD Results 80

5.3. 2 TEM Results 81
5.3. 3 Gas Phase Microcalorimetric Measurement Results 83
5.3. 4 Electrochemical Characterization Results 87
5.3. 5 Discussion 95
5. 4 THE EFFECT OF CARBON SUPPORT 99
5.4. 1 Volumetric Chemisorption Measurement Results 99
5.4. 2 Electrochemical Characterization Results 100
5.4. 3 Discussion 103
5. 5 THE EFFECT OF TIN ADDITION 104
5.5. 1 XRD Results 105
5.5. 2 XPS Results 105
5.5. 3 Gas Phase Microcalorimetric Measurement Results 106
5.5. 4 Electrochemical Characterization Results 110
5.5. 5 Discussion 116
5. 6 THE EFFECT OF TIN OXIDE PHASE 119
5.6. 1 XRD Results 119
5.6. 2 XPS Results 120
5.6. 3 Gas Phase Microcalorimetric Measurement Results 121
5.6. 4 Electrochemical Characterization Results 124
5.6. 5 Discussion 128
5. 7 CHAPTER SUMMARY 128

6. CONCLUSIONS 119

APPENDICES

A. Pt-Sn BIMETALLIC PHASE EQUILIBRIUM 161

B. STRUCTURE SENSITIVITY 162

C. XRD AND XPS FIGURES 164

D. PARTICLE SIZE CALCULATIONS 172

D. 1 PARTICLE SIZE CALCULATION BY XRD 172

D. 2 PARTICLE SIZE CALCULATION BY MICROCALORIMETRY 174

D. 3 PARTICLE SIZE CALCULATION BY TEM..... 174

E. ELECTROCHEMICAL CALCULATIONS AND MEASUREMENTS .. 179

E. 1 ELECTROCHEMICAL SURFACE AREA (ESA) CALCULATION..... 179

E. 2 Pt UTILIZATION CALCULATION..... 179

E. 3 ETHANOL ELECTRO-OXIDATION MEASUREMENTS ON GLASSY CARBON ELECTRODE 180

E. 4 ELECTRO-OXIDATION MEASUREMENTS ON CARBON 181

E. 5 ACTIVATION EXPERIMENTS ON PT/C CATALYSTS..... 183

E. 6 FIGURES 186

CURRICULUM VITAE 191

LIST OF TABLES

Table 1. 1 Reactions and Open Circuit Voltages (OCVs) for hydrogen, methanol, and ethanol fuel cell systems 5

Table 2. 1 Single Direct Ethanol Fuel Cell (DEFC) of Pt-Ru (1:1) alloy and corresponding Pt monometallic catalysts having 20 wt% Pt loading and operated in 1 M EtOH solution at 3 atm oxygen pressure published in literature. 13

Table 2. 2 Literature data of the stochiometric Pt-Sn compounds[109]. 15

Table 2. 3 Single Direct Ethanol Fuel Cell (DEFC) of Pt-Sn (20 wt% Pt loading) catalyst and operated in 1 M EtOH solution at 3 atm oxygen pressure published in literature 17

Table 2. 4 Single Direct Ethanol Fuel Cell (DEFC) of alloy and corresponding monometallic catalysts published in literature. 24

Table 2. 5 Ethanol electro-oxidation current densities on Pt-free catalysts measured in 1 M KOH+1M C_2H_5OH solution obtained from literature 27

Table 2. 6 Pore diameters and anodization conditions [188] 28

Table 2. 7 Ethanol electro-oxidation current densities on nanowires obtained from literature 29

Table 3. 2 Literature data of H_2 adsorption over Supported Pt surfaces 45

Table 3. 3 Literature data of CO adsorption over supported Pt surfaces 45

Table 4. 1 Catalysts prepared and characterized 54

Table 5. 1 Microcalorimetric measurements performed on γ-Al_2O_3 supported catalysts at 323 K 61

Table 5. 2 Hydrogen chemisorption results on γ-Al_2O_3 supported monometallic and bi-metallic catalysts. 63

Table 5. 3 Carbon monoxide chemisorption results on γ-Al_2O_3 supported monometallic and bi-metallic catalysts. 66

Table 5. 4 Oxygen chemisorption results on γ-Al_2O_3 supported monometallic and bi-metallic catalysts. 69

Table 5. 5 Particle size values obtained from different techniques 83

Table 5. 6 The surface site densities as measured by carbon monoxide and hydrogen adsorption calorimetry. 86

Table 5. 7 Dispersion values obtained from volumetric chemisorptions measurements 100

Table 5. 8 The surface site densities as measured by carbon monoxide and hydrogen adsorption calorimetry and particle size values obtained from microcalorimetry and XRD. 107

Table 5. 9 The surface site densities as measured by CO and hydrogen adsorption calorimetry on carbon supported (20%Pt-loading) Pt-Sn and Pt-SnO_2 catalysts. 121

LIST OF FIGURES

Figure 1. 1 Statistics of world primary energy consumption between 1984 and 2006: Adapted from the British Petroleum (BP) report: "Statistical review of world energy June 2008 [1]" 2

Figure 2. 1 Schematic representation of how a DEFC works. 10

Figure 3. 1 Cross section of the C80 mixing calorimeter: 1, removable lid; 2, thermal buffer zone; 3, heating elements; 4, thermopiles; 5, experimental area; 6, calorimetric block; 7, insulation layers; and 8, cooling circuit. 41

Figure 3. 2 Differential heat of adsorption thermogram obtained from microcalorimetry. 43

Figure 3. 3 Schematic representation of a typical electrochemical cell 49

Figure 3. 4 (a) Linear potential sweep, (b) Resulting current potential curve 50

Figure 3. 5 (a) Cyclic potential sweep, (b) Resulting current potential curve 51

Figure 5. 1 Differential heat of hydrogen adsorption measurements results on 1% Pt/γ-Al_2O_3, 2% Pt/γ-Al_2O_3, and 5% Pt/γ-Al_2O_3 catalysts at 323 K. 64

Figure 5. 2 Differential heat of hydrogen adsorption measurements results at 323 K on γ-Al_2O_3 supported 5% Pt and 5% Pt-Sn catalysts prepared at 15:1, 9:1, and 6:1atomic ratios. 65

Figure 5. 3 Differential heat of carbon monoxide adsorption measurements results on 1% Pt/γ-Al_2O_3, 2% Pt/γ-Al_2O_3, and 5% Pt/γ-Al_2O_3 catalysts at 323 K. 67

Figure 5. 4 Differential heat of carbon monoxide adsorption measurements results at 323 K on γ-Al_2O_3 supported 5% Pt and 5% Pt-Sn catalysts prepared at 15:1, 9:1, and 6:1atomic ratios. 68

Figure 5. 5 Differential heat of oxygen adsorption measurements results at 323 K on γ-Al_2O_3 supported 5% Pt and 5% Pt-Sn catalysts prepared at 15:1, 9:1, and 6:1atomic ratios. 70

Figure 5. 6 Cyclic voltammogram of 20% Pt/C (E-Tek) catalyst a) in 0.5 M H_2SO_4 solution b) in in 0.5 M H_2SO_4 and 0.5 M ethanol solution (Scan rate: 0.05 V/s).. 73

Figure 5. 7 Cyclic voltammogram of 20% Pt/C (E-Tek) catalyst a) in 0.5 M H_2SO_4 solution at 1 V/s, 2 V/s, 3 V/s, 4V/s, and 5V/s scan rates, upper insert shows the cyclic voltammogram of 20% Pt/C (E-Tek) catalyst in 0.5 M H_2SO_4 solution a 0.01 V/s, 0.05 V/s, 0.1 V/s and b) in 0.5 M H_2SO_4 + 0.5 M EtOH solution at 0.01 V/s, 0.05 V/s, 0.1 V/s, and 1V/s scan rates. 74

Figure 5. 8 The dependence of relation $q_{ethanol}/ q_{oxygen}$ to scan rate 77

Figure 5. 9 Cyclic voltammogram of 20% Pt/C (E-Tek) catalyst a) in 0.5 M H_2SO_4 solution at 0.05 V/s up to 0.8 V, 1 V, and 1.2 V b)in 0.5 M H_2SO_4 + 0.5 M EtOH solution at 0.05 V/s up to 0.8 V, 1 V, and 1.2 V. 78

Figure 5. 10 TEM images for catalysts (a) Pt/C (E-Tek), (b) Pt/C (pH=11), (c) Pt/C (pH=5), the insets show larger magnification of the Pt nanoparticles. 82

Figure 5. 11 Differential heat of hydrogen adsorption measurements results on 20% Pt/C (pH=5), 20% Pt/C (pH=11), and 20% Pt/C (E-Tek) catalysts at 323 K. 84

Figure 5. 12 Differential heat of carbon monoxide adsorption measurements results on 20% Pt/C (pH=5), 20% Pt/C (pH=11), and 20% Pt/C (E-Tek) catalysts at 323 K. 85

Figure 5. 13 Cyclic voltammogram of 20% Pt/C (E-Tek) catalyst in 0.5 M H_2SO_4 solution at 1 V/s, 2 V/s, 3 V/s scan rates, upper insert shows the cyclic voltammogram of 20% Pt/C (E-Tek) catalyst in 0.5 M H_2SO_4 solution at 0.01 V/s, 0.05 V/s, 0.1 V/s. 89

Figure 5. 14 Cyclic voltammogram of 20% Pt/C (E-Tek), 20% Pt/C (pH=11), and Pt/C (pH=5) catalysts (a) in 0.5 M H_2SO_4 solution at 1 V/s, (b) in 0.5 M H_2SO_4 solution at 0.05V/s..... 90

Figure 5. 15 Cyclic voltammogram of 20% Pt/C (E-Tek) catalyst in 0.5 M H_2SO_4 + 0.5 M EtOH solution at 1 V/s, 2 V/s scan rates, upper insert shows the cyclic voltammogram of 20% Pt/C (E-Tek) catalyst in 0.5 M H_2SO_4 +0.5 M EtOH solution at 0.01 V/s, 0.05 V/s, 0.1 V/s. 91

Figure 5. 16 Cyclic voltammogram of 20% Pt/C (E-Tek), 20% Pt/C (pH=11), and Pt/C (pH=5) catalysts (a) in 0.5 M H_2SO_4 +0.5 M EtOH solution at 0.05 V/s, (b) in 0.5 M H_2SO_4 +0.5 M EtOH solution at 1 V/s. 93

Figure 5. 17 Current per site measurements of 20% Pt/C (E-Tek), 20% Pt/C (pH=11), and Pt/C (pH=5) catalysts (a) in 0.5 M H_2SO_4 solution at 0.05 V/s, (b) in 0.5 M H_2SO_4 solution at 1V/s. 94

Figure 5. 18 Current per site measurements of 20% Pt/C (E-Tek), 20% Pt/C (pH=11), and Pt/C (pH=5) catalysts (a) in 0.5 M H_2SO_4 +0.5 M EtOH solution at 0.05 V/s, (b) in 0.5 M H_2SO_4 +0.5 M EtOH solution at 1V/s. 95

Figure 5. 19 Cyclic voltammetry results on 20% Pt/C (E-Tek), 20% Pt/commercial CNTs, and 20%Pt/home-made CNTs catalysts a) in 0.5 M H_2SO_4 at 0.05 V/s b) in 0.5 M H_2SO_4 + 0.5 M EtOH solution at 0.05 V/s 101

Figure 5. 20 Current per site vs. potential measurement results on 20% Pt/C (E-Tek), 20% Pt/commercial CNTs, and 20%Pt/home-made CNTs catalysts a) in 0.5 M H_2SO_4 at 0.05 V/s b) in 0.5 M H_2SO_4 + 0.5 M EtOH solution at 0.05 V/s. 103

Figure 5. 21 Differential heat of hydrogen adsorption measurements results at 323 K on carbon supported 20%Pt and 20% Pt:Sn catalysts prepared at 15:1, 9:1, 6:1, 1:1 Pt:Sn atomic ratios. 108

Figure 5. 22 Differential heat of carbon monoxide adsorption measurement results at 323 K on carbon supported 20% Pt:Sn catalysts prepared at 15:1, 9:1, 6:1, 1:1 Pt:Sn atomic ratios..... 110

Figure 5. 23 Cyclic voltammogram of carbon supported 20%Pt and 20% Pt:Sn catalysts prepared at 15:1, 9:1, 6:1, 1:1 Pt:Sn atomic ratios (a) in 0.5M H_2SO_4 solution at 0.01 V/s scan rate (b) in 0.5M H_2SO_4 solution at 0.25 V/s scan rate. 112

Figure 5. 24 Current per defect site measurements of 20%Pt and 20% Pt:Sn catalysts prepared at 15:1, 9:1, 6:1, 1:1 Pt:Sn atomic ratios (a) in 0.5 M H_2SO_4 solution at 0.05 V/s, (b) in 0.5 M H_2SO_4 solution at 0.25 V/s. 113

Figure 5. 25 Cyclic voltammograms of carbon supported 20%Pt and 20%Pt:Sn catalysts prepared at 15:1, 9:1, 6:1, 1:1 Pt:Sn atomic ratios in 0.5 M H_2SO_4+ 0.5 M EtOH solution (scan rate: 0.05 V/s). 114

Figure 5. 26 Maximum current values observed 1 V vs NHE vs poisining time obtained from linear sweep voltamogram for 20% Pt/C and Pt-Sn (6:1)/C catalysts in 0.5 M H_2SO_4 + 0.5 M EtOH solution at 0.05 V/s. 116

Figure 5. 27 Differential heat of hydrogen adsorption measurements results at 323 K on carbon supported 20%Pt and 20% Pt: SnO_2 catalysts prepared at 6:1 and 1:1 Pt: Sn atomic ratios..... 122

Figure 5. 28 Differential heat of carbon monoxide adsorption measurements results at 323 K on carbon supported 20%Pt and 20% Pt: SnO_2 catalysts prepared at 6:1 and 1:1 Pt: Sn atomic ratios. 123

Figure 5. 29 Cyclic voltammogram of 20%Pt:SnO_2(6:1)/C in 0.5 M H_2SO_4 solution at 0.05 V/s, 0.1 V/s, 0.25 V/s, 0.5V/s. 126

Figure 5. 30 Cyclic voltammogram of 20%Pt:SnO_2(6:1)/C and 20%Pt:SnO_2(1:1)/C in 0.5 M H_2SO_4 + 0.5 M EtOH solution at 0.05 V/s. 126

Figure 5. 31 Cyclic voltammogram of 20%Pt:SnO_2(6:1)/C and 20%Pt:Sn (6:1)/C in 0.5 M H_2SO_4 solution at 0.05 V/s. 127

Figure 5. 32 Cyclic voltammogram of 20%Pt:SnO_2(6:1)/C and 20%Pt:Sn (6:1)/C in 0.5 M H_2SO_4 + 0.5 M EtOH solution at 0.05 V/s. 127

Figure A. 1 The equilibrium phase diagram for Pt-Sn bi-metallic system [109]. 161

Figure B. 1 Cubo-octahedral crystal structure..... 162

Figure B. 2 Cyclic voltammograms for the electro-oxidation of 0.5 M ethanol in 0.5 M H_2SO_4 on (a) Pt (111) and Pt (110) and (b) Pt (15 15 14), Pt (554) and Pt (553), respectively. All voltammograms were recorded at a scan rate of 10 mV s^{-1}. Arrows indicate the scan directions [198]. 163

Figure C. 1 XRD Patterns of γ-Al_2O_3 supported Pt and Pt-Sn catalysts 164

Figure C. 2 XRD patterns on 20 % Pt catalysts. 165

Figure C. 3 XRD patterns on carbon supported 20% Pt and 20 % Pt:Sn catalysts prepared by polyol method at 15:1, 9:1, 6:1, 1:1 Pt:Sn atomic ratios. 165

Figure C. 4 XRD patterns on carbon supported 20 % Pt:SnO_2(6:1)/C and 20 % Pt:SnO_2(1:1)/C catalysts prepared by polyol method..... 166

Figure C. 5 XRD patterns on carbon supported 20 % Pt:SnO_2(1:1)/C and 20 % Pt:Sn(1:1)/C catalysts prepared by polyol method. 166

Figure C. 6 General XPS spectrum of 20%Pt/C and 20%Pt-Sn/C catalysts 167

Figure C. 7 C 1s XPS spectrum of 20%Pt/C and 20%Pt-Sn/C catalysts. 167

Figure C. 8 O 1s XPS spectrum of 20%Pt/C and 20%Pt-Sn/C catalysts. 168

Figure C. 9 Pt 4f XPS spectrum of 20%Pt/C and 20%Pt-Sn/C catalysts. 168

Figure C. 10 Sn 3d XPS spectrum of 20%Pt/C and 20%Pt-Sn/C catalysts. 169

Figure C. 11 General XPS spectrum of 20%Pt/C and 20%Pt-SnO_2/C catalysts .. 169

Figure C. 12 C 1s spectrum of 20%Pt/C and 20%Pt-SnO_2/C catalysts 170

Figure C. 13 O 1s spectrum of 20%Pt/C and 20%Pt-SnO_2/C catalysts. 170

Figure C. 14 Pt 4f spectrum of 20%Pt/C and 20%Pt-SnO_2/C catalysts. 171

Figure C. 15 Pt 4f spectrum of 20%Pt/C and 20%Pt-SnO_2/C catalysts. 171

Figure D. 1 X-ray diffraction pattern 173

Figure D. 3 Schematic representation of the aspect ratio (D/L) calculation 175

Figure D. 4 Particle size distribution of Pt/C (E-Tek) catalysts 175

Figure D. 5 Particle size distribution Pt/C (pH=11) catalyst. 176

Figure D. 6 Particle size distribution of Pt/C (pH=5) catalyst. 176

Figure D. 7 Aspect ratio distribution of Pt/C (E-Tek) catalyst 177

Figure D. 8 Aspect ratio distribution of catalysts Pt/C (pH=11) catalyst. 177

Figure D. 9 Aspect ratio distribution of Pt/C (pH=5) catalyst. 178

Figure E. 1 CV of Glassy carbon in 0.5 M H_2SO_4 solution (scan rate:0.01 V/s). 180

Figure E. 2 CV of Glassy carbon in 0.5 M H_2SO_4 + 0.5 M ethanol solution (scan rate: 0.01 V/s) 181

Figure E. 3 CV of carbon in 0.5 M H_2SO_4 solution (scan rate: 0.01 V/s) 182

Figure E. 4 CV of carbon in 0.5 M H_2SO_4 + 0.5 M ethanol solution (scan rate: 0.01 V/s) 182

Figure E. 5 CV of Pt/C (E-Tek) in 0.5 M H_2SO_4 solution (scan rate:0.01 V/s) (100 cycle) 183

Figure E. 6 CV of Pt/C (pH=10.8) in 0.5 M H_2SO_4 solution (scan rate:0.01 V/s) (100 cycle) 184

Figure E. 7 CV of Pt/C (E-Tek) in 0.5 M H_2SO_4 solution after oxidation in 0.5 M ethanol (scan rate:0.01 V/s) (100 cycle) 184

Figure E. 8 CV of Pt/C (pH=10.8) in 0.5 M H_2SO_4 solution after oxidation in 0.5 M ethanol (scan rate:0.01 V/s) (100 cycle) 185

Figure E. 9 Cyclic voltammogram of 20% Pt/C (pH=11) catalyst in 0.5 M H_2SO_4 solution at 1 V/s, 2 V/s, 3 V/s scan rates, upper insert shows the cyclic voltammogram of 20% Pt/C (pH=11) catalyst in 0.5 M H_2SO_4 solution at 0.01 V/s, 0.05 V/s, 0.1 V/s 186

Figure E. 10 Cyclic voltammogram of 20% Pt/C (pH=5) catalyst in 0.5 M H_2SO_4 solution at 1 V/s, 2 V/s, 3 V/s scan rates, upper insert shows the cyclic voltammogram of 20% Pt/C (pH=5) catalyst in 0.5 M H_2SO_4 solution at 0.01 V/s, 0.05 V/s, 0.1 V/s. 187

Figure E. 11 Cyclic voltammogram of 20% Pt/C (pH=11) catalyst in 0.5 M H_2SO_4 + 0.5 M EtOH solution at 1 V/s, 2 V/s scan rates, upper insert shows the cyclic voltammogram of 20% Pt/C (pH=11) catalyst in 0.5 M H_2SO_4 +0.5 M EtOH solution at 0.01 V/s, 0.05 V/s, 0.1 V/s. 188

Figure E. 12 Cyclic voltammogram of 20% Pt/C (pH=5) catalyst in 0.5 M H_2SO_4 + 0.5 M EtOH solution at 1 V/s, 2 V/s scan rates, upper insert shows the cyclic voltammogram of 20% Pt/C (pH=5) catalyst in 0.5 M H_2SO_4 +0.5 M EtOH solution at 0.01 V/s, 0.05 V/s, 0.1 V/s. 189

Figure E. 13 Schematic representation of pretreatment performed on 20% Pt/C (home-made) and 20% Pt-Sn (6:1)/C catalysts in 0.5 M H_2SO_4 + 0.5 M EtOH solution at 0.05 V/s before poisining measurements. 190

Figure E. 14 Linear sweep voltammetry measurmensts on 20% Pt/C and Pt-Sn (6:1)/C catalyst in 0.5 M H_2SO_4 + 0.5 M EtOH solution at 0.05 V/s. 190

LIST OF SYMBOLS

A	Area under the curve for H_2 reduction part excluding double layer capacitance
a	Pt loading on the electrode.
a.u.	Arbitrary Unit
β	integral breadth of peak at 2Θ values
BP	British Petroleum
cc	Cubic Centimeters (cm^3)
CMS	Carbon Microsphere
CNT	Carbon Nanotube
CNT-PAOX	Carbon Nanotube-Porous Aluminum Oxide
CV	Cyclic Voltammetry
CVD	Chemical Vapor Deposition
d	particle size, nm
D	Diameter, nm
DEFC	Direct Ethanol Fuel Cell
ΔG°	Gibbs' Free Energy of Formation, J/mol
ΔH°	Enthalpy of Formation, kJ/mol
DEMS	Differential Electrochemical Mass Spectroscopy
DFT	Density Functional Theory
DMFC	Direct Methanol Fuel Cell
E	Fuel Cell Voltage, V
EG	Ethylene Glycol
EMF	Electro Motive Force

EOR	Electro Oxidation Reaction
ESA	Electrochemical Surface Area
EtOH	Ethanol
e.v.	Electrovolt
F	Faraday Constant
fcc	Face Centered Cubic
FT-IR	Fourier Transform Infrared
GC	Glassy Carbon
hcp	hexagonal closed packed structure
HF	Hydrogen Flouride
HPLC	High Pressure Liquid Chromatography
H.S.	Hollow Sphere
K.	Charge corresponds to a fully covered monolayer for a polycrystalline Pt surface, 2100C/cm^2
K	Constant for XRD (0.8 < K <1)
L	Length, nm
λ	wavelength of the X-ray beam ($\lambda_{Cu\ K\alpha}$=1.54 A^o)
LSV	Linear Sweep Voltammetry
MeOH	Methanol
µL	Micro Liter
M	Molarity, mol/liter
MCMB	Meso Carbon Micro Bead
MPD	Maximum Power Density, mW/cm^2
MSE	Mercury Sulfate Electrode
nm	Nanometers
NW	Nanowire
N	number of electrons transferred during electro-oxidation
NHE	Normal Hydrogen Electrode

NMR	Nuclear Magnetic Resonance
OCV	Open Circuit Voltage
ORR	Oxygen Reduction Reaction
P	Pressure, Torr
Po	Initial Pressure, Torr
PEM	Proton Exchange Membrane
PAOX	Porous Aluminum Oxide
ppm	Parts per million
Q^o	Initial Heat of Adsorption, kJ/mole
$q_{ethanol}$	ethanol electro oxidation charge
q_{oxygen}	Pt oxidation charge
R	Universal Gas Constant
rxn	Reaction
RDE	Rotating disk electrode
S.A.	Surface Area
SCE	Saturated Calomel Electrode
T	Temperature, K
TEM	Transmission Electron Microscopy
θ	Coverage, moles of gas adsorbed/ 100 moles of Pt
$\theta^{saturation}$	Saturation Coverage, moles of gas adsorbed/ 100 moles of Pt
Θ	Angle (^{O})
UHV	Ultra High Vacuum
v	scan rate, V/s
V	Volt
VX	Vulcan XC72
VXR	Vulcan XC72-R
W	Work
wt %	Weight percent

XRD	X-ray Diffraction
XPS	X-ray Photoelectron Spectroscopy
ZSM	Zeolite Secony-Mobil

CHAPTER 1

INTRODUCTION AND SCOPE

1. 1 ENERGY MARKET

Energy is one of the most important and permanent needs for human welfare throughout history. The development level of countries are measured by their energy production and consumption amounts. World primary energy consumption between 1984 and 2006 is given in Figure 1.1 [1]. It is clearly observed that the need for energy is increasing sharply due to the rapid increase in world population, industrialization and urbanization. The current world energy need supllied by fossil fuels such as oil, coal, and natural gas. However, it is a common belief that these fossil fuels will be exhausted near future. According to the declining oil production model proposed by Hubbert, the global production of oil will start to decrease by 2020. In contrast, according to some pessimisic forecasts for global oil production reported that it already started to decline [2] .

It is an undeniable fact that exhaustion of fossil fuels has several negative consequences on not only the energy market but also on the life standards of mankind. For instance, purchase power decreases by increase in oil prices because oil is not only an energy resource but also it is a raw material for plastics,

elastomers, pharmaceuticals, paints and many other chemicals essential for our daily use.

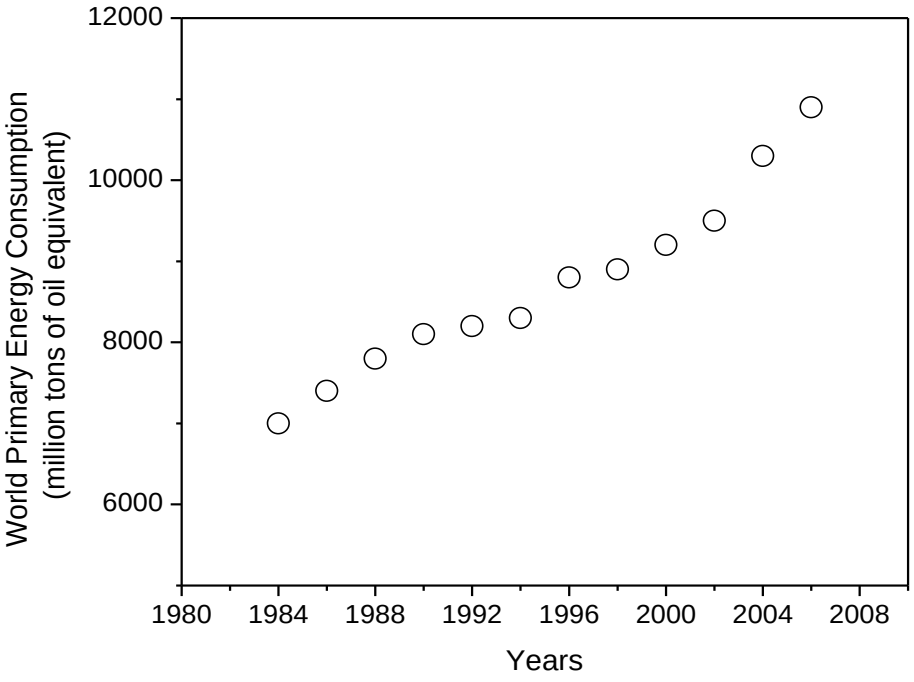

Figure 1. 1 Statistics of world primary energy consumption between 1984 and 2006: Adapted from the British Petroleum (BP) report: "Statistical review of world energy June 2008 [1]"

It goes without saying that some harmful gases such as carbon dioxide, nitrogen oxides, sulfur oxides, hydrocarbons, dust, soot, and smoke were produced while

the fossil fuels are burned and extracted, cause environmental pollution and global warming. Global warming is a main concern for all countries in the world. Some international precautions are taken and some international regulations are done throughout the world to reduce emissions. For instance, Kyoto Protocol was negotiated in 1997 at the city of Kyoto in Japan by more than 170 countries. These countires commited themselves to reduce their emissions [3].

The usage of fossil fuels for domestic, transportation, and also industry should be reduced. Research efforts on alternative energy resources, wind energy, nuclear energy, hydrothermal energy, solar energy, and hydrogen energy, increased tremendeously. Fuel cells are also the promising alternatives to fossil fuels for electrical energy generation for a clean environment due to the use of renewable fuels, such as hydrogen and alcohols. Furthermore, the efficiency of a fuel cell are higher than the efficiency of thermal energy generation system [4].

1. 2 FUEL CELLS

Fuel cells are practical power generation systems which could be used in spaceship locations, weather stations, large recreational areas, country locations, and etc. The efficiency of these devices are much more higher than conventional combustion engines since fuel cells are are not limited by thermodynamic limitations like combustion engines operating on a thermal cycle with a maximum 40% efficiency [5-13]. In ideal conditions, fuel cells can have efficiency greater than 90%, dictated by the ratio of the $\Delta G/\Delta H$ of the overall reaction carried out in fuel cells. In reality, this ideal efficiency can not be achieved due to the irreversibilities in fuel cells. The irreversibilities of a fuel cell is caused by activation losses, fuel crossover and internal currents, ohmic losses and mass transport or concentration losses [12, 14-19].

The most promising PEM fuel cell system is regarded as the hydrogen fuel cell due to its excellent performances [14]. However, the production, storage, and distribution of hydrogen are still awaiting problems for its development. Thus, alternative hydrogen carrier fuels are investigated. Alcohols such as methanol, ethanol, ethylene glycol, and propanol are considered for use in fuel cell until now due to the fact that alcohols have several advantages in comparison to hydrogen: (i) they are easily handled, transported, and stored, (ii) they have high solubility in aqueous electrolytes, (iii) liquid fuels are available at low costs. The most common fuel is methanol [14, 20-25]. On the other hand, ethanol is also preferable fuel for Direct Ethanol Fuel Cells (DEFCs) [26-32]. Table1.1 summarizes anode, cathode and overall reactions for hydrogen, methanol, ethanol fuel cell systems. Herein, thermodynamical efficiencies of hydrogen, methanol and ethanol fuel cells were regarded. If the system is reversible, the electrical work done will be equal to the *Gibbs free energy* (ΔG_f) released [5]. The electromotive force (EMF) could be calculated as follows:

$$E = \frac{-\Delta G_f}{2NF} \qquad (1\text{-}1)$$

Where,

F: Faraday constant,

E: fuel cell voltage,

ΔG_f: Gibbs free energy of formation

N: number of electrons transferred.

This fundamental equation gives the EMF or reversible open circuit voltage (OCV) of a fuel cell system.The EMF values for hydrogen, methanol, and ethanol fuel cells calculated by depending on the Equation 1 are given in Table 1.1.

Table 1. 1 Reactions and Open Circuit Voltages (OCVs) for hydrogen, methanol, and ethanol fuel cell systems [33].

Fuel Cell	Reactions		Number of electron	E_{emf} (V)
H_2	Anode	$H_2 \rightarrow 2e^- + 2H^+$	2	1.44
	Cathode	$1/2\ 0_2 + 2H^+ + 2e^- \rightarrow H_2O$		
	Overall	$2H_2 + O_2 \rightarrow 2H_2O$		
CH_3OH	Anode	$CH_3OH + H_2O \rightarrow CO_2 + 6H^+ + 6e^-$	6	1.21
	Cathode	$3/2\ 0_2 + 6H^+ + 6e^- \rightarrow 3H_2O$		
	Overall	$CH_3OH + 3/2O_2 \rightarrow CO_2 + 2H_2O$		
C_2H_5OH	Anode	$CH_3CH_2OH + 3H_2O \rightarrow 2CO_2 + 12H^+ + 12e^-$	12	1.14
	Cathode	$30_2 + 12H^+ + 12e^- \rightarrow 6H_2O$		
	Overall	$CH_3CH_2OH + 3O_2 \rightarrow 2CO_2 + 3H_2O$		

H_2 would be really the best fuel and that if there were not the H_2 production, storage, and distribution issues. In addition, DMFC shows better performance than a Direct Ethanol Fuel Cell (DEFC) in terms of thermodynamics. However, there are some disadvantages of methanol use as fuel in Direct fuel cells: (i) methanol has toxic properties and (ii) the “ideal” anodic reaction is not completely reached. In addition, methanol is mainly decomposed into CO and its principle by-products,

formaldehyde and formic acid. Platinum is the most active metal for the dissociative adsorption of methanol but it is readily poisoned by CO. Therefore, Pt-based bimetallic alloys were developed. It was reported that Pt–Ru was the best material for the methanol oxidation to carbon dioxide [34-36]. One can add that ethanol is better fuel than methanol for the portable fuel cells because ethanol is (i) easily produced, (ii) one of the less harmful chemical. The main challenge with the ethanol is the cleavage of the C–C bond. It was reported that the best anode catalyst for the DEFC was the bimetallic Pt-Sn [37-39]. However, even with that catalyst, ethanol could not be completely oxidized to CO_2 and the final products were mainly acetaldehyde and acetic acid [4, 27, 40].

1. 3 ETHANOL MARKET

Ethanol could be used as alternative vehicle fuel. However, pure ethanol is not approved as a motor vehicle fuel. For example, it could be used as a mixture of 85% ethanol and 15% of gasoline by volume called as E-85 fuel since the addition of ethanol to gasoline decrease emissions and particulate matter due to gasoline combustion. For an economic midsize vehicle, 11 liters of conventional fuel are consumed per 100 km or it needs 11 liters of gasoline for 100 km. Furthermore, for the same vehicle, 2.2 liters of gasoline and 12 liters of bio-ethanol are required for 100 km. Consequently, 1 liter of bio-ethanol could replace 0.72 liters of gasoline [41].

Commercialization of DEFCs, particularly for transportation and stationary electricity-generation markets, must be accompanied by commercialization of ethanol technologies for ethanol production, distribution, and utilization. In other words, ethanol must become readily available commodity before fuel cells can be fully commercialized. The biggest producers of ethanol from renewable resources

are Brazil and USA. These countries have particularly favorable agricultural and economic conditions [41, 42].

Ethanol could be produced by wet milling or dry milling processes. Although, wet milling process demands more power, costs more, and produces less ethanol compared to dry milling processes, wet milling process is preferable in industry because as a result of wet milling, purer starch and co-products having high market value such as corn oil, gluten feed, gluten metal, and corn steep liquor are delivered. In wet milling processes, the corn is steeped in an SO_2-water solution to make the corn grains soft enough for easy milling. Following steeping, oil, protein and a starch-rich fraction are separated. Then, starch is sent to the process for ethanol production. Finally, ethanol is produced by the following gluten separation, liquefaction, fermentation, and distillation processes. In dry milling process, corn is simply milled and mixed with water. Then it is heated before hydrolyzing, fermentation and distilling phases [42-44].

1. 4 SCOPE OF THESIS

Carbon supported Pt-Sn catalysts are active in ethanol electro-oxidation reaction but there still are questions such as how tin addition and the oxide phase of tin improve the ethanol electro-oxidation reaction were investigated in this PhD dissertation. To shed light on these questions, the role of defects and the role of Sn in relation to defects as a co- catalyst in ethanol electro-oxidation reaction were investigated. Firstly, the ethanol electro-oxidation activity on commercial 20% Pt/C (E-Tek) catalyst was investigated to find out the effect of operating parameters on ethanol electro-oxidation activity. In the second part of this study, the effect of particle size on ethanol electro-oxidation activity was explored. To reach this aim, two different carbon supported Pt (20 wt %) monometallic having

different particle size were prepared by polyol method modifying the pH of preparation solution. On the other hand, the effect of catalyst support was investigated on commercial CNT supported, home-made CNT supported, and Carbon supported Pt monometallic catalysts. These home-made CNTs were produced by CVD process on PAOX membrane. To examine the effect of support, these CNT and Carbon supported catalysts were characterized by volumetric chemisorption to find out the active metal sites on the surface. Furthermore, ethanol electro-oxidation measurements were performed by CV. Finally, the effect of tin addition and the effect of tin oxide phase were studied. Carbon supported Pt-Sn (20 wt% Pt) catalysts at 15:1, 9:1, 6:1, and 1:1 Pt: Sn atomic ratios and Pt-SnO_2 (20 wt% Pt) bimetallic catalysts at 6:1 and 1:1 Pt: Sn atomic ratios were prepared by polyol method. The characterization of these catalysts was achieved by different techniques, namely XRD, XPS, adsorption microcalorimetry, cyclic voltammetry measurements.

CHAPTER 2

LITERATURE REVIEW ON DEFC CATALYSIS

2. 1 INTRODUCTION

DEFCs are powered by ethanol, mixed with steam and fed directly to fuel cell anode. Ethanol is easier to transport and supply to the public since it is a liquid. Yet, DEFC technology is relatively new compared to that of fuel cells powered by pure hydrogen and DMFCs [4, 45, 46].

The schematic representation of DEFC is given in Figure 2.1. Chemicals constantly flow into the cell and the electricity flows out of the cell. The mixture of ethanol dissolved in water is circulated through the anodic compartment. The ethanol-water mixture by the help of anode catalyst allows the hydration of the proton exchange membrane, which transports the protons to the cathode by leaving the electrons behind, particularly for working at higher temperatures (100-130^{o}C). Electron flow results in an electric current converted to useful work. In the cathode, another catalyst is used to combine the electrons, protons and oxygen from air. The exhaust consists of water vapor and carbon dioxide when the complete ethanol electro-oxidation occurs. CO_2 is produced at anode and only protons are transported to cathode by the help of proton exchange membrane. Water is produced at cathode. The complete ethanol electro-oxidation to CO_2

involves 12 electrons per molecule passing through anode to cathode, three water molecules.

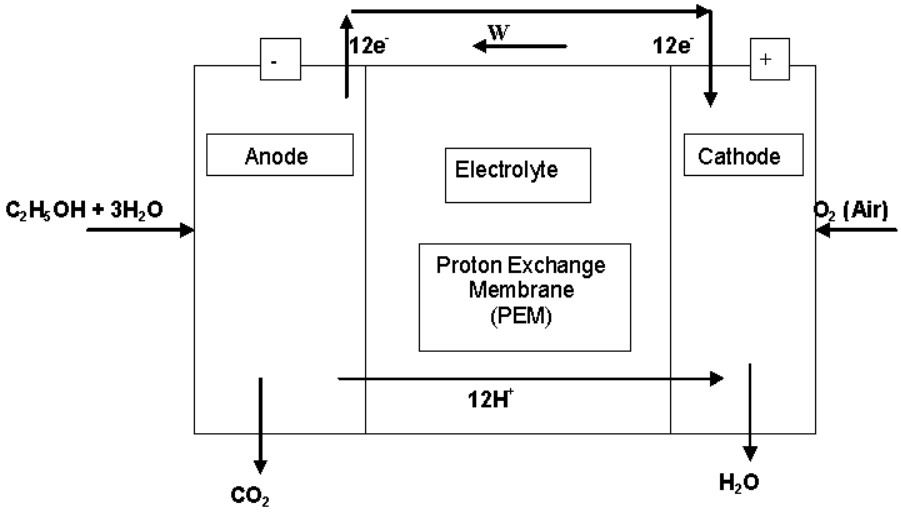

Figure 2. 1 Schematic representation of how a DEFC works.

2. 2 ETHANOL ELECTRO-OXIDATION CATALYSTS

Direct alcohol electro-oxidation catalysts are prone to poisoning by CO formed as an intermediate during the electro-oxidation reaction. Pt is the best known electro-oxidation catalyst. Pt-based multimetallic catalysts was found to be more active than monometallic Pt for alcohol electro-oxidation reaction due to their resistance

to CO poisoning [47-51]. Studies were conducted on alloys of Pt which are resistant to CO poisoning. Particularly, carbon supported Pt-Sn [4, 51-57], Pt-Ru [52, 58-65], Pt-W [66-68], Pt-Mo [69-71], Pt-Pd [72], Pt-Sn-Ru [33, 50, 73], Au [74, 75], Rh [76, 77], and Pd [72, 78-81] catalysts were investigated as anode catalysts.The more generally studied anode materials for DEFCs are the Pt–Ru and Pt–Sn binary catalysts and Pt-based tri-metallic catalysts. In consequence, Pt-Sn has been reported as one of the highly efficient DEFC anode catalyst.

2.2. 1 Pt-Ru Bi-metallic Anode Catalyst

Pt–Ru alloy catalysts revealed an enhanced ethanol electro-oxidation activity compared to pure Pt, attributed to the bi-functional mechanism and the electronic interaction between Pt and Ru [36, 82-87]. The electro-oxidation of ethanol undergoes parallel reactions producing acetaldehyde, acetic acid and carbon dioxide on Pt catalyst. Souza et al. [88] conducted an in-situ FTIR spectroscopy study for ethanol electro-oxidation reaction on Pt and Pt-Ru surfaces to understand the ability of Pt-Ru catalyst for C-C bond breaking. It was observed that the bands peaking at 1282, 1368, 1395, 1717 and 2628 cm^{-1} were indicative of acetaldehyde and acetic acid production during ethanol electro-oxidation reaction on Pt. On the contrary, for Pt-Ru electrode, only carbon dioxide was detected under the same experimental conditions by in situ FTIR spectroscopy. In conclusion, it was reported that Pt-Ru electro-catalysts were able to break down the C-C bond even at very low potentials [76, 88-97].

The amount of Ru in the Pt-Ru catalysts is an important parameter influencing the ethanol electro-oxidation reaction. It was found that there was a relatively narrow range of Pt-Ru compositions that presented a high rate of ethanol electro-oxidation it was reported that (i) at low Ru concentration, there were not enough Ru sites to

effectively assist the oxidation of adsorbed residues and the oxidation current remained almost at the levels obtained for pure Pt, (ii) for a Ru content higher than 20 wt%, the current densities increased steeply, (iii) Ru concentrations higher than 40 wt% caused the fall of current [98]. Likewise, the other studies reported that while ruthenium content increased electro-oxidation activity increased until an optimum ratio was reached [23, 45, 46, 64, 99-102].

Single DEFC tests showed that the DEFCs with Pt-Ru/C anode performed better than those with Pt/C anode [21, 27, 28, 52, 57, 103-106]. In Table 2.1, single DEFC tests performed at different temperatures and at varying Pt: Ru atomic ratios were compiled in order to enlighten the effect of operating temperature of the cell and the effect of Ru addition on cell performance. For mono-metallic Pt catalyst, the enhancing effect of temperature was clearly understood: as temperature increased, the OCV and maximum power density (MPD) of cell increased. Furthermore, it was reported that when operating temperature increased from 65^{o}C to 70^{o}C, the OCV and MPD of cell increased greatly with Pt-Ru anode [106].

A similar study was performed on Pt/C, Pt-Ru/C with different Pt-Ru atomic ratios by Liu and co-workers. It was observed that the performance and the MPD of the single fuel cell increased with increasing Ru content in the Pt-Ru/C catalysts. Furthermore, the best cell performance and the highest power density were achieved when Pt_{52} Ru_{48}/C was employed as the anode catalyst. Further increases in the mole percent of ruthenium resulted in a decrease in the performance and power density. Nevertheless, Pt-Ru/C was better as an anode catalyst than Pt/C. This result was attributed to the fact that all Pt and Pt Ru catalysts (exceptPt_{23} Ru_{77}) had a face-centered cubic (fcc) crystal structure, whereas the Pt_{23} Ru_{77} alloy was more typical of the hexagonal close packed (hcp) structure [99].

Table 2. 1 Single Direct Ethanol Fuel Cell (DEFC) of Pt-Ru (1:1) alloy and corresponding Pt monometallic catalysts having 20 wt% Pt loading and operated in 1 M EtOH solution at 3 atm oxygen pressure published in literature.

Catalyst	Operating Temperature (^oC)	OCV (mV)	MPD (mW/cm^2)	Reference
Pt/C	65	450	4	[106]
	70	550	7	[106]
	70	400	4	[57]
	80	400	5	[57]
	90	470	12	[106]
	90	420	6	[57]
	90	450	4	[28]
	100	400	5	[28]
	110	600	10	[28]
Pt-Ru/C	65	550	7	[106]
	70	650	22	[106]
	70	600	8	[57]
	80	650	10	[28]
	90	780	28	[106]
	90	600	14	[57]

Pt-Ru should combine the properties of a surface capable of oxidizing small molecules at low potentials with the ability of breaking the C-C bond present in ethanol. To investigate the effect of ruthenium oxide phase on ethanol electro-oxidation reaction, Pt–RuO_2/C and Pt–RuO_2-IrO_2 /C catalysts were prepared by a sol–gel based method to incorporate ruthenium and iridium oxides on a carbon supported platinum with 25% in their total mass related to the Pt amount. In consequence, it was found that the ethanol oxidation could proceed more efficiently on Pt–RuO_2/C than on commercially available Pt–Ru/C and Pt/C catalysts and the addition of IrO_2 to Pt–RuO_2/C composites could enhance the ethanol electro-oxidation reaction more compared to Pt-RuO_2 [107].

It is worthy to note that Pb addition to the Pt-Ru/C catalyst greatly improved the ethanol electro-oxidation activity. It was found that both the Pt-Pb and Pt-Ru-Pb catalysts exhibited significantly enhanced the catalytic activity for ethanol oxidation compared to Pt, Pt-Ru, and Pt-Sn catalysts. The promoting effect of Pb was attributed to the existence of Pb adatoms. The primary mode of action of Pb adatoms in promoting the oxidation was proposed as the removal of adsorbed CO by the bi-functional mechanism that operated for many different Pt alloys. In the case of ethanol oxidation, adsorbed CO was formed as a result of ethanol adsorption and oxidation on Pt sites at low potentials, and this blocked these sites for further ethanol oxidation [108].

2.2. 2 Pt-Sn Bi-metallic Anode Catalyst

Carbon supported Pt-Sn catalysts are commonly prepared in the absence of thermal treatment due to the fact that carbon could be burned away during the thermal preparation process. During the preparation process, Pt-Sn alloy, Pt_3Sn, and Sn and Pt oxides could be formed and the relative amounts of these species affects electrochemical activity [27]. A Platinum-tin phase equilibrium diagram was given in Appendix A (Figure A.1). Anres et al. reported that the Pt-Sn compound with the highest negative heat of formation had a very strong interaction between Pt and Sn. On the other hand, the $Pt\text{-}Sn_4$ with the smallest negative heat of formation had weak interaction between Pt and Sn (see Table 2.2) [109]. It was reported that Pt_3Sn phase improved the activity of ethanol electro-oxidation reaction rather than Pt-Sn phase [110]. Catalysts were thermally treated at 200^{o}C and 500^{o}C because thermal treatment had a significant effect on the particle size and the crystal structure of catalysts. It was reported that the formation of a predominant phase of cubic Pt_3Sn and hexagonal Pt-Sn phase rised

by thermal treatment. The amount of the hexagonal Pt-Sn phase as well as the particle size increased with increasing thermal treatment temperature. The higher electro-chemical activity was obtained in the presence of cubic Pt_3Sn [29, 38, 57, 110]. In contrast, the activity of Pt-Sn alloy for the total oxidation of ethanol to CO_2 was actually much worse than that of Pt alone. This was due to the fact that the alloying with Sn appeared to suppress the production of CH_3CHO and CO_2 but increased the selectivity to CH_3COOH [111].

Table 2. 2 Literature data of the stochiometric Pt-Sn compounds [109].

Compound	Structure	$\Delta_{formation}H$ (kJ/mol) Calorimetry
$PtSn_4$	Orthorhombic	-27,2
$PtSn_2$	Cubic	-52,3
Pt_2Sn_3	Hexagonal	-54,4
Pt-Sn	Hexagonal	-58,6
Pt_3Sn	cubic face centered	-50,2

Single DEFC tests performed at different temperatures and varying Pt: Sn atomic ratios were given in Table 2.3 in order to enlighten the effect of operating temperature of the cell and the effect of tin addition on DEFC performance. It was reported that when operating temperature increased, the OCV and MPD of the cell with Pt-Sn anode increased [9, 29, 38, 48, 66, 106, 112-117]. Single DEFC tests showed that the cells with Pt_3Sn/C anode catalyst performed better than the cells with Pt-Ru/C and Pt/C. Colmati et al. conducted a study to show the dependence of the MPD of a single DEFC with Pt/C, Pt-Ru (1:1)/C, and Pt-Sn (3:1)/C as anode material on cell temperature in the range of 70-100^{o}C. It was reported that for all investigated temperatures the MPD of the cell with Pt-Sn/C catalyst was

considerably higher than Pt-Ru/C and Pt/C catalysts [57]. Similarly, Li et al. reported that Pt-Sn had grater MPD compared to the cell with Pt-Ru catalyst operating at 90^{o}C [52].

Researchers concentrated on the effect of tin addition on ethanol electro-oxidation reaction to improve the fuel cell performance [21, 28, 29, 33, 38, 39, 50-54, 56, 57, 66, 77, 104, 106, 110, 112, 114, 116, 118-134]. To reach this aim, Tsiakaras et al. conducted a study on Pt-Sn/C catalysts at different atomic ratios by using a single DEFC at 60^{o}C and 90^{o}C. It was reported that Pt-Sn (3:2)/C catalyst revealed the highest MPD at 60^{o}C. On the contrary, the OCV and MPD of Pt-Sn (1:1)/C was smaller than that of Pt-Sn (3:2)/C catalyst, attributed to the fact that platinum active sites of catalysts with a high Sn content could be partly blocked by surface tin or its oxides [106]. Thus, there was an optimum Pt: Sn atomic ratio to reach maximum DEFC performance. In Table 2.3, other research studies were also presented seeking to investigate the effect of tin addition on ethanol electro-oxidation reaction. In the same way, other researcher also reported that Sn favored ethanol electro-oxidation activity such that the maximum power density obtained from Pt-Sn/C catalyst was three times of the value found with Pt/C alone. In conclusion, it is an undeniable fact that Sn improves the electro-catalytic performance of DEFCs [29, 38, 48, 106, 112, 113].

Pt-Sn alloy, Pt_3Sn, and Sn and Pt oxides could be formed, which the relative amounts affects electrochemical activity while carbon supported catalysts are prepared. Stannic oxide (SnO_2) and Stannous oxide (SnO) are the two main oxides of tin. The existence of these two oxides reflects the dual valence of tin, with oxidation states of +2 and +4. SnO is less well characterized than SnO_2 because its electronic band gap is not accurately known but lies somewhere in the range of 2.5-3 eV [135, 136].

Table 2. 3 Single Direct Ethanol Fuel Cell (DEFC) of Pt-Sn (20 wt% Pt loading) catalyst and operated in 1 M EtOH solution at 3 atm oxygen pressure published in literature.

Pt:Sn (atomic ratio)	Operating Temperature (^oC)	OCV (mV)	MPD (mW/cm^2)	Ref.
1:1	65	800	27	[106]
1:1	70	800	40	[106]
1:1	90	800	52	[106]
2:1	65	790	30	[106]
2:1	70	800	42	[106]
2:1	90	820	65	[106]
2:1	90	580	10	[110]
2:1	90	800	60	[21]
3:2	65	780	33	[106]
3:2	70	800	42	[106]
3:2	90	840	58	[106]
3:1	65	780	25	[106]
3:1	70	780	32	[106]
3:1	90	800	44	[106]
4:1	65	670	15	[106]
4:1	70	680	27	[106]
4:1	90	740	35	[106]
9:1	90	520	7	[110]

The oxide phases of bimetallic catalysts showed higher electro-catalytic activity rather than alloy forms. Some literature studies considering the electrochemical activity on SnO_x [56, 134, 137], RuO_x [19, 36, 99, 138-140], Co_x [141], SiO_2 [142], CeO_2 [143], MnO [144], and NiO [145] promoted Pt catalysts to emphasize the effect of oxide phases were reported in this section. Preparation method and the order of loading bi-metallic catalysts influence the formation of oxide phases.

The decoration of carbon supported Pt with Sn, the decoration of carbon supported Sn with Pt, and the co-deposition of Pt and Sn on carbon were the different preparation orders to investigate the effect of preparation orders on the formation of oxide phases and on the electrochemical activity [56]. As a result, Sn decorated Pt showed the best performance for ethanol electro-oxidation reaction and XPS data showed that Sn existed as Sn oxides in the Pt-Sn catalyst. Therefore, the promoting effect was attributed to the oxide species, rather than Sn metal or a Pt-Sn alloy. Likewise, it was indicated that SiO_2 nanoparticles may be a good candidate as the second catalyst for ethanol oxidation [146]. Zhu et al. found that Pt-Sn/C catalyst with low alloying degree could enhance the yield of acetic acid products, and the Pt-Sn/C catalyst with high alloying degree promoted the entire activity for ethanol electro-oxidation activity [127]. It was proposed that non-alloyed SnO_2 species oxidized the adsorbed poisonous intermediates to acetic acid by providing OH species, according to bi-functional mechanism. Pt-Sn alloy phase accelerated the rate of the dehydrogenation of ethanol to acetaldehyde, thus promoted the efficiency of EOR, according to electronic effect [127].

Jiang et al. conducted as study on Pt_3Sn/C catalyst prepared by a modified polyol process and treated in O_2, H_2/Ar, and Ar atmosphere, respectively. In consequence, among these treated catalysts, the as-prepared Pt-Sn/C catalyst gave the higher power density, while Ar-treated Pt-Sn/C showed the lower cell performance. This is due to the fact that more zero valence of Sn appeared in Pt-Sn/C-Ar catalyst, while more multi-valence Sn existed in the other catalysts [132, 147].

2.2. 3 Other Pt-based Bi-metallic Anode Catalysts

Other binary catalysts Pt-Pd [106], Pt-W [106], Pt-Re [148], Pt-Rh [76, 77, 83, 118, 149, 150], Pt-Pb [108, 151], Pt_3Te_x [152], Pt-Sb [119], Pt-CeO_2 [143, 153-155], Pt-ZrO_2 [143, 156], Pt-MgO [157], Pt-TiO_2 [158-162], Pt-SiO_2 [142] were investigated for ethanol electro-oxidation reaction. Generally these catalysts presented lower activity than that of Pt and lower than that of Pt-Ru.

Pt-Pd and Pt-W electrocatalysts were prepared by ethylene glycol reduction method at 1:1 Pt:Pd and Pt:W atomic ratios. According to the single DEFC performance measurements at 90^{o}C, it was found that while Pt-W showed a better ethanol electro-oxidation activity than that of Pt, Pt-Pd. On the other hand, Pt-Ru and Pt-Sn catalysts were better than Pt-Pd and Pt-W catalysts for ethanol electro-oxidation reaction [106].

Vigier et al. investigated the effect of Re on ethanol electro-oxidation reaction on carbon supported Pt, Pt-Sn, and Pt-Re catalysts by cyclic voltammetry measurements and single DEFC tests. It was reported that Pt-Sn was the best catalyst for ethanol electro-oxidation reaction. On the other hand, Pt-Re showed a better activity than that of Pt [148].

The research groups of Bergamaski, de Souza, Kowal, and Lima investigated the ethanol electro-oxidation on carbon supported Pt-Rh catalysts [76, 77, 83, 118, 149, 150]. It was shown that Pt-Rh/C catalysts enhanced the total ethanol oxidation with respect to pure Pt/C but not better than Pt-Ru. The better activity for CO_2 formation of the $Pt_{47}Rh_{53}$/C catalyst compared to Pt/C monometallic catalyst. Rhodium modifies the electronic properties of platinum in such way that the Pt-adsorbate interaction was weakened thus lowering the energy barrier for the

oxidation of adsorbates [149]. Similarly, the electrochemical oxidation of ethanol on platinum, rhodium, and platinum-rhodium electrodes was investigated using on-line differential electrochemical mass spectrometry (DEMS) and in-situ infrared spectroscopy (FTIR). In consequence, the best CO_2 yield was found on $Pt_{73}Rh_{27}$ electrodes. Furthermore, it was observed that acetaldehyde yield decreased (the ratio of CO_2/CH_3CH_2O increased) when rhodium was added to the electrode [76]. This higher efficiency was attributed to the activation of the C–C bond breaking promoted by the Rh atoms. This effect was more prominent for the materials with lower crystallite sizes due to higher alcohol adsorption strength and facilitating the C–C bond dissociation [76, 149, 163].

Carbon supported Pt-Pb and Pt-Ru-Pb catalysts were prepared by the deposition of Pb on commercial Pt and Pt-Ru catalysts. It was found that the addition of Pb increased ethanol electro-oxidation activity greatly on Pt and Pt-Ru especially at high potentials. Furthermore, it was found that no Pt-Pb and Pt-Ru-Pb alloys were formed by the help of XPS results. Hence, we could attribute the enhancing effect of Pb to the oxide phase of Pb [108, 151]. One reported that Pt-PbO_x/C exhibited significantly enhanced catalytic activity for the ethanol oxidation, observed as higher current activities and less positive reaction onset potentials when compared to the ones observed on a Pt commercial catalyst [108, 151].

Huang et al. investigated the ethanol electro-oxidation the activity of Pt_3Te_x/C catalyst. It was found that Pt_3Te/C catalyst had the highest anodic peak current density. Furthermore, as a results of cyclic voltammetry measurements, it was reported that Te addition enhance ethanol electro-oxidation activity over Pt in the following order: Pt_3Te/C> PtRu/C> Pt/C [152].

The effect of oxide phase was also investigated by many researchers. For instance, Pt, Pt–Rh, Pt–SnO_2 and Pt–Rh–SnO_2 catalysts were successfully synthesized by polyol method and deposited on high-area carbon. The activity of Pt–Rh–SnO_2/C for ethanol oxidation was found to be much higher than Pt/C and Pt–Rh/C and also superior to Pt–SnO_2/C [118]. Furthermore, Pt supported on Sb-doped SnO_2 nano-particle electro-catalysts showed enhanced electro-catalytic activities compared to Pt/C. This was attributed to the better dispersion of Pt particles on the Sb-doped SnO_2 particles as well as to the effects of SnO_2 adjacent to Pt such as the bi-functional effect and the electronic effect [119]. Likewise, The activity for ethanol electro-oxidation of carbon supported CeO_2 doped Pt catalysts was evaluated. As a result, it was reported that CeO_2 promoted Pt catalysts improved electro-catalytic activity. It was shown that CeO_2 promoted Pt-Ru and Pt catalysts exhibited best performance. It was reported that CeO_2 promoted CO oxidation at lower potentials. Pt-CeO_2/C and a series of Pt-$Ce_xZr_{1-x}O_2$/C catalyst powders with different Ce/Zr ratio were prepared and evaluated in terms of the electrochemical activity for ethanol electro-oxidation using cyclic voltammetry, steady state polarization experiments and CO-stripping technique at room temperature performance than Pt-Ru bimetallic catalyst [143, 154, 155]. TiO_2 nanotubes promoted the catalytic activity of ethanol electro-oxidation reaction [164]. Besides, another study was conducted to investigate the effect of structural water in TiO_2 nano-tubes on the electrochemical activity of ethanol oxidation by the following conclusion: (i) the existence of structural water in TiO_2 nano-tubes promoted the ethanol electro-oxidation activity, (ii) the stability of the Pt/C-TiO_2 nano-tubes catalyst was improved because of the rapid removal of CO-like poisoning species by the inherent $–OH_{ads}$ on the TiO_2 nano-tubes [162]. Pt-ZrO_2 [156] and Pt-MgO [157] were the other oxide phases catalysts evaluated as the anode catalysts for ethanol electro-oxidation reaction. Pt–ZrO_2/C catalysts were prepared and compared with the Pt/C (E-Tek) catalyst for ethanol oxidation using

cyclic voltammetry in alkaline solutions. As a result, Pt–ZrO_2/C had higher catalytic activity for ethanol electro-oxidation than Pt/C (E-Tek) catalyst [156]. In the same way, the electro-oxidation of ethanol on MgO promoted Pt/C catalysts in alkaline media was conducted. It was reported that MgO promoted Pt/C electro-catalyst was superior to Pt electro-catalyst. Moreover, the electrode with a weight ratio of Pt to MgO of 4:1 showed the highest electro-catalytic activity for ethanol electro-oxidation reaction [157]. The electro catalytic properties of Pt–SiO_2 nanocatalysts for ethanol oxidation were investigated by cyclic voltammetry. It was reported that Pt–SiO_2 nanocatalysts showed higher activity than PtRu/C (E-Tek), Pt/C (E-Tek), and Pt catalysts [142].

2.2. 4 Trimetallic Anode Catalysts

The development of novel catalysts is crucial because C-C bond cleavage on Pt catalyst and on Pt-Ru and Pt-Sn catalysts have a negative effect on fuel cells. Not only a second metal addition but also third metal addition to platinum enhances the cell performance of DEFC. Researchers paid attention to modify the Pt–Sn/C and Pt–Ru/C catalysts by adding third metal to present higher specific activity of dehydrogenation to overcome C-O and C-C bond cleavage problem during the ethanol oxidation process [28]. Mostly used tri-metallic catalyst are Pt-Sn-Ru [27, 28, 101, 104, 123, 165], Pt-Ru-Ni [165], Pt-Ru-Mo [69], Pt-Sn-Ni [124, 129, 165], Pt-Sn-Ir [107, 116, 166, 167], Pt-Sn-P [168], Pt-Sn-Rh [129, 130], Pt-Sn-CeO_2 [169]. Single DEFC test results on some of these catalysts were compiled in Table 2.4. Pt-Sn-Ru was commonly investigated tri-metallic catalyst for ethanol electro-oxidation reaction [27, 28, 101, 104, 123, 165]. Antolini et al. reported that carbon supported Pt–Ru-Sn (1:1:0.3) catalyst exhibited the highest activity for ethanol electro-oxidation while the electrochemical activity of the Pt–Sn–Ru/C (1:1:1)

catalyst was lower than that of both the binary Pt–Sn/C and Pt–Ru/C catalysts (see Table 2.4). This promoting effect of Pt-Sn-Ru (1:1:0.3) was attributed to the interactions between the Sn and Ru oxides [28]. On the contrary, Neto et al. found that the Pt-Sn/C electro-catalyst showed a superior performance for ethanol oxidation compared Pt-Ru and Pt-Ru-Sn catalysts prepared at 50:40:10, 50:25:25 and 50:10:40 Pt: Ru: Sn nominal atomic ratios. This could be due to the fact that the existence of Pt-Sn alloy probably tuned the ability of Pt to adsorb ethanol and to dissociate C–H bonds while SnO_2 species facilitated the oxidation of absorbed CO formed as an intermediate [101]. On the other hand, Rousseau et al. investigated the reaction product distribution of ethanol electro-oxidation at Pt-Sn and Pt-Ru-Sn anode catalysts in a single DEFC by using HPLC. In DEFC experiments, only three reaction products were detected: acetaldehyde, acetic acid, and carbon dioxide. It was observed that using Pt-Ru-Sn as anode catalyst improved the MPD of DEFC (See Table 2.4). Nevertheless, for the Pt–Sn/C and Pt–Sn–Ru/C anode catalysts, the formation of carbon dioxide and acetaldehyde was lowered whereas the formation of acetic acid increased in comparison that of Pt/C catalyst. In consequence, the addition of Ru to Pt–Sn only led to enhance the electrical performance of the DEFC but did not modify the product distribution and Pt-Ru-Sn tri-metallic catalyst was unable to activate C-C bond scission [104, 123]. Wang et al. reported that Pt-Ru-Mo catalyst showed superior ethanol electro-oxidation activity compared to Pt-Ru catalyst [69].

Many research studies were also dedicated to investigation of the effect of third metal addition to Pt-Sn bi-metallic catalysts. Results of researches on Pt-Sn-Ni were presented in Table 2.4. It was shown that the Ni addition decreased ethanol electro-oxidation activity and the MPD of the DEFC [124, 129, 165].

Table 2. 4 Single Direct Ethanol Fuel Cell (DEFC) of alloy and corresponding monometallic catalysts published in literature.

Catalyst	%Pt	(atomic ratio)	Operation Conditions			OCV (mV)	MPD (mW /cm^2)	Ref.
			C_{EtOH} (M)	Po_2 (atm)	T (^oC)			
Pt-Ru-Sn	20	1:0.3:1	1	3	110	720	32	[28]
	20	1:1:1	1	3	110	600	21	[28]
	20	75:15:10	1	3	80	530	3.2	[165]
	60	86:10:4	2	3	80	750	50	[104]
Pt-Ru-Ni	20	75:15:10	1	3	80	500	4	[165]
Pt-Sn-Ni	20	75:15:10	1	3	80	510	3	[165]
	40	73:0:27	2	3	90	400	8	[116]
	40	79:21:0	2	3	90	700	21	[116]
Pt-Sn-Ir	40	90:8:2	2	3	90	700	27	[116]
	40	83:16:1	2	3	90	700	28	[116]
	40	74:25:1	2	3	90	690	11	[116]
	40	67:29:4	2	3	90	700	22	[116]
	40	68:9:23	2	3	90	740	31	[116]
Pt-Sn-W	40	88:0:12	2	3	90	450	10	[66]
	40	85:8:7	2	3	90	770	35	[66]
	40	68:24:8	2	3	90	670	15	[66]
	40	62:23:15	2	3	90	680	20	[66]
Pt-Sn-P	20	3:1:1	2	2	70	703	183	[168]
	20	3:1:0	2	2	70	747	114	[168]

Riberio et al. conducted a study on the binary Pt-Ir, Pt-Sn and ternary Pt-Sn-Ir electro catalysts prepared by the Pechini–Adams method on carbon. It was found that Pt-Sn/C and Pt-Sn-Ir/C displayed better electro catalytic activity for ethanol electro-oxidation compared to Pt-Ir/C and Pt/C (see Table 2.4) [116]. Furthermore, by in situ infrared reflectance spectroscopy, adsorbed species were also investigated. As a result, linearly adsorbed CO and CO_2 species were found, indicated that the cleavage of the C-C bond in the ethanol occurred during the

electro-oxidation process [116, 167]. In the same way, the ethanol electro-oxidation activity of Pt-Sn-W catalysts prepared by Pechini–Adams method was evaluated. By in situ infrared reflectance spectroscopy, the identification of the intermediate and adsorbed species was performed and the existence of linearly adsorbed CO and CO_2 indicated that the cleavage of the C–C bond in the ethanol substrate occurred during the oxidation process [66].

Xue et al. investigated the effect of phosphorus addition to Pt-Sn catalyst to improve the ethanol electro-oxidation activity (see Table 2.4). It was found that phosphorus greatly increased the MPD from 114mW/cm^2 to 183mW/cm^2 [168].

Colmati et al. prepared carbon supported ternary Pt–Sn–Rh (1:1:0.3 and 1:1:1) alloy catalysts by the reduction of the metal precursors with formic acid. Their activity for ethanol oxidation was compared with that of binary Pt–Sn/C and Pt–Rh/C prepared with the same method. Linear sweep voltammetry measurements indicated that, for potentials higher than 0.45V versus RHE, the ternary Pt–Sn–Rh alloy catalysts exhibited higher activity for ethanol electro-oxidation, while for potentials lower than 0.45V versus RHE the electrochemical activity of the ternary catalysts was lower than that of the binary Pt–Sn catalyst. The enhanced activity for ethanol electro-oxidation on the ternary Pt–Sn–Rh catalysts was attributed to the formation of a ternary alloy and to the lower particle size [129, 130].

Neto et al. prepared Pt-Sn/CeO_2–C electrocatalysts by an alcohol-reduction process using ethylene glycol as solvent and reduction agent and CeO_2 and carbon as support. The MPD of CeO_2 promoted catalyst exhibited higher activity than Pt-Sn catalyst [169]. The enhancement of activity for alcohol electro-oxidation resulting from the addition of CeO_2 to platinum catalysts was attributed by to the bi-functional mechanism showing that CeO_2 favored the formation of chemisorbed

oxygen species and promoted the oxidation of adsorbed carbon monoxide on the surface of platinum. Díaz et al. reported that using Pt/CeO_2 electrodes, methanol and ethanol electro-oxidation were enhanced, explained either by inhibiting CO adsorption or by ceria oxygen storage facilitating the oxidation of adsorbed CO [154].

2.2. 5 Pt-free Anode Catalysts

Special attention was focused on the development of Pt-free electro-catalysts as alcohol electro-oxidation catalyst with high efficiency and low precious metal loadings to lessen the dependence on the precious metals and to reduce the cost and to accelerate the commercialization of the fuel cells. As Pt-free catalysts, Pd [155, 170-173], Pd-In_2O_3 [170], In_2O_3 [170], Ir [174], Ir_3Sn [174], Au-Pd [175, 176], Au-Pd-WC [175], and Ni [177] were investigated (see Table 2.5).

The oxidation current density of ethanol electro-oxidation reaction on Carbon microsphere (CMS) supported Pd was higher than the oxidation current density of carbon microsphere supported Pt catalyst [173]. In addition, it was reported that gold addition to Pd improved the ethanol electro-oxidation activity in alkaline media. Furthermore, Au-Pd-WC/C catalyst showed a superior ethanol electro-oxidation activity [175]. Ni and Ni hollow spheres (Ni HS) were also used as ethanol electro-oxidation catalysts in alkaline media. It was reported that Ni HS greatly enhanced the ethanol oxidation activity [177]. Carbon supported Ir_3Sn catalyst had a greater ethanol electro-oxidation activity than carbon supported Ir, Pt, and Pt_3Sn catalysts in acidic media [174]. For ethanol electro-oxidation reaction, the effect of addition In_2O_3 to Pd catalyst was investigated. It was reported that while the oxidation peak current density of Pd-In_2O_3/CNT was

reported as 61 mA/cm^2, the oxidation current density of Pd/CNT catalyst was 29 mA/cm^2. Ethanol electro-oxidation activity on In_2O_3/CNT catalyst was the lowest one [170].

Table 2. 5 Ethanol electro-oxidation current densities on Pt-free catalysts measured in 1 M KOH+1M C_2H_5OH solution obtained from literature

Catalyst	Oxidation Potential (V vs Hg/HgO)	Oxidation Current density (mA/cm^2)	Ref.
Pt/C	-0.10	40	[175]
Pt/C	-0.51	7	[173]
Pt/CMS	-0.51	12	[173]
Pd/C	-0.52	27	[173]
Pd/CMS	-0.58	65	[173]
Au-Pd/C	-0.2	60	[175]
Au-Pd-WC/C	-0.29	160	[175]
Ni	0.1	2	[177]
Ni HS	-0.1	17	[177]

2.2. 6 Nanowires Anode Catalysts

Carbon supported Pt and Pt-based anode catalysts are currently investigated and used as electro-catalysts for the electro-oxidation of liquid fuels such as methanol and ethanol. However, Pt nano-particles could be trapped in the deep cracks of carbon, reducing the reactive sites of Pt catalysts and also the Pt utilization during electrochemical oxidation of methanol and ethanol [178]. Thus, it is important to

increase Pt utilization in electro-oxidation reaction. Recently, nanowire metallic electrodes gained much attention in the area of fuel cell due to the fact that they had extremely high surface-to-volume ratios and excellent activities [80, 144, 172, 178-183].

Porous Aluminum Oxide Membrane (PAOX membrane) is an ideal template for creating highly ordered nanowire arrays because it possesses a uniform and parallel porous structure [184, 185]. Furthermore, the preparation of this membrane is not complicated. The pore system of alumina is formed by potentiostatic anodization at a constant voltage with a current change due to increased resistance in the growing oxide [184-188]. Pores grew perpendicular to the surface with oxide dissolution at the electrolyte-oxide interface [186, 187].

PAOX membrane templates are fabricated by a two step anodization process. Different electrolytes should be used to obtain PAOX templates with different pore sizes [184, 185, 188]. These pore sizes regimes and electrolytes were given in Table 2.6.

Table 2. 6 Pore diameters and anodization conditions [188].

Pore diameter (nm)	Voltage (V)	Temperature (^{o}C)	Electrolyte
5-8	15	10	10% H_2SO_4
22	27	2	3 M H_2SO_4
30	40	20	3% oxalic acid
70	30-60	1	0.3 M oxalic acid
150	130	7	10% H_3PO_4
267	160	3	10% H_3PO_4

This electrolyte dependence of pore size distribution was mainly due to the fact that the pore diameter was affected strongly by the dissolution velocity of alumina in the electrolyte chosen. Mostly used method for nanowire formation on PAOX membrane was electro-deposition method [182-185, 188-191]. In this method, a piece of PAOX membrane was attached to the surface of a glassy carbon electrode (GCE). Electro-deposition was carried out in an aqueous solution containing desired metal precursors such as Pd or Pt precursors. Then, PAOX membrane was completely removed after electro-deposition the metal (Pd or Pt) nanowire array embedded in the porous alumina template [80, 172, 178-181]. There are limited amount of studies for the use of nanowires for ethanol electro-oxidation reaction. These research studies indicated that Pt, Pd nanowires prepared by template synthesis method showed enhanced electro-catalytic activity for ethanol electro-oxidation reaction. These studies were compiled in the Table 2.7.

Table 2. 7 Ethanol electro-oxidation current densities on nanowires obtained from literature

Catalyst	Electrolyte	Oxidation Potential (V vs Ag/AgCl)	Oxidation Current density (mA/cm^2)	Reference
Pt NW	0.5M H_2SO_4+ 1M C_2H_5OH	1.1	17	[181]
Pd NW	1 M KOH+1M C_2H_5OH	-0.13	74	[172]
		-0.12	73	[80]
Pd film	1 M KOH+ 1M C_2H_5OH	-0.09	10	[172]
		-0.10	10	[80]
Pt/Ru (E-tek)	0.5M H_2SO_4+ 1M C_2H_5OH	1.1	10	[181]
	1 M KOH+ 1M C_2H_5OH	-0.15	41	[80]
		-0.15	40	[172]

It is undeniable fact that it would be nice to use metal oxide nanowires as ethanol electro-oxidation catalysts because, as has been noted, the oxide phase of metal enhances electro-oxidation activity. Unfortunately, no study was reported on metal oxide nanowires for ethanol electro-oxidation reaction. On the other hand, for methanol electro-oxidation reaction, only one study was reported until now [182]. It was reported that, for DMFC application, Platinum–ruthenium (Pt–Ru) nano-particles were successfully deposited on the surface of SnO_2 nanowires grown directly on carbon paper (Pt–Ru/SnO_2 NWs/carbon paper) by potentiostatic electro-deposition method. It was observed that Pt–Ru/SnO_2 NWs/carbon paper composite electrodes had considerably higher methanol oxidation mass activity and than the one supported on the GC electrode [182].

2.2. 7 Ethanol Electro-Oxidation Structure Sensitivity

Ethanol electro-oxidation reaction is a structure sensitive reaction. In addition, Pt is the best known catalyst for ethanol electro-oxidation reaction due to the fact that Pt is the most active catalyst for ethanol for C-C bond cleavage [111, 192-196]. Gomes et al. reported that on Pt (111), Pt (110), Pt (100) are active surfaces for breaking the C-C bond at low potentials and Pt (110) electrode displays the highest catalytic activity for the splitting of the C-C bond [29, 57, 110, 130, 197]. The bonding ability of surface atoms with C-containing atoms and the coordination number of platinum surface atoms dictate the ethanol electro-oxidation activity. It was hypothesized that Pt (100) crystal plane was the best surface to fully convert ethanol at low coverage depending on the Density Functional Theory (DFT) calculations [111].

Typical voltammograms for the ethanol electro-oxidation reaction on Pt (111), Pt (110) and on the stepped surfaces Pt (15 15 14), Pt (554) and Pt (553) in sulfuric acid solution was given in Appendix B (Figure B.1). An outstanding increase in the current occurred at 0.4 V and then a small shoulder was formed at 0.5 V, followed by a large peak with a maximum between 0.6 and 0.8 V. For Pt (111), a reproducible small increase in the current was observed at 0.44 V, attributed due to the increased availability of surface sites due to a sharp decrease of the coverage of the strongly adsorbing bi-sulfate anion. Furthermore, it was found that the maximum activity towards ethanol oxidation roughly doubled increasing the step density by going from Pt (111) to Pt (15 15 14). Further increase in the step density to Pt (554) resulted in an increase in the maximum current by a factor of three. In consequence, it is crystal clear that similar to the oxidation of CO and methanol, defects enhance the ethanol oxidation rate in sulfuric acid [198]. It was presented that C-C bond cleavage occurred through strongly chemisorbed precursor CH_2CO or CHCO only at low-coordinated surface sites. It was demonstrated that acetaldehyde was produced via the one-step concerted dehydrogenation of ethanol, occurring mainly on the close packed Pt (111).

Moreover, acetic acid was the dominant oxidation product on Pt (111) at oxidative conditions but its formation was significantly inhibited by the minority surface sites [111]. The oxidation of acetaldehyde was also investigated on Pt (111), Pt (110) and on the stepped surfaces Pt (15 15 14), Pt (554) and Pt (553) in sulfuric acid solution. In this case, it was observed that increasing the step density of the surface had a smaller effect on oxidation compared to the ethanol oxidation. Furthermore, the activity of Pt (110) in acetaldehyde electro-oxidation was very low when compared to Pt (111) and the stepped surfaces. This could be concluded as that C–C bond breaking occurred preferentially in acetaldehyde. It was reported that step poisoning was slow for ethanol oxidation when it was rapid for

acetaldehyde because of the relative ease of C–C bond breaking, which led to an adverse effect of steps on the oxidation of acetaldehyde to acetic acid [111, 198-200].

2. 3 OXYGEN REDUCTION REACTION (ORR) CATALYSTS

The material for the use as a DEFC cathode at a high activity for oxygen reduction reaction (ORR) and high ethanol tolerance is required. Research on alternative cathode catalysts is still necessary in order to find a material with an improved ORR activity and a higher ethanol tolerance than those of Pt [68, 72, 141, 171, 180, 201-213].

Pt alloys with Fe [212], Co [141, 212], Cr [212], and Ru [203, 214]were used as cathode catalyst materials to improve the activity of ORR. Lopes et al. investigated the effect of ORR on Pt-Co (3:1) cathode catalyst. Linear sweep voltammetry measurements indicated that in the cathode potential region (0.7–0.9V versus RHE) Pt/C and Pt–Co (3:1)/C showed the same activity for the oxidation of crossover ethanol. Moreover, the performance of Pt–Co/C as cathode material in DEFCs in the temperature range 60–100°C was better than that of Pt/C both in terms of mass activity and specific activity [141]. On the other hand, the electro activity of Pt-Co (1:1)/C and Pt-Cr (3:1)/C for the oxygen reduction reaction (ORR) in ethanol-containing medium was studied. It was found that these cathodes present a high tolerance to this alcohol. Furthermore, the activities were obtained in the following order: Pt-Co (1:1)/C> Pt-Cr (3:1)/C >Pt/C [141, 213]. Furthermore, it was found that the ORR activity of DEFC performance increased in the order Pt/C< Pt-Fe/C < Pt-Co/C <Pt-Cr/C [212].

Pt free electro-catalysts are currently studied as cathode catalyst materials to enhance electrochemical properties both in terms of tolerance to ethanol and high activity and selectivity toward ORR [68, 210, 211, 215]. The performances of the alcohol-tolerant electro-catalysts could be attributed to surface and/or bulk electronic properties that promote a slow rate of adsorption of the organic molecules on the catalytic surface of this type of electro-catalysts.

W_2C/C, Ag/C, and Ag–W_2C/C electro catalysts were prepared and used for the electro reduction of oxygen in alkaline solution. These Pt-free electro-catalysts showed high activities similar to those of Pt-based electro-catalyst. It was found that while W_2C/C showed catalytic activity towards oxygen reduction at higher over potential, Ag/C towards oxygen electro-reduction was higher than that of W_2C/C. Furthermore, the addition of tungsten carbides nano-crystals into Ag/C significantly enhanced the ORR performance, much better than that on pure Ag/C electro-catalysts [210].

For DMFC, carbon supported Pd–W alloy electro catalysts were prepared and ORR activity and optimum Pd: W atomic ratio was investigated. It was found that the Pd–W catalysts showed high tolerance to methanol electro-oxidation compared to a Pt catalyst. Cyclic voltammetry and rotating disk electrode measurements showed that the alloying of Pd with W enhanced the catalytic activity for the oxygen reduction reaction (ORR) as well as the stability (durability) of the electro catalyst compared to the unalloyed Pd. Furthermore, the composition $Pd_{95}W_5$ exhibited the maximum activity for ORR in the Pd–W system [68].

Park and co-workers prepared composite cathode catalyst by mixing Ni, Co, and Fe complexes into a polymer matrix followed by heating the mixture at 800^{o}C under inert atmosphere. This catalyst had alloy structures of Ni, Co and Fe. The

catalytic activity of this catalyst for ORR was compared with that of commercially available Pt/C catalyst at different ethanol concentrations. It was found that Ni-Co-Fe catalyst was less prone to ethanol oxidation at cathode even when ethanol crossover occurred through the Nafion film, preventing voltage drop at the cathode. However, the Pt/C catalyst oxidized ethanol at the cathode and caused a decrease in voltage especially at higher ethanol concentrations [211].

Verma et al. conducted a study to investigate the effect of MnO_2 cathode loading in alkaline medium for DEFC. It was reported that the power density decreased with further increase in MnO_2 loading at the cathode that for ethanol was 9.2 $mWcm^{-2}$ at 28.5 $mAcm^{-2}$ [215].

2. 4 CATALYST SUPPORTS

Carbons are stable in both acidic and basic media, which is not true for alumina and silica. Thus, carbon supported catalysts are commonly used as anode catalysts for fuel cells [35, 216]. Usually, the catalysts are formed in nano-particles and dispersed on Vulcan XC-72 carbon black surface area or other high surface are porous carbon such as carbon nanotubes (CNTs) [217, 218], mesocarbon microbeads (MCMB) [128], ZSM-5 zeolite-carbon [219], TiO_2 coated CNTs [217], and carbon xerogel [220] to obtain optimum catalyst utilization. Nevertheless, carbon black may block the pores which are important for gas or liquid diffusion during electrode reaction.

Many research studies were devoted to the preparation of the effective anodic catalyst with sufficiently high activity and CO tolerance for ethanol electro-oxidation reaction [47-51]. For instance, it was reported that carbon nano-tube

(CNT) supported anode catalysts showed higher performance than traditional carbon supported catalysts [221-226]. Multi wall carbon nanotube, single wall carbon nanotube and, traditional Vulcan supported Pt-Ru [227] and Pt-Sn [228] bimetallic catalysts were used as anode catalysts and it was reported that multi-wall carbon nanotubes gave the highest catalytic activity. The improving effect of CNTs in electrochemical activity was attributed to the peculiar texture of nanotubes accessible reagents, and perfect conductivity that improved electron transfer as well as specific interaction between catalyst particles and nanotubes [227]. As well, TiO_2 coated CNTs were used as anode catalyst support for ethanol electro-oxidation reaction and it was emphasized that the Pt catalysts which were supported by TiO_2 coated CNTs enhanced ethanol electro-oxidation activity greatly compared to CNT supported Pt catalysts [217]. Carbon xerogel was another high surface area porous carbon material used as anode catalyst support for ethanol electro-oxidation reaction. It was reported that carbon xerogel supported catalyst had a higher ethanol electro-oxidation activity than carbon black supported catalysts because carbon xerogel had a higher surface area than carbon black [220]. On the other hand, the zeolite material was used as a catalyst supported for fuel cell electrode and it resulted in lower resistance and less ohmic power losses than found that employ the use of carbon due to the fact that the zeolite material contains acidic protonic entities on its surface, making it more hydrophilic than carbon [219].

CHAPTER 3

BACKGROUND ON THE EXPERIMENTAL METHODS

In this work, adsorption calorimetry, electrochemical characterization, XRD, XPS, TEM characterization methods were used. Among them, the adsorption calorimetry and cyclic voltammetry were extensively studied in this dissertation while Transmission electron microscopy (TEM), X-ray Photoelectron Spectroscopy (XPS), and X-Ray Diffraction (XRD) are used as supporting methods to confirm the results obtained using the first group. Thus, a theoretical background is given about adsorption calorimetry and electrochemical characterization techniques in this chapter.

3. 1 ADSORPTION CALORIMETRY STUDIES

3.1 1 Theoretical Background

Heterogeneous catalysis involves specific chemical interactions between the surface of a solid and the reacting gas (or liquid phase) molecules. The catalytic cycle is generally composed of adsorption steps, surface reaction processes, and desorption steps. The energetic of these surface chemical events plays an

important role in determining the catalytic properties of the surface. Thus, the adsorption study of probe and reactive gas molecules onto surfaces has a primary importance in catalysis. Such studies led to an understanding of the nature of gas-solid interactions and give insight into the properties of the adsorbent surface.

Adsorption is a process the gas phase molecules remaining on the catalyst surface to form a higher interface concentration than in the gas phase when the gas phase molecules hit the surface of the catalyst. There are two states of adsorption process: physical adsorption and chemical adsorption. The forces of molecular interaction play role in the physical adsorption process. On the other hand, chemical bonding involves between the electrons of the interacting gas and solid in the chemical adsorption process.

Adsorption is a generally exothermic process. The amount of heat evolved during adsorption process is called as the heat of adsorption. Isosteric heat of adsorption, integral heat of adsorption, and differential heat of adsorption are the several types of heat of adsorption. Isosteric heat of adsorption, which is the isothermal differential heat related to the differential heat of adsorption is determined indirectly. On the other hand, the integral heat of adsorption and the differential heat of adsorption are measured directly by calorimetric methods. Integral heat of adsorption represents the total heat evolved in adsorbing from zero loading to some final loading at constant temperature in a closed gas-solid system that no volume work is done. The differential heat of adsorption is the change of integral heat of adsorption with respect to change in the adsorbed moles.

The heat of adsorption measurements by a suitable calorimetry is the most reliable method for evaluating the strength of the surface chemical bonding involving in the adsorption and catalytic processes. Calorimetry is the direct measurement of

the heat and gives access to the energies of transformation and combination. Heat could be measured in principal by recording (i) the temperature rise in a vessel of known heat capacity, (ii) the power of an electrical heater required exactly to compensate for the heat effect of interest, or (iii) the temperature difference across a path of known thermal conduction. This allows the classification of instruments into three groups such as heat accumulation calorimeters (adiabatic calorimeters), heat compensation calorimeters (isothermal calorimeters), and heat conduction calorimeters.

Heat accumulation calorimeters:

An adiabatic shield could be set up in to the air gap or vacuum between the measuring vessel and thermostatic bath for exothermic processes. This shield is made from a thin-walled metal area with a heater wire, which makes adiabatic-shield calorimeters very useful for measuring slow processes.

Heat compensation calorimeters:

Endothermic heat is difficult to measure evolves as a result of endothermic processes. The difficulty of measuring endothermic heat could be avoided by introducing the electrical energy into the system to balance the heat adsorbed in the process. Thus, the calorimeter is in isothermal operation and the endothermic power of the process is equal to electrical power input. In order to compensate temperature changes in exothermic processes, heat is pumped out with a thermoelectric cooler utilizing the Peltier effect, which is superimposed on the Joule heating effect produced throughout a heater. Melting of a solid, vaporization of a liquid, and a flow of cooling liquid are the alternatives to Peltier-effect cooling.

Heat conduction calorimeters:

Heat evolved by the process transferred from measuring vessel through a thermal pile wall to the surrounding heat sink for this type of microcalorimeter. Thus, a property proportional to the total heat flow rate is measured by the instrument. It is the temperature difference over the thermopile that gives the potential difference proportional to the heat flow rate from the vessel.

3.1 2 Tian-Calvet Calorimetry

The invention of Tian-Calvet calorimetry dates back to 1922. Tian introduced the electrical compensation of the thermal effect by means of Peltier effect. Tian calorimeter was a single calorimeter with only one measuring system built 7 m deep in the ground below a cellar to obtain a stable temperature for the surroundings. There were two electric piles: one was measuring the heat flow and the other one providing the cooling to operate the calorimeter at isothermal conditions. In 1948, after Calvet's modifications consisting of arranging thermocouples in a highly regular array and using two measuring systems symmetrically placed in the same thermostat, this calorimeter was called as Tian-Calvet calorimeter.

Heat conduction principle was firstly used by Tian to construct a calorimeter. The experimental space within a large calorimeter block of high heat capacity was surrounded by thermopiles of high conductivity. Thus, thermal changes in the space are integrated almost completely and the recorded heat signal is independent of the distribution of local temperatures. So, it is principally possible to measure thermal transfers by conduction directly increasing the thermal conductivity. This

increase in thermal conductivity was achieved by placing a thermopile between the internal and external vessel.

Herein, we used SETERAM C-80 calorimeter a simplified model of the standard Tian-Calvet type microcalorimeter. The technical lay-out of this type microcalorimeter was shown in Figure 3.1. In this design, there are two symmetrically positioned measuring spaces for the measuring sample and the reference. They are located in the middle of a cylindrical aluminum block sitting between the bases of two truncated cones. The set temperature is maintained by an accuracy of ±0.001 by the precision thermostat in the aluminum block. The outer shell is surrounded by heating elements. The whole block is embedded within a large insulating container. The sensitive part of the calorimeter is the conduction device connecting the outer wall of the small measuring chamber to the large isothermal metallic block.

The measurement of thermal effects in a Tian-Calvet type microcalorimetry is done by two flux-meters, one of these flux-meters is on the measurement side and the other one is on the reference side. Each of these flux-meters measures the instantaneous heat exchanged constantly between the experimental vessel and the calorimetric unit. Sample exchanges heat easily with calorimetric unit surrounding it when sample is heated or cooled. This exchange of heat is done via each of the thermopiles. The signal supplied by the thermopiles corresponds to the instantaneous heat exchanged by the sample. The calorimetric unit is regulated by a heating element coiled around it.

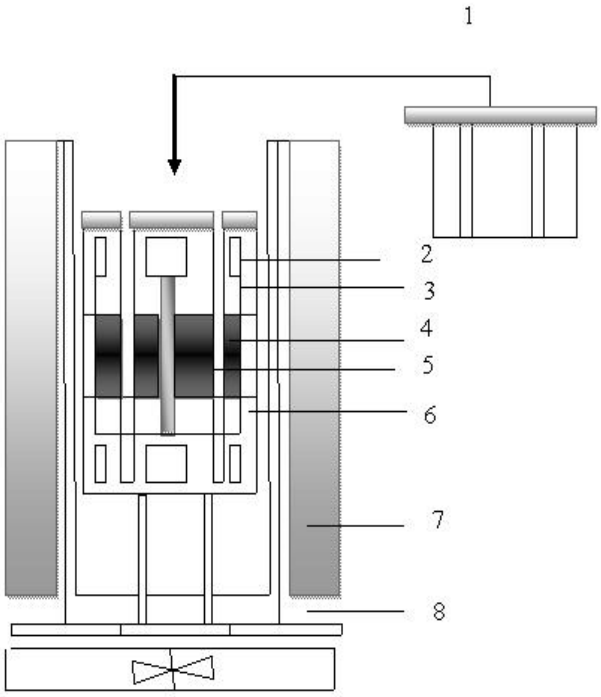

Figure 3. 1 Cross section of the C80 mixing calorimeter: 1, removable lid; 2, thermal buffer zone; 3, heating elements; 4, thermopiles; 5, experimental area; 6, calorimetric block; 7, insulation layers; and 8, cooling circuit.

3.1 3 Adsorption Structure Sensitivity

Adsorption over solid surfaces is a complex process. In certain cases, gases tend to adsorb on energetically more favorable sites and then migrate to the less favorable, weakly bond sites. For hydrogen adsorption over Ru/SiO_2 surfaces, a portal model was postulated based on ^1H NMR and adsorption calorimetry measurements [229-232]. The portal model involves adsorption and dissociation of hydrogen at defect like high energy sites and migration to planar surfaces, followed by spillover on to the support [233].

The amount of heat evolved during adsorption process is called as the heat of adsorption. Furthermore, the differential heat of adsorption is coverage dependent. An important application of adsorption calorimetry is the determination of the site energy distribution shown by plotting the differential heat of adsorption of the probe molecule as a function of coverage. A typical differential heat of adsorption curve was shown in Figure 3.2. Firstly, a sharp differential heat decrease was observed until high energetic sites were covered. These high energetic sites are edges and corners. Then a different behavior started until the low energetic sites covered. These low energetic sites are planar surfaces. The differential heat of adsorption for all of these low energetic sites is nearly same.

The high energy sites are characterized by microcalorimetry on the differential heat of adsorption curves until the plateau is reached. This could be described as step sites depending on the study reported by Norskov et al. [234]. It was shown that the heat of adsorption was directly related to the structure of the catalysts, steps sites were more active and bind adsorbates more strongly. The plateau observed on the differential heat of adsorption curve is the indication of the phenomenon that differential heat of adsorption is not a function of coverage. These sites are called as flat surfaces in the study of Norskov et al. [234]. The relative distribution of these sites could be modified by changing the particle size or by adding second or a third metal to catalyst.

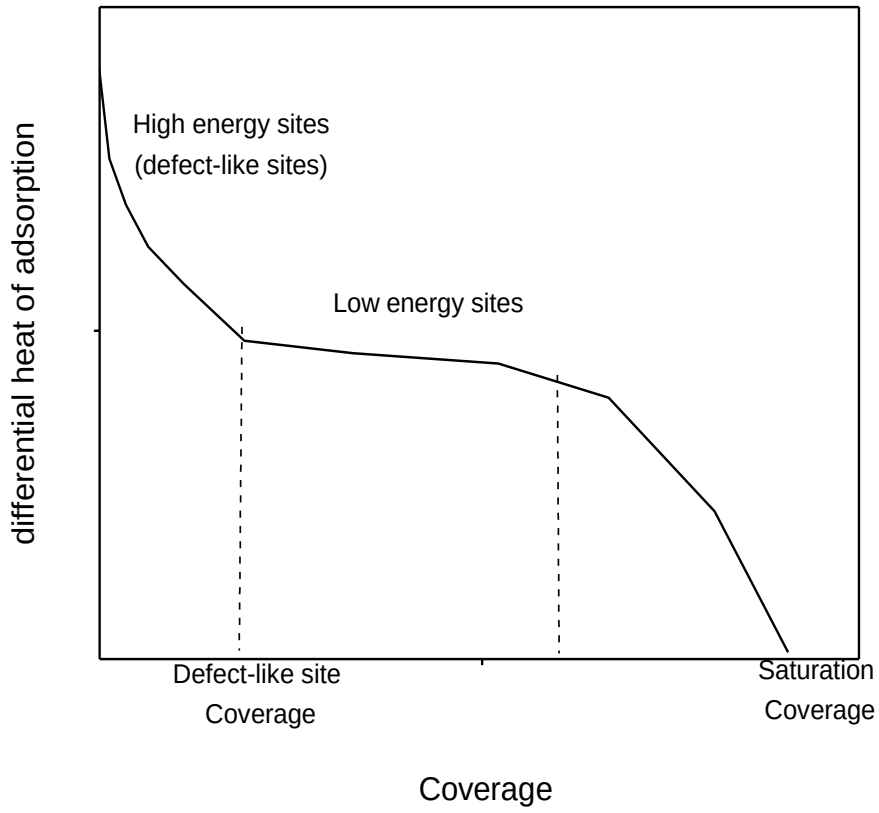

Figure 3. 2 Differential heat of adsorption thermogram obtained from microcalorimetry.

3.1.3 1 The Role of Particle Size

The relative population of defect like sites strongly depends on the metal particle size. For a perfect cubo-octahedral structure as the particle size increases, the number of corner sites remains constant, the number of edge sites slightly increases, while the number of planar surface sites increase by a large amount, resulting in a decrease in the fractional coverage of defect like sites in large

particles [235]. Uner and Uner performed hydrogen, carbon monoxide, and oxygen chemisorptions on γ-Al_2O_3 supported Pt catalysts having different platinum particle sizes [236]. In consequence, it was reported that intermediate heats decreased by increasing particle size for hydrogen chemisorption results. However, it was observed that, by increasing particle size, the initial and integral heats of adsorption of CO and oxygen stayed same. These results could be attributed to the fact that by increasing particle size number of relative population of high energy sites decreased [236].

3.1.3 2 The Role of Second Metal Addition

The addition of second metal is another way to modify the structure of monometallic catalyst. For instance, selective CO oxidation reaction, ethanol electro-oxidation, and methanol electro-oxidation reaction etc are catalyzed by platinum catalyst. However, Pt is not a very good catalyst due to the fact that CO has a poisoning effect on platinum. Many researchers proposed to add second metal to platinum to inhibit CO poisoning effect on platinum. As a consequence, Pt based bi-metallic catalysts revealed great activity on these reactions. This great activity enhancement is due to the not only inhibition of CO poisoning effect but also structure modification by addition of second metal [29, 38, 48, 106, 112, 113].

Differential heat of hydrogen and carbon monoxide adsorption data were compiled and presented in Table 3.2 to Table 3.3 to figure out the effect of second metal addition on adsorption. Pt-Sn bimetallic characterization of by using microcalorimetric method was achieved [237]. Saturation coverage decreased when tin was added. This is due to the fact that tin addition decreased the number of adsorption sites for the adsorption of carbon monoxide and hydrogen. It is clear

that initial heat of carbon monoxide and hydrogen adsorption were nearly the same for all of Pt and Pt-Sn catalyst because the electronic configuration did not change when second or third metal was added. On the other hand, the geometrical structure of these catalysts was changed because of the fact that second metal addition blocked the sites that carbon monoxide could adsorb on pure platinum.

Table 3. 1 Literature data of H_2 adsorption over Supported Pt surfaces

Catalyst	wt% Pt	Atomic ratio	T (K)	Q^0 (kJ/mole)	$\theta^{saturation}$ (μmol H_2/g catalyst)	Ref.
Pt/SiO_2	1.2	1:0:0	423	93 ± 2	37 ± 1	[237]
$Pt/K/SiO_2$	1.2	1:0:2.9	423	95 ± 2	41 ± 1	[237]
$Pt/Sn/SiO_2$	0.93	1:0.9:0	423	92 ± 2	11 ± 0.5	[237]
$Pt/Sn/K/SiO_2$	0.93	1:0.9:2.7	423	97 ± 2	19 ± 1	[237]
Pt/Cab-O-Sil	1.23	1:0	423	93	-	[238]
Pt/Sn/Cab-O-Sil	1.22	6.:1	423	93	-	[238]
Pt/Sn/Cab-O-Sil	1.22	1:1	423	93	-	[238]
Pt/Sn/Cab-O-Sil	1.23	1:3	423	76	10	[238]

Table 3. 2 Literature data of CO adsorption over supported Pt surfaces

Catalyst	wt % Pt	Atomic ratio	T (K)	Q^0 (kJ/mole)	$\theta^{saturation}$ (μmol CO/g cat.)	Ref.
$Pt/K/SiO_2$	1.2	1:0:2.9	423	140 ± 3	26 ± 1	[237]
$Pt/Sn/SiO_2$	0.93	1:0.9:0	423	135 ± 3	16 ± 0.5	[237]
$Pt/Sn/K/SiO_2$	0.93	1:0.9:3	423	138 ± 3	10 ± 0.5	[237]
Pt/Cab-O-Sil	1.23	1:0	423	144	-	[238]
Pt/Sn/Cab-O-Sil	1.22	6.:1	423	135	-	[238]
Pt/Sn/Cab-O-Sil	1.22	1:1	423	144	-	[238]
Pt/Sn/Cab-O-Sil	1.23	1:3	423	120	-	[238]

3.1.3 3 The Detection of Active Sites Involving In Liquid Phase Reaction

Gas phase adsorption measurements could be alternative to liquid phase calorimetry to count the active sites involving in liquid phase reactions. However, all of the surface sites detected by gas phase microcalorimetry are active in liquid phase reactions. It was reported that active sites detected by liquid phase hydrogenation of styrene to ethyl benzene reaction corresponds to gas phase measurements on Pd catalyst. A similar observation was made for the same reaction performed on supported Pt catalysts [235]. It was observed that the active sites for the liquid-phase hydrogenation of styrene were most likely to be edge and corner atoms, whereas the terrace atoms were not involved in the catalytic reaction.

In this PhD dissertation, the role of defect sites and the role of tin addition in ethanol electro-oxidation reaction were investigated. Thus, the differential heat of adsorption measurements could be a novel method to reach this aim. The active sites defined by cyclic voltammetry measurements could be compared to gas phase adsorption microcalorimetry measurement to figure out which sites were involved in ethanol electro-oxidation reaction. In consequence, active sites could be defined by using thermal adsorption microcalorimetry.

3. 2 ELECTRO-CHEMICAL CHARACTERIZATION STUDIES

Electrochemical characterization studies are concerned with the relation of electrical and chemical effects. As a result of the movement of electrons, charge is transported through the electrode. An electrochemical cell consists of a working electrode, a counter electrode, and a reference electrode. While working electrode is the interested electrode, reference electrode is the electrode used to standardize

the other half of the cell. The internationally accepted reference electrode is the Standard Hydrogen Electrode (SHE) or Normal Hydrogen Electrode (NHE) having all components at unit activity. Other reference electrodes are Saturated Calomel Electrode (SCE), silver-silver chloride electrode. While the potential of SCE is 0.242 V vs. NHE, the potential of silver-silver chloride electrode could be represented as 0.197 V vs. NHE. The potential of reference electrode is fixed. Thus, the changes in the system could be ascribed to the changes of working electrode. Furthermore, the potential of working electrode is controlled with respect to the reference electrode. When the energy of electrons is increased by driving electrode more negative potentials, electrons reach a level that they could transfer into vacant states. As a result of this process, electrons flow from electrode to the solution, which is called as reduction. By driving electrodes to more positive potentials, solutes in the electrolyte will meet favorable energy and will transfer there and oxidation current occurs.

Faradaic and non Faradaic processes both occur at the electrode surfaces. In Faradic processes, as a result of electron transfer oxidation or reduction current occurs, which are governed by Faraday Law. The relationship between charge and amount of product is given by Faraday Law; that the passage of 96,485.4 C causes 1 equivalent of reaction. While charge transfer reactions occur in Faradaic processes, no charge transfer reactions occur for non Faradic processes. For non faradaic processes, electrode solution interface behaves like a capacitor. A capacitor composed of two metal sheet separated by a dielectric material. Thus, there are charged species and oriented dipoles at the metal solution interface. This whole layer is called as electrical double layer.

Galvanic cells or electrolytic cells are the two types of electrochemical cells in which Faradaic processes takes place. In galvanic cell, when external connection

of electrodes by a conductor is made, reactions occur spontaneously at the electrode surface. Galvanic cells are usually used for converting chemical energy to electrical energy. Non rechargeable cells, rechargeable cells, and fuel cells are the galvanic cells. On the other hand, electrolytic cells are the one in which the reactions are effect by an external voltage which is greater than OCV. Electrolytic syntheses, electro-refining, and electroplating are the some commercial applications of electrolytic cells.

Material surface area, geometry, surface condition, mass transfer variables (diffusion, convection), surface concentration, adsorption, potential, current, quality of electricity, temperature, pressure, time, bulk concentration of electro active species, concentration of other species are the variables affecting an electrochemical cell.

Complete electrochemical behavior of a cell could be obtained through a series of step at different potentials with recording of the current vs. time curves. Moreover, more information could be obtained by sweeping potential with time and recording current vs. potential curve. A typical electrochemical cell was given in Figure 3.3. If the potential increases at certain value by time and current vs. potential is recorded. This technique is called as linear sweep voltammetry (LSV). A typical LSV potential sweep and response curve was given in Figure 3.4. For LSV, if the scan is begun at potential positive enough for the reduction, firstly non faradic currents flow. Then, electrode potential reaches the potential that reduction begins and current Faradaic currents start to flow. As the potential continues to grove in negative direction, the surface concentration decreases and mass transfer to the surface increases and reaches a maximum and then starts to decrease as the depletion of the surface concentration set in. thus, a maximum is observed on linear sweep voltammogram.

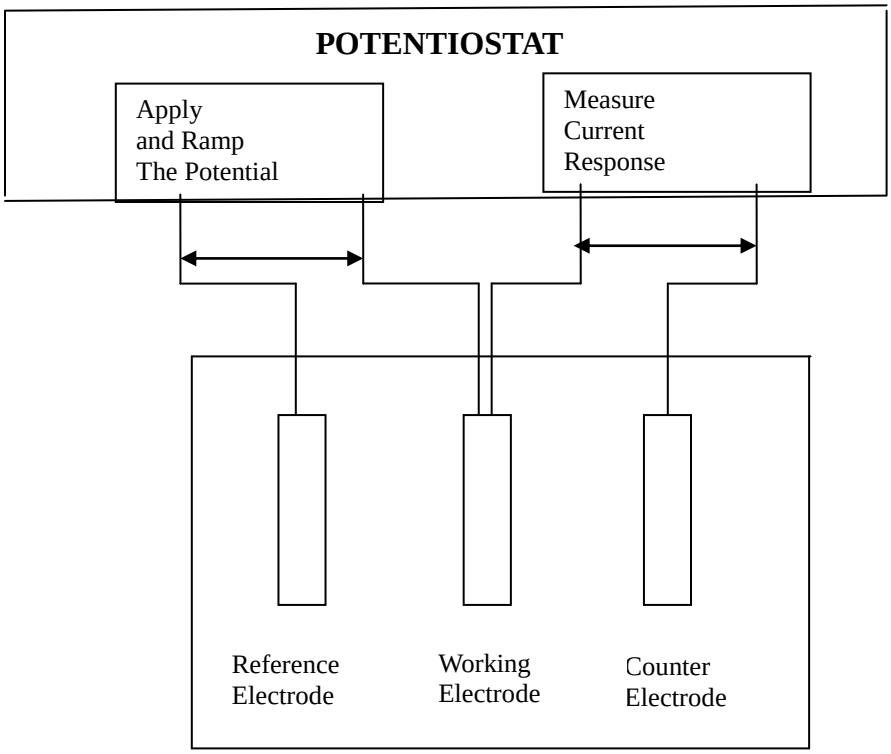

Figure 3. 3 Schematic representation of a typical electrochemical cell

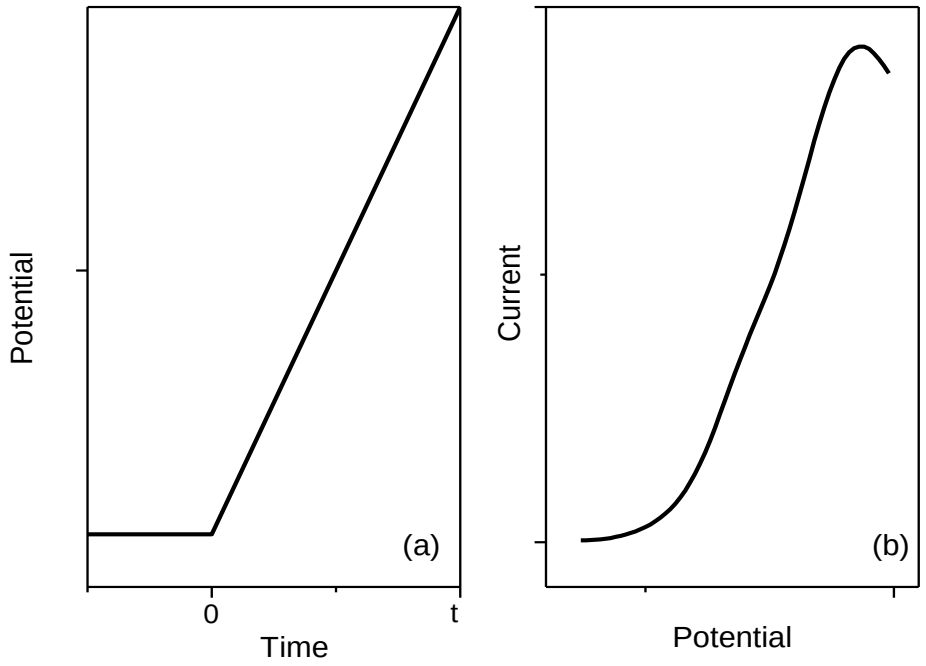

Figure 3. 4 (a) Linear potential sweep, (b) Resulting current potential curve

Cyclic voltammetry (CV) is a technique that could be achieved by reversing the potential scan. A typical CV response was shown in Figure 3.5. By reversing the potential scan, the potential increases in positive direction and on the electrode surface there is large concentration of oxidizable anion, as potential increases more in positive direction, the electrochemical balance at the surface grows more. Thus, the anion is re-oxidized an anodic currents flow.

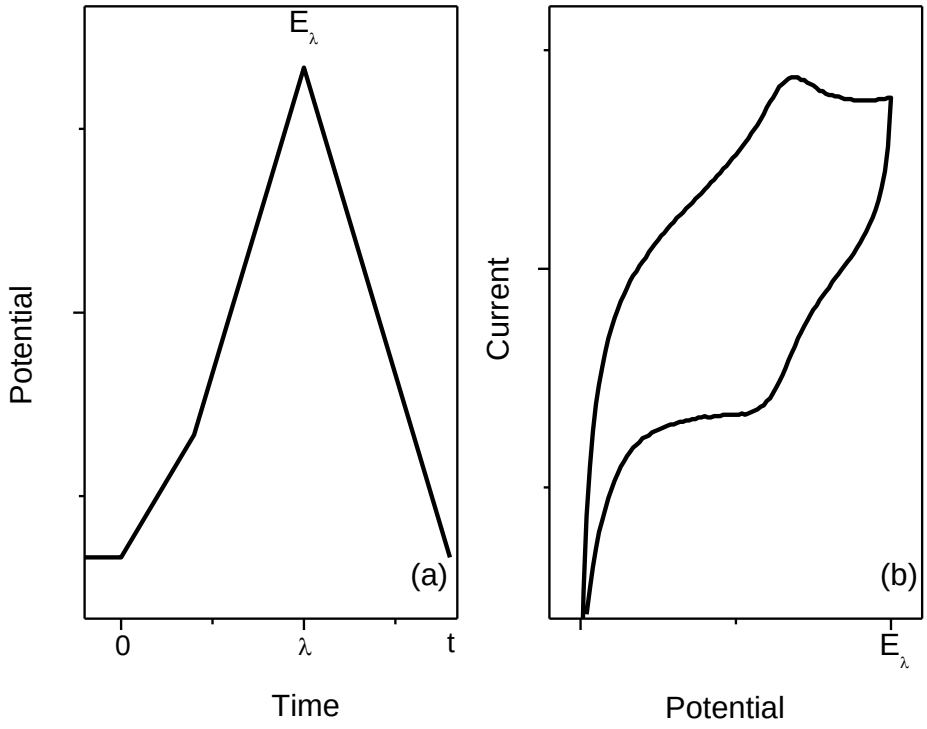

Figure 3. 5 (a) Cyclic potential sweep, (b) Resulting current potential curve

Cyclic voltammetry is a popular technique for electrochemical studies and gives fairly good information about electrochemical systems. One of them considered in this dissertation is about solid electrode surfaces. Most of the electrochemical literature studies are about polycrystalline electrodes. This kind of electrodes has a variety of small domains with different crystal surfaces. Different crystal faces shows different electrochemical activities depending upon the nature of the reaction. Thus, polycrystalline electrode represents an average electrochemical activity depending upon the number of crystal faces posses. Studies with single

crystal surfaces indicated that solid electrode properties strongly depend on the crystal plane. The most striking example is the Pt electrode. Pt metal has a cubo-octahedral crystal structure with 100 and 111 crystal planes. These crystal planes indicated different electrochemical activities. It was reported that hydrogen reduction/oxidation reaction equilibrium potential was observed at 0 V vs. NHE. Hydrogen peaks emerge at around 0.4 V vs. NHE. Furthermore, Pt started to oxidize at above 0.8 V potential oxidized and electrochemical double layer was observed between 0.65 V vs. NHE and 0.35 V vs. NHE region.

CHAPTER 4

EXPERIMENTAL

4. 1 INTRODUCTION

Catalyst preparation and characterization methods used in this PhD dissertation are summarized in the present chapter. In Table 4.1, detailed information about the catalyst preparation and the characterization methods involved in the course of dissertation was given.

Firstly, XRD and adsorption calorimetry measurements were conducted on monometallic γ-Al_2O_3 supported 1%Pt, 2%Pt, and 5%Pt monometallic and bi-metallic 5% Pt-Sn catalysts to investigate the effect of catalyst loading and the effect of Sn addition. Monometallic Pt/γ-Al_2O_3 catalysts were prepared by incipient wetness impregnation method. Moreover, Sn containing Pt/γ-Al_2O_3 catalysts were prepared by sequential impregnation method. Results on these measurements were explained in Chapter 5.1.

Commercial Pt/C (E-Tek) (20% Pt loading) was employed as ethanol electro-oxidation reaction catalyst to explore the effect of scan rate and the effect of potential change. The results of this study were presented in Chapter 5.2.

Table 4. 1 Catalysts prepared and characterized

Catalyst	wt% Pt	Atomic ratio	Preparation Method	Investigation Method
Pt /γ-Al_2O_3	1	1:0	Impregnation	adsorption calorimetry
	2	1:0		
	5	1:0		
Pt-Sn/γ-Al_2O_3	5	15:1	Sequential impregnation	adsorption calorimetry
	5	9:1		
	5	6:1		
Pt/C (E-Tek)	20	1:0	Polyol	XRD, adsorption calorimetry, TEM, CV
Pt/C (pH=11)	20	1:0		
Pt/C (pH=5)	20	1:0		
Pt/ commercial CNT	20	1:0	Polyol	chemisorption CV
Pt/home-made CNT	20	1:0		
Pt-Sn/C	20	15:1	Polyol	XRD, adsorption calorimetry, XPS, CV
	20	9:1		
	20	6:1		
	20	1:1		
Pt-SnO_2/C	20	9:1	Polyol	XRD, adsorption calorimetry, XPS, CV
	20	6:1		

XRD, XPS, TEM, adsorption calorimetry, and cyclic voltammetry measurements were performed on three sets of monometallic carbon supported Pt (20%) catalysts by polyol method to investigate the effect of particle size on ethanol electro-oxidation reaction. Two different catalyst having two different particle size were prepared at pH=5 and pH=11. Results on these measurements were given in Chapter 5.3.

Chapter 5.4 was also focused on the effect of support for ethanol electro-oxidation reaction. In order to investigate the effect of support, volumetric chemisorption measurements and cyclic voltammetry measurements were conducted on 20% Pt/C (E-Tek), 20% Pt/commercial CNT, and 20%Pt/home-made CNTs catalysts.

Home made CNTs were prepared by template synthesis method via chemical vapor deposition method.

Pt-Sn/C (20% Pt loading) catalysts were prepared by polyol method at 15:1 to 1:1 Pt: Sn atomic ratios to investigate the effect of tin addition on ethanol electro-oxidation reaction. To characterize catalysts, XRD, XPS, hydrogen and carbon monoxide adsorption measurements, and cyclic voltammetry measurements were conducted. Experimental results of the effect of tin addition on ethanol electro-oxidation reaction are presented in Chapter 5.5.

Pt-SnO_2/C (20 % Pt loading) catalysts were prepared at 9:1 and 6:1 Pt: Sn atomic ratios by polyol method to find how tin oxide improves ethanol electro-oxidation reaction activity. XRD, XPS, adsorption calorimetry, and cyclic voltammetry measurements performed together. Results on these measurements were explained in Chapter 5.6.

4. 2 PREPARATION METHODS

4.2. 1 Incipient Wetness Impregnation Method

All of the Pt /γ-Al_2O_3 monometallic samples were prepared by incipient wetness impregnation of Pt from a solution of tetraammine platinum (II) chloride hydride on γ-Al_2O_3. Approximately 2 mL of solution per gram support was needed to bring incipient wetness. The slurries obtained after impregnation were dried overnight at room temperature and calcined at 410^{o}C for 3 hours.

Pt-Sn samples were prepared by the sequential impregnation of Pt from a solution of tetraammine platinum (II) chloride hydride, Tin (II) chloride dehydrate on γ-Al_2O_3. For Pt-Sn catalysts, tetraammine platinum (II) chloride hydride was dissolved in 20 mL pure water and impregnated on alumina. After calcinations at 410^oC for 3 hours, Tin (II) chloride dehydrate salt was dissolved in 20 mL water and impregnated on the Pt/γ-Al_2O_3 followed by drying at room temperature overnight. Then, it was calcined at 410^oC for 3 hours.

4.2. 2 Polyol Method

For monometallic Pt catalysts, the appropriate amounts of Pt salt $H_2PtCl_6.6H_2O$ (Aldrich) and carbon (Vulcan XC 72-R) were dissolved in 200 mL ethylene glycol (EG) mixture per gram support and slurry was obtained. For Pt: Sn/C (20 % Pt loading) samples, appropriate amounts of Pt salt $H_2PtCl_6.6H_2O$ (Aldrich), Sn salt $SnCl_2.2H_2O$ (Aldrich) and carbon (Vulcan XC 72-R) were dissolved in 200 mL EG mixture per gram support and a slurry was obtained. For Pt-SnO_2/C (20% Pt loading) samples, firstly appropriate amount of $SnCl_2 \cdot 2H_2O$ was dissolved in 200 mL EG and refluxed at 190^oC for 30 min under constant stirring. Then a yellow solution was obtained indicating the formation of tin oxide. The resulting tin oxide and Pt salt $H_2PtCl_6.6H_2O$ (Aldrich) were mixed at the desired atomic ratios and slurry was obtained. Consequently, for all Pt/C, Pt-Sn/C, and Pt-SnO_2/C catalysts, the pH of the slurry was raised to 11 by the addition of 1M KOH solution and the temperature was increased to 130^oC and kept constant at this temperature for 2 h. The slurry suspension was rapidly cooled down in a water bath. Following cooling, this slurry was filtered and dried.

For monometallic catalysts, it was observed that pH had an influencing effect on the catalyst particle size. Thus, two sets of monometallic catalysts were prepared

to ensure to have two different catalysts having different particle size. One of them was prepared at pH=11 and the other one was prepared at pH=5.

4.2. 3 Preparation of CNTs

Home-made CNTs were synthesized by template synthesis method as described in literature [239]. Firstly, PAOX membranes were prepared by two step anodization method as described in literature [184, 185]. Thick Al foils were rinsed with acetone and then anodized for 2 hours. After 2 hour anodization, anodized foil was etched for 30 min. followed by 19 hours anodization at 20 V in 10% H_2SO_4 solution. Cathodization was performed for 2 hours after 19 hours anodization to remove the oxide layer from the Al surface. CNT-PAOX membranes were prepared via non-catalytic method by chemical vapor deposition (CVD) at a temperature of ca. 700^{o}C in propylene and argon flow on PAOX membrane to obtain aligned catalyst free CNTs embedded in an alumina matrix. Propylene was used as a gaseous carbon source. The PAOX membranes were arranged perpendicular to the gas flow in a quartz tube CVD reactor and fixed between two iron rings. After CNT-PAOX membranes were prepared, some of these membranes were kept and the other ones were etched in HF solution to obtain powder CNTs.

4. 3 CATALYST CHARACTERIZATION TECHNIQUES

4.3 1 X-Ray Diffraction Measurements

XRD patterns of 5%Pt/γ-Al_2O_3, 5%Pt-Sn/γ-Al_2O_3, 20%Pt/C, 20%Pt-Sn/C and 20%Pt-SnO_2/C catalysts were obtained with a Rigaku X-Ray powder diffractometer using Cu-Kα radiation ($\lambda_{Cu\text{-}K\alpha}$=1.54 A^o) in METU Chemistry Department. The angular resolution in the 2θ scans was 0.05^o for the wide angle 2θ scans. The scan range was from 20^o to 90^o, and the scan rate was 2^o/min.

4.3 2 X-ray Photoelectron Spectroscopy Measurements

Surface characterization of 20%Pt/C, 20%Pt-Sn/C, and 20%Pt-SnO_2/C catalysts by X-ray Photoelectron Spectroscopy (XPS) was performed for quantification of surface composition. The X-ray photoelectron spectra were obtained using Al-K_α source radiation with a SPECS spectrometer. Measurements were performed at METU Central Laboratory.

4.3 3 Transmission Electron Microscopy Measurements

Transmission electron microscopy (TEM) measurements were performed on 20%Pt/C (E-Tek), 20%Pt/C (pH=11), and 20% Pt/C (pH=5) catalysts. These measurements were conducted in Darmstadt Technical University (DTU). Nanostructure characterization was performed employing a CM20STEM instrument (FEI, Eindhoven, The Netherlands), operating at 200 kV. Sample preparation followed standard techniques: fine dispersion of the catalyst materials in acetone in an ultrasonic bath and deposition of a droplet of suspension on a lacy carbon grid. Low magnification images revealed the homogeneity of the sample, while high-resolution imaging was utilized to analyze the size and respective shape of the Pt nano crystallites.

4.3 4 Volumetric Chemisorption Measurements

The volumetric chemisorption measurements performed on 20%Pt/C (E-Tek), 20%Pt/commercial CNTs, and 20% Pt/home-made CNTs catalysts to obtain dispersion values on a home built adsorption apparatus consisting a multiport high vacuum Pyrex glass manifold in connection with a turbo molecular pump backed by a mechanical pump.

4.3 5 Gas Phase Microcalorimetric Measurements

Gas phase microcalorimetric measurements were performed at 323 K by using a Tian-Calvet type heat flow calorimeter (Seteram C-80) connected to a gas handling system and a volumetric adsorption apparatus employing Baratron capacitance manometers in the range of 10^{-4}-10 Torr. In this manifold, a Pfeifer turbo molecular pump station backed by a diaphragm pump was used. The sample and the reference cells were connected to each other and to the manifold by a Pyrex tee. Stainless steel bellows were used to connect the sample of stainless steel Cajon Ultra Torr unions.

The pre-reduced catalyst was loaded into the sample cell and empty cell was inserted into the reference port of the microcalorimetry. Prior to the introduction of subsequent doses of gas, the catalyst was reduced in-situ by hydrogen gas at 523 K. After the reduction process, the catalyst was evacuated for approximately 10 h, while the catalyst bed cooled down. The measurements of differential heats were conducted by introducing small doses of gas on to the samples. The resulting heat response for each dose was recorded as a function of time and integrated to determine the energy released. The amount of gas adsorbed was determined volumetrically by the dose and equilibrium pressures. The equilibrium pressure was recorded when the calorimeter reached the thermal equilibrium, i.e. the heat signal decreased to the background level. The procedure was repeated until the surface was saturated, i.e. no detectable heat signal was observed, or until the upper limit of the pressure measurement (10 Torr) was reached.

4.3 6 Voltammetric Measurements

4.3.6. 1 Preparation of working electrode

About 7 mg of the powdered catalyst was suspended in 1000 μL Nafion® solution for about 1 h to obtain the catalyst ink. Then 6μl of this catalyst ink was spread on the surface of the glassy carbon electrode, polished with alumina before deposition, using a micropipette. It was dried at room temperature to remove the solvent.

4.3.6. 2 Preparation of reference electrode

All potential of working electrodes was measured by normal hydrogen reference electrode (NHE). This reference electrode was prepared by electro-deposition of palladium on platinum foil. This foil was inserted in a special glass cell with containing base solution. Before each experiment this electrode was saturated with hydrogen by cathodic polarization in 0.5 M H_2SO_4.

4.3.6. 3 Electro-chemical measurements

Electrochemical measurements were carried out in a conventional three-electrode cell at room temperature with an IVIUMSTAT potentiostat. A Pt wire was used as the counter electrode. The working electrode was a glassy carbon disk with a diameter of 3 mm held in a Teflon cylinder. A home-made Normal hydrogen reference electrode (NHE) was used. The base cyclic voltammetry experiments were carried out in 0.5 M H_2SO_4 solution. The evaluation of ethanol oxidation on glassy carbon electrode was performed in 0.5 M H_2SO_4 + 0.5 M ethanol solution at room temperature.

CHAPTER 5

RESULTS AND DISCUSSION

5. 1 THE CHARACTERIZATION OF γ-Al_2O_3 SUPPORTED Pt CATALYSTS

The microcalorimetric measurements of hydrogen, carbon monoxide, and oxygen were conducted on monometallic (1%Pt, 2%Pt, and 5%Pt) and bi-metallic (5% Pt-Sn) γ-Al_2O_3 supported platinum catalysts to investigate the effect of catalyst loading and the effect of tin addition on the heat of adsorption measurements. While the monometallic Pt/γ-Al_2O_3 catalysts were prepared by incipient wetness impregnation method, tin containing Pt/γ-Al_2O_3 catalysts were prepared by sequential impregnation method. These catalysts, their compositions, the microcalorimetric measurement details were given in Table 5.1

Table 5. 1 Microcalorimetric measurements performed on γ-Al_2O_3 supported catalysts at 323 K

Catalyst	wt % Pt	Atomic ratio	Adsorbed gas
Pt /γ-Al_2O_3	1	1:0	H_2 and CO
	2	1:0	H_2 and CO
	5	1:0	H_2, CO, and O_2

Pt-Sn/γ-Al_2O_3	5	15:1	
	5	9:1	H_2, CO, and O_2
	5	6:1	

5.1. 1 Hydrogen Chemisorption Measurements

The hydrogen chemisorption measurements were performed at 323 K on the γ-Al_2O_3 supported Pt, Pt-Sn catalysts on varying 15:1 to 6:1 Pt: Sn ratios. Initial heat of adsorption, defect-like site saturation coverages, and total saturation coverage values were given in Table 5.2. The hydrogen chemisorptions measurements were performed on Pt/γ-Al_2O_3 catalysts to investigate the effect of Pt loading on hydrogen adsorption. The hydrogen chemisorption measurement results on the Pt/γ-Al_2O_3 catalysts having 1% Pt, 2% Pt, and 5%Pt loading were given in Figure 5.1. The initial heat of hydrogen adsorption value on the Pt/γ-Al_2O_3 catalysts having 1% Pt, 2% Pt, and 5%Pt loading were 129, 98, and 80 kJ/mole, respectively. These initial heat of adsorption values agreed well with the literature values, which were reported as 100-140 kJ/mole [237, 238]. For all of these monometallic catalysts, firstly, differential heat of hydrogen adsorption exhibited a sharp differential heat decrease, attributed to the saturation of high energy defect like sites of platinum [234, 237, 238]. Then, the differential heat values remained constant by exhibiting a plateau attributed to the low energy sites. Further differential heat of hydrogen decrease was observed until the saturation coverage was reached. While 1% Pt/γ-Al_2O_3 catalyst had the highest saturation coverage, 5% Pt/γ-Al_2O_3 catalyst had the lowest saturation coverage value. The energies of low energy sites (intermediate heats) did not change much when the Pt loading increased from 1% Pt to 2% Pt. However, when 5% Pt loading was reached, there was a considerable decrease in the energies of low energy sites.

Table 5. 2 Hydrogen chemisorption results on γ-Al_2O_3 supported monometallic and bi-metallic catalysts.

Catalyst	wt % Pt	Atomic ratio	Q^0 (kJ/mole)	$\theta^{defects}$ (mol H/ mol Pt)	$\theta^{saturation}$ (mol H/ mol Pt)
Pt	1	1:0	129	12	88
	2	1:0	98	8	42
	5	1:0	70	7	33
Pt-Sn	5	15:1	74	6	17
	5	9:1	74	5	13
	5	6:1	110	3	7

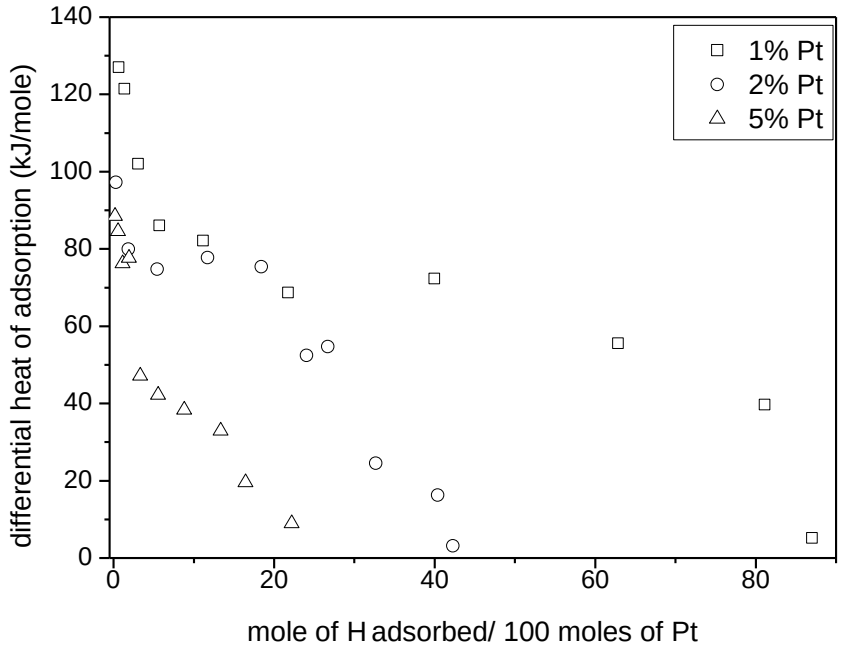

Figure 5. 1 Differential heat of hydrogen adsorption measurements results on 1% Pt/γ-Al_2O_3, 2% Pt/γ-Al_2O_3, and 5% Pt/γ-Al_2O_3 catalysts at 323 K.

The hydrogen chemisorption measurements were performed on 5%Pt-Sn/γ-Al_2O_3 catalysts to investigate the effect of tin addition on the hydrogen adsorption. The hydrogen chemisorption measurement results on the 5%Pt-Sn/γ-Al_2O_3 catalysts prepared at 15:1, 9:1, 6:1 atomic ratios were given in Figure 5.2. These measurements indicated that when the Sn amount increased saturation coverage decreased. The initial heat of hydrogen adsorption values for 5%Pt-Sn/γ-Al_2O_3 catalysts were given in Table 5.2. The initial heat of adsorption values did not change much when tin amount increased from 15:1 to 6:1. The defect site coverage value of 5%Pt-Sn (15:1)/γ-Al_2O_3 catalyst was 3 mol H/ 100 mol Pt,

smaller than 5%Pt/γ-Al_2O_3 catalyst. This was due to fact when tin was added the defect like saturation coverage decreased (Table 5.2). However, the defect site saturation coverage slightly decreased when Pt: Sn atomic ratio increased from 15:1 to 9:1 and 6:1. The energies of low energy sites did not change when tin amount increased but for 5%Pt-Sn (6:1)/γ-Al_2O_3, these sites were lost. This could be attributed to the fact that when Pt: Sn atomic ratio was reached 6:1, platinum low energy sites were completely blocked by tin. Furthermore, it is clear that tin addition caused a decrease in saturation coverages.

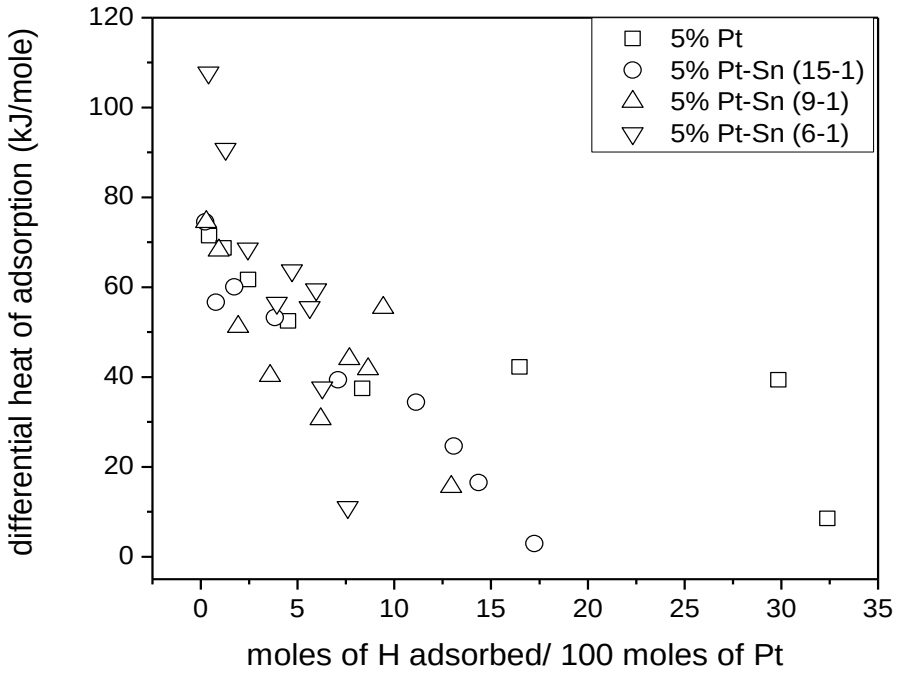

Figure 5. 2 Differential heat of hydrogen adsorption measurements results at 323 K on γ-Al_2O_3 supported 5% Pt and 5% Pt-Sn catalysts prepared at 15:1, 9:1, and 6:1atomic ratios.

5.1. 2 Carbon Monoxide Chemisorption Measurement Results

The carbon monoxide chemisorption measurements were performed at 323 K on the γ-Al_2O_3 supported Pt, Pt-Sn catalysts on varying 15:1 to 6:1 ratios. Initial heat of adsorption, defect-like coverage values, saturation coverage values of these catalysts were given in Table 5.3. Carbon monoxide chemisorptions thermograms of these mono-metallic and bi-metallic catalysts were given in Figure 5.3 and Figure 5.4. Initial heats of carbon monoxide chemisorption on these catalysts were in agreement with previous microcalorimetric studies, for which heats of carbon monoxide chemisorption of 135-144 kJ/mol for SiO_2 supported Pt.

Table 5. 3 Carbon monoxide chemisorption results on γ-Al_2O_3 supported monometallic and bi-metallic catalysts.

Catalyst	wt % Pt	Atomic ratio	Q^0 (kJ/mole)	$\theta^{defects}$ (mol CO/ mol Pt)	$\theta^{saturation}$ (mol CO/ mol Pt)
Pt	1	1:0	230	10	82
	2	1:0	210	7	44
	5	1:0	130	5	18
Pt-Sn	5	15:1	160	4	7
	5	9:1	148	3	7
	5	6:1	178	2	4

In Figure 5.3, the carbon monoxide heat of adsorption thermogram on 1% Pt/γ-Al_2O_3, 2% Pt/γ-Al_2O_3, and 5% Pt/γ-Al_2O_3 catalysts were given. Similar to hydrogen chemisorption measurements, while 1% Pt/γ-Al_2O_3 had the highest saturation coverage value, lowest saturation coverage value observed for 5% Pt/γ-Al_2O_3 catalyst. This is due to the agglomeration of platinum particles when

catalysts loading increased. The intermediate heats for carbon monoxide adsorption decreased when Pt loading increased. While the intermediate heats for 1% Pt/γ-Al_2O_3 catalyst were higher than 2% Pt/γ-Al_2O_3, 5% Pt/γ-Al_2O_3 catalysts, the intermediate heats on 2% Pt/γ-Al_2O_3, 5% Pt/γ-Al_2O_3 catalysts were the same.

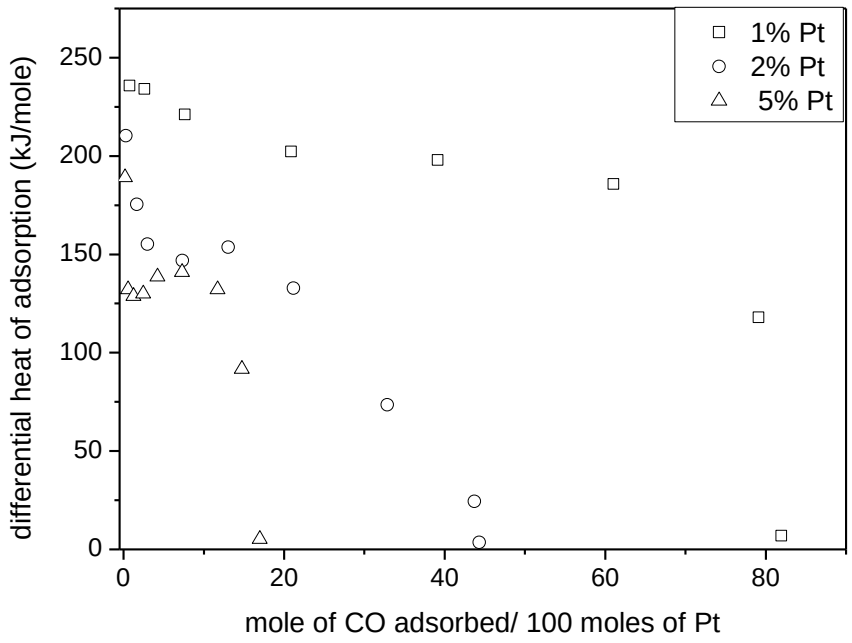

Figure 5. 3 Differential heat of carbon monoxide adsorption measurements results on 1% Pt/γ-Al_2O_3, 2% Pt/γ-Al_2O_3, and 5% Pt/γ-Al_2O_3 catalysts at 323 K.

In Figure 5.4, the differential heat of carbon monoxide adsorption measurements on the 5%Pt-Sn/γ-Al_2O_3 catalysts prepared at 15:1, 9:1, 6:1 atomic ratios were given. Initial heat of carbon monoxide adsorption was consistent with the literature data. Saturation coverage values of these catalysts decreased by the addition of tin. The intermediate heats were nearly the same for all of these catalysts except for 5%Pt-Sn (6:1)/γ-Al_2O_3. For 5%Pt-Sn (6:1)/γ-Al_2O_3 catalyst, low energy sites were lost due to the fact that tin blocked these sites.

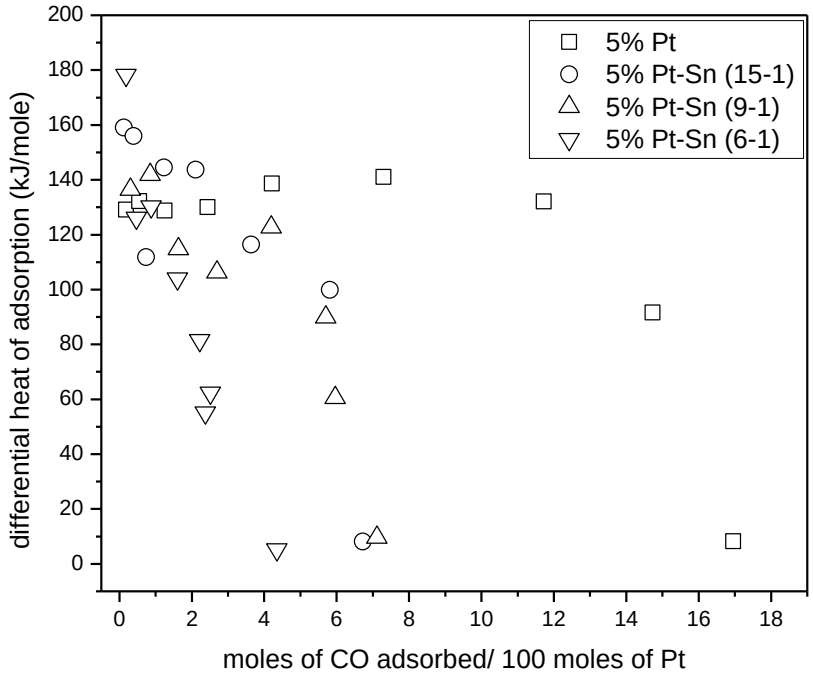

Figure 5. 4 Differential heat of carbon monoxide adsorption measurements results at 323 K on γ-Al_2O_3 supported 5% Pt and 5% Pt-Sn catalysts prepared at 15:1, 9:1, and 6:1atomic ratios.

5.1. 3 Oxygen Chemisorption Results

The differential heat of oxygen adsorption measurements on the γ-Al_2O_3 supported 5% Pt and 5%Pt-Sn catalysts measured at 323 K. Initial heat of adsorption values and saturation coverage values were represented in Table 5.4 Differential heat of oxygen adsorption thermograms on these catalysts were shown in Figure 5.5. The results showed that when the Sn amount increased from 1:0 to 9:1, saturation coverage did not changed. On the contrary, when 6:1 atomic ratio reached saturation coverage decreased. Furthermore, the intermediate heats were nearly the same for oxygen adsorption on 5% Pt, 5%Pt-Sn (15:1), and 5%Pt-Sn (9:1) catalysts. On the other hand, these heats were lowered for 5%Pt-Sn (6:1) catalyst.

Table 5. 4 Oxygen chemisorption results on γ-Al_2O_3 supported monometallic and bi-metallic catalysts.

Catalyst	wt % Pt	Atomic ratio	Q^0 (kJ/mole)	$\theta^{saturation}$ (mol H / mol Pt)
Pt	5	1:0	170	3.2
Pt-Sn	5	15:1	200	3.2
	5	9:1	192	2.8
	5	6:1	180	1.0

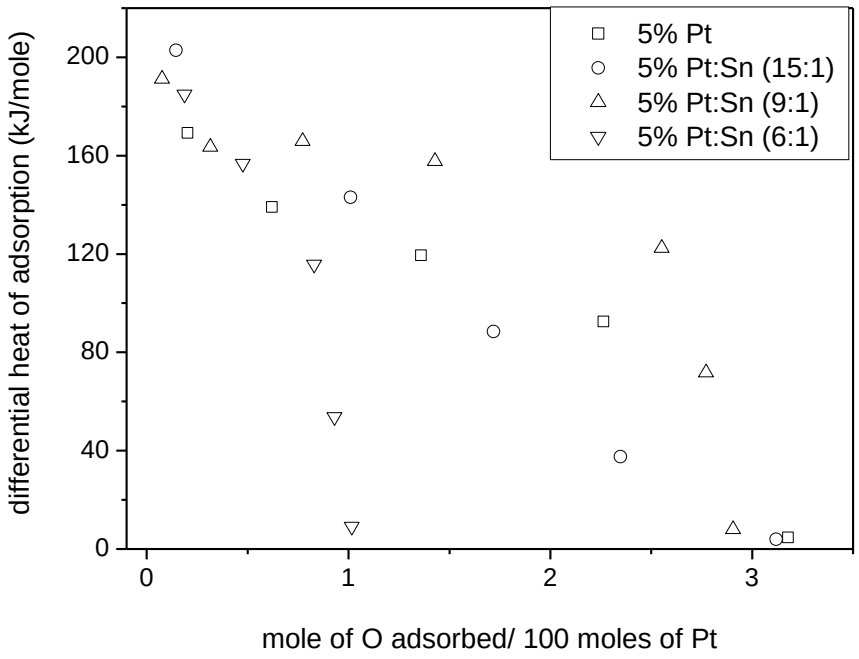

Figure 5. 5 Differential heat of oxygen adsorption measurements results at 323 K on γ-Al_2O_3 supported 5% Pt and 5% Pt-Sn catalysts prepared at 15:1, 9:1, and 6:1atomic ratios.

5.1. 4 Discussion

The differential heat of hydrogen, carbon monoxide, and oxygen chemisorption measurements were performed on monometallic (1%Pt, 2%Pt, and 5%Pt) and bi-metallic (5% Pt-Sn) γ-Al_2O_3 supported platinum catalysts to investigate the effect of catalyst loading and the effect of tin addition on the heat of adsorption measurements.

The effect of catalyst loading was evaluated depending upon the differential heat of hydrogen and carbon monoxide adsorption measurements on monometallic 1%Pt/ γ-Al_2O_3, 2%Pt/ γ-Al_2O_3, and 5%Pt/γ-Al_2O_3 supported catalysts. It was observed that when Pt loading increased saturation coverage of hydrogen and carbon monoxide adsorption decrease due to agglomeration of platinum particles at high catalyst loading. Thus, the dispersion of platinum particles at high metal loading catalysts was lower, site distribution of changes by increasing metal loading.

The effect of second metal addition was investigated both on γ-Al_2O_3 supported Pt catalyst. The effect of tin addition was explored by using hydrogen, carbon monoxide, and oxygen adsorption results. It was observed that by the increasing amount of tin, saturation coverage values decreased. The intermediate heats remained same for Pt-Sn catalysts.

For all these catalysts, it was observed that adsorbed hydrogen amounts were greater than adsorbed CO. This is believed to be due to a weakly bound hydrogen that exists on the metal surfaces at H: M stoichiometries greater than 1. This could be explained depending upon the portal model adsorption. According to this model, hydrogen adsorption occurs via two pathways. The first involves rapid, dissociative adsorption at low coordination sites to produce weakly bound, highly mobile hydrogen. The second pathway is adsorption directly onto the basal planes, which occurs at an intrinsically slower rate. Since the weakly bound hydrogen adsorbed at low-coordination sites is highly mobile, it can then either migrate to strongly bound states, spill over to the support, or recombine with another hydrogen atom and desorb. As a result of recombination and desorption of hydrogen from the sites from basal plane, these sites would be available for the hydrogen adsorption.

5. 2 THE EFFECT OF SCAN RATE AND THE EFFECT OF POTENTIAL CHANGE ON 20% Pt/C (E-TEK) CATALYST FOR ETHANOL ELECTRO-OXIDATION REACTION

The characteristics of the cyclic voltammogram recorded depend on a number of factors such as the rate of the electron transfer reactions, the chemical reactivity of the electro-active species, and the voltage scan rate. Herein, the effect of scan rate and the effect of voltage difference on ethanol electro-oxidation reaction were investigated.

5.2. 1 The Effect of Scan Rate

Cyclic voltammogram of 20% Pt/C (E-Tek) in 0.5 M H_2SO_4 solution was given in Figure 5.6-a. The equilibrium potential for the hydrogen reduction/oxidation reaction is to be 0.0 V vs. NHE for any case. It was observed that below 0.35 V vs. NHE hydrogen adsorption and desorption peaks appear. At potentials higher than 0.75 V vs. NHE, Pt is oxidized. If potential is further increased to more than 1.2 V vs. NHE oxygen reduction can be observed. The peaks observed at 0.1 V and 0.2 V (NHE) were attributed to the existence of Pt (100) and Pt (110) crystal surfaces [240-243].

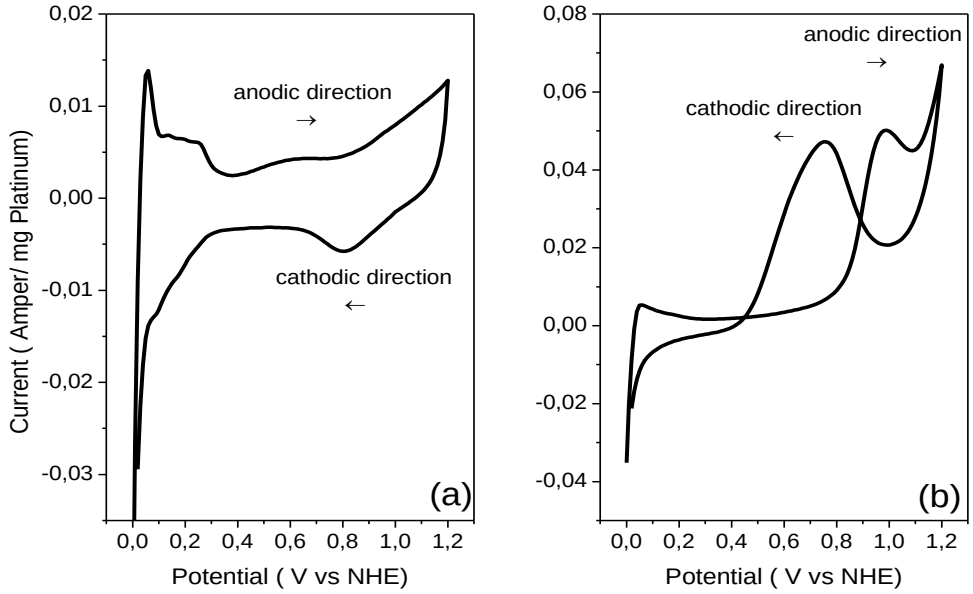

Figure 5. 6 Cyclic voltammogram of 20% Pt/C (E-Tek) catalyst a) in 0.5 M H_2SO_4 solution b) in in 0.5 M H_2SO_4 and 0.5 M ethanol solution (Scan rate: 0.05 V/s).

Cyclic voltammogram of 20% Pt/C (E-Tek) catalyst in 0.5 M H_2SO_4 and 0.5 M ethanol solution at 0.05 V/s scan rate was shown in Figure 5.6-b. Surface chemisorbed ethanol was oxized at around 1 V potential. By increasing potential further, Pt surface is oxidized at 1.2 V. When potential was reversed, bulk ethanol was oxidized via surface Pt oxide at around 0.7 V [198]. From sulfuric acid oxidation voltammogram and from ethanol electro-oxidation voltammogram, it is clear that oxidation currents at 1.2 V overlaped. This indicates that surface chemisorbed ethanol was oxidized at 1.0 V completely, then at this potential Pt surface is oxidized and when potential was reversed bulk ethanol was oxidized.

The voltage scan rate could be obtained from the slope of the current vs. potential diagram. If the scan rate is altered, the current response also changes. The above voltammograms were recorded at a single scan rate at 0.05 V/s. A series of cyclic voltammograms taken at 0.01 V/s, 0.05 V/s, 0.1 V/s, 1 V/s, 2 V/s, 3 V/s, 4 V/s, 5 V/s scan rates for 20% Pt/C (E-Tek) catalyst in 0.5 M H_2SO_4 solution are presented in Figure 5.7-a.

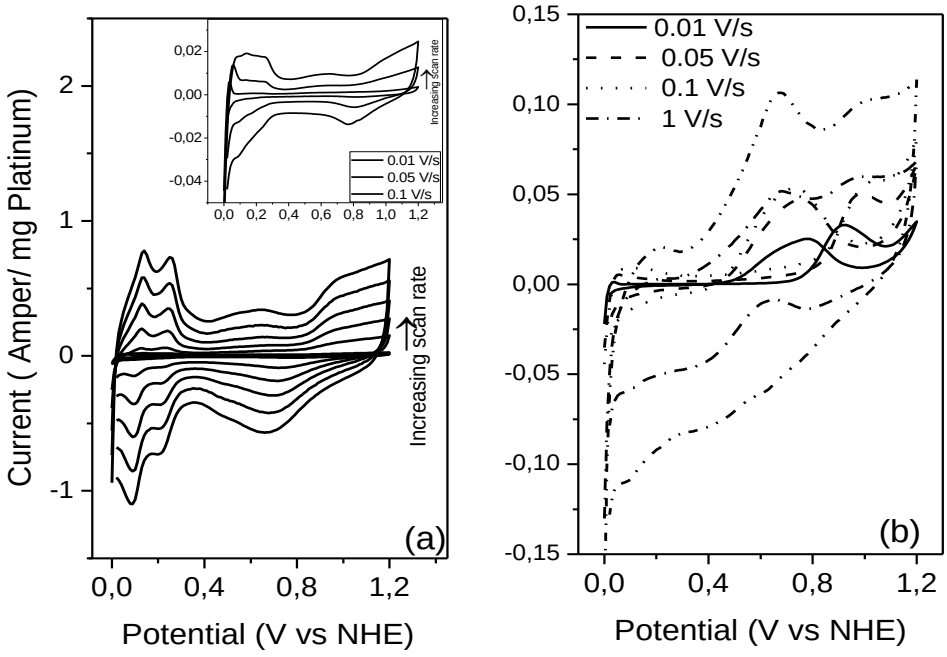

Figure 5. 7 Cyclic voltammogram of 20% Pt/C (E-Tek) catalyst a) in 0.5 M H_2SO_4 solution at 1 V/s, 2 V/s, 3 V/s, 4V/s, and 5V/s scan rates, upper insert shows the cyclic voltammogram of 20% Pt/C (E-Tek) catalyst in 0.5 M H_2SO_4 solution a 0.01 V/s, 0.05 V/s, 0.1 V/s and b) in 0.5 M H_2SO_4 + 0.5 M EtOH solution at 0.01 V/s, 0.05 V/s, 0.1 V/s, and 1V/s scan rates.

It was observed that at low scan rates (0.01 V/s-0.1 V/s), two well resolved peaks (hydrogen adsorption-reduction peaks) for polycrystalline platinum were not observed. However, these peaks were visible at higher scan rates. For 0.01 V/s and 0.05 V/s, sharp hydrogen adsorption evolution peaks were observed but these sharp peaks were not visible above these scan rates. In hydrogen region at high scan rates (1V/s to 5 V/s), two well resolved peaks occurred at the same voltage by increasing scan rate. This could be attributed to the fact that this process is reversible. For a reversible scan rate, peak potential is independent of scan rate [5].

Ethanol electro-oxidation measurements were also conducted in 0.5 M H_2SO_4 and 0.5 M ethanol solution to investigate the effect of scan rate on ethanol electro-oxidation reaction. Ethanol electro-oxidation measurements at different scan rates were given in Figure 5.7-b. These electrochemical measurements for ethanol electro-oxidation reaction was performed at small scan rates (0.01 V/s to 0.1 V/s) due to the fact that it was impossible to oxidize ethanol at 1 V/s high scan rate shown in Figure 5.7-b. This could be attributed to the fact that time taken to record would be short not enough to oxidize ethanol at 1 V/s high scan rate. It was observed that shape of the both cyclic voltammograms did not change by changing scan rate. On the other hand, the current increased by increasing scan rate and scan time. When the scan rate was decreased, cyclic voltammogram will take longer to record. This could be attributed to the fact that, by altering scan rate, the size of the diffusion layer would be changed. For instance, in slow scan rates, the size of the diffusion layer would be higher than it was at faster rates due to the fact that the flux to the electrode surface was smaller at slow scan rates. Magnitude of the current is directly related to the flux towards to electrode. That is why, at small scan rates, magnitude of the current was smaller than ones recorded at higher rates. Consequently, the voltage scan had a strong effect the behavior of current potential curve recorded [5].

In sulfuric acid solution, Pt was oxidized above 0.75 V vs NHE when potential increased. When potential was reversed, an oxygen reduction was observed at around 0.75 V vs NHE potential. The magnitude of the oxygen reduction currents increased by incresing scan rate (Figure 5.7-b). Furthermore, for ethanol electro-oxidation reaction, ethanol was oxidized at around 1 V vs NHE potential by the oxygen adsorbed on Pt. Likewise, when the scan rate increased, the magnitude of the ethanol electro-oxidation current increased. In order to show that the oxidation of ethanol achieved via oxygen adsorbed on Pt, the charge of the surface ethanol per the charge of oxygen evolution ($q_{ethanol}/ q_{oxygen}$)versus scan rate is presented in Figure 5.8. It was observed that while the highest $q_{ethanol}/ q_{oxygen}$ ratio was obtained for at 0.01 V/s, the lowest $q_{ethanol}/ q_{oxygen}$ was found at 0.1 V/s scan rate. It is clear that ethanol was oxidized by adsorbed oxygen on Pt at small scan rates [5, 198, 240-243].

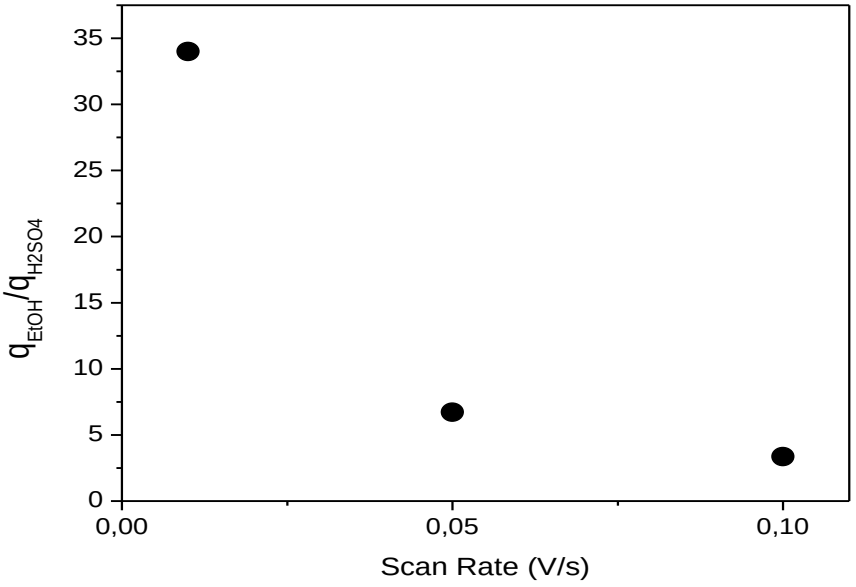

Figure 5. 8 The dependence of relation $q_{ethanol}/ q_{oxygen}$ to scan rate

5.2. 2 The Effect of Potential Change

The potential of working electrode is controlled with respect to reference electrode of which potential is fixed. It is equivalent to observing or controlling the energy of electrons within the working electrode. The energy of electrons is raised when the electrode is driven to more negative potentials at which they can reach a level high enough to transfer into vacant electronic states on species in the electrolyte. A flow of electrons from electrode to solution which is called reduction current occurs. When, the energy of electrons is lowered by driving the electrode to more positive potentials, an oxidation current occurs [5]. Cyclic voltammogram of 20% Pt/C (E-Tek) in 0.5 M H_2SO_4 solution which was performed at different potentials

is given in Figure 5.9-a. When potential difference was increased, i.e., when the working electrode was driven to more positive potentials, it was observed that at reverse potential swept, highest oxygen reduction peak was observed for 1.2 V. Ethanol electro-oxidation cyclic voltammogram in 0.5 M H_2SO_4 + 0.5 M ethanol solution is given in Figure 5.9-b. It was observed that oxygen was not enough to oxidize ethanol at 0.8 V. By increasing potential, it was observed that ethanol oxidized and current values increased considerably.

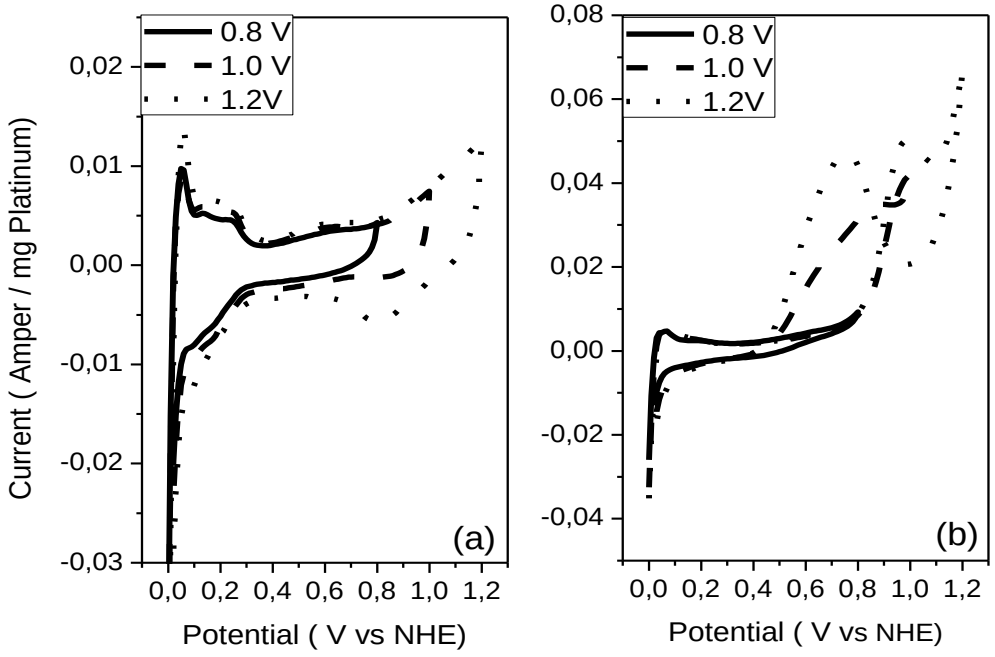

Figure 5. 9 Cyclic voltammogram of 20% Pt/C (E-Tek) catalyst a) in 0.5 M H_2SO_4 solution at 0.05 V/s up to 0.8 V, 1 V, and 1.2 V b)in 0.5 M H_2SO_4 + 0.5 M EtOH solution at 0.05 V/s up to 0.8 V, 1 V, and 1.2 V.

5.2. 3 Discussion

The ethanol electro-oxidation, the effect of scan rate and the effect of potential change on commercially available 20%Pt/C (E-Tek) catalyst were investigated. It was reported that total current values increased by increasing scan rate. It was observed that when scan rate altered the total current changed because the thickness of the diffusion layer changed. Furthermore, it was observed that at high scan rates as 1 V/s, it was impossible to oxidize ethanol the fact that time taken to record would be short not enough to oxidize ethanol at 1 V/s high scan rate.

5. 3 THE EFFECT OF PLATINUM PARTICLE SIZE FOR ETHANOL ELECTRO-OXIDATION

The particle size effect for ethanol electro-oxidation over 20% Pt/C catalysts was investigated by XRD, TEM, microcalorimetry, and cyclic voltammetry. Two sets of carbon supported Pt catalysts were prepared by the polyol method by modifying the pH of the starting mixture as 5 and 11, knowing the fact that a pH increase resulted in a decrease of the catalyst particle size [244]. In addition, a commercial Pt/C (E-Tek) catalyst was also studied for comparison. The defect site densities were determined by adsorption microcalorimetry. Finally, ethanol electro-oxidation was investigated by cyclic voltammetry. Before electro-oxidation measurements, the effect of scan rate on ethanol electro-oxidation reaction was investigated on these catalysts. A series of cyclic voltammograms were taken at 0.01 V/s, 0.05 V/s, 0.1 V/s, 1 V/s, 2 V/s, 3 V/s scan rates for these catalysts in 0.5 M H_2SO_4 solution. Prior to every experiment, the electrode was activated in 0.5 M H_2SO_4 by cycling potential between 0.0 to 1.2 V at 0.05 V/s scan rate. Furthermore, the evaluation of the ethanol oxidation reaction on carbon supported platinum catalysts was carried out by adding the appropriate amount of ethanol to adjust the concentration of electrolytic solution to 0.5 M at the potentials between 0.0 and 1.2 V. To investigate the effect of scan rate on ethanol electro-oxidation reaction, the scan rate was altered at 0.01 V/s, 0.05 V/s, 0.1 V/s, 1 V/s, 2 V/s scan rates.

5.3. 1 XRD Results

XRD patterns of the Pt/C catalysts are given in Appendix C (Figure C. 2). The diffraction peak at around 25^o was attributed to the (002) plane of the hexagonal structure of Vulcan XC-72R carbon. The diffraction peaks at around 39^o, 46^o, 68^0 and 81^o are due to diffraction of Pt (111), (200), (220) and (311) planes,

respectively. The particle size values were calculated using the Scherrer equation and are presented in Table 5.5. It was observed that Pt/C (E-Tek) had the smallest particle size. The particle size of the Pt/C catalyst prepared at pH=11 was smaller than the particle size of the catalyst prepared at pH=5.

5.3. 2 TEM Results

The TEM images of the synthesized 20%Pt/C (pH=11) and 20% Pt/C (pH=5) and the commercial monometallic catalyst are shown in Figure 5.10. For the Pt/C (E-Tek) commercial catalyst and the Pt/C (pH=11) catalysts, particles were more homogenously distributed as compared to the Pt/C (pH=5) catalyst.

By counting over 200 particles, the number-mean particle diameter versus relative frequency diagrams were obtained for all of these catalysts and given Appendix D (Figure D.3 to Figure D.6). In addition, the aspect ratio (the ratio of the length of the minor axis to that of the major axis) versus relative population of the particles are also presented in Appendix D (Figure D.7 to Figure D.9). Mean particle sizes and mean aspect ratios determined from the analysis are given in Table 5.5.

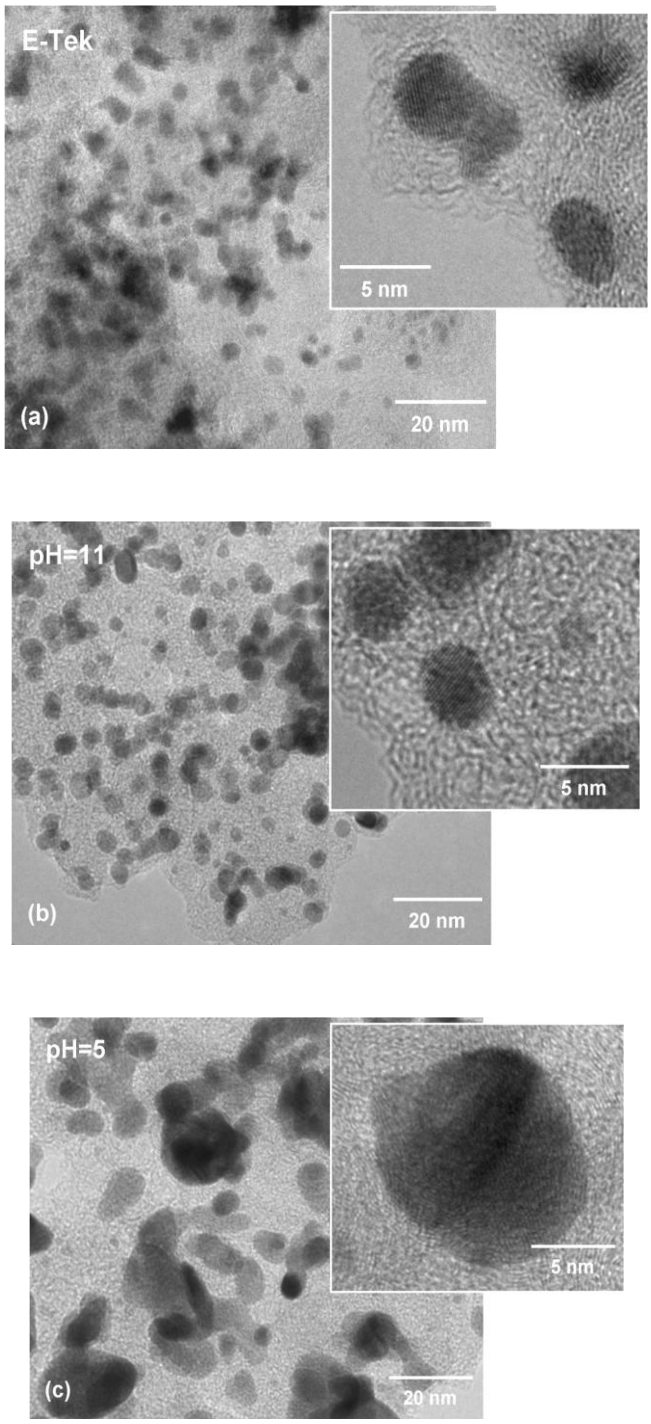

Figure 5. 10 TEM images for catalysts (a) Pt/C (E-Tek), (b) Pt/C (pH=11), (c) Pt/C (pH=5), the insets show larger magnification of the Pt nanoparticles.

Table 5. 5 Particle size values obtained from different techniques

Catalysts	Particle size (nm)				Mean-aspect ratio from TEM
	H/Pt	CO/Pt	XRD	TEM	
Pt/C (E-Tek)	3.1	4.0	2.7<d<3.4	3.3	0.76
Pt/C (pH=11)	2.7	4.1	3.1<d<3.9	4.4	0.87
Pt/C(pH=5)	12.5	33.0	11.2<d<14.0	6.7	0.85

For Pt/C (E-Tek) catalyst, a mean particle size was found as 3.3 nm and the aspect ratio of most of the particles were 0.76, which can be interpreted that most of the particles are not symmetrical. For the Pt/C (pH=11)/C catalyst, the aspect ratio of the platinum particles was approximately 0.87, indicating that most of the platinum particles are nearly symmetrical. Furthermore, the mean diameter for the Pt/C (pH=11)/C catalyst is about 4.4 nm. In consequence, these two catalysts have not only different particle sizes but also different shapes. On the other hand, the platinum particles were not homogenously distributed in the Pt/C (pH=5) catalyst. The mean particle size was obtained as 6.7 nm and the aspect ratio of distribution of the platinum particles were nearly 0.85, indicating that here also most of the platinum particles are nearly symmetrical.

5.3. 3 Gas Phase Microcalorimetric Measurement Results

The differential heats of hydrogen and carbon monoxide adsorption measurements were performed on Pt/C (E-Tek), Pt/C (pH=11), and Pt/C (pH=5) (20% Pt loading) catalysts by using Tian-Calvet type heat flow calorimeter at 323 K. The results of these measurements were given in Figure 5.11 and Figure 5.12.

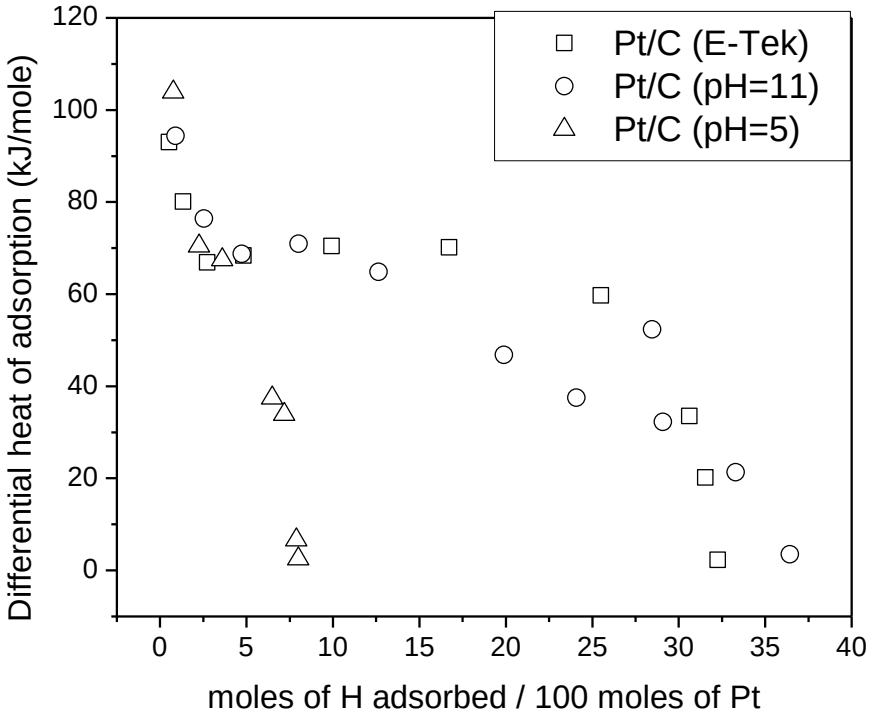

Figure 5. 11 Differential heat of hydrogen adsorption measurements results on 20% Pt/C (pH=5), 20% Pt/C (pH=11), and 20% Pt/C (E-Tek) catalysts at 323 K.

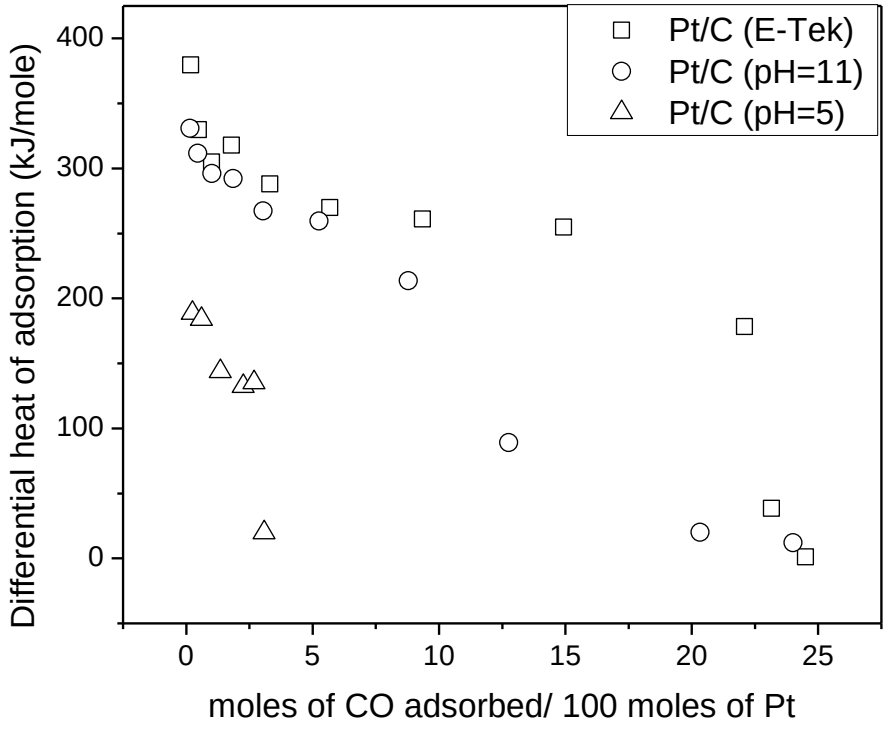

Figure 5. 12 Differential heat of carbon monoxide adsorption measurements results on 20% Pt/C (pH=5), 20% Pt/C (pH=11), and 20% Pt/C (E-Tek) catalysts at 323 K.

Initial heats of adsorption, saturation coverages of the defect-like sites, and overall saturation coverages for these catalysts for hydrogen and carbon monoxide adsorption are also given in Table 5.6. Initial heat of hydrogen adsorption on Pt/C (E-Tek) is 92 kJ/mole, which is in agreement with the literature values reported as 110-140 kJ/mole [237, 238]. Differential heat of hydrogen adsorption on Pt/C (E-Tek) exhibited a sharp decrease from ~92 kJ/mol to 65 kJ/mol up to hydrogen coverage of 0.06 mol H/mol Pt. This behavior was attributed to the saturation of

high energy defect-like sites of platinum [235, 245]. The differential heat values remained constant at this value until the hydrogen coverage reached ~0.27 mol H/mol Pt, exhibiting a plateau attributed to the low-energy sites as shown in Figure 5.11. Further decrease was observed until the saturation coverage of 0.32 mol H/mol Pt was reached. A similar behavior was observed for the Pt/C (pH=11) catalyst such that the differential heat of hydrogen adsorption curve exhibited a sharp differential heat decrease from ~95 to 68 kJ/mol up to ~0.05 mol H/mol Pt coverage. Further increments in the hydrogen doses resulted in a plateau at 68 kJ/mol until a 0.20 mol H/mol Pt coverage value was reached. Hence, the catalyst surface was saturated at 0.37 mol H/mol Pt coverage, as indicated in Figure 5.11. The only difference observed between both catalysts Pt/C (E-Tek) and Pt/C (pH=11) was that the heats of hydrogen adsorption for low energy sites (flat surfaces) were higher for the latter. When taking the Pt/C (pH=5) catalyst into consideration, only a sharp differential heat decrease was observed when compared with Pt/C (pH=11) and Pt/C (E-Tek). The defect sites were saturated at ~ 0.02 mol H/mol Pt and the surface was saturated at around 0.08 mol H/mol Pt coverage.

Table 5. 6 The surface site densities as measured by carbon monoxide and hydrogen adsorption calorimetry.

Catalysts	Q^0 (kJ/mole)		$Q_{integral}$ (kJ/mole)		$\theta^{saturation}$ (mol H or CO/ mol Pt)	
	H_2	CO	H_2	CO	H/Pt	CO/Pt
Pt/C (E-Tek)	92	370	109	260	0.32	0.25
Pt/C (pH=11)	95	340	112	231	0.37	0.24
Pt/C(pH=5)	105	200	73	98	0.08	0.03

The differential heats of carbon monoxide adsorption measurements on Pt/C (pH=5), Pt/C (pH=11), and Pt/C (E-Tek) (20% Pt loading) catalysts at 323 K are given in Figure 5.12. Differential heat of carbon monoxide adsorption on Pt/C (E-Tek) decreased from 370 kJ/mole to 260 kJ/mole and on Pt/C (pH=11) decreased from 340 kJ/mole to 260 kJ/mole up to ~0.04 mol CO/mol Pt coverage reached. A plateau was observed for the CO differential heats of adsorption curves on Pt/C (E-Tek) and Pt/C (pH=11) at ~260 kJ/mole up to ~0.20 mol CO/mol Pt of carbon monoxide and ~0.17 mol CO/mol Pt of carbon monoxide adsorbed, respectively. Moreover, further increments in the coverage resulted in a decrease of heats of adsorption until 0.25 mol CO/mol Pt for Pt/C (E-Tek) and 0.24 mol CO/mol Pt for the Pt/C (pH=11) saturation coverage values was reached. A sharp differential heat decrease was observed for Pt/C (pH=5) catalyst until ~0.02 mol CO/mol Pt saturation coverage was reached. The low coverage values indicated that the intermediate energy sites for Pt/C (pH=5) catalysts were lost when compared with Pt/C (E-Tek) and Pt/C (pH=11). All of the coverage values are consolidated in Table 5.6. It was observed that adsorbed hydrogen amounts were greater than adsorbed CO. This is believed to be due to a weakly bound hydrogen that exists on the metal surfaces at H: M stoichiometries greater than 1.

The saturation coverages of H and CO were taken as the particle dispersions assuming 1:1 stoichiometry of H: Pt or CO: Pt. Particle size values of these catalysts were estimated using the $d(nm) = 100/D(\text{dispersion})$ empirical correlation [246]. An average particle size value was also calculated as such and is given in Table 5.5.

5.3. 4 Electrochemical Characterization Results

The ethanol electro-oxidation activity was evaluated on the Pt/C (E-Tek), Pt/C (pH=11), and Pt/C (pH=5) catalysts in a 0.5 M H_2SO_4 solution at 25^{o}C to

investigate the particle size effect in ethanol electro-oxidation reaction. Prior to the measurement of ethanol electro-oxidation activities, the surface of the electrodes were activated for 100 cycles in the potential range of 0.0 to 1.2 V which was swept at 0.05V s^{-1}. The steady state cyclic voltammograms of these catalysts in 0.5 M H_2SO_4 solution are presented in Figure 5.13 and Figure 5.14. The voltage scan rate could be obtained from the slope of the current vs. potential diagram. If the scan rate is altered, the current response also changes. A series of cyclic voltammograms were taken at 0.01 V/s, 0.05 V/s, 0.1 V/s, 1 V/s, 2 V/s, 3 V/s, scan rates for 20% Pt/C (E-Tek), 20% Pt/C (pH=11), and 20% Pt/C (pH=5) catalysts in 0.5 M H_2SO_4 solution. These results for 20% Pt/C (E-Tek) were presented in Figure 5.13. Results for 20% Pt/C (pH=11) and 20% Pt/C (pH=5) catalysts were given in Appendix E (Figure E.9 and Figure E.10).

Two well resolved peaks (hydrogen adsorption-evolution peaks) for polycrystalline platinum were not observed at low scan rates (0.01 V/s-0.1 V/s). However, these peaks were visible at higher scan rates. For 0.01 V/s and 0.05 V/s, sharp hydrogen adsorption evolution peaks were observed but these sharp peaks were not visible above these scan rates. In hydrogen region at high scan rates (1V/s to 3 V/s), two well resolved peaks occurred at the same voltage by increasing scan rate. The voltammetric features of these platinum catalysts are consistent with literature data for a typical polycrystalline platinum electrode in 0.5M H_2SO_4 solution electrolyte. At the hydrogen adsorption-desorption region below 0.35 V vs. NHE, well defined peaks were observed for Pt/C (E-Tek) and for Pt/C (pH=11). These peaks are attributed to the existence of (100) and (110) platinum crystal facets [194, 240, 247]. On the other hand, these peaks were not recorded for Pt/C (pH=5) catalyst. Furthermore, the results indicated that while the activity of the 20%Pt/C (E-Tek) and Pt/C (pH=11) were nearly same for sulfuric acid electro-oxidation, which was superior to 20% Pt/C (pH=5) (see Figure 5.14).

This could be attributed to the scarceness of defect sites. Kumar et al. reported that edges and corner sites acts as gateways or portals through which hydrogen dissociative adsorbing onto planar surfaces. When these portals are blocked, the results are drastic decrease in the hydrogen amount. Thus, in this case, the scarceness of defect-like sites acting as adsorption-desorption portals obstructed the accessibility of the low-energy sites. It is already established that liquid phase reactions were reported to take place on the defect-like sites [231, 233, 235].

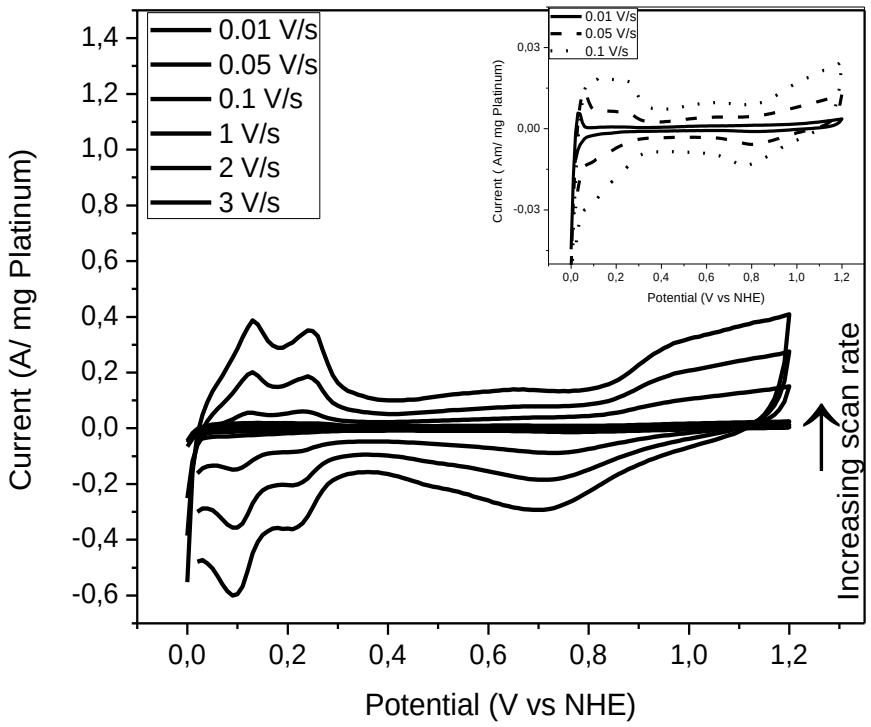

Figure 5. 13 Cyclic voltammogram of 20% Pt/C (E-Tek) catalyst in 0.5 M H_2SO_4 solution at 1 V/s, 2 V/s, 3 V/s scan rates, upper insert shows the cyclic voltammogram of 20% Pt/C (E-Tek) catalyst in 0.5 M H_2SO_4 solution at 0.01 V/s, 0.05 V/s, 0.1 V/s.

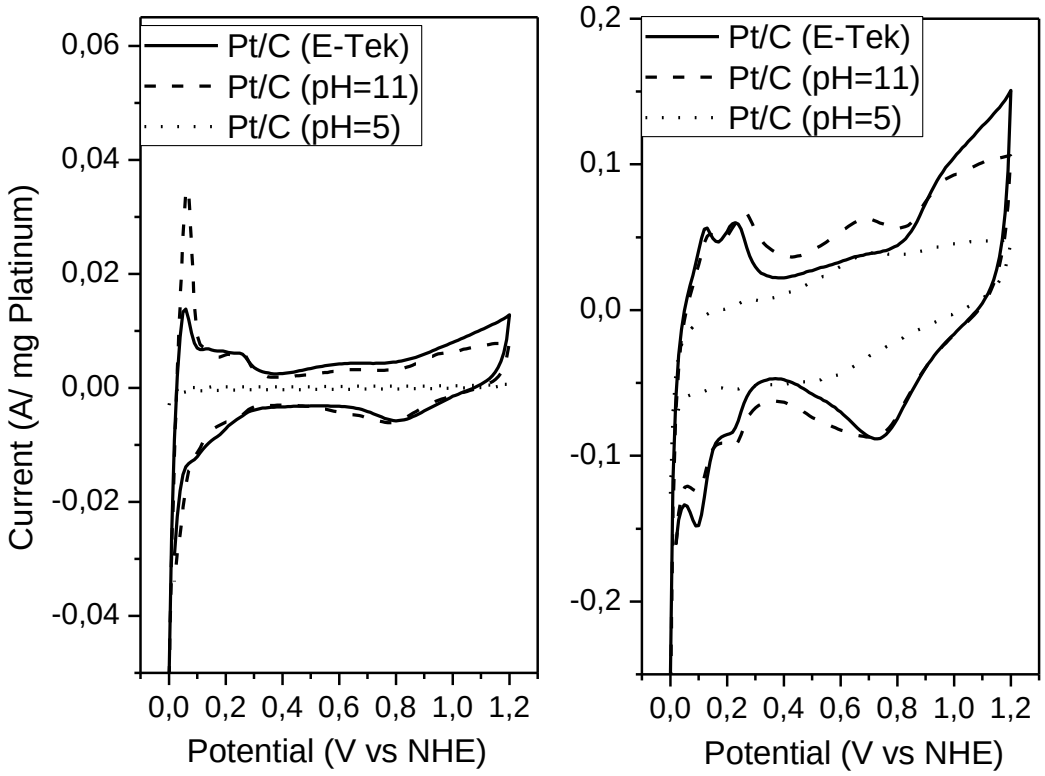

Figure 5. 14 Cyclic voltammogram of 20% Pt/C (E-Tek), 20% Pt/C (pH=11), and Pt/C (pH=5) catalysts (a) in 0.5 M H_2SO_4 solution at 1 V/s, (b) in 0.5 M H_2SO_4 solution at 0.05V/s.

Ethanol electro-oxidation measurements were also conducted in 0.5 M H_2SO_4 and 0.5 M ethanol solution to investigate the effect of scan rate on ethanol electro-oxidation reaction on 20% Pt/C (E-Tek), 20% Pt/C (pH=11), 20% Pt/C (pH=5) catalysts. For 20% Pt/C (E-Tek) catalyst, ethanol electro-oxidation measurements at different scan rates on these catalysts were shown in Figure 5.15. For 20% Pt/C

(pH=11), 20% Pt/C (pH=5) catalysts, results were given in Appendix D (Figure E.11 and Figure E.12).

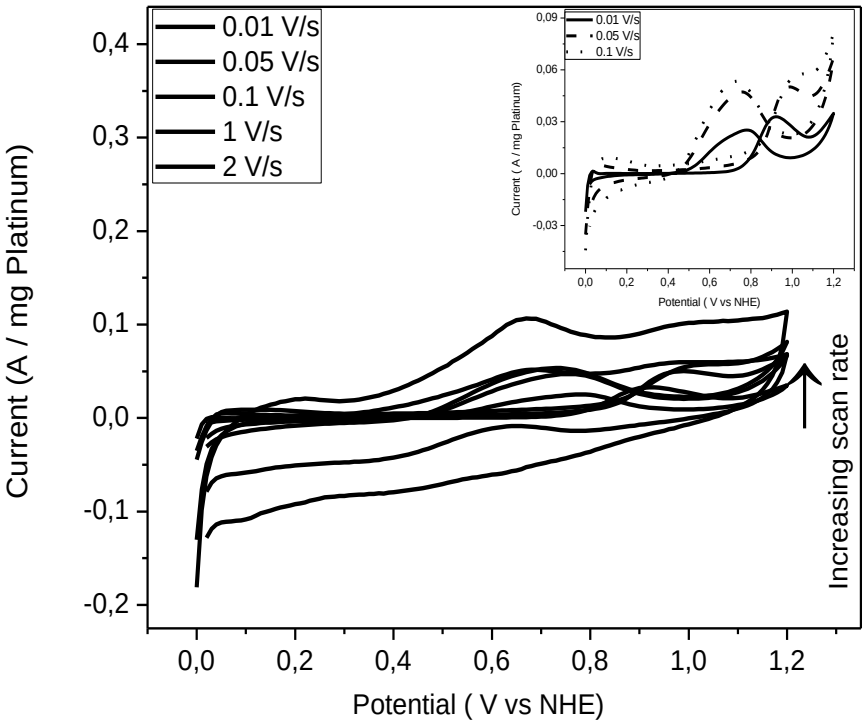

Figure 5. 15 Cyclic voltammogram of 20% Pt/C (E-Tek) catalyst in 0.5 M H_2SO_4 + 0.5 M EtOH solution at 1 V/s, 2 V/s scan rates, upper insert shows the cyclic voltammogram of 20% Pt/C (E-Tek) catalyst in 0.5 M H_2SO_4 +0.5 M EtOH solution at 0.01 V/s, 0.05 V/s, 0.1 V/s.

These electrochemical measurements for ethanol electro-oxidation reaction was performed at 0.01 V/s, 0.05 V/s, 0.1 V/s, 1 V/s, 2 V/s as shown in Figure 5.15, At small scan rates (0.01 V/s to 0.1 V/s), it was observed that ethanol was oxized at

aroud 1 V potential and Pt was oxidized at 1.2 V by increasing potential further. Furthermore, bulk ethanol was oxidized via surface Pt oxide at around 0.7 V by reversing the potential [198]. At high scan rates (1 V/s and 2 V/s), the time taken to record to voltammetry would be short enough not to oxidize ethanol completely.

Ethanol electro-oxidation measurements at 0.05 V/s and 1V/s scan rates performed in the presence of 0.5 M ethanol concentration on Pt/C (E-Tek), Pt/C (pH=11), and Pt/C (pH=5) catalysts are shown in Figure 5.16. Ethanol oxidation on the catalysts commenced at 0.3-0.4V and was fully developed at 1.2 V. Maximum current density in forward scan was used to investigate the electro catalytic activity of these catalysts because it is more indicative of the CO removal rate via bi-functional mechanisms [248, 249]. The results indicated that the activity of the Pt/C (E-Tek) catalyst for ethanol electro-oxidation and reduction of ethanol was superior to Pt/C (pH=11) and Pt/C (pH=5).

To understand whether this low activity of 20% Pt/C (pH=5) catalyst were due to the low amount of defect-like sites or not, per site activity of these catalysts were determined and presented in Figure 5.17 and Figure 5.18 for sulfuric acid and ethanol electro-oxidation voltammograms at 0.05 V/s and 1 V/s, respectively. For both of these measurements, it was observed that the current per site values were nearly the same for for 20% Pt/C (E-Tek) and Pt/C (pH=11) catalysts at 0.05 V/s and 1 V/s scan rates for sulfuric acid electro-oxidation and ethanol electro-oxidation. However, considering sulfuric acid and ethanol electro-oxidation voltammograms at 0.05 V/s, it was observed that current per sites values for Pt/C (pH=5) catalyst were significantly lower than the ones measured for 20% Pt/C (E-Tek) and Pt/C (pH=11) catalysts. On the other hand, the current per site values for Pt/C (pH=5) catalyst were nearly the same for 20% Pt/C (E-Tek) and Pt/C (pH=11) catalysts.

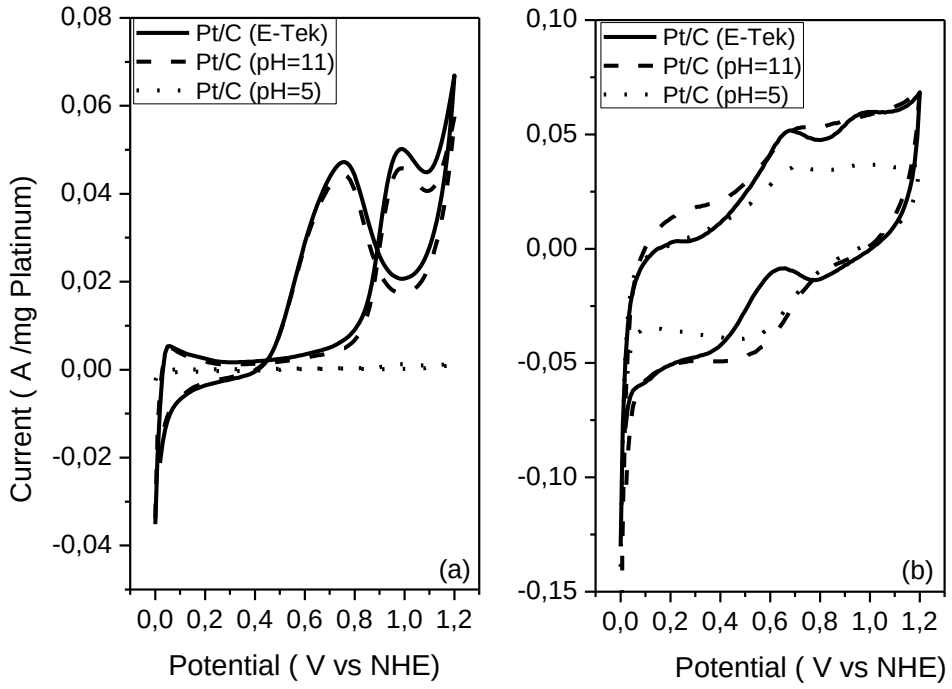

Figure 5. 16 Cyclic voltammogram of 20% Pt/C (E-Tek), 20% Pt/C (pH=11), and Pt/C (pH=5) catalysts (a) in 0.5 M H_2SO_4 +0.5 M EtOH solution at 0.05 V/s, (b) in 0.5 M H_2SO_4 +0.5 M EtOH solution at 1 V/s.

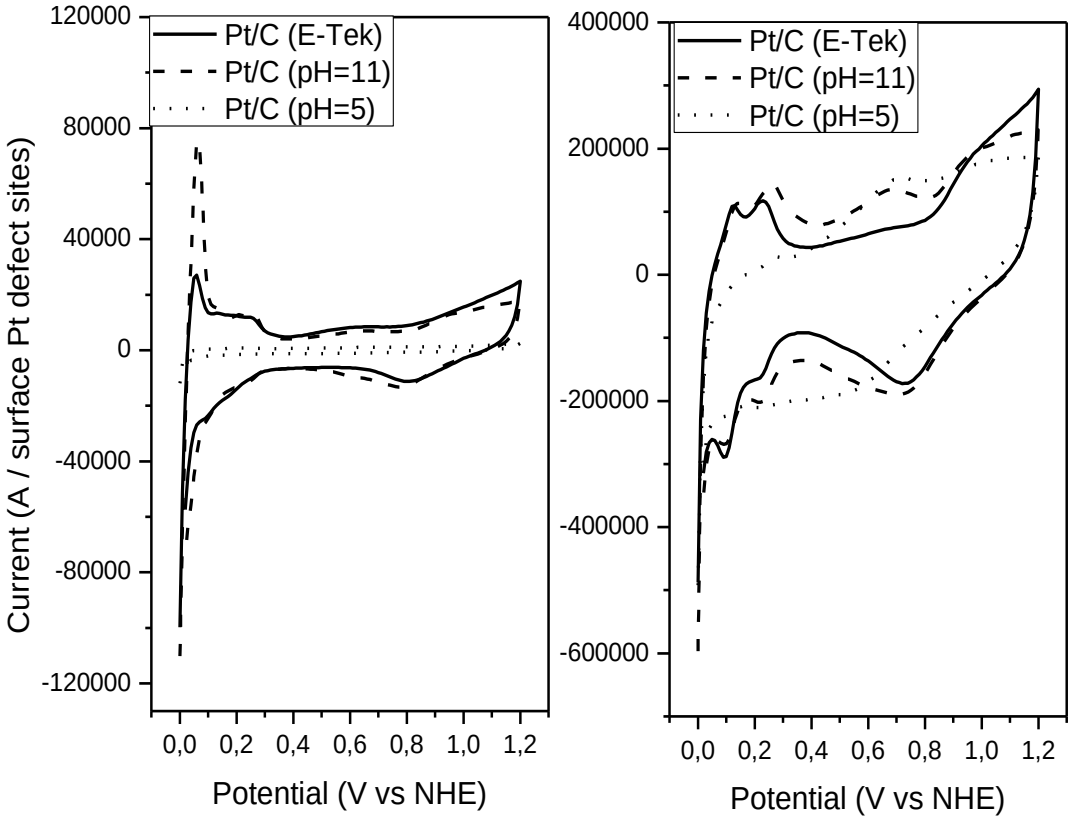

Figure 5. 17 Current per site measurements of 20% Pt/C (E-Tek), 20% Pt/C (pH=11), and Pt/C (pH=5) catalysts (a) in 0.5 M H_2SO_4 solution at 0.05 V/s, (b) in 0.5 M H_2SO_4 solution at 1V/s.

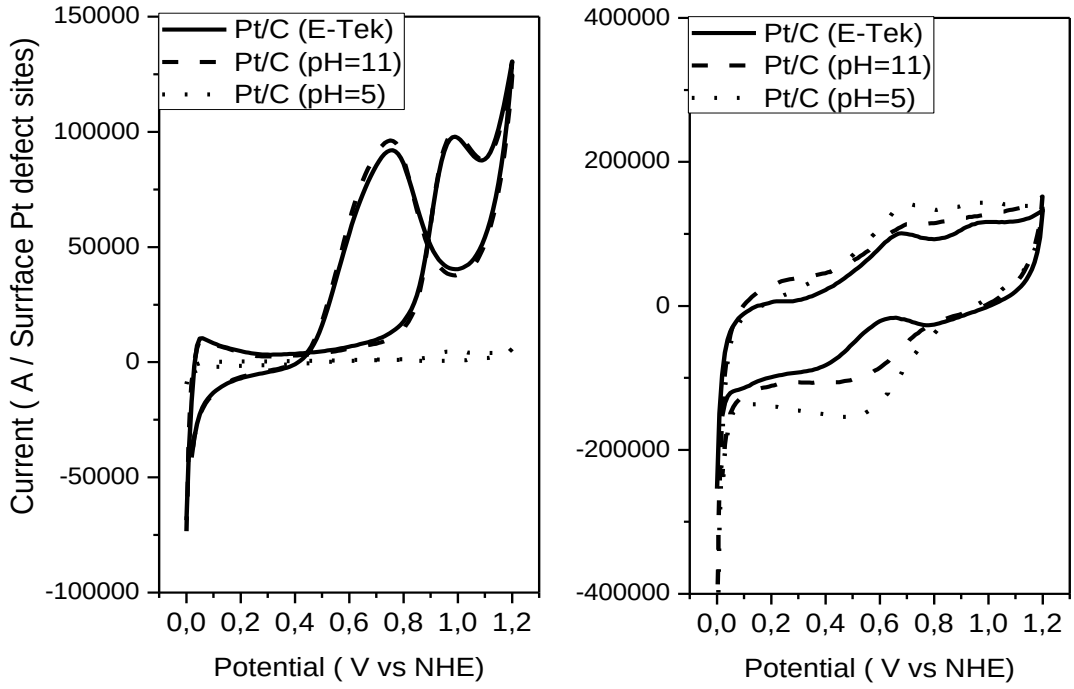

Figure 5. 18 Current per site measurements of 20% Pt/C (E-Tek), 20% Pt/C (pH=11), and Pt/C (pH=5) catalysts (a) in 0.5 M H_2SO_4 +0.5 M EtOH solution at 0.05 V/s, (b) in 0.5 M H_2SO_4 +0.5 M EtOH solution at 1V/s.

5.3. 5 Discussion

Particle size of Pt/C (E-Tek), Pt/C (pH=11), and Pt/C (pH=11) catalysts were estimated by XRD, TEM and adsorption microcalorimetry measurements and are presented in Table 5.5. For the size of the Pt/C (E-Tek) particles, there is a good agreement between XRD and TEM data, indicating a narrow particle size distribution. Likewise, for Pt/C (pH=11), particle size values obtained from XRD and TEM agree well. On the contrary, there is not an agreement between XRD and TEM data for the Pt/C (pH=5) catalysts, indicating a non-symmetrical behavior.

The heat of adsorption was directly related to the structure of the catalysts. Differential heats of CO and H_2 adsorption data were used to determine the population and the strength of the defect-like sites present in the catalysts. The high-energy sites, characterized by microcalorimetry on the differential heat of adsorption curves until the plateau was reached, were described as defect-like sites based on previous experimental [231, 232, 235, 236, 245] and theoretical [234] studies. Steps sites are more active and they bind adsorbates more strongly. One can realize that the plateau observed on the differential heat of adsorption curve is an indication that the differential heat of adsorption is not a function of coverage. These sites were identified as flat surfaces in accordance with Norskov et al. [234]. For polycrystalline surfaces, the site energy distribution of catalysts depends on the average particle size of the catalyst and as a result it depends on the detailed geometric structure of the surface atoms of the catalyst. Uner and Uner [236] performed hydrogen adsorption measurements on 2% Pt/ γ-Al_2O_3 calcined at different temperatures to vary the particle size of catalysts. They reported that hydrogen chemisorption sites with low and intermediate heats were lost when the metal particle size of 2% Pt/γ-Al_2O_3 was increased.

The difference observed between Pt/C (E-Tek) and Pt/C (pH=11) catalysts was that the heats of hydrogen and carbon monoxide adsorption values for low energy sites (flat surfaces) were higher for the latter. When the particle size increased, the saturation coverage of CO and H_2 decreased. This behavior was attributed to the loss of low energy sites (flat surfaces).

Electrochemical measurements were performed on these catalysts to investigate the particle size effect in the ethanol electro-oxidation activity. Two well resolved peaks were observed at hydrogen region at high scan rates (NHE) at cyclic voltammetry measurements performed in 0.5 M H_2SO_4 solution. Markovíc et

al.[240, 247] attributed these peaks to the existence of Pt (100) and Pt (110) crystal surfaces. They conducted studies on single crystal platinum surfaces and indicated that the peak located at around 0.12 V was related to the adsorption/desorption process of hydrogen on Pt (110) single crystal surfaces. On the other hand, they reported that the peak at around 0.24 V was related to a hydrogen adsorption-desorption process on Pt (100) single crystal surfaces. In this study, these peaks were not observed for the Pt/C (pH=5) catalyst. This was due to the loss of low-energy sites with increasing Pt particle size. Consequently, hydrogen and carbon monoxide differential heat of adsorption measurements and cyclic voltammogram experiments performed in sulfuric acid. This indicated that an increase in particle size results in the loss of low-energy sites (flat surfaces). On the other hand, current per site measurements indicated that current per site values were nearly the same for for 20% Pt/C (E-Tek) and Pt/C (pH=11) catalysts at 0.05 V/s and 1 V/s scan rates for sulfuric acid electro-oxidation and ethanol electro-oxidation. These two catalysts have different particle shapes since the aspect ratio distribution of these catalysts was different. When ethanol electro-oxidation data and the relative densities of the surface sites were compared, it was clearly seen that the E-Tek catalyst had the highest density of defect sites while the total coverages (dispersions) of hydrogen and CO on both Pt/C (E-Tek) and Pt/C (pH=11) catalysts were the same. These catalysts have different number of defect sites. It is clearly demonstrated that the defect sites determine the ethanol electro-oxidation activities, which is governed by the shape difference between Pt/C (pH=11) and Pt/C (E-Tek) catalyst.

Considering the Pt/C (pH=5) catalyst, it was observed that while current per sites values for Pt/C (pH=5) catalyst were significantly lower than the ones measured for 20% Pt/C (E-Tek) and Pt/C (pH=11) catalysts for sufuric acid and ethanol electro-oxidation measurements at 0.05 Vs scan rate, the current per site values for

Pt/C (pH=5) catalyst were nearly the same for 20% Pt/C (E-Tek) and Pt/C (pH=11) catalysts for sufuric acid and ethanol electro-oxidation measurements at 1 V/s scan rate. This could be attributed to the fact that by altering scan rate, the size of the diffusion layer would be changed. For instance, in slow scan rates (0.05 V/s) , the size of the diffusion layer would be higher than it was at faster rates (1 V/s) due to the fact that the flux to the electrode surface was smaller at slow scan rates.

5. 4 THE EFFECT OF CARBON SUPPORT

Activated carbon, carbon black, carbon nanotubes, and carbon nanofibers are many different carbon materials were investigated especially as catalysts and catalyst supports. The effect of the surface area, pore size, and the surface chemistry of carbon supports on catalytic activity and selectivity as well as the material stability are the current topics under investigation. In the present study, the effect of support for ethanol electro-oxidation reaction was investigated on 20% Pt/C (E-Tek), 20% Pt/commercial CNT, and 20%Pt/home-made CNTs catalysts. Home-made CNTs were prepared by template synthesis method via chemical vapor deposition (CVD) method .The metal dispersions were determined from volumetric chemisorption measurements. By using these dispersion values, per site activity of these catalysts were explored. 20% Pt/commercial CNTs and 20% Pt/home-made CNTs were prepared by polyol method.These catalysts were tested as anode catalysts for the ethanol electro-oxidation reaction at room temperature by cyclic voltammetry. Ethanol electro-oxidation measurements were performed on 20% Pt/C (E-Tek), 20% Pt/commercial CNTs, and 20%Pt/home-made CNTs catalysts in 0.5 M H_2SO_4 +0.5 M ethanol solution at 0.05 V/s scan rate and 1.2 V vs NHE.

5.4. 1 Volumetric Chemisorption Measurement Results

Volumetric chemisorption measurements were performed on 20%Pt/C (E-Tek), 20%Pt/ commercial CNTs, and 20% Pt/home-made CNTs catalysts to define platinum dispersion on these catalysts. Dispersion measurement results of these catalysts are given in Table 5.7. While the dispersion values of commercial 20%Pt/C (E-Tek) catalyst and the dispersion of 20%Pt/home-made CNTs were nearly the same, the platinum dispersion on 20%Pt/commercial CNTs catalysts

was around 16%, which was significantly lower than both 20%Pt/C (E-Tek) and 20%Pt/commercial CNTs catalysts.

Table 5. 7 Dispersion values obtained from volumetric chemisorption measurements

Catalyst	mol H / mol Pt	Dispersion (%)
Pt/C (E-Tek)	0.28	28
Pt/home-made CNTs	0.29	29
Pt/commercial-CNTs	0.16	16

5.4. 2 Electrochemical Characterization Results

The sulfuric acid and ethanol electro-oxidation measurements were also performed on glassy carbon and carbon powder. These voltammograms were given in Appendix E (Figure E.1 to Figure E.4). It was observed that current values were nearly the same for glassy carbon and Carbon support loaded electrode. The ethanol electro-oxidation activity was evaluated on 20% Pt/C (E-Tek), 20% Pt/commercial CNTs, and 20%Pt/home-made CNTs catalysts in a 0.5 M H_2SO_4 solution to investigate the support effect in ethanol electro-oxidation reaction. The steady state cyclic voltammograms of these catalysts in 0.5 M H_2SO_4 solution were presented in Figure 5.19-a. The activity of the 20% Pt/C (E-Tek) catalyst and 20%Pt/home-made CNTs for the sulfuric acid electro-oxidation was superior to 20% Pt/commercial CNTs. Ethanol electro-oxidation measurements performed in the presence of 0.5 M ethanol concentration on 20% Pt/C (E-Tek), 20%

Pt/commercial CNTs, and 20%Pt/home-made CNTs catalysts were shown in Figure 5.19-b. Ethanol oxidation on the catalysts commenced at 0.3-0.4V and was fully developed at 1.2 V. Maximum current density in forward scan was used to investigate the electro-catalytic activity of these catalysts because it is more indicative of the CO removal rate via bi-functional mechanisms. The results indicated that the activity of the20%Pt/home-made CNTs for the sulfuric acid electro-oxidation was superior to 20% Pt/commercial CNTs.

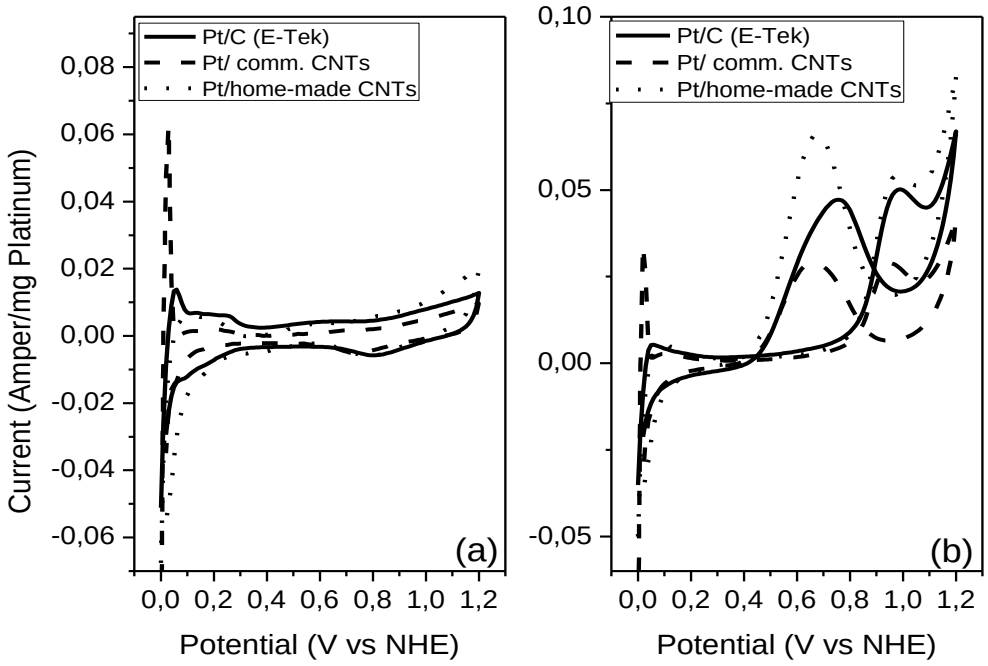

Figure 5. 19 Cyclic voltammetry results on 20% Pt/C (E-Tek), 20% Pt/commercial CNTs, and 20%Pt/home-made CNTs catalysts a) in 0.5 M H_2SO_4 at 0.05 V/s b) in 0.5 M H_2SO_4 + 0.5 M EtOH solution at 0.05 V/s .

To differentiate whether the differences are due to the supports or to the metal, per site activity of these catalysts were determined and presented in Figure 5.20-a and Figure 5.20-b for sulfuric acid and ethanol electro-oxidation voltammograms, respectively.For both of these measurements, it was observed that the current per site values were nearly the same for all of the catalysts. In conclusion, only metal dispersion improved ethanol electro-oxidation reaction and support did not have any improving effect on ethanol electro-oxidation reaction. The exception is the large weakly bound hydrogen peak apparent for the commercial CNTs which might be due to hydrogen spillover effects on defect rich CNT surface sites [250, 251].

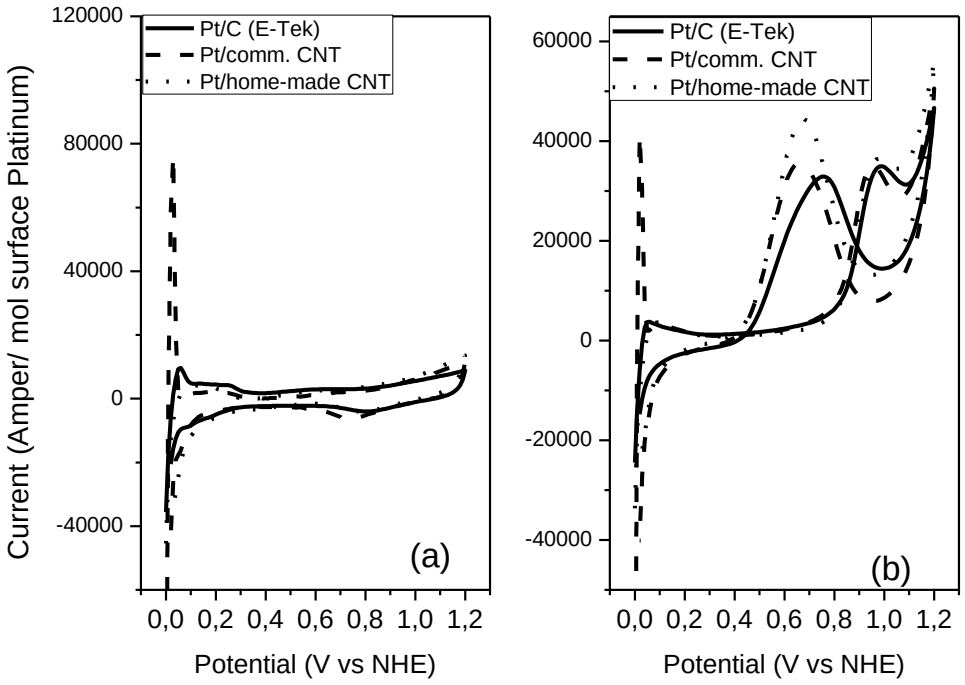

Figure 5. 20 Current per site vs. potential measurement results on 20% Pt/C (E-Tek), 20% Pt/commercial CNTs, and 20%Pt/home-made CNTs catalysts a) in 0.5 M H_2SO_4 at 0.05 V/s b) in 0.5 M H_2SO_4 + 0.5 M EtOH solution at 0.05 V/s.

5.4. 3 Discussion

The effect of carbon support material was investigated by using different carbon materials as support. Finally, it was found that the electrocatalytic activities per Pt surface site values were nearly the same regardless of the carbon support used. Under the conditions used in this study, ethanol electro-oxidation reaction depended only on the metal dispersions and support did not have any effect.

5. 5 THE EFFECT OF TIN ADDITION

The role of tin addition in ethanol electro-oxidation reaction was investigated. Thus, the differential heat of adsorption measurements could be a novel method to reach this aim. The active sites defined by cyclic voltammetry measurements could be compared to gas phase adsorption microcalorimetry measurement to figure out which sites are involving in ethanol electro-oxidation reaction. In conclusion, the microcalorimetric measurements of carbon monoxide adsorption and hydrogen adsorption, and cyclic voltammetric measurements were performed on 20%Pt: Sn/C catalysts prepared by polyol method at different Pt: Sn atomic ratios. Pt: Sn/C (20% Pt loading) catalysts were prepared by polyol method varying the Pt: Sn atomic ratio 15:1 to 1:1. These catalysts were characterized by XRD, adsorption calorimetry, and tested as anode catalysts for the ethanol electro-oxidation reaction at room temperature by cyclic voltammetry to investigate the effect of Sn addition on the ethanol electro-oxidation activity. Cyclic voltammetric measurements on 20% Pt/C, 20%Pt-Sn (15:1)/C, 20%Pt-Sn (9:1)/C, 20%Pt-Sn (6:1)/C, and 20%Pt-Sn (1:1)/C catalysts were performed in 0.5 M H_2SO_4 and 0.5 M ethanol solutions. At two different scan rates (0.05 V/s and 0.25 V/s scan rates), cyclic voltammograms were taken in 0.5 M H_2SO_4 solution on 20%Pt-Sn/C catalysts. Ethanol electro-oxidation reaction was also evaluated on 20%Pt-Sn/C catalysts by adding the appropriate amount of ethanol to adjust the concentration of electrolytic solution to 0.5 M at the potentials between 0.0 and 0.8 V.

Furthermore, in order to investigate the poisoning capacity of monometallic Pt/C catalyst and bi-metallic Pt-Sn (6:1)/C catalyst, poisoning measurements were performed by linear sweep voltammetry technique. Linear sweep voltammetry measurements were performed between 0.4 V vs NHE and 1.6 V vs NHE in 0.5 M H_2SO_4 +0.5 M ethanol solution at 0.05 V/s scan rate. Prior to linear sweep

voltammetry measurements, a surface pretreatment was applied on electrode. According to this pretretament, firstly 1.6 V vs NHE constant potential was applied for 30 s and then potential was held constant at 0.0 V vs NHE for 10 s in order to activate the surface before poisoning. In the second part of the pretreatment, potential was kept constant at 0.4 vs NHE for 1 s, 10 s, 20 s, 40 s, 60 s, 120 s, 200 s, and 600 s to poision the catalyst surface because the poisoning of the Pt surface commenced at around 0.4 vs NHE potential. After this pretreatment, linear sweep voltammetry measurements were performed to oxidize the surface adsorbed poision.

5.5. 1 XRD Results

XRD patterns of the 20%Pt/C and 20%Pt-Sn/C catalysts were given in Appendix C (Figure C.3). The diffraction peak at around 25^{o} was attributed to diffraction at the (002) plane of the hexagonal structure of Vulcan XC-72R carbon. The diffraction peaks at around 39^{o}, 46^{o}, 68^{o}, and 81^{o} were due to diffraction at the Pt (111), (200), (220) and (311) planes, respectively. The diffraction peaks of Pt are clearly broadened with increasing tin content. The mean Pt particle diameters of the 20%Pt-Sn/C catalysts were calculated from the Pt (111) diffraction peak via the Scherrer equation [252]. The mean Pt particle diameter decreases from 3.6 to 1.2 nm with increasing tin content. This was attributed to Pt-Pt ensembles were separated by Sn particles inhibiting the agglomeration of Pt particles during the synthesis process.

5.5. 2 XPS Results

The surface composition of 20%Pt/C (pH=11), 20%Pt-Sn/C catalysts was investigated for understanding the oxidation states of the species by means of XPS. General XPS spectra of these catalysts were given in Appendix C (Figure

C.6). To reach this aim, Pt 4f and Sn 3d core levels were analyzed. The charging effects were corrected by using the C 1s peak of which the most intense component was set at 284.6 eV and used as internal reference. C 1s spectra were given in Appendix C (Figure C.7).

In Appendix C (Figure C.9), the Pt 4f regions of the XPS spectrum of the Pt/C (pH=11) and Pt-Sn/C were represented. The spectrum reveals the doublets containing a low energy band (Pt $4f_{7/2}$) and a high energy band (Pt $4f_{5/2}$). There are three possible oxidation states of platinum consisting of Pt^{0}, Pt^{2+} and Pt^{4+}.The binding energy increases by the oxidation state of the Pt. When Sn amount increased, a negative shift was observed in binding energies. This could be attributed to the fact that there was more zero valence Pt in Pt-Sn (1:1) catalyst.

The Sn 3d core level doublet spectra of 20% Pt-Sn/C catalysts were demonstrated in Appendix C (Figure C.10). The foremost component was the Sn $3d_{5/2}$ component appearing at 486.4 eV binding energy. Similarly, it was observed that there is a negative shift in binding energies by the increasing amount of tin. This could be attributed that tin was in more zero valence compared to other ones.

5.5. 3 Gas Phase Microcalorimetric Measurement Results

The differential heats of hydrogen and carbon monoxide heat of adsorption measurements were performed on 20%Pt-Sn/C catalysts by using Tian-Calvet type heat flow calorimeter at 323 K to define the effect of Sn addition. Initial heat of adsorption, defect-like sites (highly active sites) coverages, and total coverage values for 20%Pt-Sn/C catalysts for hydrogen and carbon monoxide adsorption were given in Table 5.8. The initial heat of hydrogen and carbon monoxide

adsorption values of 20%Pt:Sn/C catalysts were in agreement with the ones reported in literature for Pt and Pt-Sn catalysts [237, 238].

adsorption values of 20%Pt:Sn/C catalysts were in agreement with the ones reported in literature for Pt and Pt-Sn catalysts [237, 238].

Table 5. 8 The surface site densities as measured by carbon monoxide and hydrogen adsorption calorimetry and particle size values obtained from microcalorimetry and XRD.

Catalysts	Q^0 (kJ/mole)		$\theta^{defects}$ (mol H or CO/ mol Pt)		$\theta^{saturation}$ (mol H or CO/ mol Pt)		Particle size (nm)		
							Calorimetry		d_{XRD}
	H_2	CO	H/Pt	CO/Pt	H/Pt	CO/Pt	$*d_{H/Pt}$	$*d_{CO/Pt}$	
Pt/C	89	330	0.07	0.05	0.36	0.24	2.8	4.1	3.3<d<4.1
Pt:Sn(15:1)	150	330	0.05	0.05	0.23	0.12	4.3	8.3	3.1<d<3.8
Pt:Sn (9:1)	119	370	0.04	0.03	0.23	0.09	4.3	11.1	2.8<d<3.6
Pt:Sn (6:1)	149	320	0.04	0.03	0.13	0.03	7.7	33.3	2.6<d<3.2
Pt:Sn (1:1)	140	300	0.02	0.02	0.03	0.02	33.3	50.0	1.0<d<1.2

Taking the hydrogen chemisorption measurements on these catalysts into consideration, one could see that hydrogen saturation coverage decreased when the Sn amount increased (see Figure 5. 21). Furthermore, we noted that if Pt:Sn atomic ratio decreased from 15:1 to 9:1 and 6:1, the defect-like site saturation coverage

values slightly decreased by increasing Sn amount and these values were approximately same for Pt-Sn(9:1)/C and Pt-Sn(6:1)/C catalysts (Table 5.8). Moreover, when the Pt: Sn atomic ratio decreased 1:1 value, it was seen that the defect-like site coverage value considerably decreased. Furthermore, the energy of plateau observed on the hydrogen chemisorption thermogram decreased by increasing Sn amount. In addition, this plateau was lost for Pt: Sn (1:1)/C catalyst. Thus, the presence of these plateaus could be attributed to the presence of low energy sites.

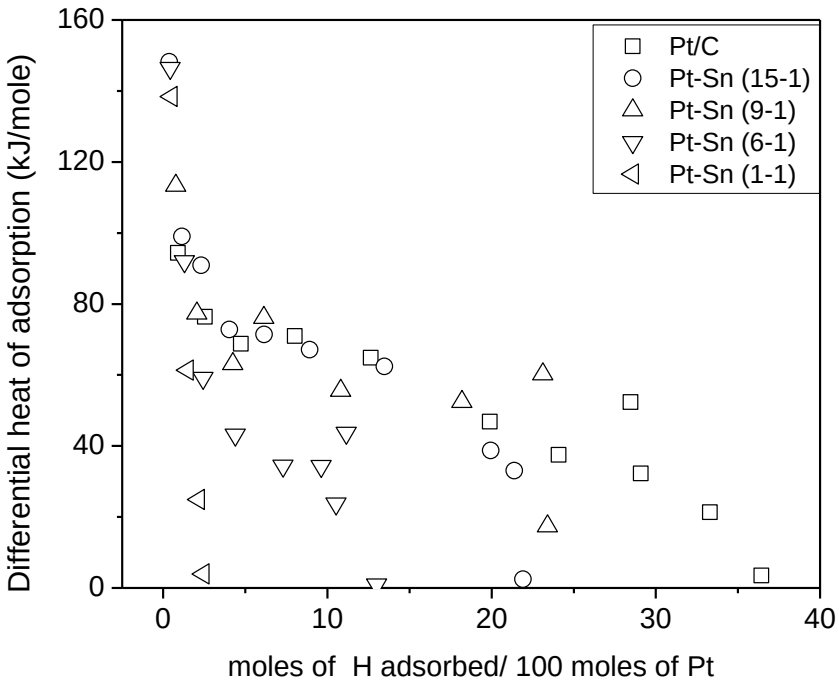

Figure 5. 21 Differential heat of hydrogen adsorption measurements results at 323 K on carbon supported 20%Pt and 20% Pt:Sn catalysts prepared at 15:1, 9:1, 6:1, 1:1 Pt:Sn atomic ratios.

For carbon monoxide chemisorption measurements on 20%Pt-Sn/C catalysts, similar to the hydrogen adsorption measurements on 20%Pt: Sn/C catalysts, defect-like site coverages decreased by increasing Sn amount (see Figure 5. 22). Defect-like site coverage values were approximately same for 15:1, 9:1, and 6:1 but it decreased much when 1:1 atomic ratio was attained. The energies of the plateaus decreased when Sn amount increased. These plateaus were completely lost when 1:1 atomic ratio was reached. This behavior was attributed to the loss of low energy sites by adding more Sn. Also, total coverage values reported for carbon monoxide adsorption measurements on these catalysts indicated that when Sn amount increased total coverage values decreased (Table 5.8).

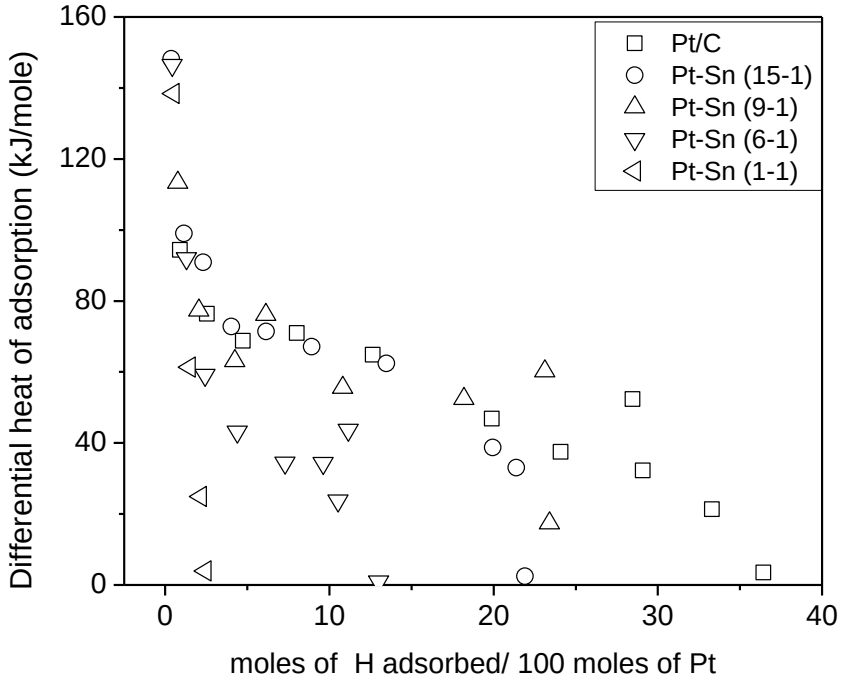

Figure 5. 22 Differential heat of carbon monoxide adsorption measurement results at 323 K on carbon supported 20% Pt:Sn catalysts prepared at 15:1, 9:1, 6:1, 1:1 Pt:Sn atomic ratios

5.5. 4 Electrochemical Measurements

The ethanol electro-oxidation activity was evaluated on the 20%Pt: Sn/C catalysts in the 0.5 M H_2SO_4 solution at 25^oC to investigate the effect of Sn addition in ethanol electro-oxidation activity. Prior to ethanol electro-oxidation measurements, the surface of electrodes was activated and then cyclic voltammetric measurements were performed in the absence of ethanol in 0.5 M H_2SO_4 solution. The cyclic voltammograms which were taken at 0.05 V/s and 0.25 V/s scan rates of 20%Pt:

Sn/C catalysts prepared at 15:1, 9:1, 6:1, and 1:1 Pt-Sn atomic ratios in the 0.5 M H_2SO_4 solution. Furthermore, these measurements on Pt-Sn catalysts were compared with monometallic Pt catalyst and results on these measurements were shown in Figure 5.23. From Figure 5.23, it is clear that Pt/C catalyst and Pt-Sn (15:1)/ C catalyst showed nearly the same activity. In our previous study (in the first part of this study), it was reported that two well resolved peaks (hydrogen adsorption-evolution peaks) for polycrystalline platinum were not observed at low scan rates (0.01 V/s-0.1 V/s). However, these peaks were visible at higher scan rates. For 0.01 V/s and 0.05 V/s, sharp hydrogen adsorption evolution peaks were observed but these sharp peaks were not visible above these scan rates. In our case, for Pt/C and Pt-Sn (15:1)/c catalysts, this situation still exists. However, for Pt-Sn (9:1)/C, Pt-Sn (6:1)/C, and Pt-Sn (1:1)/C catalysts, these peaks were clearly observed at high scan rate (0.25 V/s) and at even small scan rate (0.05 V/s). At hydrogen region, the best current value of hydrogen adsorption-evolution peaks was obtained for Pt-Sn (1:1)/C catalyst. Then, this activity was obtained in the order of Pt-Sn (9:1)/C > Pt-Sn (6:1)/C > Pt-Sn (15:1)/C and Pt /C.

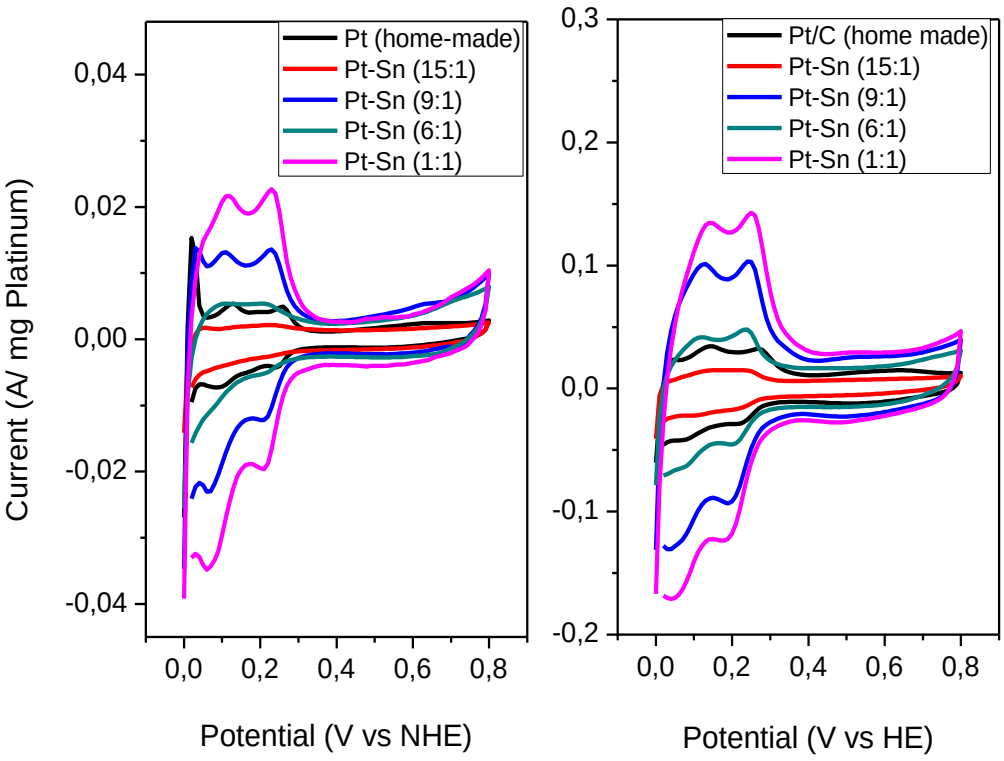

Figure 5. 23 Cyclic voltammogram of carbon supported 20%Pt and 20% Pt:Sn catalysts prepared at 15:1, 9:1, 6:1, 1:1 Pt:Sn atomic ratios (a) in 0.5M H_2SO_4 solution at 0.01 V/s scan rate (b) in 0.5M H_2SO_4 solution at 0.25 V/s scan rate.

Per site activity of these catalysts were determined in 0.5 M sulfuric acid at 0.05 V/s and 0.25 V/s, respectively and presented in Figure 5.24. For both of these measurements, it was observed that the current per site values were nearly the same for Pt/C (home-made) and Pt-Sn (15:1)/C catalysts, which was lower than Pt (9:1)/C, Pt-Sn (6:1)/C, and Pt-Sn (1:1)/C catalysts. Moreover, for Pt (9:1)/C and Pt-Sn (6:1)/C catalysts, the current per site values were also nearly the same. The best current per site hydrogen activity was obtained for Pt-Sn (1:1)/C catalyst.

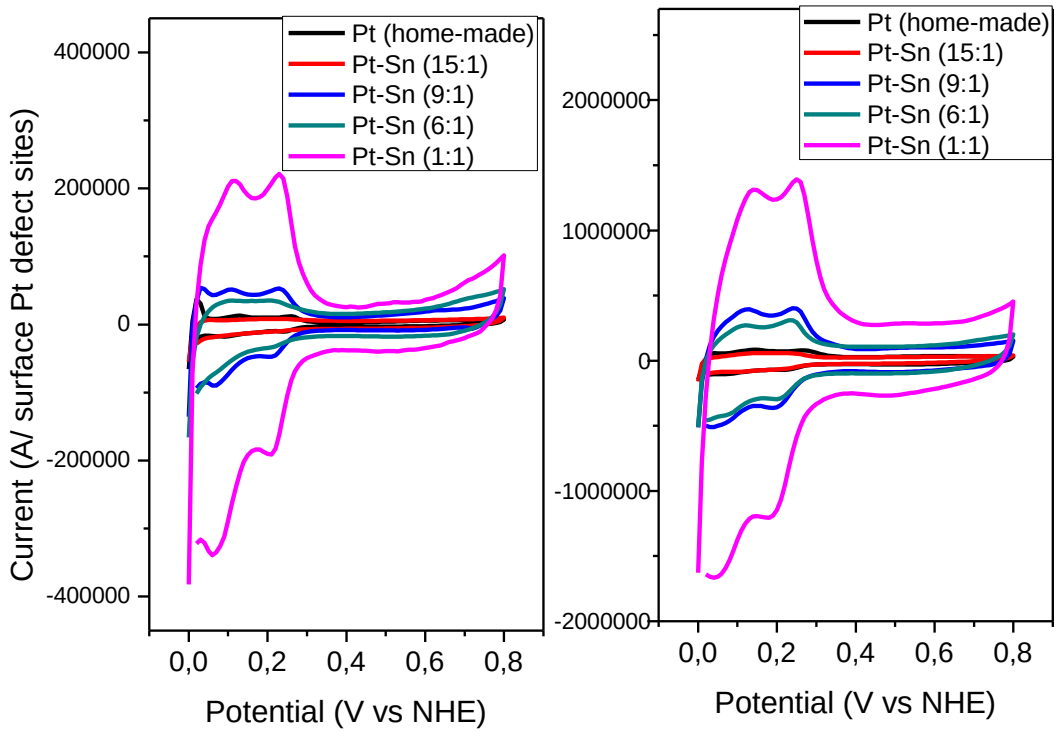

Figure 5. 24 Current per defect site measurements of 20%Pt and 20% Pt:Sn catalysts prepared at 15:1, 9:1, 6:1, 1:1 Pt:Sn atomic ratios (a) in 0.5 M H_2SO_4 solution at 0.05 V/s, (b) in 0.5 M H_2SO_4 solution at 0.25 V/s.

The catalytic activities of 20%Pt: Sn/C catalysts were investigated by cyclic voltammetry in 0.5 M H_2SO_4 and 0.5M ethanol solution and presented in Figure 5. 25. Results on these catalysts indicated the fact that when Pt:Sn atomic ratio decreased 15:1 to 6:1, oxidation current values observed at 0.8 V potential increased, significantly. When Pt: Sn atomic ratio decreased 6:1 to 1:1, a decrease

in oxidation current value was observed. It was obvious that Pt-Sn (6:1)/C catalyst was the most active catalyst for ethanol electro-oxidation reaction.

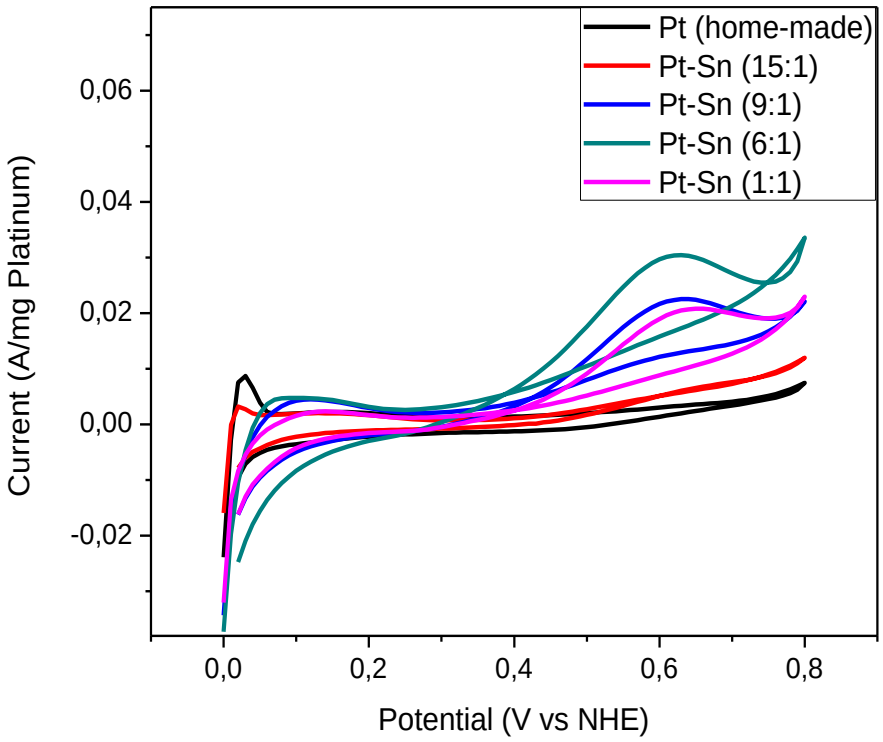

Figure 5. 25 Cyclic voltammograms of carbon supported 20%Pt and 20%Pt:Sn catalysts prepared at 15:1, 9:1, 6:1, 1:1 Pt:Sn atomic ratios in 0.5 M H_2SO_4+ 0.5 M EtOH solution (scan rate: 0.05 V/s).

Poisoning measurements were performed by linear sweep voltammetry technique in 0.5 M H_2SO_4 +0.5 M ethanol solution at 0.05 V/s scan rate to investigate the poisoning capacity of monometallic Pt/C catalyst and bi-metallic Pt-Sn (6:1)/C catalyst. Prior to linear sweep voltammetry measurements, a surface pretreatment was applied on electrode given in Appendix E (Figure E.13). According to this pretreatment, firstly 1.6 V vs NHE constant potential was applied for 30 s and then potential was held constant at 0.0 V vs NHE for 10 s in order to activate the surface before poisoning. In the second part of the pretreatment, The surface of the catalyst was poisoned by holding potential at 0.4 V for 1 s, 10 s, 20 s, 40 s, 60 s, 120 s, 200 s, and 600 s. As a result of these measurements, it was observed that the the current from the poison adsorbed on Pt/C catalyst surface was higher than current value obtained for Pt-Sn (6:1)/C catalyst given in Appendix E (Figure E.14). Furthermore, for Pt-Sn (6:1)/C catalysts, this surface adsorbed material was oxidized at lower potential than one adsorbed on Pt/C catalyts (Figure 5.26). The maximum current values of the surface poisoning material which was accumulated on these catalysts surfaces at varying times was plotted in Figure 5.26. It was observed that for both of these catalysts, poisoning oxidation current increased by increasing time and stayed constant. This behaviour was ascribed as the surface of the catalyst was poisoned completely. All of these outcomes indicated that tin improves the poisoning resistance of Pt catalysts.

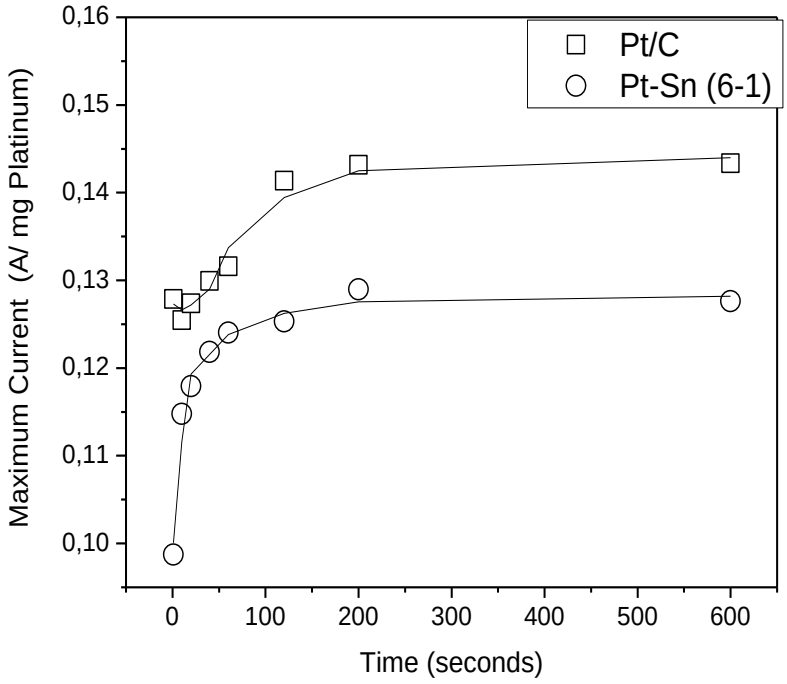

Figure 5. 26 Maximum current values observed 1 V vs NHE vs poisining time obtained from linear sweep voltamogram for 20% Pt/C and Pt-Sn (6:1)/C catalysts in 0.5 M H_2SO_4 + 0.5 M EtOH solution at 0.05 V/s.

5.5. 5 Discussion

The characterization results of 20%Pt: Sn/C catalysts presented so far could be summarized. The ethanol electrochemical activity depends on the Sn content effect and the available Pt sites. Two well resolved peaks for polycrystalline platinum existed at around 0 V potential. It was noted that these peaks could be an evidence of existence of these low energetic sites. It was reported that the peak located at

around 0.2 V is related with Pt (110) crystal surface and the other located at around 0.24 V is related with Pt (100) surface. These peaks were also observed for 20%Pt: Sn/C catalysts. For Pt/C and Pt-Sn (15:1)/c catalysts, these peaks were not as visible as ones for Pt-Sn (9:1)/C, Pt-Sn (6:1)/C, and Pt-Sn (1:1)/C catalysts. These peaks were clearly observed at high scan rate (0.25 V/s) and at even small scan rate (0.05 V/s). At hydrogen region, the best current value of hydrogen adsorption-evolution peaks was obtained for Pt-Sn (1:1)/C catalyst. Then, this activity was obtained in the order of Pt-Sn (9:1)/C > Pt-Sn (6:1)/C > Pt-Sn (15:1)/C and Pt /C. During the preparation process, Pt-Sn alloy, Pt_3Sn, and Sn and Pt oxides could be formed and the relative amounts of these species affects electrochemical activity. Considering the enthalpies of formation diagram of solid alloys of the platinum-tin system (Figure A.1), one could conclude that during the preparation process of Pt-Sn (15:1), Pt-Sn (9:1), and Pt-Sn (6:1) could be formed from Pt and Pt_3Sn. Considering the Pt-Sn molar ratios, Pt/C catalyst and Pt-Sn (15:1) catalysts were so close to each other and these catalysts includes Pt more Pt_3Sn . Thus, the current per site activity for Pt-Sn (15:1) was more like Pt/C catalyst. On the other hand, considering Pt-Sn (9:1) and Pt-Sn (6:1) catalysts, the Pt-Sn molar ratios are close for these catalysts. For these catalysts, also current per site activities were nearly same, which was greatly higher than Pt-Sn (15:1) and Pt/C catalysts due to the fact that Pt_3Sn phase was more dominant than Pt for Pt-Sn (9:1) and Pt-Sn (6:1) catalysts, which improved the catalyst activity. Pt-Sn (1:1) was completely different region on phase diagram: it only consisted from Pt-Sn phase. Microcalorimetric data could help to prove this hypothesis as following: the microcalorimetric measurements on Pt-Sn (1:1)/ C catalysts indicated that that the energies of plateaus, the indication of low energetic sites, decreased with increased tin content. These plateaus were lost for Pt: Sn (1:1)/C catalyst. The decrease of the energies of plateues could be interpreted as low energetic sites were lost one by one. Not all of the low energetic sites were lost when the appropriate amount of Sn

added to form Pt: Sn (15:1)/C catalyst. This behavior was observed especially for CO adsorption. It was observed that further increments in the Sn amount resulted further decrement of low energetic sites.

Pt-Sn (6:1)/C catalyst was better than Pt-Sn (1:1)/C catalyst and also had the highest ethanol electro-oxidation activity because Pt-Sn (6:1)/C catalyst had the highest Pt-Sn molar ratio which was close to Pt_3Sn. Colmati et al. [29] reported that Pt_3Sn phase improved the activity of ethanol electro-oxidation reaction rather than Pt-Sn phase. For that study, catalysts were thermally treated at 200^oC and 500^oC because thermal treatment has a significant effect on the particle size and the crystal structure of catalysts. Thermal treatment at 200^oC temperature gave rise to the formation of a predominant phase of cubic Pt_3Sn and, to a lesser extent, a hexagonal Pt-Sn phase. The amount of the hexagonal Pt-Sn phase as well as the particle size increased with increasing thermal treatment temperature. The higher electro-chemical activity was obtained in the presence of cubic Pt_3Sn [13]. As a conclusion for Pt:Sn (1:1) catalyst hexagonal Pt-Sn phases could be dominant so the electrochemical activity low hydrogen and carbon monoxide total coverages were observed. On the other hand, for Pt: Sn (6:1) cubic Pt_3Sn phase could be dominant because the higher electrochemical activity is obtained for this catalyst site.

Poisoning measurements were performed by linear sweep voltammetry technique in 0.5 M H_2SO_4 +0.5 M ethanol solution at 0.05 V/s scan rate to investigate the poisoning capacity of monometallic Pt/C catalyst and bi-metallic Pt-Sn (6-1)/C catalyst. As as result of these measurements it was observed that Pt-Sn (6:1)/C catalyst was more resistant compared to Pt catalyst.

5. 6 THE EFFECT OF TIN OXIDE PHASE

The oxide phase of bimetallic catalysts indicates more electro-catalytic activity than alloy forms, as it was reported in previous chapters. In Chapter 2, we reported that although there are many research studies on oxide phases of bi-metallic catalysts (SnO_x, RuO_x, Co_x, SiO_2, CeO_2, MnO, and NiO promoted Pt catalysts) to investigate the electrochemical activities, "how and why oxide phase of bimetallic catalyst improves electro-oxidation activity?" were still awaiting questions.

Herein, it is our main concern "How and why the oxides phase of Sn promoted Pt bimetallic catalysts increase ethanol electro-oxidation activity?". Thus, XRD, XPS, the microcalorimetric measurements of carbon monoxide and hydrogen, and cyclic voltammetric measurements were performed on 20%Pt:SnO_2/C catalysts prepared at 6:1 and 1:1 Pt:Sn atomic ratios. These results were compared with the ones obtained for 20% Pt/C monometallic catalyst and 20%Pt-Sn (6:1)/C bi-metallic catalyst. The activation of electrode surface was performed in 0.5 M H_2SO_4 by cycling potential between 0.0 to 0.8 V at 0.05 V/s scan rate before starting electrochemical measurements. Cyclic voltammograms of 20%Pt-SnO_2 (6:1)/C and 20%Pt-SnO_2 (1:1)/C catalysts were taken in 0.5 M H_2SO_4 solution on 20%Pt-Sn/C catalysts. In order to investigate ethanol electro-oxidation activity, cyclic voltammograms of 20%Pt-SnO_2 (6:1)/C and 20%Pt-SnO_2 (1:1)/C catalysts were also taken in 0.5 M H_2SO_4 + 0.5 M Ethanol solution at the potentials between 0.0 and 0.8 V.

5.6. 1 XRD Results

XRD patterns of the 20%Pt-SnO_2 (6:1)/C and 20%Pt-SnO_2 (1:1)/C catalysts were given in Appendix C (Figure C.5). Furthermore, the XRD patterns of 20%Pt-SnO_2 (1:1)/C and 20%Pt-Sn (1:1)/C catalysts were given in Appendix C (Figure C.6) to

compare the differences between the oxide catalyst and the alloy catalyst. At around 25^{o} and Pt (111), (200), (220) and (311) planes were detected from XRD patterns of these catalysts. Furthermore, peaks at around 34° and 52° were related to tin oxide. Tin oxide phase was more significant on the XRD patterns of SnO_2 promoted catalysts than Pt-Sn catalysts. The diffraction peaks of Pt are clearly broadened with increasing tin content. The mean Pt particle diameters of the Pt-Sn/C catalysts were calculated from the Pt (111) diffraction peak via the Scherer equation [24] and given in Table 5.9. The mean Pt particle diameter decreases from 3.6 to 1.2 nm with increasing tin content. This phenomenon could be attributed to Pt-Pt ensembles were separated by tin particles inhibiting the agglomeration of Pt particles during the synthesis process. The mean Pt particle diameter of the Pt-SnO_2 catalyst were also calculated by Scherer equation and given in Table 5.9. It was observed that when Sn amount increased 6:1 to 1:1 particle size decreased 2.5 nm to 2 nm.

5.6. 2 XPS Results

Surface composition investigation on 20%Pt/C (pH=11), 20%Pt-SnO_2 (6:1)/C, and 20%Pt-SnO_2 (1:1)/C catalysts was performed by means of XPS. The XPS spectra of 20%Pt/C (pH=11), 20%Pt-SnO_2 (6:1)/C, and 20%Pt-SnO_2 (1:1)/C catalysts were given in Appendix C (Figure C.11). C 1s peak was used to correct XRD spectra, which the most intense component was set at 284.6 eV. and used as internal reference. C 1s spectra was given in Appendix C (Figure C.7).

In Appendix C (Figure C.14), the Pt 4f regions of the XPS spectrum of the Pt/C (pH=11), 20%Pt-SnO_2 (6:1)/C, and 20%Pt-SnO_2 (6:1)/C, and 20%Pt-SnO_2 (1:1)/C were represented. There is a negative shift via increase of tin amount. Thus, it could be concluded that oxidation state of 20%Pt-SnO_2 (1:1)/C was Pt^0.

The Sn 3d core level doublet spectra of 20% Pt-Sn/C catalysts were demonstrated in Appendix C (Figure C.15). Similarly, it was observed that there is a negative shift the increase of tin amount. This could be attributed that 20%Pt-SnO_2 (1:1)/C have more zero valence compared to other ones. The oxidation state of tin was higher for 20%Pt-SnO_2 (6:1)/C than 20%Pt-Sn (1:1)/C catalyst.

5.6. 3 Gas Phase Microcalorimetric Measurement Results

Gas phase hydrogen and carbon monoxide adsorption measurements were performed on 20% Pt-SnO_2 (6:1) and 20% Pt-SnO_2 (1:1) catalysts at 323 K by using a Tian-Calvet type heat flow calorimeter and were given in Figure 5.27 and Figure 5. 28. The initial heats, defect-like sites coverages, and saturation coverages were given in Table 5.9.

Table 5. 9 The surface site densities as measured by CO and hydrogen adsorption calorimetry on carbon supported (20%Pt-loading) Pt-Sn and Pt-SnO_2 catalysts.

Catalyst	Q^0 (kJ/mole)		$\theta^{defects}$ (mol H or CO/ mol Pt)		$\theta^{saturation}$ (mol H or CO/ mol Pt)	
	H_2	CO	H/Pt	CO/Pt	H/Pt	CO/Pt
Pt-SnO_2 (6:1)	150	400	0.06	0.04	0.24	0.16
Pt-SnO_2 (1:1)	160	500	0.04	0.02	0.11	0.02
Pt-Sn (1:1)	140	300	0.02	0.02	0.03	0.02
Pt	89	330	0.07	0.05	0.36	0.24

Hydrogen adsorption measurements on 20% Pt-SnO_2 (6:1) and 20% Pt-SnO_2 (1:1) catalysts indicated that the increase in tin amount resulted in a decrease in

saturation coverages (see Figure 5. 27). It is obvious that total coverage and defect-like coverage decreased when tin amount increased. Furthermore, when tin amount increased, the energies of plateaus decreased as it was observed for Pt-Sn alloy catalysts. The most distinguished difference was that there was still a plateau for Pt-SnO_2 (1:1) catalyst unlike Pt-Sn (1:1) alloy catalyst.

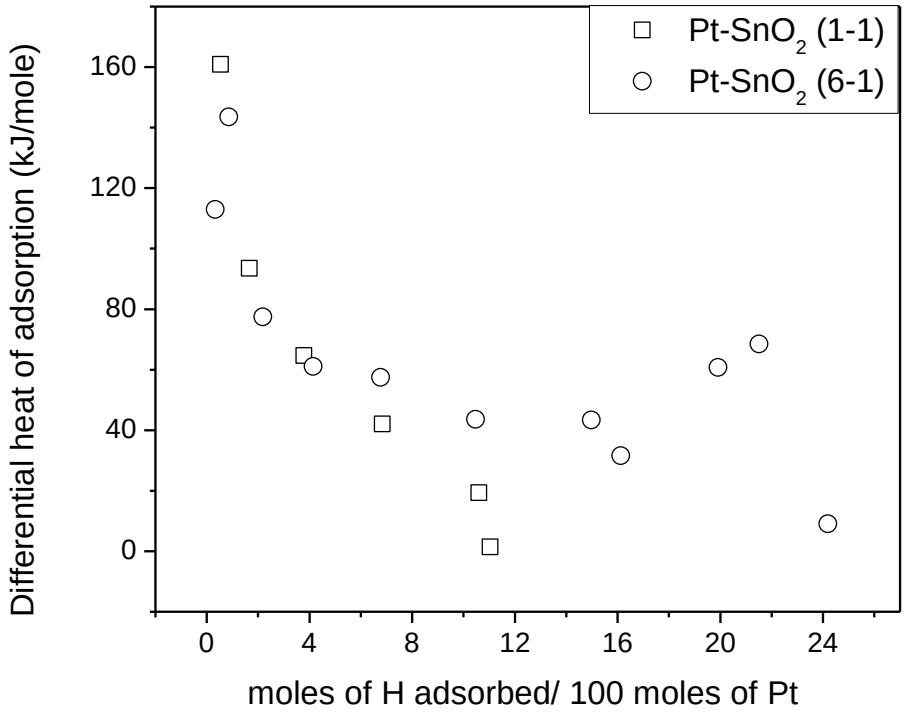

Figure 5. 27 Differential heat of hydrogen adsorption measurements results at 323 K on carbon supported 20%Pt and 20% Pt: SnO_2 catalysts prepared at 6:1 and 1:1 Pt: Sn atomic ratios.

Carbon monoxide chemisorption measurements on 20% Pt-SnO_2 (6:1) and 20% Pt-SnO_2 (1:1) catalysts were given in Figure 5.28. These results indicated that when the Pt: Sn atomic ratio decreased to 6:1 to 1:1 defect-like site coverage decreased. Total coverage values reported for carbon monoxide adsorption measurements on both type of catalysts also indicated that when tin amount increased total coverage values decreased (Table 5.9).

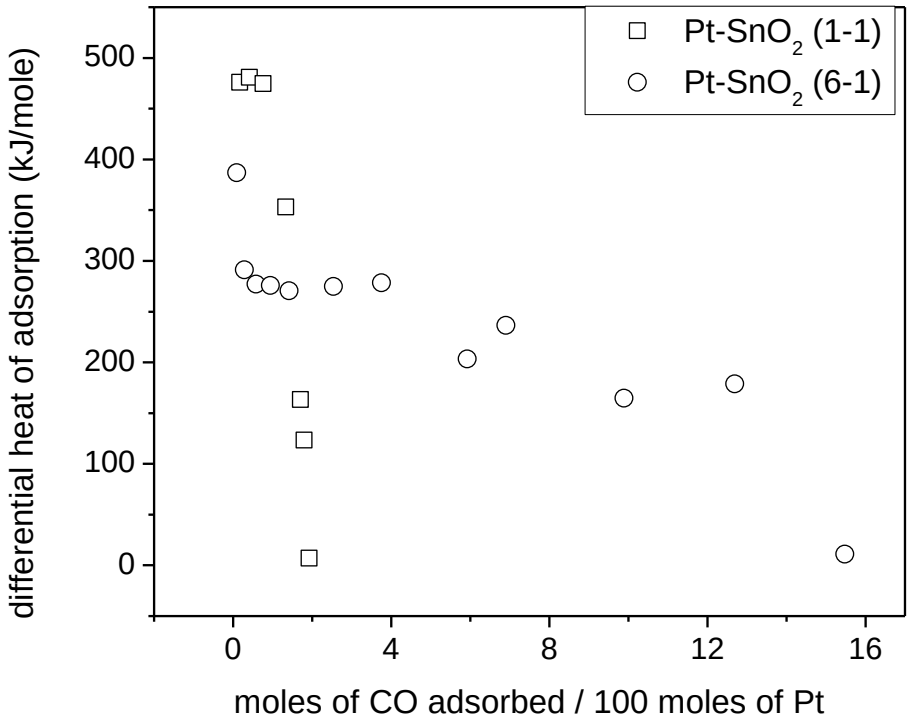

Figure 5. 28 Differential heat of carbon monoxide adsorption measurements results at 323 K on carbon supported 20%Pt and 20% Pt: SnO_2 catalysts prepared at 6:1 and 1:1 Pt: Sn atomic ratios.

The initial heats of adsorption values reported in Table 5.9 indicated that Pt-SnO_2 catalysts had higher initial heat of carbon monoxide values like the case observed for hydrogen chemisorption measurements. The initial heats of carbon monoxide adsorption values for Pt-Sn alloy catalysts were slightly different than the value measured for home made catalyst. However these initial heats of carbon monoxide values for Pt-SnO_2 catalysts were measured as ~ 470 kJ/mol (greatly different than the values measured ~ 310 kJ/mole for the alloy catalysts and homemade catalysts). This significant difference could be the indicative of the effect of chemical state. In this case, by the help of oxide phases surface oxidation of CO occurred. Furthermore, the energies of plateau were smaller for Pt-SnO_2 (6:1) catalyst than Pt/C homemade catalyst. These plateaus were completely lost for Pt-SnO_2 (1:1) catalysts.

5.6. 4 Electrochemical Characterization Results

The ethanol electro-oxidation activity was evaluated on the carbon supported Pt-SnO_2 catalysts in the 0.5 M H_2SO_4 solution to investigate the effect of Sn addition and the effect of chemical state of Sn in ethanol electro-oxidation activity. Prior to ethanol electro-oxidation measurements, the surface of electrodes was activated and then cyclic voltammetric measurements were performed in the absence of ethanol in 0.5 M H_2SO_4 solution. The cyclic voltammogram measurements performed on carbon supported 20%Pt-SnO_2 prepared at 6:1 and 1:1 atomic ratios catalysts in 0.5 M H_2SO_4 solution indicated that peaks at hydrogen adsorption-desorption region similar to the polycrystalline platinum catalysts. For 20% Pt-SnO_2/C catalyst, cyclic voltammogram was taken at different scan rates in 0.5 M H_2SO_4 solution. It was observed that these hydrogen adsorption-desorption current becomes more visible by increasing scan rate due to overcome external diffusion limitations. The voltammogram curve for ethanol electro-oxidation on Pt-SnO_2 (6:1)/C and Pt-SnO_2 (1:1)/C catalyst were presented in Figure 5.29. Oxidation

current values observed at 0.6 V potential for Pt-SnO_2 (6:1)/C catalyst were higher than Pt-SnO_2 (1:1)/C catalyst. The comparison of oxide promoted catalysts and Pt-Sn catalysts were given in Figure 5.29 and Figure 5.30. It was observed that Pt-SnO_2 (6:1)/C catalyst showed higher ethanol electro-oxidation activity than Pt-Sn (6:1)/C catalysts. Furthermore, the hydrogen adsorption desorption peak for Pt-SnO_2 (6:1)/C catalyst is more clear than Pt-Sn (6:1)/C catalyst in sulfuric acid voltammogram.

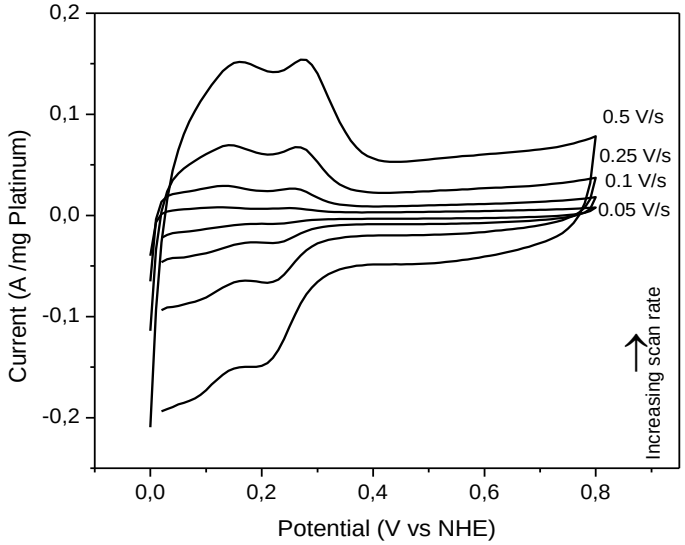

Figure 5. 29 Cyclic voltammogram of 20%Pt:SnO_2(6:1)/C in 0.5 M H_2SO_4 solution at 0.05 V/s, 0.1 V/s, 0.25 V/s, 0.5V/s.

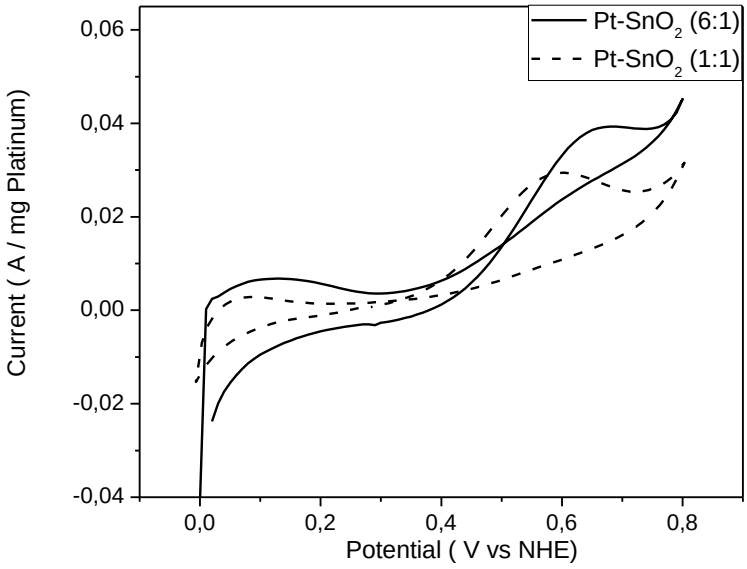

Figure 5. 30 Cyclic voltammogram of 20%Pt:SnO_2(6:1)/C and 20%Pt:SnO_2(1:1)/C in 0.5 M H_2SO_4 + 0.5 M EtOH solution at 0.05 V/s.

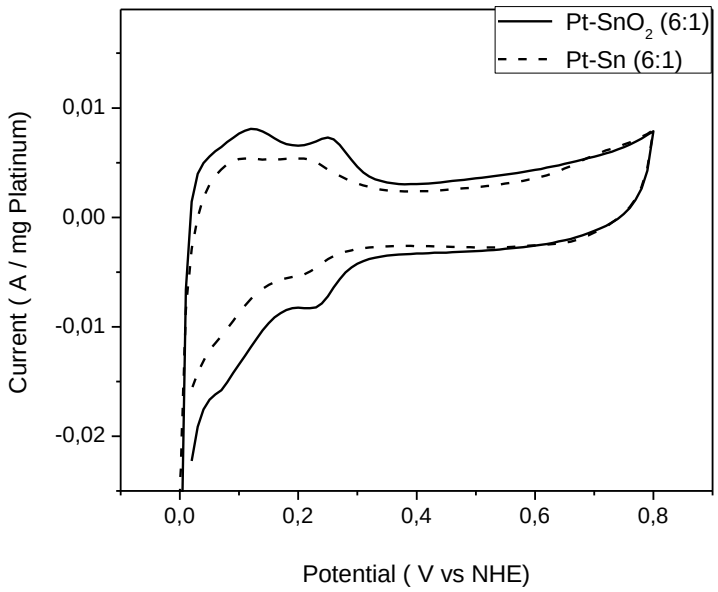

Figure 5. 31 Cyclic voltammogram of 20%Pt:SnO_2(6:1)/C and 20%Pt:Sn (6:1)/C in 0.5 M H_2SO_4 solution at 0.05 V/s.

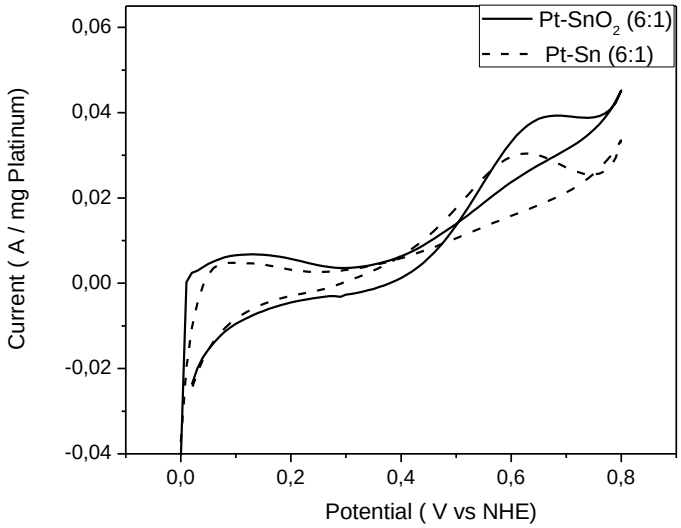

Figure 5. 32 Cyclic voltammogram of 20%Pt:SnO_2(6:1)/C and 20%Pt:Sn (6:1)/C in 0.5 M H_2SO_4 + 0.5 M EtOH solution at 0.05 V/s.

5.6. 5 Discussion

In this chapter, the effect of tin oxide on ethanol electro-oxidation activity was investigated. From the XRD pattern of 20% Pt-SnO_2 (6:1) and 20% Pt-SnO_2 (1:1) catalysts, it was observed that tin oxide was formed. Furthermore, the initial heat of adsorption values of 20% Pt-SnO_2 (6:1) and 20% Pt-SnO_2 (1:1) catalysts obtained from CO chemisorptions was 160 kJ/mol which was greater than 20%Pt monometallic and 20% Pt-Sn/C catalysts. This difference could be attributed to the fact that surface adsorbed CO was oxidized on the surface by the help of lattice oxygen of tin. In conclusion, the presence of tin oxide increased the initial heat of adsorption 160 kJ/mole above which is heat of CO oxidation reaction value. Furthermore, the energies of plateau were smaller for Pt-SnO_2 (6:1) catalyst than Pt/C homemade catalyst. These plateaus were completely lost for Pt-SnO_2 (1:1) catalysts. Finally, it was observed that oxide phase of tin improves the ethanol electro-oxidation activity. The voltammogram curve for ethanol electro-oxidation on Pt-SnO_2 (6:1)/C and Pt-SnO_2 (1:1)/C catalyst were presented in Figure 5.29. Oxidation current values observed at 0.6 V potential for Pt-SnO_2 (6:1)/C catalyst were higher than Pt-SnO_2 (1:1)/C catalyst. Furthermore, it was observed that Pt-SnO_2 (6:1)/C catalyst showed higher ethanol electro-oxidation activity than Pt-Sn (6:1)/C catalysts. The hydrogen adsorption desorption peak for Pt-SnO_2 (6:1)/C catalyst was much more visible than Pt-Sn (6:1)/C catalyst in sulfuric acid voltammogram, which could be attributed to the fact that there is low contact between Pt and SnO_2 particles.

5. 7 CHAPTER SUMMARY

In this dissertation, different parameters affecting the ethanol electro-oxidation are being investigated such as the effect of platinum particle size, the effect of catalyst

support, the effect of second metal addition, the effect of oxide phase of tin. Firstly, adsorption calorimetry measurements were conducted on monometallic (1%Pt, 2%Pt, and 5%Pt) and bi-metallic (5% Pt-Sn) γ-Al_2O_3 supported Pt catalysts to investigate the effect of catalyst loading and the effect of Sn addition. It was observed that when Pt loading increased saturation coverage of hydrogen and carbon monoxide adsorption decrease due to agglomeration of platinum particles at high catalyst loading. Thus, the dispersion of platinum particles at high metal loading catalysts was low. The effect of second metal addition was also investigated both on γ-Al_2O_3 supported Pt catalysts: It was observed that by the increasing amount of tin, saturation coverage values decreased. The intermediate heats remained same for Pt-Sn catalysts.

Secondly, carbon supported mono-metallic and bi metallic catalysts were prepared by polyol method. Before starting measurements on these catalysts, ethanol electro-oxidation reaction was investigated on 20% Pt/C (E-Tek) catalyst to assess the ethanol electro-oxidation reaction and to find out optimum conditions. It was reported that total current values increased by increasing scan rate. It was observed that when scan rate altered the total current changed because the thickness of the diffusion layer changed. Furthermore, it was observed that at high scan rates 1 V/s it was impossible to oxidize ethanol the fact that time taken to record would be short not enough to oxidize ethanol at 1 V/s high scan rate.

Platinum particle size investigations indicated that depending on the shape of the catalyst particles, a different number of defect sites are present on the catalyst particles, controlling catalytic activity. Current per site activities of these Pt/C (E-Tek), Pt/C (pH=11), and Pt/C (pH=5) catalysts indicated that current per sites values for Pt/C (pH=5) catalyst were significantly lower than the ones measured for 20% Pt/C (E-Tek) and Pt/C (pH=11) catalysts at low scan rates. However, the

current per site values for Pt/C (pH=5) catalyst were nearly the same for 20% Pt/C (E-Tek) and Pt/C (pH=11) catalysts for sulfuric acid and ethanol electro-oxidation measurements at high scan rates. It can be concluded that current per site activities were nearly the same for 20% Pt/C (E-Tek), Pt/C (pH=11), and Pt/C (pH=5) catalysts far above diffusion limitation region. These results could be interpreted as the ethanol electro-oxidation reaction and sulfuric acid electro-oxidation reaction takes place at the defects sites unless diffusion limitations play role in the electro-oxidation reaction.

CNTs having high surface area compared to conventional carbon was used as support to explore the effect of carbon support in ethanol electro-oxidation activity on 20% Pt/C (E-Tek), 20% Pt/commercial CNTs, and 20%Pt/home-made CNTs catalyst. It was found that the electrocatalytic activities per Pt surface site values were nearly the same regardless of the carbon support used. Under the conditions used in this study, ethanol electro-oxidation reaction depended only on the metal dispersions and support did not have any effect.

The effect of tin addition on ethanol electro-oxidation reaction were conducted on Pt:Sn/C (20% Pt loading) catalysts. It was reported that the ethanol electrochemical activity depends on the Sn content effect and the available Pt sites. When Sn amount increased total coverage values decreased and the electrochemical activity increased. Pt:Sn (6:1)/C catalysts showed the highest ethanol electro-oxidation activity. Low energetic sites are partly blocked by addition of Sn. When Pt:Sn 1:1 atomic ratio was reached all of the low energetic sites were lost. Thus, Pt-Sn (6:1)/C catalyst was better than Pt-Sn (1:1)/C catalyst and also had the highest ethanol electro-oxidation activity because Pt-Sn (6:1)/C catalyst had the highest Pt-Sn molar ratio which was close to Pt_3Sn. As a conclusion for Pt:Sn (1:1) catalyst hexagonal Pt-Sn phases could be dominant so

the electrochemical activity low hydrogen and carbon monoxide total coverages were observed. On the other hand for Pt:Sn (6:1) cubic Pt_3Sn phase could be dominant because the higher electrochemical activity is obtained for this alloy catalyst. Poisoning measurements on monometallic Pt/C catalyst and bi-metallic Pt-Sn (6:1)/C catalyst indicated Pt-Sn (6:1)/C catalyst was more resistant compared to Pt catalyst.

The effect of tin oxide on ethanol electro-oxidation activity was investigated on 20% Pt-SnO_2 catalysts. The formation of tin oxide on these catalysts was observed from both XRD and XPS spectra. Furthermore, the initial heats of adsorption values of 20% Pt-SnO_2 (6:1) and 20% Pt-SnO_2 (1:1) catalysts obtained from CO chemisorptions were 160 kJ/mol greater than 20%Pt monometallic and 20% Pt-Sn/C catalysts. This difference could be attributed to the fact that surface adsorbed CO was oxidized on the surface by the help of lattice oxygen of tin. In conclusion, the presence of tin oxide increased the initial heat of adsorption 160 kJ/mole above which was heat of CO oxidation reaction value. Pt-SnO_2 (6:1)/C catalyst showed higher ethanol electro-oxidation activity than Pt-Sn (6:1)/C catalysts. Furthermore, the hydrogen adsorption desorption peak for Pt-SnO_2 (6:1)/C catalyst was more clear than Pt-Sn (6:1)/C catalyst in sulfuric acid voltammogram, which could be attributed to the fact that there was low contact between Pt and SnO_2 particles.

CHAPTER 6

CONCLUSIONS

The aim of this study was to investigate the role of defects and the role of Sn in relation to defects as a co-catalyst in ethanol electro-oxidation reaction. In experimental study, the population of defects was determined by microcalorimetry. Furthermore, electro-oxidation activity measurements were performed by cyclic voltammetry measurements. Firstly, the different supports were used to understand whether the support properties affect the properties of the metal deposited. It was shown that electrocatalytic activities per Pt surface site values were nearly the same regardless of the carbon support used. Under the conditions used in this study, ethanol electro-oxidation reaction depended only on the metal dispersions and support did not have any effect. Then, the effect of particle size on ethanol electro-oxidation reaction was explored . Platinum particle size investigations indicated current per site activities were nearly the same for 20% Pt/C (E-Tek), Pt/C (pH=11), and Pt/C (pH=5) catalysts far above diffusion limitation region. These results could be interpreted as the ethanol electro-oxidation reaction and sulfuric acid electro-oxidation reaction takes place at the defects sites unless diffusion limitations play role in the electro-oxidation reaction. Finally, the role of tin relation to defects was studied. We found that the ethanol electrochemical activity depends on the Sn content effect and the available Pt sites.

Pt-Sn (6:1)/C catalyst was better than Pt-Sn (1:1)/C catalyst and also had the highest ethanol electro-oxidation activity because Pt-Sn (6:1)/C catalyst had the highest Pt-Sn molar ratio which was close to Pt_3Sn. As a conclusion for Pt:Sn (1:1) catalyst hexagonal Pt-Sn phases could be dominant so the electrochemical activity low hydrogen and carbon monoxide total coverages were observed.

REFERENCES

[1] statistical review of world energy 2010, http://www.bp.com/productlanding, (last accessed 3th September, 2010)

[2] Hubbert peak theory, http://en.wikipedia.org/wiki/Hubbert_peak_theory, (last accessed 3th September, 2010)

[3] Kyoto protocol, http://en.wikipedia.org/wiki/Kyoto_Protocol, (last accessed 3th September, 2010)

[4] W.J. Zhou, S.Q. Song, W.Z. Li, Z.H. Zhou, G.Q. Sun, Q. Xin, S. Douvartzides, P. Tsiakaras, Direct ethanol fuel cells based on PtSn anodes: the effect of Sn content on the fuel cell performance, Journal of Power Sources, 140 (2005) 50-58.

[5] A.J. Bard, L.R. Faulkner, Electrochemical Methods Fundamentals and Applications, 2001.

[6] A.K. Shukla, M.K. Ravikumar, K.S. Gandhi, Direct methanol fuel cells for vehicular applications, in: 3rd Indo-German Seminar on Modern Aspects of Electrochemistry, Bangalore, India, 1996, pp. 117-122.

[7] K.M. McGrath, G.K.S. Prakash, G.A. Olah, Direct methanol fuel cells, Journal of Industrial and Engineering Chemistry, 10 (2004) 1063-1080.

[8] U.B. Demirci, Direct liquid-feed fuel cells: Thermodynamic and environmental concerns, Journal of Power Sources, 169 (2007) 239-246.

[9] U.B. Demirci, Theoretical means for searching bimetallic alloys as anode electrocatalysts for direct liquid-feed fuel cells, Journal of Power Sources, 173 (2007) 11-18.

[10] A. Kundu, J.H. Jang, J.H. Gil, C.R. Jung, H.R. Lee, S.H. Kim, B. Ku, Y.S. Oh, Micro-fuel cells - Current development and applications, Journal of Power Sources, 170 (2007) 67-78.

[11] K. Xu, D.T. Pierce, A. Li, J.X. Zhao, Nanocatalysts in direct methanol fuel cell applications, Synthesis and Reactivity in Inorganic Metal-Organic and Nano-Metal Chemistry, 38 (2008) 394-399.

[12] X.W. Yu, P.G. Pickup, Recent advances in direct formic acid fuel cells (DFAFC), Journal of Power Sources, 182 (2008) 124-132.

[13] E. Kjeang, N. Djilali, D. Sinton, Microfluidic fuel cells: A review, Journal of Power Sources, 186 (2009) 353-369.

[14] D. Kareemulla, S. Jayanti, Comprehensive one-dimensional, semi-analytical, mathematical model for liquid-feed polymer electrolyte membrane direct methanol fuel cells, Journal of Power Sources, 188 (2009) 367-378.

[15] G. Andreadis, P. Tsiakaras, Ethanol crossover and direct ethanol PEM fuel cell performance modeling and experimental validation, Chemical Engineering Science, 61 (2006) 7497-7508.

[16] A.Y. Leykin, O.A. Shkrebko, M.R. Tarasevich, Ethanol crossover through alkali-doped polybenzimidazole membrane, Journal of Membrane Science, 328 (2009) 86-89.

[17] V. Paganin, E. Sitta, T. Iwasita, W. Vielstich, Methanol crossover effect on the cathode potential of a direct PEM fuel cell, Journal of Applied Electrochemistry, 35 (2005) 1239-1243.

[18] G.C. Li, P.G. Pickup, Analysis of performance losses of direct ethanol fuel cells with the aid of a reference electrode, Journal of Power Sources, 161 (2006) 256-263.

[19] A.S. Arico, P. Creti, E. Modica, G. Monforte, V. Baglio, V. Antonucci, Investigation of direct methanol fuel cells based on unsupported Pt-Ru anode catalysts with different chemical properties, in: 3rd Electrocatalysis Meeting (ECS 99), Portoroz, Slovenia, 2000, pp. 4319-4328.

[20] E. Elsarrag, Experimental study of using fuel cells in dwellings for energy saving lighting and other low power applications, International Journal of Hydrogen Energy, 33 (2008) 4427-4432.

[21] S.Q. Song, W.J. Zhou, Z.H. Zhou, L.H. Jiang, G.Q. Sun, Q. Xin, V. Leontidis, S. Kontou, P. Tsiakaras, Direct ethanol PEM fuel cells: The case of platinum based anodes, International Journal of Hydrogen Energy, 30 (2005) 995-1001.

[22] F. Vigier, S. Rousseau, C. Coutanceau, J.M. Leger, C. Lamy, Electrocatalysis for the direct alcohol fuel cell, in: 12th International Symposium on Relations between Homogeneous and Heterogeneous Catalysis, Florence, ITALY, 2005, pp. 111-121.

[23] A.O. Neto, E.G. Franco, E. Arico, M. Linardi, E.R. Gonzalez, Electro-oxidation of methanol and ethanol on Pt-Ru/C and Pt-Ru-Mo/C electrocatalysts prepared by Bonnemann's method, in: International Workshop on Interfaces: Ceramic and metal Interfaces: Control at the Atomic Level, Oviedo, Spain, 2002, pp. 2987-2992.

[24] K.G. Stanley, Q.M.J. Wu, T. Vanderhoek, S. Nikumb, Fabrication of a micromachined direct methanol fuel cell, in: W. Kinsner, A. Sebak, K. Ferens (Eds.) IEEE Canadian Conference on Electrical and Computer Engineering, Winnipeg, Canada, 2002, pp. 450-454.

[25] L.P.L. Carrette, K.A. Friedrich, M. Huber, U. Stimming, Improvement of CO tolerance of proton exchange membrane (PEM) fuel cells by a pulsing technique, in: Annual Meeting of the Deutsche-Bunsen-Gasellschaft-fur-Physikakusche-Chemie, Wurzburg, Germany, 2000, pp. 320-324.

[26] Y.S. Li, T.S. Zhao, Z.X. Liang, Performance of alkaline electrolyte-membrane-based direct ethanol fuel cells, Journal of Power Sources, 187 (2009) 387-392.

[27] E. Antolini, Catalysts for direct ethanol fuel cells, Journal of Power Sources, 170 (2007) 1-12.

[28] E. Antolini, F. Colmati, E.R. Gonzalez, Effect of Ru addition on the structural characteristics and the electrochemical activity for ethanol oxidation of carbon supported Pt-Sn alloy catalysts, Electrochemistry Communications, 9 (2007) 398-404.

[29] F. Colmati, E. Antolini, E.R. Gonalez, Ethanol oxidation on carbon supported Pt-Sn electrocatalysts prepared by reduction with formic acid, Journal of the Electrochemical Society, 154 (2007) B39-B47.

[30] M. Cimenti, J.M. Hill, Direct utilization of ethanol on ceria-based anodes for solid oxide fuel cells, Asia-Pacific Journal of Chemical Engineering, 4 (2009) 45-54.

[31] M. Cimenti, J.M. Hill, Thermodynamic analysis of solid oxide fuel cells operated with methanol and ethanol under direct utilization, steam reforming, dry reforming or partial oxidation conditions, Journal of Power Sources, 186 (2009) 377-384.

[32] R. Muccillo, E.N.S. Muccillo, F.C. Fonseca, D.Z. de Florio, Characteristics and performance of electrolyte-supported solid oxide fuel cells under ethanol and hydrogen, Journal of the Electrochemical Society, 155 (2008) B232-B235.

[33] W.J. Zhou, S.Q. Song, W.Z. Li, G.Q. Sun, Q. Xin, S. Kontou, K. Poulianitis, P. Tsiakaras, Pt-based anode catalysts for direct ethanol fuel cells, in: 14th International Conference on Solid State Ionics, Monterey, CA, 2003, pp. 797-803.

[34] W.M. Chen, G.Q. Sun, Z.X. Liang, Q. Mao, H.Q. Li, G.X. Wang, Q. Xin, H. Chang, C.H. Pak, D.Y. Seung, The stability of a PtRu/C electrocatalyst at anode potentials in a direct methanol fuel cell, Journal of Power Sources, 160 (2006) 933-939.

[35] H.S. Liu, C.J. Song, L. Zhang, J.J. Zhang, H.J. Wang, D.P. Wilkinson, A review of anode catalysis in the direct methanol fuel cell, Journal of Power Sources, 155 (2006) 95-110.

[36] D.R. Rolison, P.L. Hagans, K.E. Swider, J.W. Long, Role of hydrous ruthenium oxide in Pt-Ru direct methanol fuel cell anode electrocatalysts: The importance of mixed electron/proton conductivity, in: Symposium on Electrochemistry at Nanostructed Materials, at the 215th Meeting of the American-Chemical-Society, Dallas, Texas, 1998, pp. 774-779.

[37] F.L.S. Purgato, P. Olivi, J.M. Leger, A.R. de Andrade, G. Tremiliosi, E.R. Gonzalez, C. Lamy, K.B. Kokoh, Activity of platinum-tin catalysts prepared by the Pechini-Adams method for the electrooxidation of ethanol, Journal of Electroanalytical Chemistry, 628 (2009) 81-89.

[38] Y.L. Guo, Y.Z. Zheng, M.H. Huang, Enhanced activity of PtSn/C anodic electrocatalyst prepared by formic acid reduction for direct ethanol fuel cells, Electrochimica Acta, 53 (2008) 3102-3108.

[39] B. Hoyos, C. Sanchez, J. Gonzalez, Pt-based anode catalysts for direct ethanol fuel cells, Dyna-Colombia, 74 (2007) 195-202.

[40] D. Chu, C. Walker, S. Gilman, Effect of Ru on unsupported Pt-Ru alloys for methanol electro-oxidation at different temperatures, in: D.H. Doughty, B. Vyas, T. Takamura, J.R. Huff (Eds.) Symposium on Materials for Electrochemical Energy Storage and Conversion - Batteries, Capacitors and Fuel Cells, at the 1995 MRS Spring Meeting, San Francisco, Ca, 1995, pp. 25-30.

[41] S. Kim, B.E. Dale, Global potential bioethanol production from wasted crops and crop residues, Biomass & Bioenergy, 26 (2004) 361-375.

[42] E. Viola, M. Cardinale, R. Santarcangelo, A. Villone, F. Zimbardi, Ethanol from eel grass via steam explosion and enzymatic hydrolysis, Biomass & Bioenergy, 32 (2008) 613-618.

[43] J.M. Kelzer, P.J. Kononoff, L.O. Tedeschi, T.C. Jenkins, K. Karges, M.L. Gibson, Evaluation of protein fractionation and ruminal and intestinal digestibility of corn milling co-products, Journal of Dairy Science, 93 (2010) 2803-2815.

[44] A. Hideno, H. Inoue, K. Tsukahara, S. Fujimoto, T. Minowa, S. Inoue, T. Endo, S. Sawayama, Wet disk milling pretreatment without sulfuric acid for enzymatic hydrolysis of rice straw, Bioresource Technology, 100 (2009) 2706-2711.

[45] C. Lamy, E.M. Belgsir, J.M. Leger, Electrocatalytic oxidation of aliphatic alcohols: Application to the direct alcohol fuel cell (DAFC), in: Workshop on Electrocatalysis in Ditect and Indirect Methanol Fuel Cells, Portoroz, Slovenia, 1999, pp. 799-809.

[46] A.O. Neto, T.R.R. Vasconcelos, R. Da Silva, M. Linardi, E.V. Spinace, Electro-oxidation of ethylene glycol on PtRu/C and PtSn/C electrocatalysts prepared by alcohol-reduction process, Journal of Applied Electrochemistry, 35 (2005) 193-198.

[47] E.V. Spinace, A.O. Neto, T.R.R. Vasconcelos, M. Linardi, Electro-oxidation of ethanol using PtRu/C electrocatalysts prepared by alcohol-reduction process, Journal of Power Sources, 137 (2004) 17-23.

[48] C. Lamy, S. Rousseau, E.M. Belgsir, C. Coutanceau, J.M. Leger, Recent progress in the direct ethanol fuel cell: development of new platinum-tin

electrocatalysts, in: 54th Annual ISE Meeting, Sao Pedro, Brazil, 2003, pp. 3901-3908.

[49] N.H. Li, S.G. Sun, S.P. Chen, Studies on the role of oxidation states of the platinum surface in electrocatalytic oxidation of small primary alcohols, Journal of Electroanalytical Chemistry, 430 (1997) 57-67.

[50] W.J. Zhou, Z.H. Zhou, S.Q. Song, W.Z. Li, G.Q. Sun, P. Tsiakaras, Q. Xin, Pt based anode catalysts for direct ethanol fuel cells, Applied Catalysis B-Environmental, 46 (2003) 273-285.

[51] W.J. Zhou, W.Z. Li, S.Q. Song, Z.H. Zhou, L.H. Jiang, G.Q. Sun, Q. Xin, K. Poulianitis, S. Kontou, P. Tsiakaras, Bi- and tri-metallic Pt-based anode catalysts for direct ethanol fuel cells, in: 8th Grove Fuel Cell Symposium, London, England, 2003, pp. 217-223.

[52] H.Q. Li, G.Q. Sun, L. Cao, L.H. Jiang, Q. Xin, Comparison of different promotion effect of PtRu/C and PtSn/C electrocatalysts for ethanol electro-oxidation, Electrochimica Acta, 52 (2007) 6622-6629.

[53] J.B. Joo, Y.J. Kim, W. Kim, P. Kim, J. Yi, Preparation and Characterization of a PtSn Nanocatalyst for Use in Ethanol Electro-Oxidation, in: International Conference on Nanoscience and Nanotechnology, Gwangju, South Korea, 2007, pp. 5130-5134.

[54] E.E. Switzer, T.S. Olson, A.K. Datye, P. Atanassov, M.R. Hibbs, C.J. Cornelius, Templated Pt-Sn electrocatalysts for ethanol, methanol and CO oxidation in alkaline media, Electrochimica Acta, 54 (2009) 989-995.

[55] I. Honma, T. Toda, Temperature dependence of kinetics of methanol electro-oxidation on PtSn alloys, Journal of the Electrochemical Society, 150 (2003) A1689-A1692.

[56] G.C. Li, P.G. Pickup, Decoration of carbon-supported Pt catalysts with Sn to promote electro-oxidation of ethanol, Journal of Power Sources, 173 (2007) 121-129.

[57] F. Colmati, E. Antolini, E.R. Gonzalez, Effect of temperature on the mechanism of ethanol oxidation on carbon supported Pt, PtRu and Pt3Sn electrocatalysts, Journal of Power Sources, 157 (2006) 98-103.

[58] T. Oka, H. Mizuseki, Y. Kawazoe, Activation barriers of CO oxidation on Pt-M (M = Ru, Sn) alloys, Journal of the Japan Institute of Metals, 70 (2006) 495-499.

[59] M. Shibamine, A. Yamada, M. Umeda, S. Tanaka, Alcohol electrooxidation at Pt-Ru sputter-deposited electrode, Electrical Engineering in Japan, 163 (2008) 14-21.

[60] J.S. Guo, G.Q. Sun, Q. Wang, G.X. Wang, Z.H. Zhou, S.H. Tang, L.H. Jiang, B. Zhou, Q. Xin, Carbon nanofibers supported Pt-Ru electrocatalysts for direct methanol fuel cells, Carbon, 44 (2006) 152-157.

[61] P.L. Hagans, K.E. Swider, D.R. Rolison, The chemical state of Ru in Pt-Ru direct methanol fuel cell anode electrocatalysts, in: J. McBreen, S. Mukerjee, S. Srinivasan (Eds.) Symposium on Electrode Materials and Processes for Energy Conversion and Storage IV, at the 191st Meeting of the Electrochemical-Society, Montreal, Canada, 1997, pp. 86-105.

[62] C.M. Zhou, H.J. Wang, J.H. Liang, F. Peng, H. Yu, J. Yang, Effects of RuO2 Content in Pt/RuO2/CNTs Nanocatalyst on the Electrocatalytic Oxidation Performance of Methanol, in: 14th International Congress on Catalysis, Dalian, Peoples are in China, 2008, pp. 1093-1098.

[63] J.H. Jiang, A. Kucernak, Synthesis of highly active nanostructured PtRu electrocatalyst with three-dimensional mesoporous silica template, Electrochemistry Communications, 11 (2009) 623-626.

[64] D.F. Silva, A. Oliveira, E.S. Pino, M. Linardi, E.V. Spinace, PtRu/C electrocatalysts prepared using gamma-irradiation, Journal of Power Sources, 170 (2007) 303-307.

[65] N. Jha, A.L.M. Reddy, M.M. Shaijumon, N. Rajalakshmi, S. Ramaprabhu, Pt-Ru/multi-walled carbon nanotubes as electrocatalysts for direct methanol fuel cell, in: International Workshop on Hydrogen Energy - Production Storage and Application, Jaipur, India, 2006, pp. 427-433.

[66] J. Ribeiro, D.M. dos Anjos, J.M. Leger, F. Hahn, P. Olivi, A.R. Andrade, G. Tremiliosi-Filho, K.B. Kokoh, Effect of W on PtSn/C catalysts for ethanol electrooxidation, Journal of Applied Electrochemistry, 38 (2008) 653-662.

[67] E.J. McLeod, V.I. Birss, Sol-gel derived WOx and WOx/Pt films for direct methanol fuel cell catalyst applications, Electrochimica Acta, 51 (2005) 684-693
.
[68] A. Sarkar, A.V. Murugan, A. Manthiram, Low cost Pd-W nanoalloy electrocatalysts for oxygen reduction reaction in fuel cells, Journal of Materials Chemistry, 19 (2009) 159-165.

[69] Z.B. Wang, G.P. Yin, Y.G. Lin, Synthesis and characterization of PtRuMo/C nanoparticle electrocatalyst for direct ethanol fuel cell, Journal of Power Sources, 170 (2007) 242-250.

[70] D.M. Han, Z.P. Guo, R. Zeng, C.J. Kim, Y.Z. Meng, H.K. Liu, Multiwalled carbon nanotube-supported Pt/Sn and Pt/Sn/PMo12 electrocatalysts for methanol electro-oxidation, International Journal of Hydrogen Energy, 34 (2009) 2426-2434.

[71] D.C. Papageorgopoulos, M. Keijzer, F.A. de Bruijn, The inclusion of Mo, Nb and Ta in Pt and PtRu carbon supported 3electrocatalysts in the quest for improved CO tolerant PEMFC anodes, Electrochimica Acta, 48 (2002) 197-204.

[72] T. Lopes, E. Antolini, E.R. Gonzalez, Carbon supported Pt-Pd alloy as an ethanol tolerant oxygen reduction electrocatalyst for direct ethanol fuel cells, International Journal of Hydrogen Energy, 33 (2008) 5563-5570.

[73] C.Z. He, H.R. Kunz, J.M. Fenton, Electro-oxidation of hydrogen with carbon monoxide on Pt/Ru-based ternary catalysts, Journal of the Electrochemical Society, 150 (2003) A1017-A1024.

[74] D. Zhao, B.Q. Xu, Platinum covering of gold nanoparticles for utilization enhancement of Pt in electrocatalysts, Physical Chemistry Chemical Physics, 8 (2006) 5106-5114.

[75] X. Guo, D.J. Guo, X.P. Qiu, L.Q. Chen, W.T. Zhu, A simple one-step preparation of high utilization AuPt nanoparticles supported on MWCNTs for methanol oxidation in alkaline medium, Electrochemistry Communications, 10 (2008) 1748-1751.

[76] J.P.I. de Souza, S.L. Queiroz, K. Bergamaski, E.R. Gonzalez, F.C. Nart, Electro-oxidation of ethanol on Pt, Rh, and PtRh electrodes. A study using DEMS and in-situ FTIR techniques, Journal of Physical Chemistry B, 106 (2002) 9825-9830.

[77] A. Kowal, M. Li, M. Shao, K. Sasaki, M.B. Vukmirovic, J. Zhang, N.S. Marinkovic, P. Liu, A.I. Frenkel, R.R. Adzic, Ternary Pt/Rh/SnO2 electrocatalysts for oxidizing ethanol to CO2, Nature Materials, 8 (2009) 325-330.

[78] Y. Wang, S.Y. Wang, X. Wang, CeO2 Promoted Electro-Oxidation of Formic Acid on Pd/C Nano-Electrocatalysts, Electrochemical and Solid State Letters, 12 (2009) B73-B76.

[79] H.P. Liu, J.Q. Ye, C.W. Xu, S.P. Jiang, Y.X. Tong, Electro-oxidation of methanol, 1-propanol and 2-propanol on Pt and Pd in alkaline medium, Journal of Power Sources, 177 (2008) 67-70.

[80] H. Wang, C.W. Xu, F.L. Cheng, S.P. Jiang, Pd nanowire arrays as electrocatalysts for ethanol electrooxidation, Electrochemistry Communications, 9 (2007) 1212-1216.

[81] L.D. Zhu, T.S. Zhao, J.B. Xu, Z.X. Liang, Preparation and characterization of carbon-supported sub-monolayer palladium decorated gold nanoparticles for the electro-oxidation of ethanol in alkaline media, Journal of Power Sources, 187 (2009) 80-84.

[82] C.E. Lee, S.H. Bergens, Deposition of Ru adatoms on Pt using organometallic chemistry - Electro-oxidation of methanol, ethanol, 1,2-ethanediol, and D-glucose over a Pt-Ru-ads surface optimized for oxidation of methanol, Journal of the Electrochemical Society, 145 (1998) 4182-4185.

[83] F.H.B. Lima, E.R. Gonzalez, Ethanol electro-oxidation on carbon-supported Pt-Ru, Pt-Rh and Pt-Ru-Rh nanoparticles, Electrochimica Acta, 53 (2008) 2963-2971.

[84] E. Antolini, T. Lopes, E.R. Gonzalez, An overview of platinum-based catalysts as methanol-resistant oxygen reduction materials for direct methanol fuel cells, Journal of Alloys and Compounds, 461 (2008) 253-262.

[85] D. Chakraborty, I. Chorkendoff, T. Johannessen, Metamorphosis of the mixed phase PtRu anode catalyst for direct methanol fuel cells after exposure of methanol: In situ and ex situ characterizations, Journal of Power Sources, 173 (2007) 110-120.

[86] D.L. Boxall, G.A. Deluga, E.A. Kenik, W.D. King, C.M. Lukehart, Rapid synthesis of a Pt1Ru1/carbon nanocomposite using microwave irradiation: A

DMFC anode catalyst of high relative performance, Chemistry of Materials, 13 (2001) 891-900.

[87] C. Eickes, E. Brosha, F. Garzon, G. Purdy, P. Zelenay, T. Morita, D. Thompsett, Electrochemical and XRD characterization of Pt-Ru blacks for DMFC anodes, in: M. Murthy, T.F. Fuller, J.W. VanZee, S. Gottesfeld (Eds.) 3rd Symposium on Proton Conducting Membrane Fuel Cells, Salt Lake City, UT, 2002, pp. 450-467.

[88] J.P.I. Souza, F.J.B. Rabelo, I.R. deMoraes, F.C. Nart, Performance of a co-electrodeposited Pt-Ru electrode for the electro-oxidation of ethanol studied by in situ FTIR spectroscopy, Journal of Electroanalytical Chemistry, 420 (1997) 17-20.

[89] T. Yajima, H. Uchida, M. Watanabe, In-situ ATR-FTIR spectroscopic study of electro-oxidation of methanol and adsorbed CO at Pt-Ru alloy, Journal of Physical Chemistry B, 108 (2004) 2654-2659.

[90] A. Bourane, D. Bianchi, Oxidation of CO on a Pt/A1(2)O(3) catalyst: from the surface elementary steps to light-off tests IV. Kinetic study of the reduction by CO of strongly adsorbed oxygen species, Journal of Catalysis, 220 (2003) 3-12.

[91] T. Yajima, N. Wakabayashi, H. Uchida, M. Watanabe, Adsorbed water for the electro-oxidation of methanol at Pt-Ru alloy, Chemical Communications, (2003) 828-829.

[92] A. Bourane, D. Bianchi, Oxidation of CO on a Pt/Al2O3 catalyst: From the surface elementary steps to lighting-off tests - II. Kinetic study of the oxidation of adsorbed CO species using mass spectroscopy, Journal of Catalysis, 209 (2002) 114-125.

[93] A. Bourane, O. Dulaurent, D. Bianchi, Comparison of the coverage of the linear CO species on Pt/Al2O3 measured under adsorption equilibrium conditions by using FTIR and mass spectroscopy, Journal of Catalysis, 195 (2000) 406-411.

[94] A. Bourane, O. Dulaurent, D. Bianchi, Heats of adsorption of linear and multibound adsorbed CO species on a Pt/Al2O3 catalyst using in Situ infrared spectroscopy under adsorption equilibrium, Journal of Catalysis, 196 (2000) 115-125.

[95] G.L. Chen, In-situ FTIR spectroscopic studies of electro oxidation of ethanol in alkaline media at a nm-Pt/GC electrode, Spectroscopy and Spectral Analysis, 20 (2000) 770-772.

[96] G. Orozco, C. Gutierrez, Adsorption and electro-oxidation of carbon monoxide, methanol, ethanol and formic acid on osmium electrodeposited on glassy carbon, Journal of Electroanalytical Chemistry, 484 (2000) 64-72.

[97] A. Kabbabi, R. Faure, R. Durand, B. Beden, F. Hahn, J.M. Leger, C. Lamy, In situ FTIRS study of the electrocatalytic oxidation of carbon monoxide and methanol at platinum-ruthenium bulk alloy electrodes, Journal of Electroanalytical Chemistry, 444 (1998) 41-53.

[98] G.A. Camara, R.B. de Lima, T. Iwasita, Catalysis of ethanol electro oxidation by PtRu: the influence of catalyst composition, Electrochemistry Communications, 6 (2004) 812-815.

[99] Z.L. Liu, X.Y. Ling, X.D. Su, J.Y. Lee, L.M. Gan, Preparation and characterization of Pt/C and Pt-Ru/C electrocatalysts for direct ethanol fuel cells, Journal of Power Sources, 149 (2005) 1-7.

[100] A.O. Neto, M.J. Giz, J. Perez, E.A. Ticianelli, E.R. Gonzalez, The electro-oxidation of ethanol on Pt-Ru and Pt-Mo particles supported on high-surface-area carbon, Journal of the Electrochemical Society, 149 (2002) A272-A279.

[101] A.O. Neto, R.R. Dias, M.M. Tusi, M. Linardi, E.V. Spinace, Electro-oxidation of methanol and ethanol using PtRu/C, PtSn/C and PtSnRu/C electrocatalysts prepared by an alcohol-reduction process, Journal of Power Sources, 166 (2007) 87-91.

[102] E. Spinace, A.O. Neto, M. Linardi, Electro-oxidation of methanol and ethanol using PtRu/C electrocatalysts prepared by spontaneous deposition of platinum on carbon-supported ruthenium nanoparticles, Journal of Power Sources, 129 (2004) 121-126.

[103] C. Lamy, J.M. Leger, Recent progresses in materials for the direct methanol fuel cell, in: O. Savadogo, P.R. Roberge (Eds.) 2nd International Symposium on New Materials for Fuel Cell and Modern Battery Systems, Montreal, Canada, 1997, pp. 477-488.

[104] S. Rousseau, C. Coutanceau, C. Lamy, J.M. Leger, Direct ethanol fuel cell (DEFC): Electrical performances and reaction products distribution under operating conditions with different platinum-based anodes, Journal of Power Sources, 158 (2006) 18-24.

[105] S.Q. Song, W.J. Zhou, Z.X. Liang, R. Cai, G.Q. Sun, Q. Xin, V. Stergiopoulos, P. Tsiakaras, The effect of methanol and ethanol cross-over on the performance of PtRu/C-based anode DAFCs, Applied Catalysis B-Environmental, 55 (2005) 65-72.

[106] P.E. Tsiakaras, PtM/C (M = Sn, Ru, Pd, W) based anode direct ethanol-PEMFCs: Structural characteristics and cell performance, Journal of Power Sources, 171 (2007) 107-112.

[107] M.L. Calegaro, H.B. Suffredini, S.A.S. Machado, L.A. Avaca, Preparation, characterization and utilization of a new electrocatalyst for ethanol oxidation obtained by the sol-gel method, Journal of Power Sources, 156 (2006) 300-305.

[108] G.C. Li, P.G. Pickup, The promoting effect of Pb on carbon supported Pt and Pt/Ru catalysts for electro-oxidation of ethanol, Electrochimica Acta, 52 (2006) 1033-1037.

[109] P. Anres, M. Gaune-Escard, J.P. Bros, E. Hayer, Enthalpy of formation of the (Pt-Sn) system, Journal of Alloys and Compounds, 280 (1998) 158-167.

[110] F. Colmati, E. Antolini, E.R. Gonzalez, Ethanol oxidation on a carbon-supported Pt75Sn25 electrocatalyst prepared by reduction with formic acid: Effect of thermal treatment, Applied Catalysis B-Environmental, 73 (2007) 106-115.

[111] H.F. Wang, Z.P. Liu, Comprehensive mechanism and structure-sensitivity of ethanol oxidation on platinum: New transition-state searching method for resolving the complex reaction network, Journal of the American Chemical Society, 130 (2008) 10996-11004.

[112] P. Bommersbach, M. Mohamedi, D. Guay, Electro-oxidation of ethanol at sputter-deposited platinum-tin catalysts, Journal of the Electrochemical Society, 154 (2007) B876-B882.

[113] C. Lamy, A. Lima, V. LeRhun, F. Delime, C. Coutanceau, J.M. Leger, Recent advances in the development of direct alcohol fuel cells (DAFC), in: 7th Meeting on Ulmer Elektrochemische Tage, Ulm, Germany, 2000, pp. 283-296.

[114] L.H. Jiang, G.Q. Sun, Z.H. Zhou, Q. Xin, Preparation and characterization of PtSn/C anode electrocatalysts for direct ethanol fuel cell, in: 3rd Asia-Pacific Congress on Catalysis, Dalian, Peopleas are in China, 2003, pp. 665-670.

[115] V. Rao, Hariyanto, C. Cremers, U. Stimming, Investigation of the ethanol electro-oxidation in alkaline membrane electrode assembly by differential electrochemical mass spectrometry, Fuel Cells, 7 (2007) 417-423.

[116] J. Riberio, D.M. dos Anjos, K.B. Kokoh, C. Coutanceau, J.M. Leger, P. Olivi, A.R. de Andrade, G. Tremiliosi-Filho, Carbon-supported ternary PtSnIr catalysts for direct ethanol fuel cell, Electrochimica Acta, 52 (2007) 6997-7006.

[117] W.J. Zhou, B. Zhou, Z.H. Zhou, W.Z. Li, S.Q. Song, Z. Wei, G.Q. Sun, Q. Xin, A novel route to prepare Pt-based electrocatalysts for direct methanol (ethanol) fuel cells, in: B. Zhou, S. Hermans, G.A. Somorjai (Eds.) Symposium on Nanotechnology in Catalysis held at the 2002 Fall ACS 224th National Meeting, Boston, MA, 2004, pp. 183-200.

[118] A. Kowal, S.L. Gojkovic, K.S. Lee, P. Olszewski, Y.E. Sung, Synthesis, characterization and electrocatalytic activity for ethanol oxidation of carbon supported Pt, Pt-Rh, Pt-SnO2 and Pt-Rh-SnO2 nanoclusters, Electrochemistry Communications, 11 (2009) 724-727.

[119] K.S. Lee, I.S. Park, Y.H. Cho, D.S. Jung, N. Jung, H.Y. Park, Y.E. Sung, Electrocatalytic activity and stability of Pt supported on Sb-doped SnO2 nanoparticles for direct alcohol fuel cells, Journal of Catalysis, 258 (2008) 143-152.

[120] J.M. Leger, S. Rousseau, C. Coutanceau, F. Hahn, C. Lamy, How bimetallic electrocatalysts does work for reactions involved in fuel cells? Example of ethanol oxidation and comparison to methanol, in: 55th Annual Meeting of the International-Society-of-Electrochemistry, Thessaloniki, Greece, 2004, pp. 5118-5125.

[121] D.R. Lycke, E.L. Gyenge, Electrochemically assisted organosol method for Pt-Sn nanoparticle synthesis and in situ deposition on graphite felt support: Extended reaction zone anodes for direct ethanol fuel cells, Electrochimica Acta, 52 (2007) 4287-4298.

[122] C. Panja, N. Saliba, B.E. Koel, Adsorption of methanol, ethanol and water on well-characterized Pt-Sn surface alloys, Surface Science, 395 (1998) 248-259.

[123] G. Sine, D. Smida, M. Limat, G. Foti, C. Comninellis, Microemulsion synthesized Pt/Ru/Sn nanoparticles on BDD for alcohol electro-oxidation, Journal of the Electrochemical Society, 154 (2007) B170-B174.

[124] E.V. Spinace, M. Linardi, A.O. Neto, Co-catalytic effect of nickel in the electro-oxidation of ethanol on binary Pt-Sn electrocatalysts, Electrochemistry Communications, 7 (2005) 365-369.

[125] F. Vigier, C. Coutanceau, F. Hahn, E.M. Belgsir, C. Lamy, On the mechanism of ethanol electro-oxidation on Pt and PtSn catalysts: electrochemical and in situ IR reflectance spectroscopy studies, Journal of Electroanalytical Chemistry, 563 (2004) 81-89.

[126] W.J. Zhou, B. Zhou, W.Z. Li, Z.H. Zhou, S.Q. Song, G.Q. Sun, Q. Xin, S. Douvartzides, A. Goula, P. Tsiakaras, Performance comparison of low-temperature direct alcohol fuel cells with different anode catalysts, Journal of Power Sources, 126 (2004) 16-22.

[127] M.Y. Zhu, G.Q. Sun, Q. Xin, Effect of alloying degree in PtSn catalyst on the catalytic behavior for ethanol electro-oxidation, Electrochimica Acta, 54 (2009) 1511-1518.

[128] Y.X. Bai, J.F. Li, X.P. Qiu, J.J. Wu, J.S. Wang, J.Y. Xi, W.T. Zhu, L.Q. Chen, Mesocarbon microbeads supported PtSn catalysts for electrochemical oxidation of ethanol, Journal of Materials Science, 42 (2007) 4508-4512.

[129] A. Bonesi, G. Garaventa, W.E. Triaca, A.M.C. Luna, Synthesis and characterization of new electrocatalysts for ethanol oxidation, in: 2nd National/1st Latin American Congress on Hydrogen and Sustainable Energy Sources, Posadas, Argentina, 2007, pp. 3499-3501.

[130] F. Colmati, E. Antolini, E.R. Gonzalez, Preparation, structural characterization and activity for ethanol oxidation of carbon supported ternary Pt-Sn-Rh catalysts, Journal of Alloys and Compounds, 456 (2008) 264-270.

[131] D.M. dos Anjos, F. Hahn, J.M. Leger, K.B. Kokoh, G. Tremiliosi, Ethanol electrooxidation on Pt-Sn and Pt-Sn-W bulk alloys, in: 16th Brazillian Symposium of Electrochemistry and Electroanalytical Chemistry, Aguas de Lindoia, Brazil, 2007, pp. 795-802.

[132] L.H. Jiang, Z.H. Zhou, W.Z. Li, W.J. Zhou, S.Q. Song, H.Q. Li, G.Q. Sun, Q. Xin, Effects of treatment in different atmosphere on Pt3Sn/C electrocatalysts for ethanol electro-oxidation, Energy & Fuels, 18 (2004) 866-871.

[133] L.H. Jiang, G.Q. Sun, S.G. Sun, J.G. Liu, S.H. Tang, H.Q. Li, B. Zhou, Q. Xin, Structure and chemical composition of supported Pt-Sn electrocatalysts for ethanol oxidation, Electrochimica Acta, 50 (2005) 5384-5389.

[134] L. Jiang, L. Colmenares, Z. Jusys, G.Q. Sun, R. Behm, Ethanol electrooxidation on novel carbon supported Pt/SnOx/C catalysts with varied Pt : Sn ratio, in: 5th International Conference on Electrocatalysis from Theory to Industrial Applications, Kotor, Montenegro, 2006, pp. 377-389.

[135] M. Batzill, K. Katsiev, J.M. Burst, U. Diebold, A.M. Chaka, B. Delley, Gas-phase-dependent properties of SnO2 (110), (100), and (101) single-crystal surfaces: Structure, composition, and electronic properties, Physical Review B, 72 (2005).

[136] U. Diebold, The surface science of titanium dioxide, Surface Science Reports, 48 (2003) 53-229.

[137] K. Ke, K. Waki, Fabrication and characterization of multiwalled carbon nanotubes-supported Pt/SnO_x nanocomposites as catalysts for electro-oxidation of methanol, Journal of the Electrochemical Society, 154 (2007) A207-A212.

[138] A.S. Arico, P. Creti, H. Kim, R. Mantegna, N. Giordano, V. Antonucci, Analysis of the electrochemical characteristics of a direct methanol fuel cell based on a Pt-Ru/C anode catalyst, Journal of the Electrochemical Society, 143 (1996) 3950-3959.

[139] W.L. Xu, T.H. Lu, C.P. Liu, W. Xing, Nanostructured PtRu/C as anode catalysts prepared in a pseudomicroemulsion with ionic surfactant for direct methanol fuel cell, Journal of Physical Chemistry B, 109 (2005) 14325-14330.

[140] M.K. Jeon, J.Y. Won, S.I. Woo, Improved performance of direct methanol fuel cells by anodic treatment, Electrochemical and Solid State Letters, 10 (2007) B23-B25.

[141] T. Lopes, E. Antolini, F. Colmati, E.R. Gonzalez, Carbon supported Pt-Co (3 : 1) alloy as improved cathode electrocatalyst for direct ethanol fuel cells, Journal of Power Sources, 164 (2007) 111-114.

[142] B. Liu, J.H. Chen, X.X. Zhong, K.Z. Cui, H.H. Zhou, Y.F. Kuang, Preparation and electrocatalytic properties of Pt-SiO2 nanocatalysts for ethanol electrooxidation, Journal of Colloid and Interface Science, 307 (2007) 139-144.

[143] Y.X. Bai, J.J. Wu, X.P. Qiu, J.Y. Xi, J.S. Wang, J.F. Li, W.T. Zhu, L.Q. Chen, Electrochemical characterization of Pt-CeO2/C and Pt-CexZr1-xO2/C catalysts for ethanol electro-oxidation, Applied Catalysis B-Environmental, 73 (2007) 144-149.

[144] G.Y. Zhao, H.L. Li, Electrochemical oxidation of methanol on Pt nanoparticles composited MnO2 nanowire arrayed electrode, Applied Surface Science, 254 (2008) 3232-3235.

[145] Z.B. Wang, G.P. Yin, J. Zhang, Y.C. Sun, P.F. Shi, Co-catalytic effect of Ni in the methanol electro-oxidation on Pt-Ru/C catalyst for direct methanol fuel cell, Electrochimica Acta, 51 (2006) 5691-5697.

[146] S. Sen Gupta, S.S. Mahapatra, J. Datta, A potential anode material for the direct alcohol fuel cell, in: 8th Grove Fuel Cell Symposium, London, England, 2003, pp. 169-174.

[147] L.H. Jiang, Z.H. Zhou, W.J. Zhou, S.L. Wang, G.X. Wang, G.Q. Sun, Q. Xin, Synthesis, characterization and performance of PtSn/C electrocatalyst for direct ethanol fuel cell, Chemical Journal of Chinese Universities-Chinese, 25 (2004) 1511-1516.

[148] F. Vigier, C. Coutanceau, A. Perrard, E.M. Belgsir, C. Lamy, Development of anode catalysts for a direct ethanol fuel cell, Journal of Applied Electrochemistry, 34 (2004) 439-446.

[149] K. Bergamaski, E.R. Gonzalez, F.C. Nart, Ethanol oxidation on carbon supported platinum-rhodium bimetallic catalysts, Electrochimica Acta, 53 (2008) 4396-4406.

[150] F.H.B. Lima, E.R. Gonzalez, Electrocatalysis of ethanol oxidation on Pt monolayers deposited on carbon-supported Ru and Rh nanoparticles, Applied Catalysis B-Environmental, 79 (2008) 341-346.

[151] H.B. Suffredini, G.R. Salazar-Banda, L.A. Avaca, Enhanced ethanol oxidation on PbOx-containing electrode materials for fuel cell applications, Journal of Power Sources, 171 (2007) 355-362.

[152] M.H. Huang, F. Wang, L.R. Li, Y.L. Guo, A novel binary Pt_3Tex/C nanocatalyst for ethanol electro-oxidation, Journal of Power Sources, 178 (2008) 48-52.

[153] J.S. Wang, J.Y. Xi, Y.X. Bai, Y. Shen, J. Sun, L.Q. Chen, W.T. Zhu, X.P. Qiu, Structural designing of Pt-CeO_2/CNTs for methanol electro-oxidation, Journal of Power Sources, 164 (2007) 555-560.

[154] D.J. Diaz, N. Greenletch, A. Solanki, A. Karakoti, S. Seal, Novel nanoscale ceria-platinum composite electrodes for direct alcohol electro-oxidation, Catalysis Letters, 119 (2007) 319-326.

[155] C.W. Xu, P.K. Shen, Y.L. Liu, Ethanol electrooxidation on Pt/C and Pd/C catalysts promoted with oxide, Journal of Power Sources, 164 (2007) 527-531.

[156] Y.X. Bai, J.J. Wu, J.Y. Xi, J.S. Wang, W.T. Zhu, L.Q. Chen, X.P. Qiu, Electrochemical oxidation of ethanol on Pt-ZrO2/C catalyst, Electrochemistry Communications, 7 (2005) 1087-1090.

[157] C.W. Xu, P.K. Shen, X.H. Ji, R. Zeng, Y.L. Liu, Enhanced activity for ethanol electro oxidation on Pt-MgO/C catalysts, Electrochemistry Communications, 7 (2005) 1305-1308.

[158] H.Q. Song, X.P. Qiu, F.S. Li, W.T. Zhu, L.Q. Chen, Ethanol electro-oxidation on catalysts with TiO2 coated carbon nanotubes as support, Electrochemistry Communications, 9 (2007) 1416-1421.

[159] B. Lei, J.J. Xue, D.P. Jin, S.G. Ni, H.B. Sun, Fabrication, annealing, and electrocatalytic properties of platinum nanoparticles supported on self-organized TiO2 nanotubes, Rare Metals, 27 (2008) 445-450.

[160] Q.Z. Jiang, X. Wu, M. Shen, Z.F. Ma, X.Y. Zhu, Low-Pt content carbon-supported Pt-Ni-TiO2 nanotube electrocatalyst for direct methanol fuel cells, Catalysis Letters, 124 (2008) 434-438.

[161] H.Q. Song, X.P. Qiu, F.H. Li, Effect of heat treatment on the performance of TiO_2-Pt/CNT catalysts for methanol electro-oxidation, Electrochimica Acta, 53 (2008) 3708-3713.

[162] H.Q. Song, X.P. Qiu, D.J. Guo, F.S. Li, Role of structural H2O in TiO2 nanotubes in enhancing Pt/C direct ethanol fuel cell anode electro-catalysts, Journal of Power Sources, 178 (2008) 97-102.

[163] F.H.B. Lima, D. Profeti, W.H. Lizcano-Valbuena, E.A. Ticianelli, E.R. Gonzalez, Carbon-dispersed Pt-Rh nanoparticles for ethanol electro-oxidation. Effect of the crystallite size and of temperature, Journal of Electroanalytical Chemistry, 617 (2008) 121-129.

[164] H.Q. Song, X.P. Qiu, X.X. Li, F.S. Li, W.T. Zhu, L.Q. Chen, TiO_2 nanotubes promoting Pt/C catalysts for ethanol electro-oxidation in acidic media, Journal of Power Sources, 170 (2007) 50-54.

[165] E. Ribadeneira, B.A. Hoyos, Evaluation of Pt-Ru-Ni and Pt-Sn-Ni catalysts as anodes in direct ethanol fuel cells, Journal of Power Sources, 180 (2008) 238-242.

[166] M.M. Hefny, S. AbdelWanees, Electro-oxidation at a coated iridium electrode, Electrochimica Acta, 41 (1996) 1419-1422.

[167] Y.M. Liang, H.M. Zhang, H.X. Zhong, X.B. Zhu, Z.Q. Tian, D.Y. Xu, B.L. Yi, Preparation and characterization of carbon-supported PtRuIr catalyst with excellent CO-tolerant performance for proton-exchange membrane fuel cells, Journal of Catalysis, 238 (2006) 468-476.

[168] X.Z. Xue, J.J. Ge, T. Tian, C.P. Liu, W. Xing, T.H. Lu, Enhancement of the electrooxidation of ethanol on Pt-Sn-P/C catalysts prepared by chemical deposition process, Journal of Power Sources, 172 (2007) 560-569.

[169] A.O. Neto, L.A. Farias, R.R. Dias, M. Brandalise, M. Linardi, E.V. Spinace, Enhanced electro-oxidation of ethanol using PtSn/CeO2-C electrocatalyst prepared by an alcohol-reduction process, Electrochemistry Communications, 10 (2008) 1315-1317.

[170] D.B. Chu, J. Wang, S.X. Wang, L.W. Zha, J.G. He, Y.Y. Hou, Y.X. Yan, H.S. Lin, Z.W. Tian, High activity of Pd-In2O3/CNTs electrocatalyst for electro-oxidation of ethanol, Catalysis Communications, 10 (2009) 955-958.

[171] Y.H. Xu, X.Q. Lin, Facile fabrication and electrocatalytic activity of Pt0.9Pd0.1 alloy film catalysts, Journal of Power Sources, 170 (2007) 13-19.

[172] C.W. Xu, H. Wang, P.K. Shen, S.P. Jiang, Highly ordered Pd nanowire arrays as effective electrocatalysts for ethanol oxidation in direct alcohol fuel cells, Advanced Materials, 19 (2007) 4256.

[173] C.W. Xu, L.Q. Cheng, P.K. Shen, Y.L. Liu, Methanol and ethanol electrooxidation on Pt and Pd supported on carbon microspheres in alkaline media, Electrochemistry Communications, 9 (2007) 997-1001.

[174] L. Cao, G.Q. Sun, H.Q. Li, Q. Xin, Carbon-supported IrSn catalysts for a direct ethanol fuel cell, Electrochemistry Communications, 9 (2007) 2541-2546.

[175] M. Nie, H.L. Tang, Z.D. Wei, S.P. Jiang, P.K. Shen, Highly efficient AuPd-WC/C electrocatalyst for ethanol oxidation, Electrochemistry Communications, 9 (2007) 2375-2379.

[176] C.W. Xu, Z.Q. Tian, Z.C. Chen, S.P. Jiang, Pd/C promoted by Au for 2-propanol electrooxidation in alkaline media, Electrochemistry Communications, 10 (2008) 246-249.

[177] C.W. Xu, Y.H. Hu, J.H. Rong, S.P. Jiang, Y.L. Liu, Ni hollow spheres as catalysts for methanol and ethanol electrooxidation, Electrochemistry Communications, 9 (2007) 2009-2012.

[178] X.Y. Zhang, D.H. Dong, D. Li, T. Williams, H.T. Wang, P.A. Webley, Direct electrodeposition of Pt nanotube arrays and their enhanced electrocatalytic activities, Electrochemistry Communications, 11 (2009) 190-193.

[179] J.W. Guo, T.S. Zhao, J. Prabhuram, R. Chen, C.W. Wong, Preparation and characterization of a PtRu/C nanocatalyst for direct methanol fuel cells, Electrochimica Acta, 51 (2005) 754-763.

[180] J. Kim, T. Momma, T. Osaka, Cell performance of Pd-Sn catalyst in passive direct methanol alkaline fuel cell using anion exchange membrane, Journal of Power Sources, 189 (2009) 999-1002.

[181] X.Y. Zhang, W. Lu, J.Y. Da, H.T. Wang, D.Y. Zhao, P.A. Webley, Porous platinum nanowire arrays for direct ethanol fuel cell applications, Chemical Communications, (2009) 195-197.

[182] M.S. Saha, R.Y. Li, X.L. Sun, Composite of Pt-Ru supported SnO2 nanowires grown on carbon paper for electrocatalytic oxidation of methanol, Electrochemistry Communications, 9 (2007) 2229-2234.

[183] G.Y. Zhao, C.L. Xu, D.J. Guo, H. Li, H.L. Li, Template preparation of Pt-Ru and Pt nanowire array electrodes on a Ti/Si substrate for methanol electro-oxidation, Journal of Power Sources, 162 (2006) 492-496.

[184] J.J. Schneider, J. Engstler, Carbon and polymer filaments in nanoporous alumina, European Journal of Inorganic Chemistry, (2006) 1723-1736.

[185] J.J. Schneider, N. Engstler, K.P. Budna, C. Teichert, S. Franzka, Freestanding, highly flexible, large area, nanoporous alumina membranes with complete through-hole pore morphology, European Journal of Inorganic Chemistry, (2005) 2352-2359.

[186] O. Jessensky, F. Muller, U. Gosele, Self-organized formation of hexagonal pore arrays in anodic alumina, Applied Physics Letters, 72 (1998) 1173-1175.

[187] O. Jessensky, F. Muller, U. Gosele, Self-organized formation of hexagonal pore structures in anodic alumina, Journal of the Electrochemical Society, 145 (1998) 3735-3740.

[188] C.S. Cojocaru, J.M. Padovani, T. Wade, C. Mandoli, G. Jaskierowicz, J.E. Wegrowe, A.F.I. Morral, D. Pribat, Conformal anodic oxidation of aluminum thin films, Nano Letters, 5 (2005) 675-680.

[189] W.C. Choi, S.I. Woo, Bimetallic Pt-Ru nanowire network for anode material in a direct-methanol fuel cell, Journal of Power Sources, 124 (2003) 420-425.

[190] S.M. Choi, J.H. Kim, J.Y. Jung, E.Y. Yoon, W.B. Kim, Pt nanowires prepared via a polymer template method: Its promise toward high Pt-loaded electrocatalysts for methanol oxidation, Electrochimica Acta, 53 (2008) 5804-5811.

[191] G.Y. Zhao, C.L. Xu, D.J. Guo, H. Li, H.L. Li, Template preparation of Pt nanowire array electrode on Ti/Si substrate for methanol electro-oxidation, Applied Surface Science, 253 (2007) 3242-3246.

[192] H.A. Gasteiger, N. Markovic, P.N. Ross, E.J. Cairns, CO Electro-oxidation On Well-Characterized Pt-Ru Alloys, Journal of Physical Chemistry, 98 (1994) 617-625.

[193] H.A. Gasteiger, N.M. Markovic, P.N. Ross, Electro-oxidation of CO and H_2/CO Mixtures on a Well Characterized Pt_3Sn Electrode Surface, Journal of Physical Chemistry, 99 (1995) 8945-8949.

[194] N.M. Markovic, T.J. Schmidt, V. Stamenkovic, R. P.N., Fuel Cells, in, 2001, pp. 105.

[195] N.S. Marinkovic, N.M. Markovic, R.R. Adzic, Hydrogen Adsorption on Single Crystal Platinum Electrodes In Alkaline Solutions, Journal of Electroanalytical Chemistry, 330 (1992) 433-452.

[196] N.M. Markovic, H.A. Gasteiger, S.T. Sarraf, P.N. Ross, Kinetic and Mechanistic Studies of H_2 Oxidation and Generation on Pt Single Crystal Surfaces, Abstracts of Papers of the American Chemical Society, 210 (1995) 225.

[197] J.F. Gomes, B. Busson, A. Tadjeddine, G. Tremiliosi, Ethanol electro-oxidation over Pt(h k l): Comparative study on the reaction intermediates probed by FTIR and SFG spectroscopies, in: 58th Annual Meeting of the International-Society-of-Electrochemisty, Banff, Canada, 2007, pp. 6899-6905.

[198] S.C.S. Lai, M.T.M. Koper, Electro-oxidation of ethanol and acetaldehyde on platinum single-crystal electrodes, in: Conference on Electrocatalysis Theory and Experiment at the Interface, Southampton, England, 2008, pp. 399-416.

[199] Gewirth, Armstrong, Nestoridi, Schmickler, Wieckowski, Wittstock, Ren, Janik, Rossmeisl, Wang, Jinnouchi, Korzeniewski, Behm, Tryk, Savinova, Kucernak, Markovic, Strasser, Gross, Neurock, Herrero, Koper, Sun, Lai, Gomes, Thompsett, Electro-oxidation of ethanol and acetaldehyde on platinum single-crystal electrodes Discussion, Faraday Discussions, 140 (2008) 417-437.

[200] S.C.S. Lai, S.E.F. Kleyn, V. Rosca, M.T.M. Koper, Mechanism of the Dissociation and Electrooxidation of Ethanol and Acetaldehyde on Platinum As Studied by SERS, Journal of Physical Chemistry C, 112 (2008) 19080-19087.

[201] L. Demarconnay, C. Coutanceau, J.M. Leger, Study of the oxygen electroreduction at nanostructured PtBi catalysts in alkaline medium, Electrochimica Acta, 53 (2008) 3232-3241.

[202] M.K. Jeon, K.R. Lee, W.S. Lee, H. Daimon, A. Nakahara, S.I. Woo, Investigation of Pt/WC/C catalyst for methanol electro-oxidation and oxygen electro-reduction, Journal of Power Sources, 185 (2008) 927-931.

[203] L.H. Jiang, A. Hsu, D. Chu, R.R. Chen, Oxygen reduction on carbon supported Pt and PtRu catalysts in alkaline solutions, Journal of Electroanalytical Chemistry, 629 (2009) 87-93.

[204] W.Z. Li, Z.H. Zhou, W.J. Zhou, H.Q. Li, X.S. Zhao, G.X. Wang, G.Q. Sun, Q. Xin, Preparation and characterization of Pt/C cathode catalysts for direct methanol fuel cells - Effect of different preparation and treatment methods, Chinese Journal of Catalysis, 24 (2003) 465-470.

[205] W.Z. Li, S.Q. Song, W.J. Zhou, G.Q. Sun, Q. Xin, C. Poulianitis, P. Tsiakaras, Direct methanol fuel cells: The influence of methanol on the reduction of oxygen over Pt/C catalysts with different particle sizes, in: Patras Conference on Solid State Ionics - Transport Properties, Patras, Greece, 2004, pp. 112-119.

[206] W.Z. Li, W.J. Zhou, H.Q. Li, Z.H. Zhou, B. Zhou, G.Q. Sun, Q. Xin, Nano-stuctured Pt-Fe/C as cathode catalyst in direct methanol fuel cell, Electrochimica Acta, 49 (2004) 1045-1055.

[207] X.W. Li, Q.H. Huang, Z.Q. Zou, B.J. Xia, H. Yang, Low temperature preparation of carbon-supported Pd-Co alloy electrocatalysts for methanol-tolerant oxygen reduction reaction, Electrochimica Acta, 53 (2008) 6662-6667.

[208] S.F. Luna, F.J.R. Varela, R.D. Klapco, O. Savadogo, Performance of Pd/C Cathode Electro-Catalysts for the ORR in Sulfuric Acid Containing Small Organic Molecules, in: T. Fuller, K. Shinohara, V. Ramani, P. Shirvanian, H. Uchida, S. Cleghorn, M. Inaba, S. Mitsushima, P. Strasser, H. Nakagawa, H.A. Gasteiger, T. Zawodzinski, C. Lamy (Eds.) Proton Exchange Membrane Fuel Cells 8, Pts 1 and 2, 2008, pp. 761-767.

[209] A.M.C. Luna, A. Bonesi, W.E. Triaca, V. Baglio, V. Antonucci, A.S. Arico, Pt-Fe cathode catalysts to improve the oxygen reduction reaction and methanol tolerance in direct methanol fuel cells, Journal of Solid State Electrochemistry, 12 (2008) 643-649.

[210] H. Meng, P.K. Shen, Novel Pt-free catalyst for oxygen electroreduction, Electrochemistry Communications, 8 (2006) 588-594.

[211] N. Park, T. Shiraishi, K. Kamisugi, Y. Hara, K. Iizuka, T. Kado, S. Hayase, NiCoFe/C cathode electrocatalysts for direct ethanol fuel cells, Journal of Applied Electrochemistry, 38 (2008) 371-375.

[212] C.V. Rao, B. Viswanathan, ORR Activity and Direct Ethanol Fuel Cell Performance of Carbon-Supported Pt-M (M = Fe, Co, and Cr) Alloys Prepared by Polyol Reduction Method, Journal of Physical Chemistry C, 113 (2009) 18907-18913.

[213] F.J.R. Varela, O. Savadogo, Ethanol-tolerant Pt-alloy cathodes for direct ethanol fuel cell (DEFC) applications, Asia-Pacific Journal of Chemical Engineering, 4 (2009) 17-24.

[214] F.J.R. Varela, S.E.G. Ramirez, R.D. Klapco, Evaluation of the Performance of Ru/C Electrocatalysts for the ORR in the Absence and Presence Of C2H5OH: Application in Direct Fuel Cells, Journal of New Materials for Electrochemical Systems, 12 (2009) 9-15.

[215] A. Verma, A.K. Jha, S. Basu, Manganese dioxide as a cathode catalyst for a direct alcohol or sodium borohydride fuel cell with a flowing alkaline electrolyte, Journal of Power Sources, 141 (2005) 30-34.

[216] E. Auer, A. Freund, J. Pietsch, T. Tacke, Carbons as supports for industrial precious metal catalysts, Applied Catalysis a-General, 173 (1998) 259-271.

[217] Z.Q. Tian, S.P. Jiang, Y.M. Liang, P.K. Shen, Synthesis and characterization of platinum catalysts on muldwalled carbon nanotubes by intermittent microwave irradiation for fuel cell applications, Journal of Physical Chemistry B, 110 (2006) 5343-5350.

[218] J.H. Zeng, F.B. Su, J.Y. Lee, W.J. Zhou, X.S. Zhao, Methanol oxidation activities of Pt nanoparticles supported on microporous carbon with and without a graphitic shell, Carbon, 44 (2006) 1713-1717.

[219] H.L. Pang, J.H. Chen, L. Yang, B. Liu, X.X. Zhong, X.G. Wei, Ethanol electrooxidation on Pt/ZSM-5 zeolite-C catalyst, Journal of Solid State Electrochemistry, 12 (2008) 237-243.

[220] D.Y. Zhang, Z.F. Ma, G.X. Wang, J. Chen, G.C. Wallace, H.K. Liu, Preparation of low loading Pt/C catalyst by carbon xerogel method for ethanol electrooxidation, Catalysis Letters, 122 (2008) 111-114.

[221] M. Carmo, V.A. Paganin, J.M. Rosolen, E.R. Gonzalez, Alternative supports for the preparation of catalysts for low-temperature fuel cells: the use of carbon nanotubes, Journal of Power Sources, 142 (2005) 169-176.

[222] Z.M. Cui, C.P. Liu, J.H. Liao, W. Xing, Highly active PtRu catalysts supported on carbon nanotubes prepared by modified impregnation method for methanol electro-oxidation, Electrochimica Acta, 53 (2008) 7807-7811.

[223] J.L. Figueiredo, M.F.R. Pereira, P. Serp, P. Kalck, P.V. Samant, J.B. Fernandes, Development of carbon nanotube and carbon xerogel supported catalysts for the electro-oxidation of methanol in fuel cells, in: 1st International Conference on Carbon for Energy Storage and Environment Protection, Orleans, France, 2005, pp. 2516-2522.

[224] Y. Kim, Y. Seo, Y. Cho, K. Kim, W. Chung, Effect of CNTs support diameter on Pt particles size and distribution, in: C.K. Rhee (Ed.) 7th International Symposium on Nanocomposites and Nanoporous Materials (ISNAM7), Gyeongju, South Korea, 2006, pp. 231-234.

[225] J. Shi, Z. Wang, H.L. Li, Electrochemical fabrication of polyaniline/multi-walled carbon nanotube composite films for electrooxidation of methanol, Journal of Materials Science, 42 (2007) 539-544.

[226] H.P. Yuan, D.J. Guo, X.P. Qiu, W.T. Zhu, L.Q. Chen, Influence of metal oxides on Pt catalysts for methanol electrooxidation using electrochemical impedance spectroscopy, Journal of Power Sources, 188 (2009) 8-13.

[227] E. Frackowiak, G. Lota, T. Cacciaguerra, F. Beguin, Carbon nanotubes with Pt-Ru catalyst for methanol fuel cell, Electrochemistry Communications, 8 (2006) 129-132.

[228] J. Zhao, P. Wang, W.X. Chen, R. Liu, X. Li, Q.L. Nie, Microwave synthesis and characterization of acetate-stabilized Pt nanoparticles supported on carbon for methanol electro-oxidation, Journal of Power Sources, 160 (2006) 563-569.

[229] F. Engelke, S. Bhatia, T.S. King, M. Pruski, Dynamics of Hydrogen at the Surface of Supported Dynamics of Hydrogen At The Surface Of Supported Ruthenium, Physical Review B, 49 (1994) 2730-2738.

[230] R.L. Narayan, T.S. King, Hydrogen adsorption states on silica-supported Ru-Ag and Ru-Cu bimetallic catalysts investigated via microcalorimetry, Thermochimica Acta, 312 (1998) 105-114.

[231] D.O. Uner, N. Savargoankar, M. Pruski, T.S. King, The effects of alkali promoters on the dynamics of hydrogen chemisorption and syngas reaction kinetics on Ru/SiO2 surfaces, in: G.F. Froment, K.C. Waught (Eds.) Dynamics of Surfaces and Reaction Kinetics in Heterogeneous Catalysis, 1997, pp. 315-324.

[232] N. Savargaonkar, R.L. Narayan, M. Pruski, D.O. Uner, T.S. King, Structure sensitive hydrogen adsorption: Effect of Ag on Ru/SiO2 catalysts, Journal of Catalysis, 178 (1998) 26-33.

[233] P.M. Kumar, S. Badrinarayanan, M. Sastry, Nanocrystalline TiO2 studied by optical, FTIR and X-ray photoelectron spectroscopy: correlation to presence of surface states, Thin Solid Films, 358 (2000) 122-130.

[234] J.K. Norskov, T. Bligaard, A. Logadottir, S. Bahn, L.B. Hansen, M. Bollinger, H. Bengaard, B. Hammer, Z. Sljivancanin, M. Mavrikakis, Y. Xu, S. Dahl, C.J.H. Jacobsen, Universality in heterogeneous catalysis, Journal of Catalysis, 209 (2002) 275-278.

[235] H. Kivrak, A. Mastalir, Z. Kiraly, D. Uner, Determination of the dispersion of supported Pt particles by gas-phase and liquid-phase measurements, Catalysis Communications, 10 (2009) 1002-1005.

[236] D. Uner, M. Uner, Adsorption calorimetry in supported catalyst characterization: Adsorption structure sensitivity on Pt/-gamma-Al2O3, in: 3rd International Symposium on Calorimetry and Thermal Effects in Catalysis, Lyon, France, 2004, pp. 107-112.

[237] R.D. Cortright, J.A. Dumesic, Effects of potassium on silica-supported Pt and Pt/Sn catalysts for isobutane dehydrogenation, Journal of Catalysis, 157 (1995) 576-583.

[238] R.D. Cortright, J.A. Dumesic, Microcalorimetric, Spectroscopic, and Kinetic Studies of Silica-Supported Pt and Pt-Sn Catalysts for Isubtane Dehydrogenation, Journal of Catalysis, 148 (1994) 771-778.

[239] B.B. Schaack, W. Schrader, T. Schuth, Detection of Structural Elements of Different Zeolites in Nucleating Solutions by Electrospray Ionization Mass Spectrometry, Angewandte Chemie-International Edition, 47 (2008) 9092-9095.

[240] N.M. Markovic, H.A. Gasteiger, P.N. Ross, Oxygen Reduction on Platinum Low Index Single Crystal Surfaces In Sulfuric Acid Solution- Rotating Ring Pt (hkl) Disk Studies, Journal of Physical Chemistry, 99 (1995) 3411-3415.

[241] N.M. Markovic, M.L. Avramovivic, N.S. Marinkovic, R.R. Adzic, Structural Effects In Electrocatalysis-Ethylene-Glycol Oxidation on Platinum Single Crystal Surfaces, Journal of Electroanalytical Chemistry, 312 (1991) 115-130.

[242] N.M. Markovic, R.R. Adzic, B.D. Cahan, E.B. Yeager, Structural Effects In Electrocatalyis- Oxygen Reduction on Platinum Low Index Single Crystal Surfaces In Perchloric Acid Solutions, Journal of Electroanalytical Chemistry, 377 (1994) 249-259.

[243] N.M. Markovic, H.A. Gasteiger, N. Philip, Oxygen reduction on platinum low-index single-crystal surfaces in alkaline solution: Rotating ring disk(Pt(hkl)) studies, Journal of Physical Chemistry, 100 (1996) 6715-6721.

[244] X.X. Li, X.P. Qiu, H.P. Yuan, L.Q. Chen, W.T. Zhu, Size-effect on the activity of anodic catalysts in alcohol and CO electrooxidation, in: Meeting of the International-Battery-Material-Association, Shenzhen, Peoples are In China, 2007, pp. 353-360.

[245] Z. Kiraly, A. Mastalir, A. Csaszar, H. Demir, D. Uner, G.H. Findenegg, Liquid chromatography as a novel method for determination of the dispersion of supported Fd particles, Journal of Catalysis, 245 (2007) 267-271.

[246] W.Q. Zou, R.D. Gonzalez, The Preparation of Silica Supported Pd Catalysts-The Effect of Pretreatment Variables on Particle Size, in: 5th Trilateral United-States / Japan / China Symp on Catalysis, Evanston, Il, 1991, pp. 73-86.

[247] N.M. Markovic, H.A. Gasteiger, B.N. Grgur, P.N. Ross, Oxygen reduction reaction on Pt(111): effects of bromide, Journal of Electroanalytical Chemistry, 467 (1999) 157-163.

[248] H.A. Gasteiger, N. Markovic, P.N. Ross, E.J. Cairns, Electro-oxidation of Small Organic Molecules on Well Characterized Pt-Ru Alloys, in: International

Symposium on Progress in Electrocatalysis: Theory and Practice, Ferrara, Italy, 1993, pp. 1825-1832.

[249] M. Watanabe, S. Motoo, Electrocatalysis by Ad-Atoms 2. Enhancement of Oxidation of Methanol on Pt by Ruthenium Ad-atoms, Journal of Electroanalytical Chemistry, 60 (1975) 267-273.

[250] A. Lueking, R.T. Yang, Hydrogen spillover from a metal oxide catalyst onto carbon nanotubes - Implications for hydrogen storage, Journal of Catalysis, 206 (2002) 165-168.

[251] A. Lueking, R.T. Yang, Hydrogen spillover from a metal oxide catalyst onto carbon nanotubes - Implications for hydrogen storage (vol 206, pg 165, 2002), Journal of Catalysis, 211 (2002) 565-565.

[252] B.E. Warren, X-Ray Diffraction, Addison-Wesley, USA, 1969.

APPENDIX A

Pt-Sn BIMETALLIC PHASE EQUILIBRIUM

Platinum-tin system forms five different intermetallic phases which have different crytal structures such as $PtSn_4$, $PtSn_2$, $PtSn_3$, Pt-Sn, and Pt_3Sn. The equilibrium phase diagram that exhibited five intermediate stochiometric phases were given in Figure A. 1 [109].

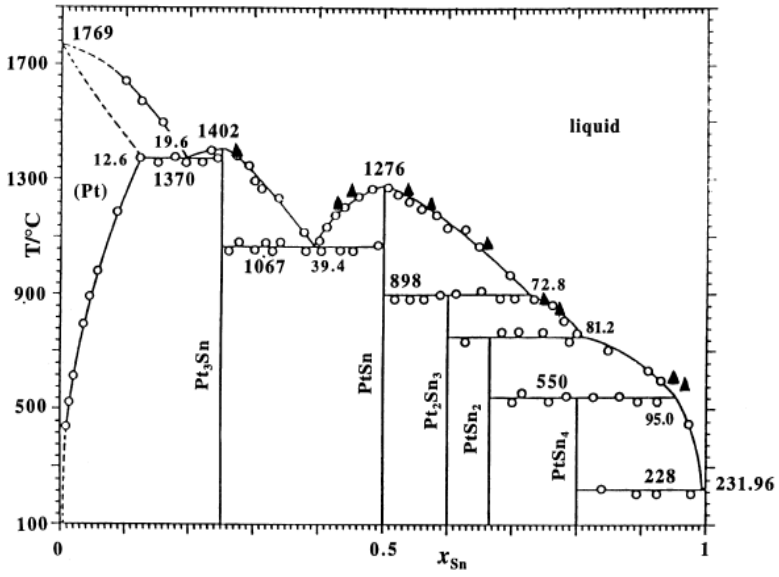

Figure A. 1 The equilibrium phase diagram for Pt-Sn bi-metallic system [109].

APPENDIX B

STRUCTURE SENSITIVITY

Pt particle has a cubo-octahedral crystal structure as shown in Figure B.1. Furthermore, different facets of metal exhibit different electrochemical activities as shown in Figure B.2 and Figure B.3.

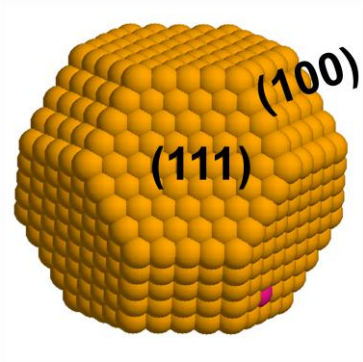

Figure B. 1 Cubo-octahedral crystal structure

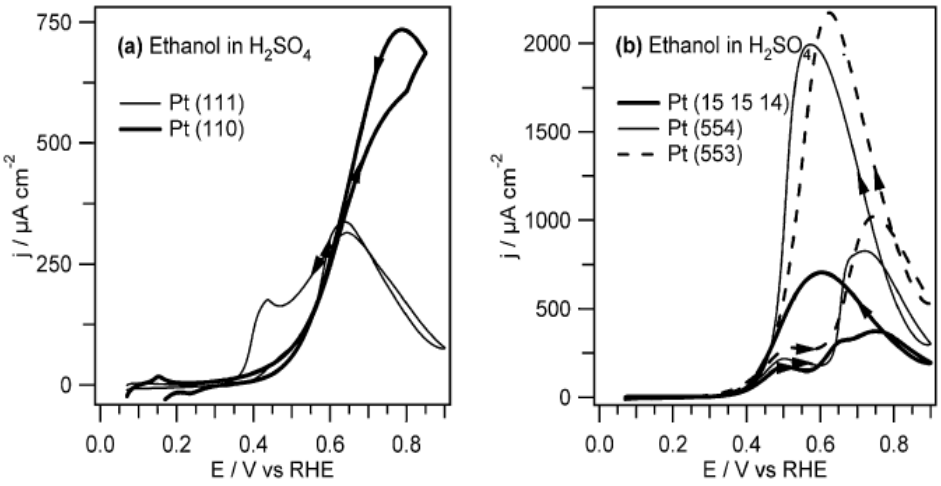

Figure B. 2 Cyclic voltammograms for the electro-oxidation of 0.5 M ethanol in 0.5 M H_2SO_4 on (a) Pt (111) and Pt (110) and (b) Pt (15 15 14), Pt (554) and Pt (553), respectively. All voltammograms were recorded at a scan rate of 10 mV s^{-1}. Arrows indicate the scan directions [198].

APPENDIX C

XRD AND XPS FIGURES

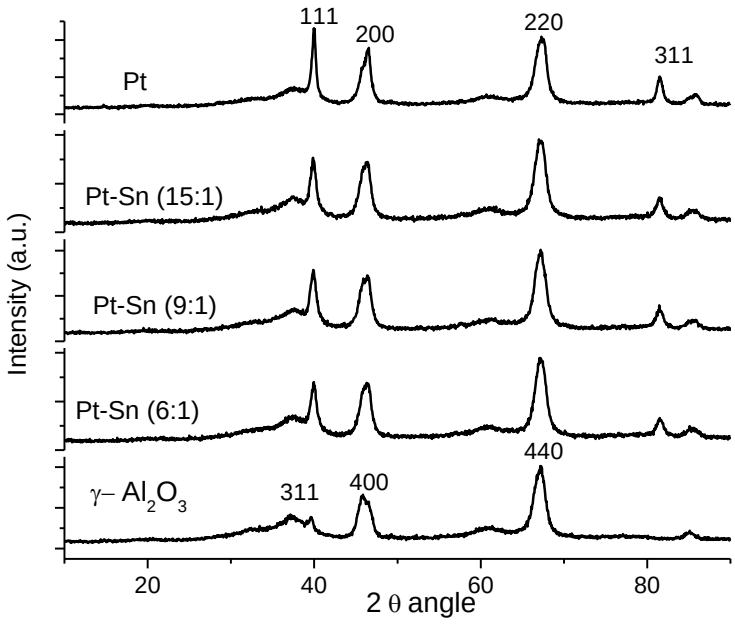

Figure C. 1 XRD Patterns of γ-Al_2O_3 supported Pt and Pt-Sn catalysts

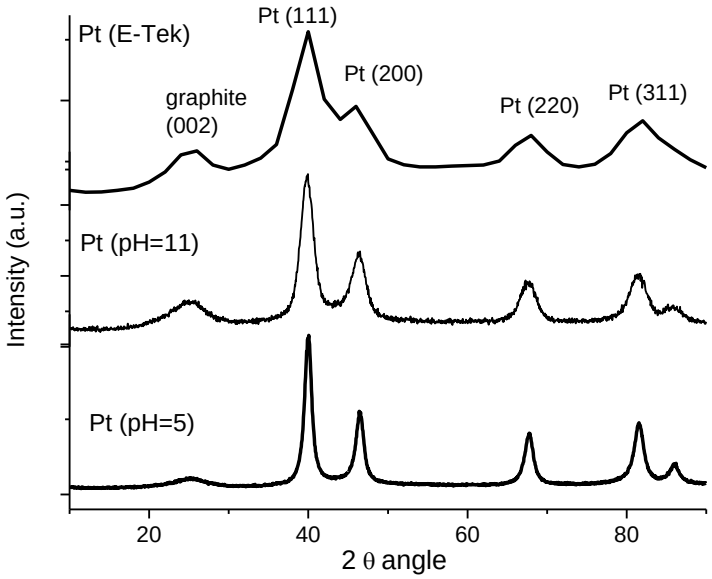

Figure C. 2 XRD patterns on 20 % Pt catalysts.

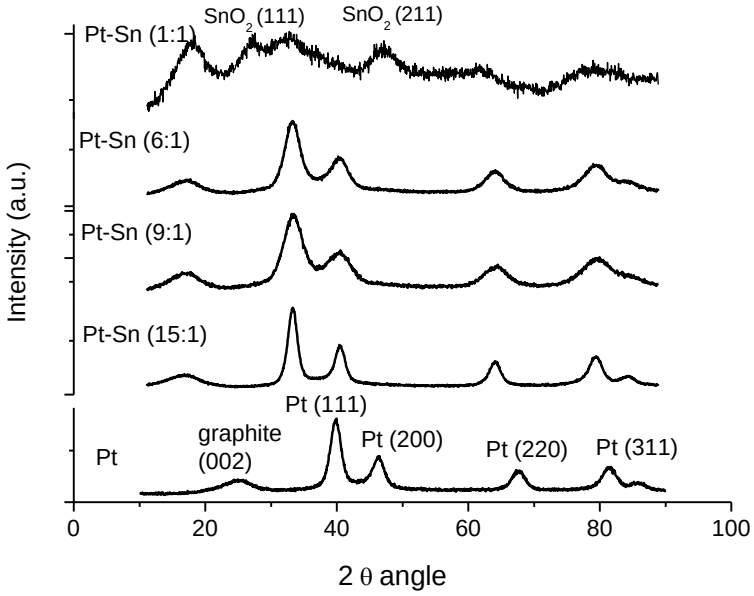

Figure C. 3 XRD patterns on carbon supported 20% Pt and 20 % Pt:Sn catalysts prepared by polyol method at 15:1, 9:1, 6:1, 1:1 Pt:Sn atomic ratios.

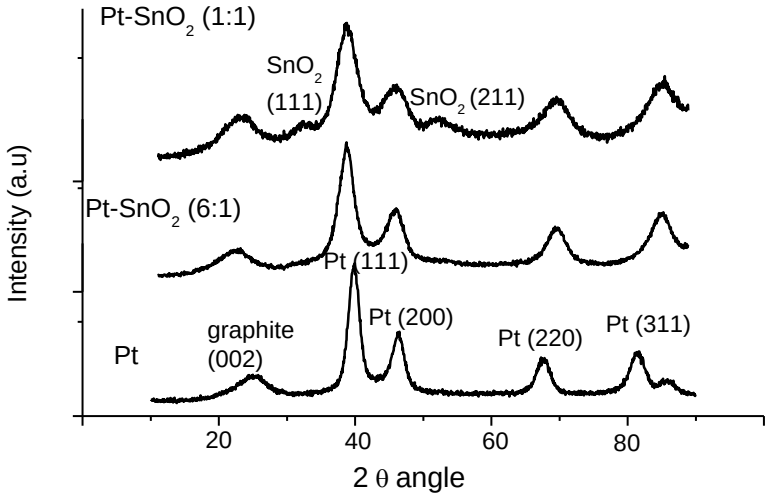

Figure C. 4 XRD patterns on carbon supported 20 % Pt:SnO_2(6:1)/C and 20 % Pt:SnO_2(1:1)/C catalysts prepared by polyol method.

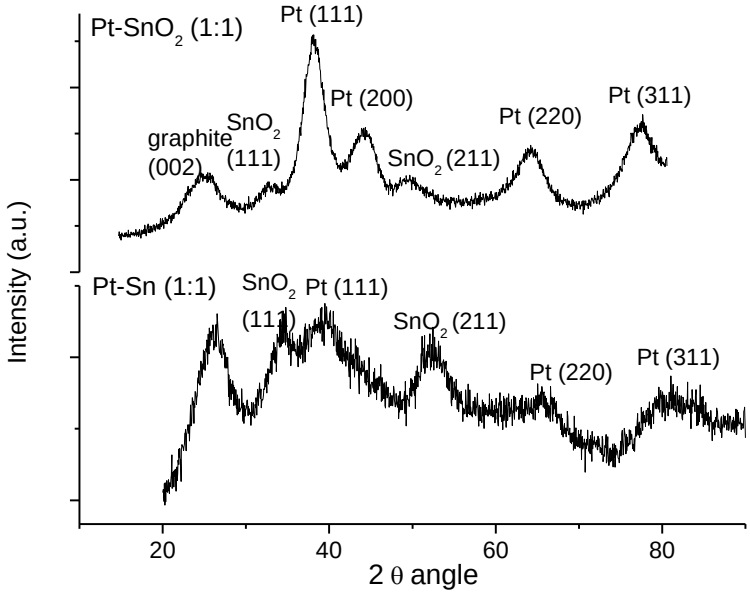

Figure C. 5 XRD patterns on carbon supported 20 % Pt:SnO_2(1:1)/C and 20 % Pt:Sn(1:1)/C catalysts prepared by polyol method.

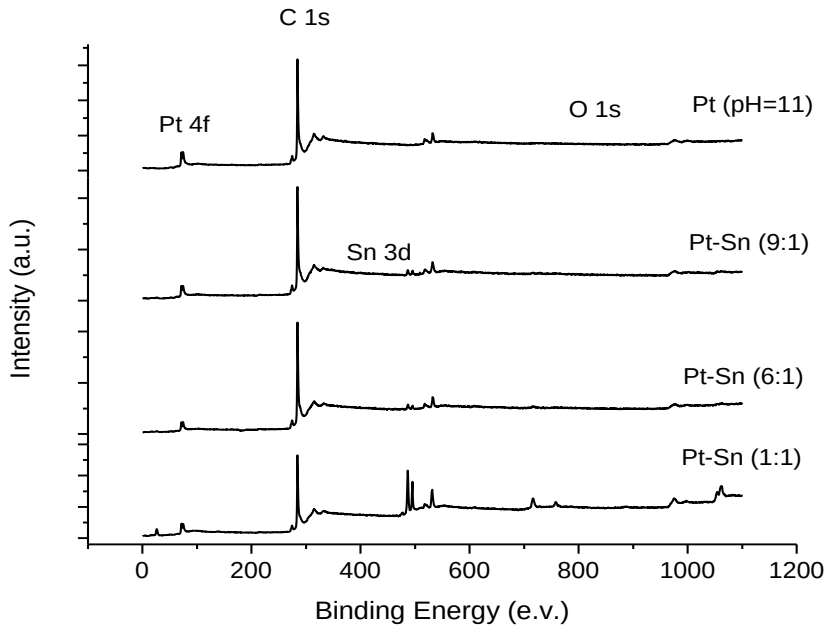

Figure C. 6 General XPS spectrum of 20%Pt/C and 20%Pt-Sn/C catalysts

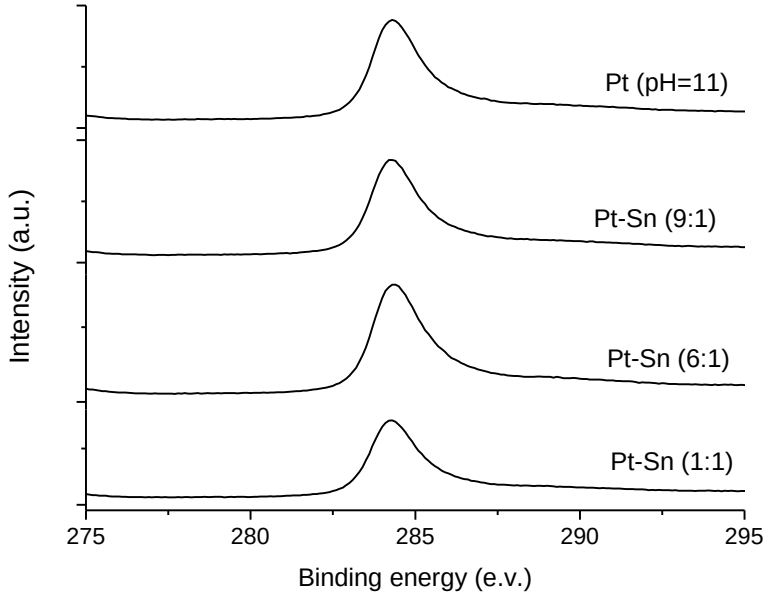

Figure C. 7 C 1s XPS spectrum of 20%Pt/C and 20%Pt-Sn/C catalysts.

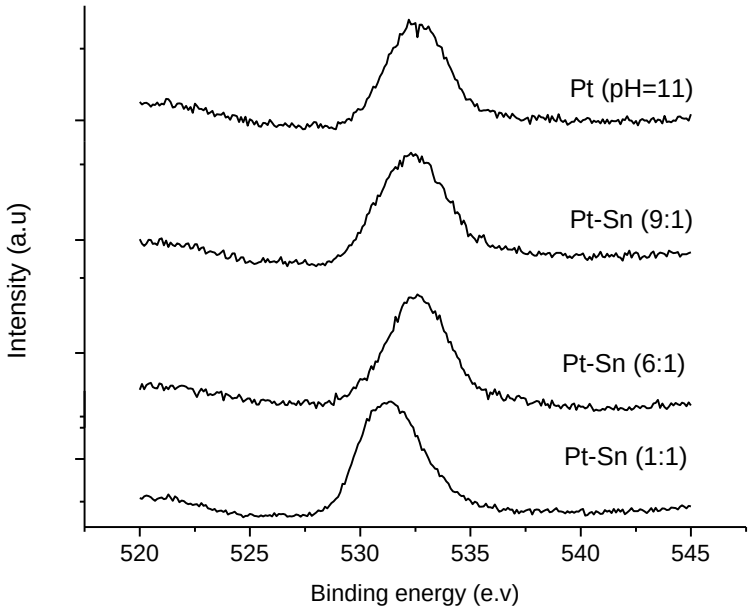

Figure C. 8 O 1s XPS spectrum of 20%Pt/C and 20%Pt-Sn/C catalysts.

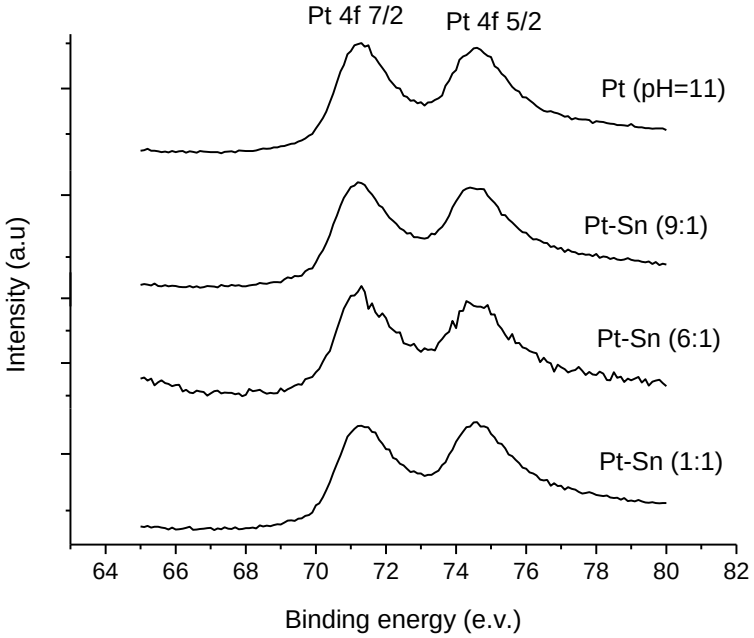

Figure C. 9 Pt 4f XPS spectrum of 20%Pt/C and 20%Pt-Sn/C catalysts.

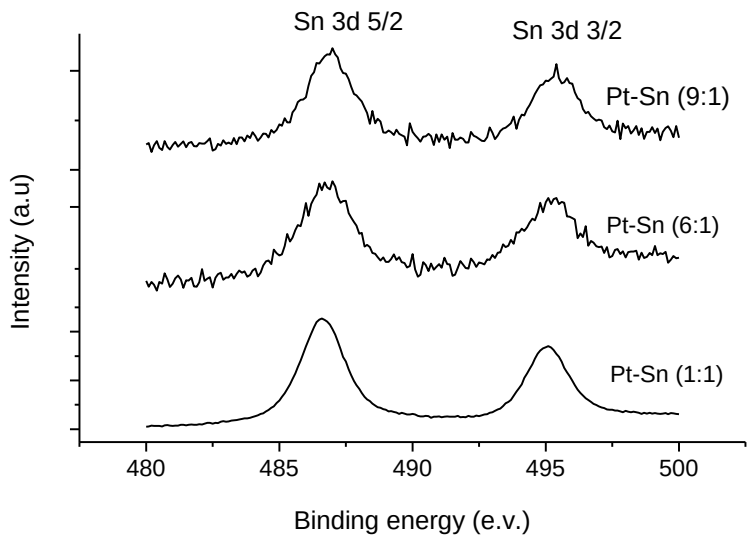

Figure C. 10 Sn 3d XPS spectrum of 20%Pt/C and 20%Pt-Sn/C catalysts.

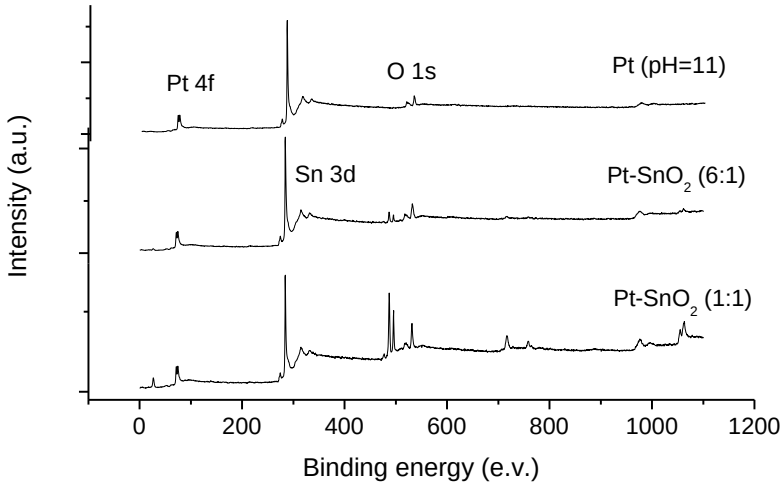

Figure C. 11 General XPS spectrum of 20%Pt/C and 20%Pt-SnO_2/C catalysts

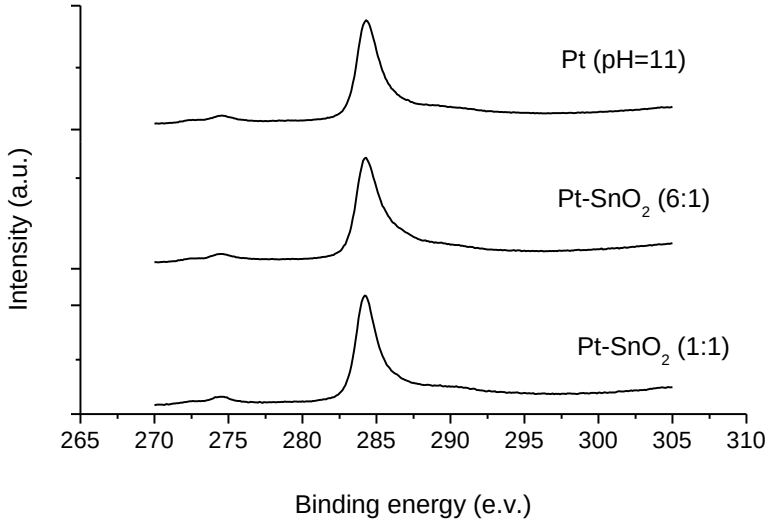

Figure C. 12 C 1s spectrum of 20%Pt/C and 20%Pt-SnO_2/C catalysts

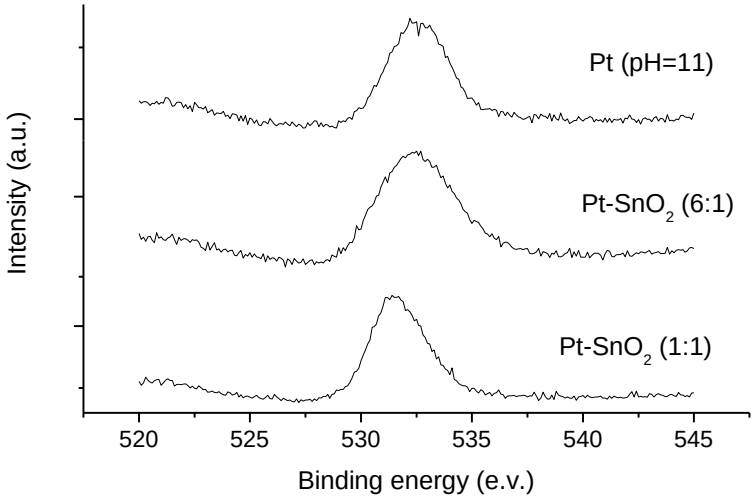

Figure C. 13 O 1s spectrum of 20%Pt/C and 20%Pt-SnO_2/C catalysts.

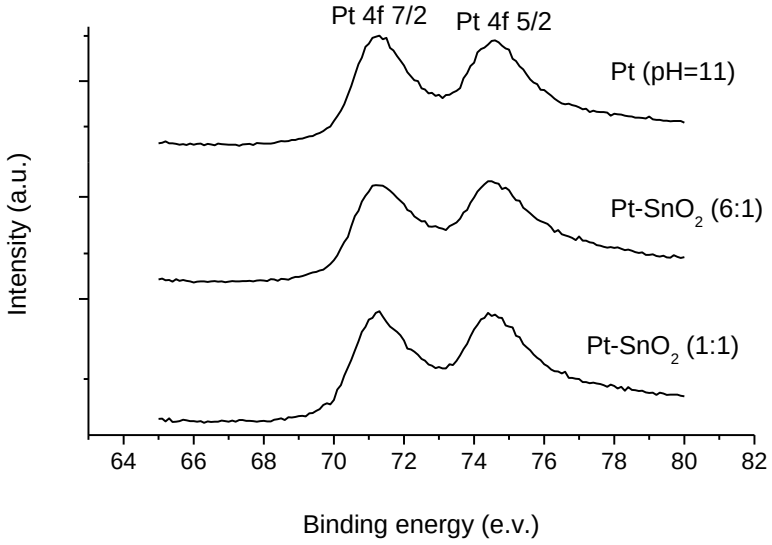

Figure C. 14 Pt 4f spectrum of 20%Pt/C and 20%Pt-SnO_2/C catalysts.

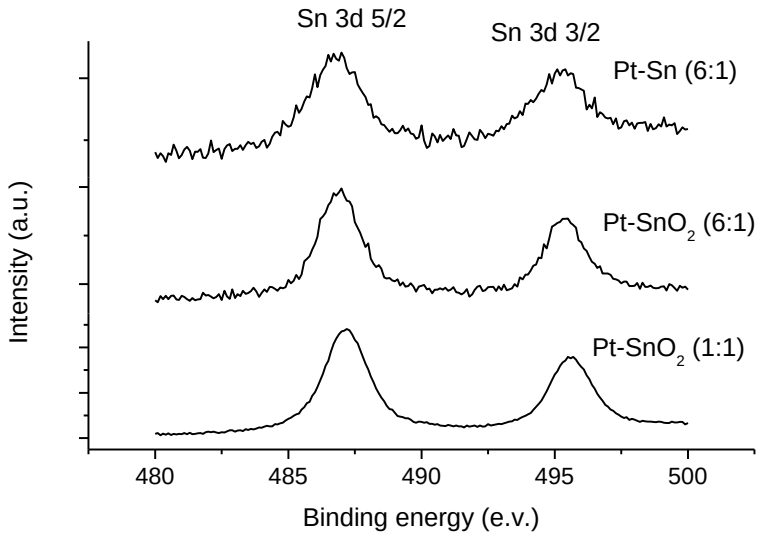

Figure C. 15 Pt 4f spectrum of 20%Pt/C and 20%Pt-SnO_2/C catalysts.

APPENDIX D

PARTICLE SIZE CALCULATIONS

D. 1 PARTICLE SIZE CALCULATION BY XRD

Scherrer equation and XRD spectra was used to calculate the particle size of the catalysts. XRD spectra was given in Figure D.1. Scherrer's equation is given as following:

$$d = \frac{K\lambda}{\beta \cos\Theta} \qquad \text{(D- 1)}$$

where

β is the integral breadth of peak at 2Θ values ($\beta = \Theta_1 - \Theta_2$)

λ is the wavelength of the X-ray beam ($\lambda_{Cu\ K\alpha}$=1.54 nm).

Θ is the half of the deviation of the diffracted beam and

d is the interplanar spacing for a plane.

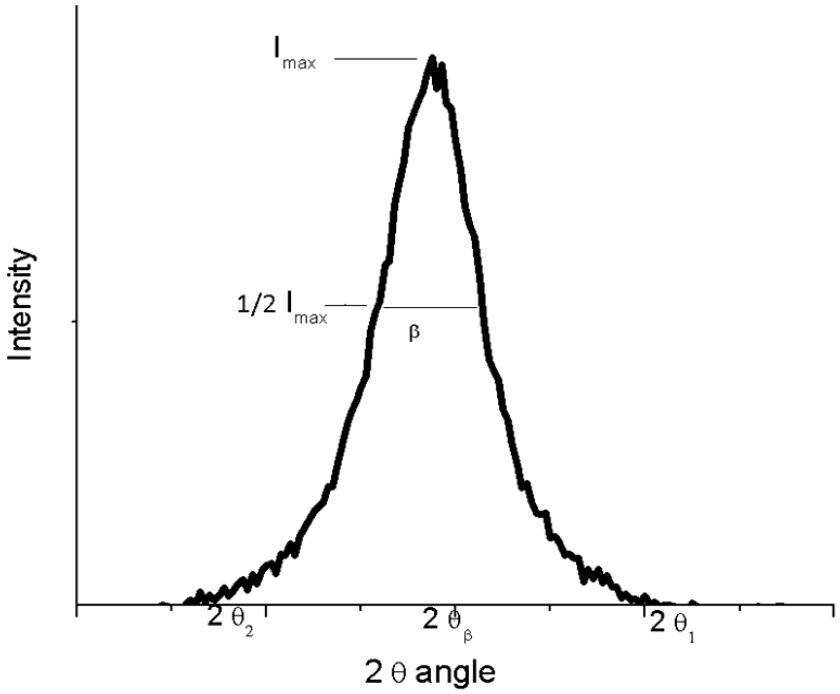

Figure D. 1 X-ray diffraction pattern

Sample calculation for Pt/C (E-Tek) catalyst:

$\beta = 3.8^{o} * 2 * \pi/360 = 0.066$ rad

$2\Theta_{\beta} = 39.95^{o}$

$0.8 < K < 1$

$$\frac{0.8*0.154}{0.066* \text{Cos}\,(39.95/2)} < d < \frac{1*0.154}{0.066* \text{Cos}\,(39.95/2)} \quad (2.7 \text{ nm} < d < 3.4 \text{ nm})$$

D. 2 PARTICLE SIZE CALCULATION BY MICROCALORIMETRY

Dispersion of catalyst could be obtained from adsorption thermogram. A typical differential heat of adsorption thermogram was shown in Figure D.2.The saturation coverage (while the differential heat of adsorption reaches the zero, saturation coverage obtained). There is a relation between the particle size and the dispersion as;

$$\text{Dispersion (\%)} = 100 / d\ (\text{nm}) \qquad \text{(D- 2)}$$

Sample calculation for Pt/C (E-Tek) catalyst:

Dispersion (%) = 20moles of CO gas adsorbed / mole of Pt

$$d\ (\text{nm}) = \frac{100}{28} = 3.57\ \text{nm}$$

D. 3 PARTICLE SIZE CALCULATION BY TEM

Particle size distribution and aspect ratio distribution could be obtained from TEM images by counting the particles and measuring their diameter and length. The aspect ratio is the ratio of the length of the minor axis to that of the major axis (see Figure D.3.).

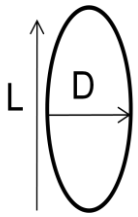

Figure D. 2 Schematic representation of the aspect ratio (D/L) calculation

TEM images were taken for Pt/C (E-Tek), Pt/C (pH=11), and Pt/C (pH=5) catalysts. Figures of mean particle sizes distribution and mean aspect ratios determined from the analysis were given as follows:

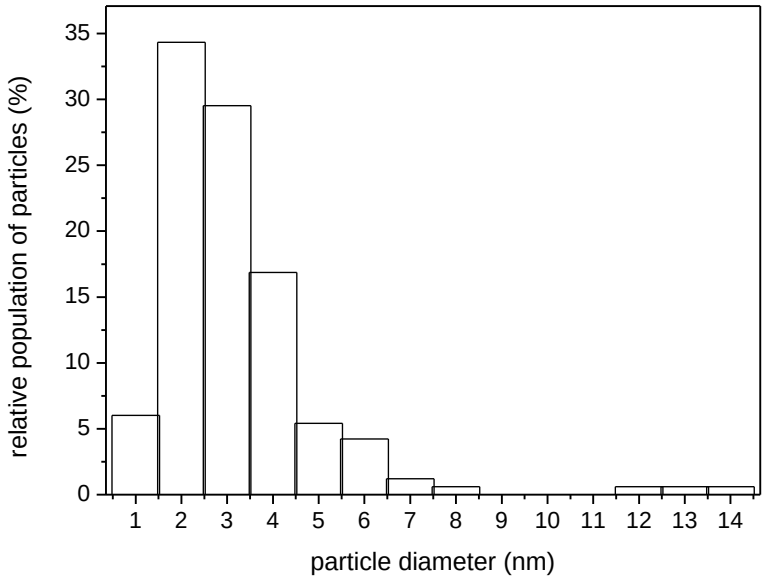

Figure D. 3 Particle size distribution of Pt/C (E-Tek) catalysts

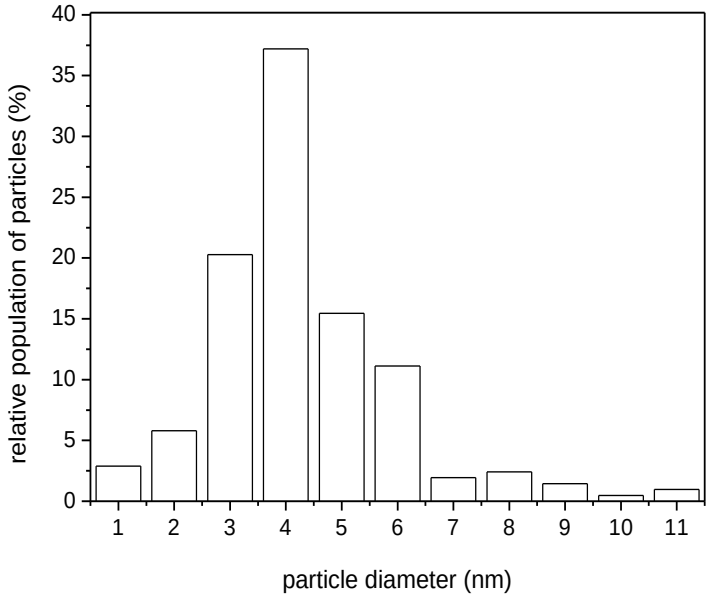

Figure D. 4 Particle size distribution Pt/C (pH=11) catalyst.

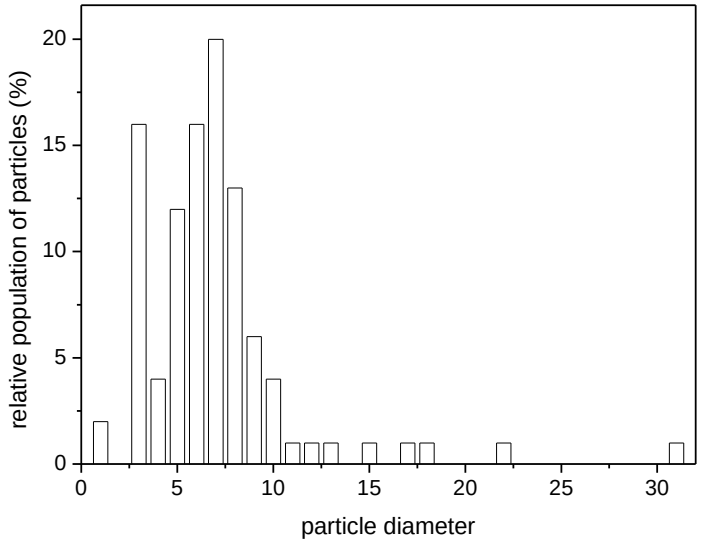

Figure D. 5 Particle size distribution of Pt/C (pH=5) catalyst.

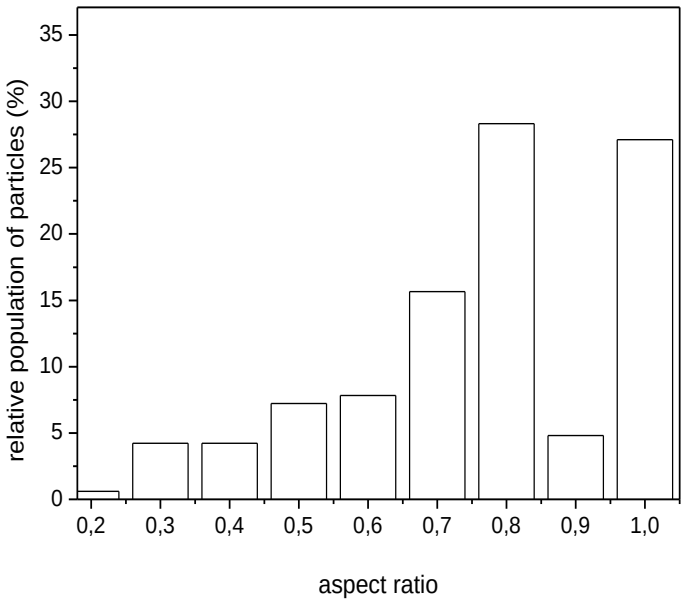

Figure D. 6 Aspect ratio distribution of Pt/C (E-Tek) catalyst

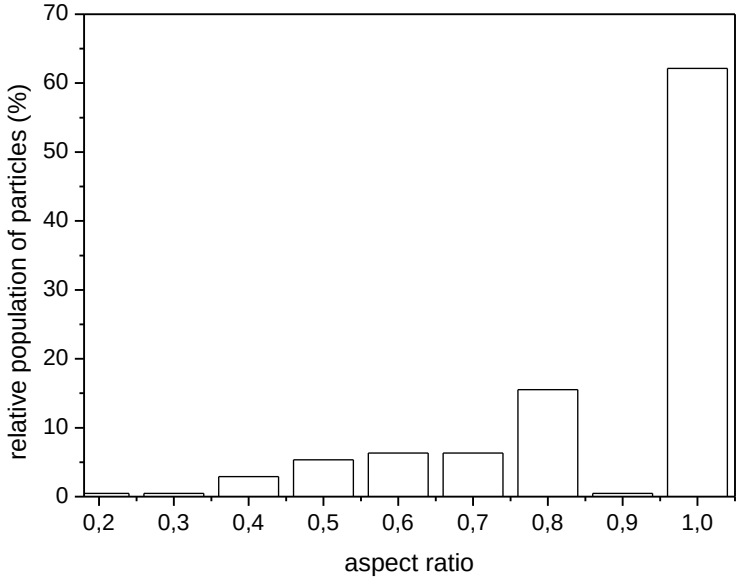

Figure D. 7 Aspect ratio distribution of catalysts Pt/C (pH=11) catalyst.

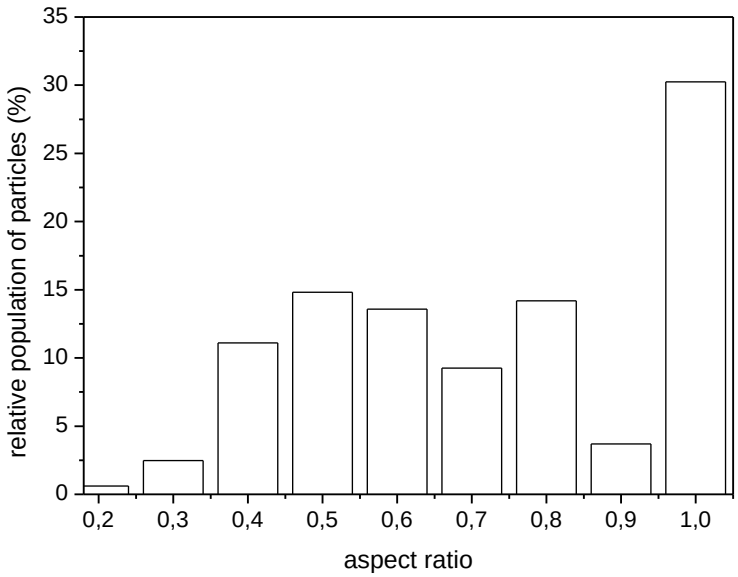

Figure D. 8 Aspect ratio distribution of Pt/C (pH=5) catalyst.

APPENDIX E

ELECTROCHEMICAL CALCULATIONS AND MEASUREMENTS

E. 1 ELECTROCHEMICAL SURFACE AREA (ESA) CALCULATION

By integrating the area under the hydrogen reduction peak. Electro-chemical surface area could be found

$$E.S.A.=A/(K*v*a) \quad \text{(E- 1)}$$

Where

A is the integral of hydrogen reduction (A/V cm^2),
K= 0.21 mC/cm^2 (1 C= 1 A. 1 s),
v is scan rate (mV/s),
a is the Pt loading on the electrode ($\mu g/cm^2$).

E. 2 Pt UTILIZATION CALCULATION

The Pt utilization is stated by the ratio of electrochemical surface area (ESA) to total metal surface area (SA).

E. 3 ETHANOL ELECTRO-OXIDATION MEASUREMENTS ON GLASSY CARBON ELECTRODE

Cyclic voltammetry measurements were performed on the graphite support in 0.5 M H_2SO_4 solution and small amounts of ethanol were added this electrolyte to observe the ethanol oxidation on the glassy carbon support. When the concentration of ethanol was increased by order of magnitude, concentration change did not make considerable effect on the glassy carbon electrode. This is a desirable situation because when the catalysts are added on to the surface of the glassy carbon electrode there will be no additional effect coming from the oxidation of ethanol on the glassy carbon electrode (see Figure E.1 and Figure E.2).

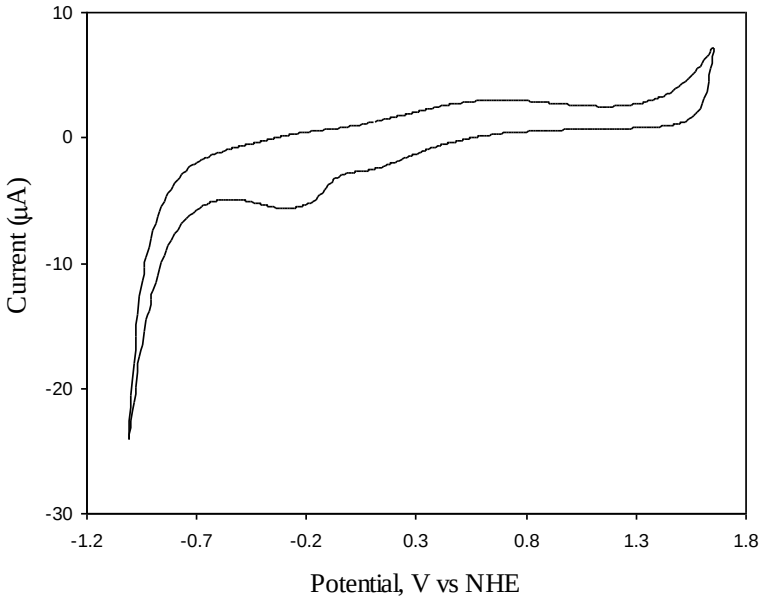

Figure E. 1 CV of Glassy carbon in 0.5 M H_2SO_4 solution (scan rate:0.01 V/s)

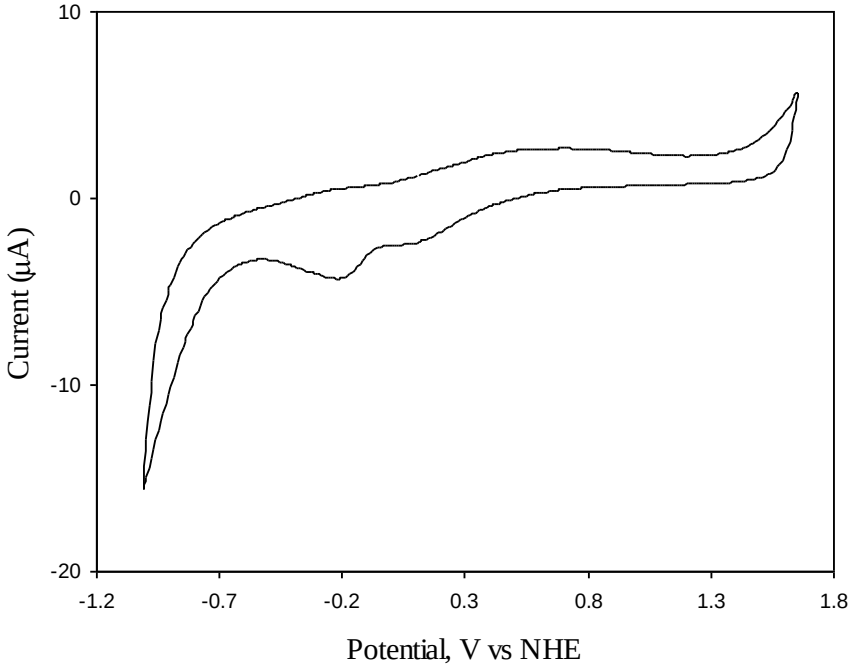

Figure E. 2 CV of Glassy carbon in 0.5 M H_2SO_4 + 0.5 M ethanol solution (scan rate: 0.01 V/s)

E. 4 ELECTRO-OXIDATION MEASUREMENTS ON CARBON

Cyclic voltammetry measurements were performed on C (Vulcan XC-72 R) to observe the activity of ethanol oxidation reaction on C support. Carbon was dispersed in water and Nafion mixture and an ink was obtained. This mixture was spread on the glassy carbon electrode. The evaluation of ethanol oxidation was carried out in 0.5 M ethanol concentration in 0.5 M H_2SO_4 solution (see Figure E.3 and Figure E.4).

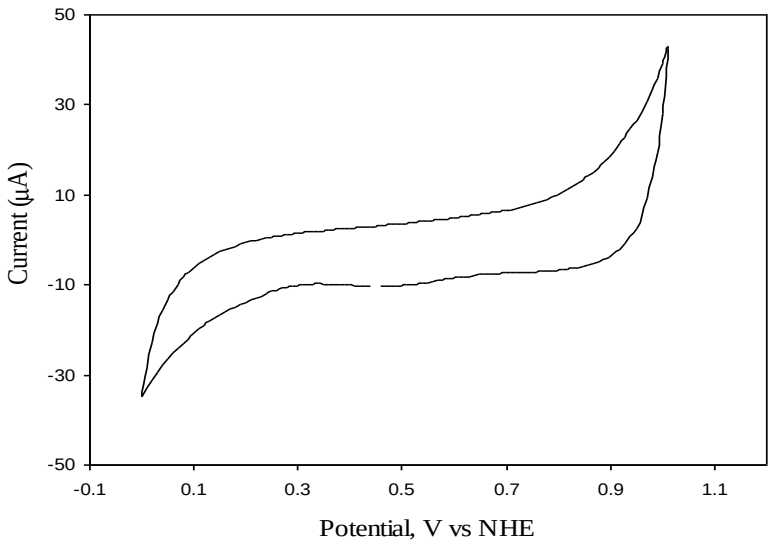

Figure E. 3 CV of carbon in 0.5 M H_2SO_4 solution (scan rate: 0.01 V/s)

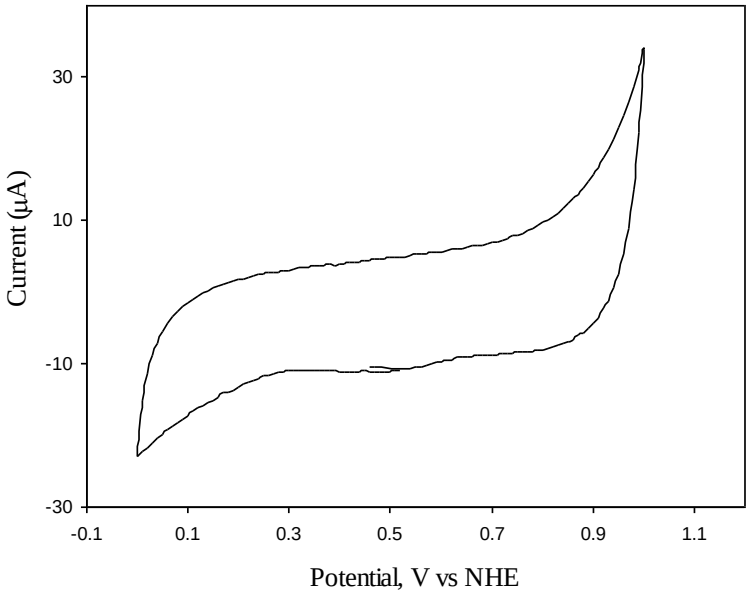

Figure E. 4 CV of carbon in 0.5 M H_2SO_4 + 0.5 M ethanol solution (scan rate: 0.01 V/s)

E. 5 ACTIVATION EXPERIMENTS ON PT/C CATALYSTS

Activation was performed before every experiment. Activation was performed in 0.5 M H2SO4 solution applying 100 cycle to remove the surface adsorbed species from Pt surface. In Figure E.5 and Figure E.6, activation experiments were given on Pt/C (E-Tek) and Pt/C (pH=11), respectively. It was observed that hydrogen peaks and oxidation peaks increased by applying cyclization.

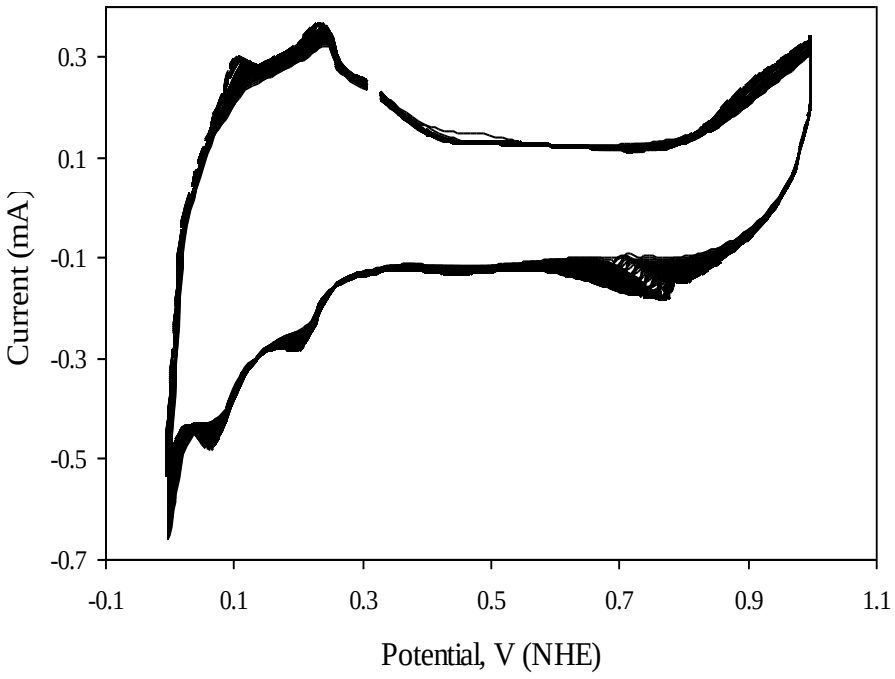

Figure E. 5 CV of Pt/C (E-Tek) in 0.5 M H_2SO_4 solution (scan rate:0.01 V/s) (100 cycle)

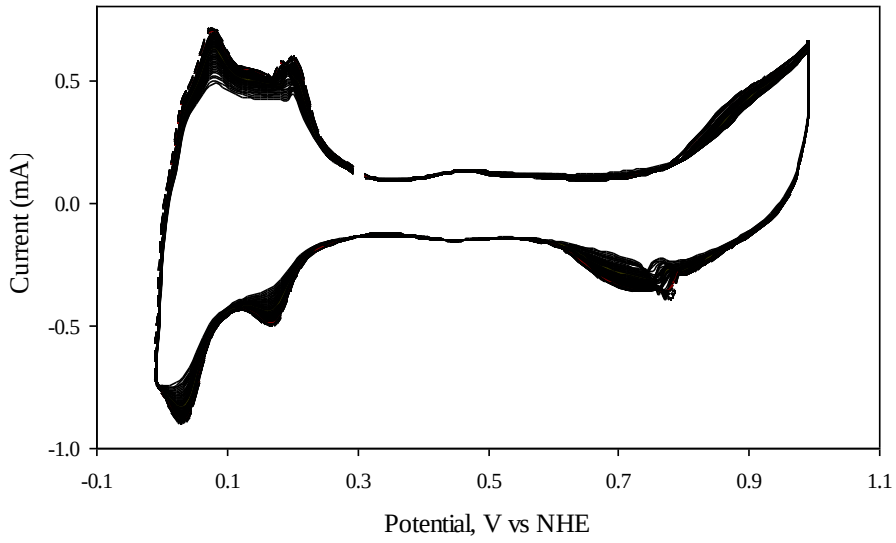

Figure E. 6 CV of Pt/C (pH=10.8) in 0.5 M H_2SO_4 solution (scan rate:0.01 V/s) (100 cycle)

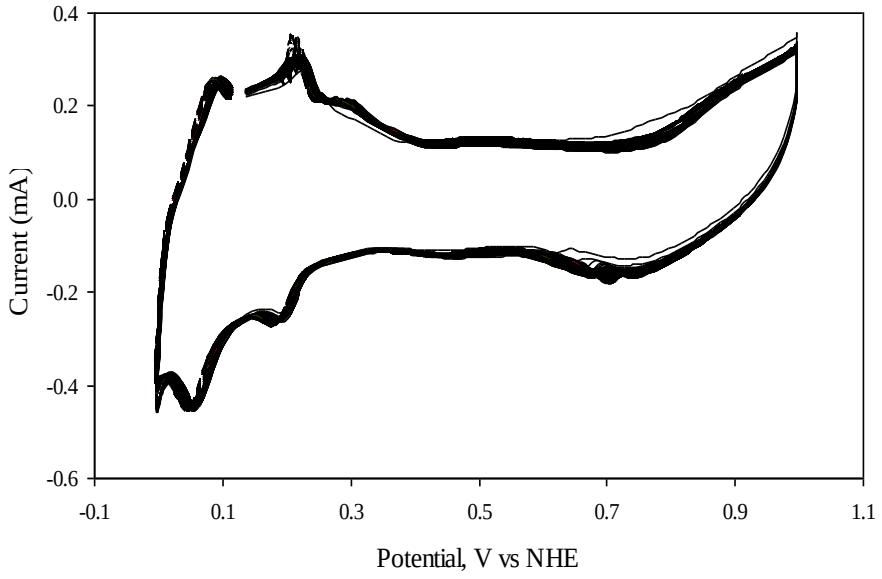

Figure E. 7 CV of Pt/C (E-Tek) in 0.5 M H_2SO_4 solution after oxidation in 0.5 M ethanol (scan rate:0.01 V/s) (100 cycle)

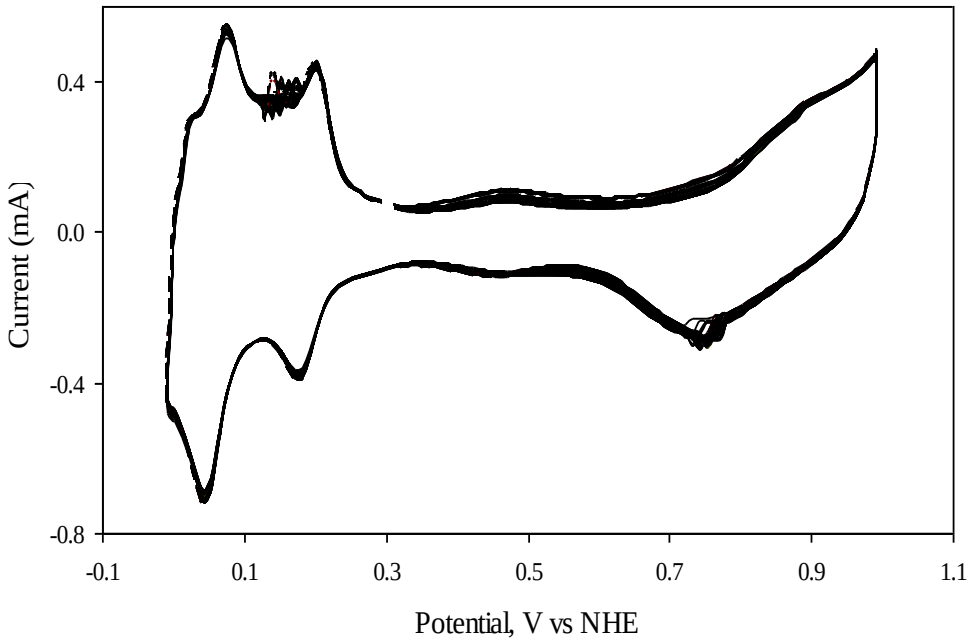

Figure E. 8 CV of Pt/C (pH=10.8) in 0.5 M H_2SO_4 solution after oxidation in 0.5 M ethanol (scan rate:0.01 V/s) (100 cycle)

E. 6 FIGURES

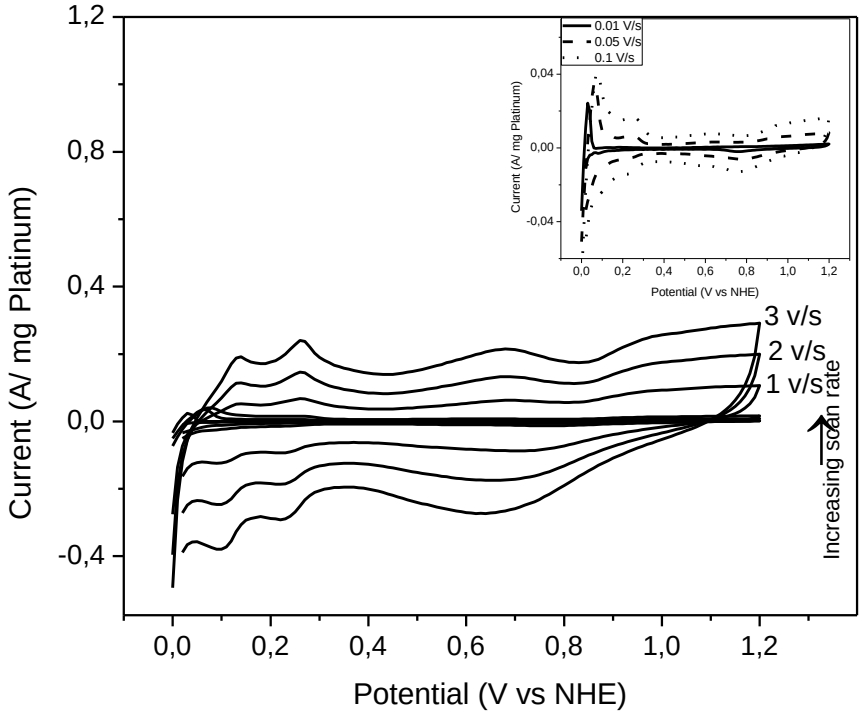

Figure E. 9 Cyclic voltammogram of 20% Pt/C (pH=11) catalyst in 0.5 M H_2SO_4 solution at 1 V/s, 2 V/s, 3 V/s scan rates, upper insert shows the cyclic voltammogram of 20% Pt/C (pH=11) catalyst in 0.5 M H_2SO_4 solution at 0.01 V/s, 0.05 V/s, 0.1 V/s

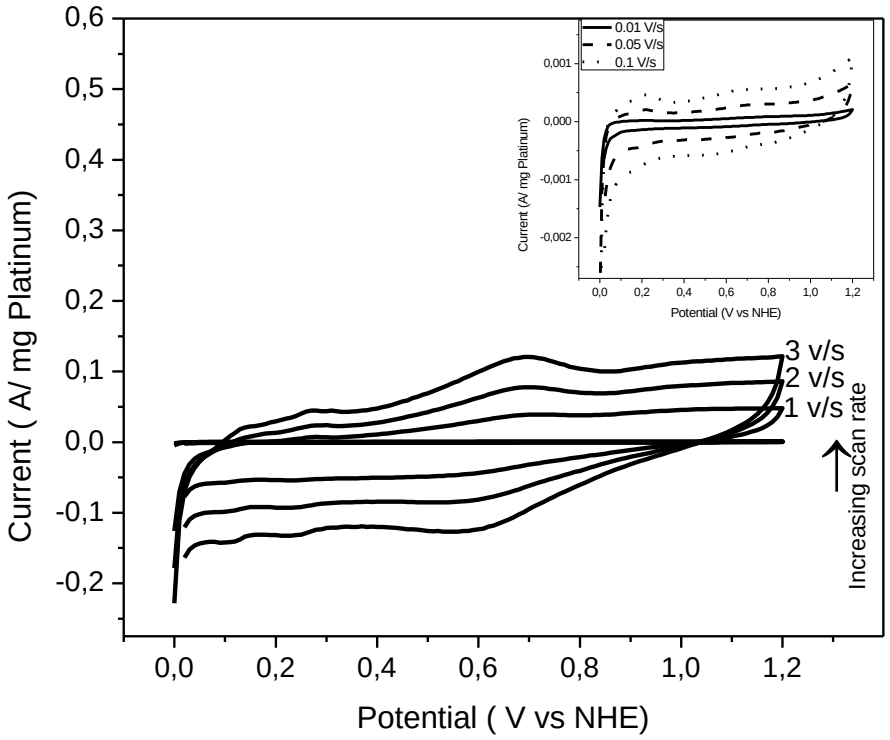

Figure E. 10 Cyclic voltammogram of 20% Pt/C (pH=5) catalyst in 0.5 M H_2SO_4 solution at 1 V/s, 2 V/s, 3 V/s scan rates, upper insert shows the cyclic voltammogram of 20% Pt/C (pH=5) catalyst in 0.5 M H_2SO_4 solution at 0.01 V/s, 0.05 V/s, 0.1 V/s.

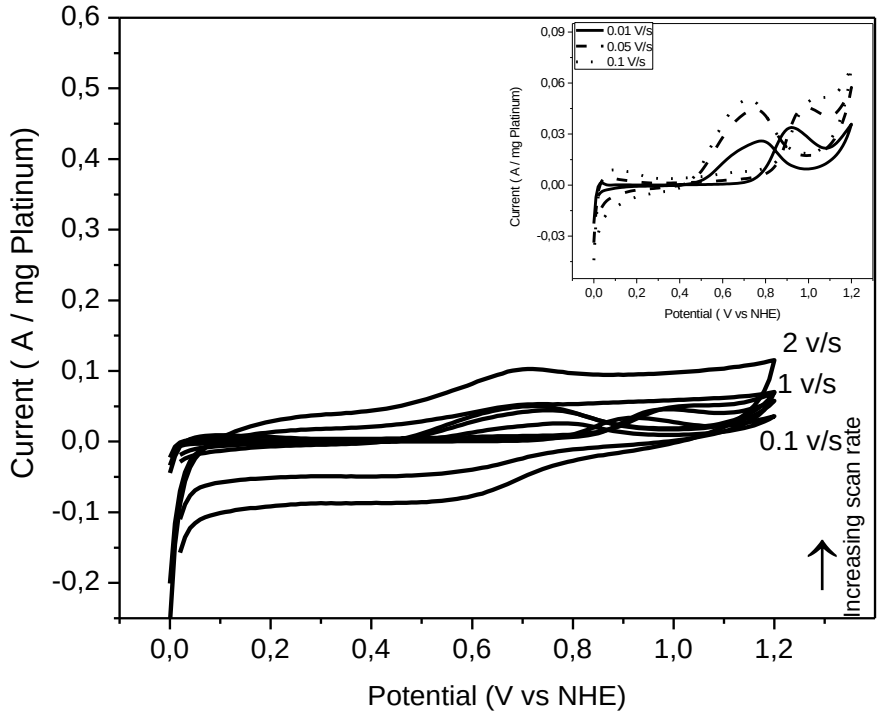

Figure E. 11 Cyclic voltammogram of 20% Pt/C (pH=11) catalyst in 0.5 M H_2SO_4 + 0.5 M EtOH solution at 1 V/s, 2 V/s scan rates, upper insert shows the cyclic voltammogram of 20% Pt/C (pH=11) catalyst in 0.5 M H_2SO_4 +0.5 M EtOH solution at 0.01 V/s, 0.05 V/s, 0.1 V/s.

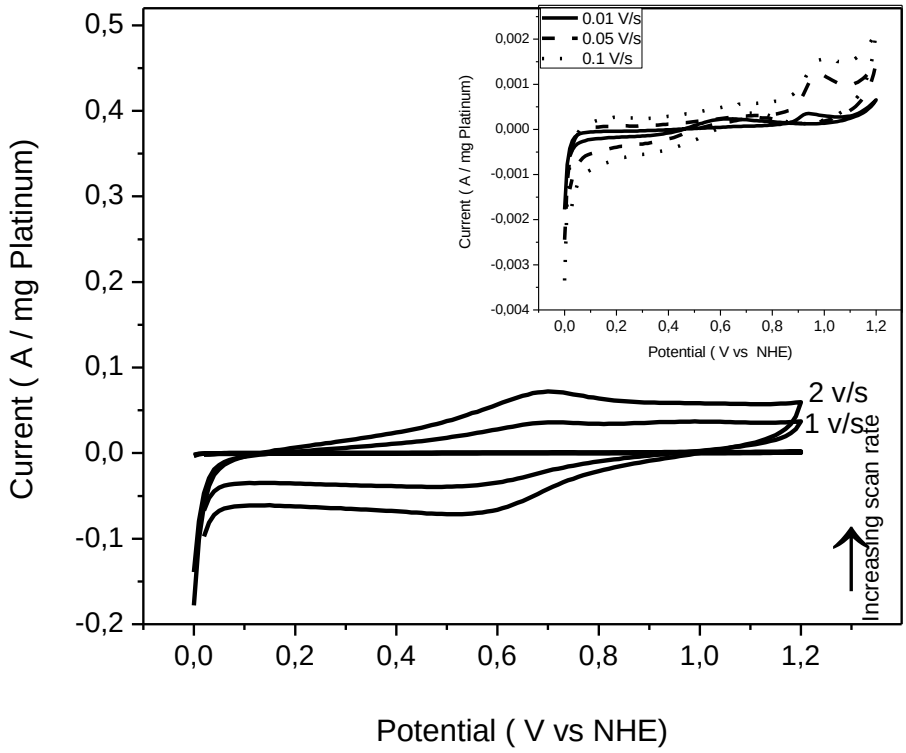

Figure E. 12 Cyclic voltammogram of 20% Pt/C (pH=5) catalyst in 0.5 M H_2SO_4 + 0.5 M EtOH solution at 1 V/s, 2 V/s scan rates, upper insert shows the cyclic voltammogram of 20% Pt/C (pH=5) catalyst in 0.5 M H_2SO_4 +0.5 M EtOH solution at 0.01 V/s, 0.05 V/s, 0.1 V/s.

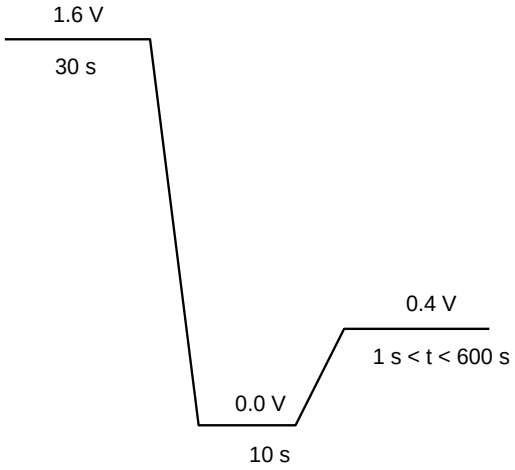

Figure E. 13 Schematic representation of pretreatment performed on 20% Pt/C (home-made) and 20% Pt-Sn (6:1)/C catalysts in 0.5 M H_2SO_4 + 0.5 M EtOH solution at 0.05 V/s before poisining measurements.

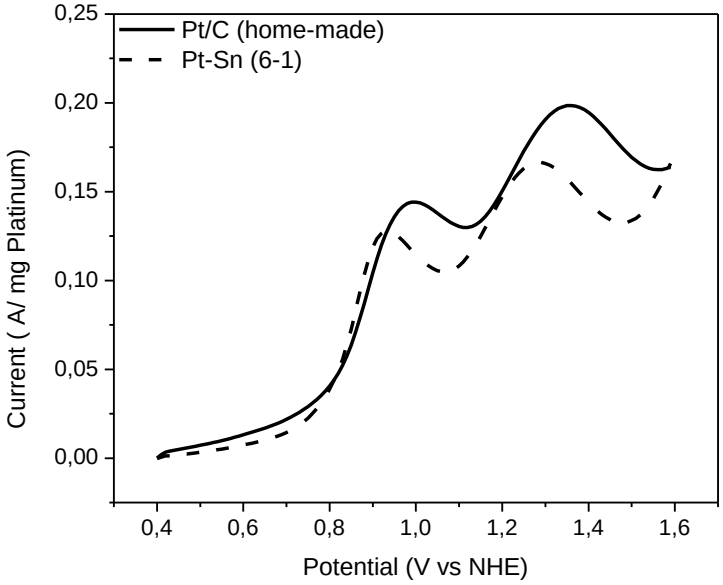

Figure E. 14 Linear sweep voltammetry measurmensts on 20% Pt/C and Pt-Sn (6:1)/C catalyst in 0.5 M H_2SO_4 + 0.5 M EtOH solution at 0.05 V/s.

CURRICULUM VITAE

Hilal Demir-Kivrak
Middle East Technical University
Department of Chemical Engineering
06531 Ankara/Turkey

Phone: +90 312 210 43 86
Fax: +90 312 210 26 00
E-mail: hilalkivrak@googlemail.com

PERSONAL INFORMATION

Nationality: Turkish (TC)
Gender: Female
Date and Place of Birth: 21th September 1980, Bursa

EDUCATION

Degree	Institution	Year of Graduation
Ph. D.	METU Chemical Engineering	2010
B. Sc.	Eskisehir Osmangazi University Chemical Engineering	2002
High School	Bilecik Ertugrulgazi High School	1998

WORK EXPERIENCE

Year	Place	Enrollment
2001 August	Eskisehir Arcelik Refrigerator Industry	Internship
2001 July	Eskisehir 1st Military Aerospace Supply and Maintenance Center	Internship
2000 July	Bilecik Marmara Pulp and Pack Industry	Internship

HONORS and AWARDS

2007 – 2008	Ph.D. Abroad Research Scholarship, TUBİTAK
2002	2nd Rank Student Award, Department of Chemical Engineering, Eskisehir Osmangazi University.
1998	3rd Rank Student Award, Bilecik Ertugrulgazi High School

MEMBERSHIPS

2006 -	Catalysis Society of Turkey
2006 - 2009	Middle East Technical University, Tae Kwon Do club
2010-	Middle East Technical University, Outdoor sports club

FOREIGN LANGUAGES

Advanced English

PROFESSIONAL

Year

2009 September, Visiting Scientist;
Technical University of Darmstadt, Department of Inorganic Chemistry, Germay *"*Production of PAOX membrane and synthesis of Carbon Nanotubes on PAOX membrane by chemical vapor deposition method*"*

2008 -2009 (July-February) Visiting Scientist;
Iowa State University, Department of Chemical and Biological Engineering, IA U.S.A **"**Cu deposition on Ti and Ta during alkaline corrosion*"*

2002- 2010, Research Assistant;
Middle East Technical University (METU), Department of Chemical Engineering, Ankara, Turkey (on leave from Selcuk University for OYP program).

PUBLICATIONS

Refereed Journals:

1. Z. Király, Á. Mastalir, Á. Császár, H. Demir, D. Uner, G. H. Findenegg, ‘‘Liquid chromatography as a novel method for determination of the dispersion of supported Pd particles’’, Journal of Catalysis 2007, 245, 265-269.

2. H. Kivrak, Á. Mastalir, Z. Király, D. Uner, “Determination of the dispersion of supported Pt particles by gas-phase and liquid-phase measurements”, Catalysis Communications 2009, 10, 1002-1005.

3. H. Kivrak, S. Kuliyev, H. Tempel, J. J. Schneider, D. Uner, “Carbon Nanotube Structures As Support For Ethanol Elelctro-Oxidation Catalysis”, International Journal of Chemical Reactor Engineering 2010, Manuscript Submitted.

4. H. Kivrak, S. Kuliyev, H.J. Kleebe, D. Uner, “Ethanol Electro-oxidation Reaction over Pt/C Catalysts: The Effect of Platinum Particle Size” manuscript in preparation.

5. H. Kivrak, S. Kuliyev, D. Uner, “Ethanol Electro-oxidation Reaction over Pt/C Catalysts: The Effect of Tin Addition” manuscript in preparation.

6. H. Kivrak, S. Kuliyev, D. Uner, “Ethanol Elelectro-oxidation Reaction over Pt/C Catalysts: The Effect of Tin Oxide Phase” manuscript in preparation.

7. H. Kivrak, H. Tempel, S. Kuliyev, J. J. Schneider, D. Uner, “TiO_2-Carbon Nanotube Structures For Photo-electrocatalysis“ manuscript in preparation.

National and International Conference Presentations:

1. H. Ö. Olcay, H. Demir, D. Uner, E. Şeker, “Sol-gel yontemi ile hazirlanan mixed –oksit katalizorlerin uzerinde Etanol buhar reformlamasi”, Ulusal Kimya Mühendisligi Kongresi 6, Izmir-Türkiye, September 2004, Poster Presentation.

2. H. Ö. Olcay, H. Demir, D. Uner, E. Şeker, ‘Ethanol steam reforming on sol-gel prepared mixed oxide catalysts’, 19th North American Catalysis Meeting, Philadelphia, Pennsylvania, U.S.A. May 2005, Poster Presentation.

3. H. Demir, E. Şeker, D.Uner, 'Microcalorimetric characterization of sol gel prepared SiO_2 supported Pd and ZnO catalysts', EuropaCAT VII, Sofia, Bulgaria, September 2005, Poster Presentation.

4. H. Demir, H. Olcay, E. Seker, D. Uner, 'Steam reforming of ethanol over sol-gel-synthesized mixed oxide catalysts', 1st International Hydrogen Congress, Istanbul, Turkey, July 2005, Poster Presentation.

5. H. Demir, D.Uner, 'Microcalorimetric studies to investigate the effect of Sn addition to elucidate CO poisioning on γ-Al_2O_3 supported Pt-Sn direct ethanol fuel cell catalysts', NanoTR-II, Ankara, Turkey, May 2006, Poster Presentation.

6. H. Demir, Z. Kiraly, D. Uner, 'Microcalorimetric characterization of γ- Al_2O_3 supported Pd and Pt catalysts', TOCAT 5, Tokyo, Japan, July 2006, Poster Presentation.

7. H. Demir, D.Uner, 'Microcalorimetric Studies to Investigate the Effect of Sn Addition to Elucidate CO Poisioning on Pt-Sn Direct Ethanol Fuel Cell', European Materials Research Society Fall meeting, Warsaw, Poland, September 2006, Poster Presentation.

8. H. Demir, D. Uner, "Iki metallic Pt-Sn etanol elektro oksitlenme katalizorlerinin sentezi ve karakterizasyonuSynthesis and characterization of Pt-Sn bimetallic ethanol electro-oxidation catalysts", Ulusal Kimya Muhendisligi Kongresi 7, Eskisehir, Turkey; September 2006, Poster Presentation.

9. Á. Császár, Á. Mastalir, Z. Király, H. Demir, D. Üner, 'Determination of metal dispersion by various instrumental techniques', 20th Conference of the European Colloid and Interface Society, Budapest, Hungary, September 2006, Oral Presentation.

10. H. Demir, D. Uner, 'Microcalorimetric Studies to Investigate the Effect of Sn Addition to Elucidate CO Poisoning on γ-Al_2O_3 Supported Pt –based Direct Ethanol Fuel Cell Catalysts', First National Catalysis Congress (NCC 1), Güzelyurt, Nothern Cyprus, January 2007, Poster Presentation.

11. H. D. Kivrak, D.Uner, 'Mechanism Elucidation of the Ethanol Electro-oxidation Reactions on Pt-Sn catalysts', EuropaCAT VIII, Turku, Finland, September 2007, Poster Presentation.

12. H. Kivrak, Z. Király, Á. Mastalir, D. Uner, 'What are the active sites of a commercial 5% Pt γ-Al_20_3 catalyst in liquid phase reactions?', 2nd National Catalysis Congress (NCC-2) , Erzurum, Turkey, June 2008, Poster Presentation.

13. H. Kivrak, S. Kuliyev, D. Uner, 'Structural Characterization and Activity for Ethanol Electro-oxidation of Carbon Supported Pt–Sn Bimetallic Catalysts Prepared by Polyol Method', 2nd National Catalysis Congress (NCC-2), Erzurum, Turkey, June 2008, Oral Presentation.

14. H. Kivrak, S. Kuliyev, D. Uner, 'Synthesis and characterization of carbon supported Pt-Sn and Pt-SnO_2 catalysts to investigate the effect of oxide phase in ethanol electro-oxidation reaction.' AIChE Annual Meeting, Philadelphia, PA, U.S.A., November 2008, Poster Presentation.

15. H. Kivrak, D. Uner, 'Direct ethanol fuel cells as alternative energy generation systems' Global Conference on Global Warming Istanbul, Turkey. July 2009, Oral Presentation.

16. H. Kivrak, S. Kuliyev, and D. Uner, 'Polyol metodu İle hazırlanan Pt/C katalizör parçacık boyutunun etanol elektro-oksitlenme tepkimesine etkilerinin belirlenmesi', 23. Ulusal Kimya Kongresi, Sivas-Turkiye, Haziran 2009, Poster Presentation.

17. H. Kivrak, S. Kuliyev, and D. Uner, Synthesis and characterization of carbon supported Pt-Sn and Pt-SnO_2 catalysts to investigate the effect of oxide phase in ethanol electro-oxidation reaction' National Catalysis Workshop, Tubitak-MAM Energy Institute, Gebze-Turkey, March 2009, Oral Presentation.

18. H. Kivrak. S. Kuliyev, D. Uner, "Role of defects on ethanol electro-oxidation reaction",13th European Conference on Applications of Surface and Interface Analysis, the ECASIA'09, Antalya-Turkey, October 2009, Oral Presentation.

19. H. Kivrak, I. Ozoran. D Uner, "Selective CO oxidation reaction on Pt-Sn", 13th European Conference on Applications of Surface and Interface Analysis, the ECASIA'09, Antalya-Turkey, October 2009, Poster Presentation.

20. H. Kivrak. S. Kuliyev, D. Uner, H. Kleebe, J. J. Schneider "Part I-Size and shape effects in supported metal catalysts via Microcalorimetry and TEM: Part II-On the applications on CNT-PAOX composite structure", 5th TU Darmstad-

METU Joint Graduate Workshop on Nanotechnology, Ankara-Turkey, November 2010, Oral Presentation.

21. H. Kivrak, K. R. Hebert, "A Hyride Precursor Deposition Method Application: Cu deposition on Ti", EMCC6, Antalya-Turkey, March 2010, Poster Presentation.

22. H. Kıvrak, H. Tempel, S. Kuliyev, J. J. Schneider, D. Üner, "TiO2-Carbon Nanotube Structures for Electrocatalysis", NCC-3, April 2010, Zonguldak-Turkey, Oral Presentation.

23. D. Uner, H. Kivrak, Hermann Tempel, S. Kuliyev, J. J. Schneider,"TiO_2-carbon nanotube structures for photoelectrocatalysis", TOCAT6/APCAT 5, Sapporo-Japan, July 2010, Poster Presentation.

24. H. Kivrak. S. Kuliyev, D. Uner, "The Effect of tin addition on ethanol electro-oxidation reaction", 6th EFCATS Summer School, "Catalysis and Surface Science for Renewables and Energy", Izmir-Turkey, September 2010, Oral Presentation.

Summer Schools:

1. 6th EFCATS Summer School, "*Catalysis and Surface Science for Renewables and Energy*", September 13-19, 2010, Izmir, Turkey

2. "*Solid State NMR and Recent Developments*", 30 October-1 November, 2007, Middle East Technical University Central Laboratory, Ankara, Turkey.

3. First Anatolian School on Catalysis (ASC-I), September 25-October 6, 2006, Middle East Technical University, Ankara, Turkey, (Workshop I: *Master class Catalysis*. Workshop II: *Computational Catalysis*.)